The University Of Sheffield.

Metal Matrix Composites with Diamond for Abrasion Resistance

This thesis submitted in partial fulfilment of the requirements for the degree of Doctor of Philosophy (PhD)

By

Haydar Swiry Rahi Al-Shabbani

Department of Materials Science and Engineering

Faculty of Engineering

The University of Sheffield

November 2018

Abstract

Metal matrix composites (MMCs) have been used in many applications (such as automotive, aerospace and construction) for many decades. Recently, there have been interesting developments in this type of composite, applying them in electronic and thermal applications such as with semiconductors, in electronic packaging and heat sinks. This is particularly the case for composites of a metal matrix with diamond which are considered a modern sub-class of metal matrix composites. However, while the thermal properties are exceptional, this class of composites has not been extensively examined for mechanical and tribological behaviour, and it may be possible to apply these composites in practical applications, especially those that require extreme mechanical and tribological strength, for example cutting resistance for security applications.

Therefore, this research looks for a composite material consisting of metal matrix and diamond particles, which resists abrasive cutting. This progresses through a series of steps, developing methods to process the material, understanding the mechanics of abrasive behaviour and optimizing the composite structure to resist abrasive cutting.

Gas Infiltration (GI) casting under gas pressure has been applied to metal matrices with relatively low melting point (aluminium (Al) and tin (Sn)) to obtain a significant penetration of the metal into a preform of diamond particles. Different diamond particle sizes (63-75, 212-250, 420-500 μm) were used to strengthen the Al matrix and diamond coated with a thin Ti layer was used to attempt to enhance the bonding forces between the aluminium matrix and diamond. Al-1 wt. % Mg as a matrix alloy was utilised to investigate the possible effect of Mg on bonding phases and to reduce the surface tension of molten aluminium during the infiltration process. Epoxy was also used as a matrix with diamond in this research by gravity infiltration.

Tribological and microstructural tests were performed on the samples, and the results show that the surface modification (Ti coating) of diamond particles has an important role for enhancing the bonding between the aluminium matrix and diamond reinforcement as is apparent under SEM observation, thus improving wear resistance. The coating layer works to either catalyse the graphitisation of diamond surfaces to then dissolve carbon in the metal, or reacts at the diamond surfaces to form carbide crystallites at the interface. This may be one of the reasons contributing to the bonding between the different matrices and diamond. The presence of some of these phases was indicated with XRD patterns and Raman spectra.

The principal characterization method was by abrasion cutting tests, which have been carried out on all the samples made. One particle size range, 420-500 μm, of diamond coated by Ti, has been used to manufacture composites with different matrices (titanium (Ti), nickel (Ni), copper (Cu), tin (Sn) and epoxy) using different production methods (PM and SPS) for the transition metal matrices due to their high melting points. The abrasion cutting tests of these composites showed that the bonding between the metal matrix and diamond reinforcement and the processing temperature, have an important role in enhancing the abrasion wear resistance of composites, rather than the hardness of matrices.

ACKNOWLEDGEMENT

I would like to thank my home university (University of Al-Qadisiyah/Iraq) and the Iraqi Cultural Attaché-London, which is representative of the Iraqi Ministry of Higher Education and Scientific Research in the UK, for their financial support of my PhD study.

I would like to express my faithful gratitude and deep thank to my supervisor *Dr. Russell Goodall* for his remarkable suggestions, encouragement and guidance through the research; I am really indebted to him for giving opportunities to deeply discuss my experiment issues and suggest alternative worth ideas in my research and even his support in securing finance for research materials.

I should not forget to record my special deep thanks and gratitude to my second supervisor *Professor Matthew Marshall* for his worth suggestion and guidance, especially about developing the tribological rig tester and strategies in my research. All these supports help to achieve success experiments.

I would like to thank the technicians in foundry place (*Dr. Lisa Hollands, Mr. Kyle Arnold and Mr. Neil Hind*) in the department of materials science and engineering, technicians in Sorby Center/ SEM staff (*Dr. Le Ma and Dr. Cheryl Shaw*) all for their available help and support at any time when needed and *Dr Erardo Elizondo* for introducing me to infiltration process.

I would like to thank all my friends and colleagues here in Sheffield for their support and kindness, who make my PhD journey more creative,

Final appreciated, gratitude and grateful words should express to my extended family (Mum, Dad, brothers and sisters) and my small family (wife and daughter) for their encouragement, kindness, support, patient and understanding my busyness during the entire period of this work and the long journey. Special appreciate to my little angel inspiration, who has come to life while I am writing this thesis, inspired me additional creative moment in writing. Thank you all.

Author's Statement

The thesis is submitted to the University of Sheffield, UK in order to achieve the Doctor of Philosophy Degree in Materials Engineering. This work was done by the author in the period from January 2015 to November 2018 under supervision of Dr. Russell Goodall & Prof. Matthew Marshall at the Department of Materials Science and Engineering at the University of Sheffield.

I confirm to best of my knowledge that this work is original, and no part or similar work of the thesis has been submitted for any degree or qualification at other university.

Haydar Al-shabbani / 2018

List of Contents

List of Figures

List of Tables

Chapter 1 Introduction

Currently, there is interest in new advanced composite materials in many new areas, especially those relating to modern electronic and electrical devices which demand very high heat flux, in some cases exceeding the thermal conductivity of copper by many times [1]. Diamond/metal composites could be suitable candidates for those requirements due to their attractive thermal conductivity [2], relatively low coefficients of thermal expansion, acceptable strength to weight ratio (high specific strength), long-term performance and easy set up for net shape products [1]. Therefore, it could be said these advanced composites are becoming the choice of the current century for investigation in thermal management applications [1]. In addition there are other important potential applications which could be considered for materials of this type, such as diamond reinforced abrasives for abrasive cutting and high-performance brake disks [3].

Further, there are unexplored potential applications for this type of composite include being used to impart resistance to abrasive cutting rather than being the cutting medium themselves. For such applications insufficient mechanical data exist for these modern composites, particularly for those with high volume fraction of diamond (50 Vol. % or more) [4]. Therefore, this study will primarily utilize the gas pressure infiltration technique to manufacture diamond/aluminium composites with diamond content above 50 Vol. %, with other manufacturing methods and matrix materials explored to understand their roles. These composites will then be investigated from abrasive and cutting resistance aspects and an attempt will be made to optimize the material composition and processing in order to obtain the best resistance to cutting forces.

1.1 Motivation of Study

The levels of reported crime involving the use of angle grinders have risen in the last few years; for example, during the period of the current work three examples of this type of crime were reported in national news. These thieves stole thousands of pounds and damaged property estimated to cost further thousands of pounds. An investigation carried out by the BBC in 2014, calculated that, for one particular gang who used an angle grinder and a pickaxe, the cost of stolen goods and damage to property was about £109k. This gang stole six ticket machines in railway stations in London and Hertfordshire between 19th April and 23rd May before finally being captured due to footage on CCTV cameras; one of those photos is shown in Figure (1-1) [5].

Figure (1-1): Thieves use angle grinders and pickaxes in railway stations in London while the station is unattended [5].

This type of crime seems to be coming more common among gangs worldwide. In 2016, the Italian State Police in Acireale, Sicily announced an important operation, which was called Caterpillar, to arrest a net of thieves using CCTV images as shown in Figure (1-2), These images show a man attempting to cut into an ATM machine in a petrol station. These thieves confessed to police that they stole from different banks and stores by using a digger to make an opening hole through the wall of the targeted property [6].

Figure (1-2): Thieves use an angle grinder to cut ATM machine beside petrol pump in Sicily-Italy [6].

The most recent angle grinder gang thefts were reported [7] in May 2018 when thieves used an angle grinder to attempt to take money from Castle Donington ATMs at night in 24-hour petrol stations in Leicestershire, UK. Even though they failed to get money from this attempt, significant damage occurred to the ATM machine [7].

There are other angle grinder thieves that have been reported in the press, where the criminals released a video on their Instagram accounts and described how they cut a locked moped and stole it. This video was taken on London streets in 2017 and some captured photos from the video are shown in Figure (1-3)[8].

Figure (1-3): Thieves use an angle grinder to cut a locked moped in London streets [8].

This problem of theft will still occur as long as the grinding wheels, which are normally reinforced with hard materials such as SiC or Al_2O_3, can easily cut through barrier materials which do not have suitable abrasive wear resistance. Diamond/metal composites have been utilized in machining and abrasive tools, which are exposed to extreme stresses, such as grinding wheels, cut-off blades and drills for metals and concrete cutting. These products can be produced by powder metallurgy because their content of diamond volume fraction is normally from 10 to 30 Vol. % [4]. However, there are unexplored potential applications for this type of composite in other areas, being used to impart resistance to abrasive cutting rather than being the cutting medium themselves. For such applications insufficient mechanical data for these modern composites, particularly for those with high volume fraction of diamond up to 50 Vol. % or more, are available [4].

Therefore, in this study the gas pressure infiltration technique was utilised to manufacture diamond/aluminium composites with diamond content above 50 Vol. % in addition to other techniques like Powder Metallurgy (PM) and Spark Plasma Sintering (SPS). This research will investigate these composites from abrasive and cutting resistance aspects and attempt to optimize the material composition and processing in order to obtain the best

resistance to abrasive cutting. In addition, different matrices with different manufacturing processes will be used to obtain the highest abrasive cutting resistance of produced materials.

1.2 Aims of the Study

The primary aim of this study is to create novel diamond-metal composites and assess their suitability for applications requiring abrasive cutting resistance (for example in security) like padlocks or physical barriers for important secured sites or objects, which may be targets of thieves using portable angle grinders.

The objectives to achieve these aims are:

1) To process testable samples of diamond-metal composites, using gas infiltration, spark plasma sintering and powder metallurgy. The metal matrices are Al, Ti, Ni, Cu, and Sn, in addition to Epoxy.
2) To design and validate an abrasion cutting resistance test method, where both the cutting of the samples, and the wear of the abrasive cutting wheels used can be monitored with time.
3) To use this cutting test to evaluate the performance of different samples, with different processing methods, reinforcements, reinforcement particle sizes, reinforcement surface modifications, and matrices to identify the most likely to be effective in the applications needing abrasive cutting resistance.
4) To study the nature of the interaction between the diamond particles and the metal matrices, in order to understand better the nature of this interaction, and the effect that on the performance.

1.3 Thesis Outline

This thesis contains 11 chapters, the current chapter, which is the general introduction, is the first one. The 2nd, 3rd, and 4th chapters deal with background, previous studies, production methods of Metal Matrix Composites (MMCs), relevant works of Metal Matrix with Diamond Composites MMDCs and wear resistance, especially abrasive wear of cutting wheels and composites. Chapter 5 details all procedures and processes for making MMCs and equipment that has been used in manufacturing and tests that were carried out in this study. The 6th and 7th chapters discuss the developed equipment and devices that were created or improved to manufacture and estimate performance for abrasive wear resistance. Chapters 8 and 9 deal with results of abrasive wear resistance of different

MMCs in regard to manufacturing methods, matrices, and reinforcements and compares these results with each other and the matrix. Chapter 10 gives more detailed discussions of wear tests and compares them with other work. Finally, Chapter 11 is the conclusion of this study and recommendations for future work.

Chapter 2 Metal Matrix Composites (MMCs)

Historical Background:

The usage of composite material in a very basic manner started several centuries ago when Egyptian Pharaohs used to reinforce mud walls with bamboo shoots in houses and make multi laminate wood in 1500 BC [9]. In the 1930s advanced composites emerged when glass fiber reinforced polymers [9]–[11] were used to fabricate boats and aircraft [9].
Composite materials have been developed in many ways since this time period and the progress in the composite developments have met aerospace challenges in addition to other applications such as automotive and domestic applications [12],[13]. Composites have become very attractive materials with high specific strength (high strength-to-weight ratio), light weight, high stiffness [13], good fatigue and corrosion resistance, and complicated geometry parts which can be manufactured [10]. These exclusive properties have led to the replacement of some of the more traditional materials such as polymers, metals, ceramics and wood in many applications by composites [12],[13]. In this era, significant progress has been made in advanced composite technologies with, for example, changes from the use of E-glass / Phenolic to the graphite / polyamide composites. This may be considered a big achievement at that time when the graphite / polyamide composites have been applied in the space shuttle orbiter [12]. Efforts have continued to focus on combining different materials or the same materials in a different form [14] to obtain the potential weight savings [12], specific performance and properties [14]. In the 1960s there was an increasing concentration on cost and increase in efficiency requirement by potential weight savings that can be obtained by applying advanced composites. These demands led to developments in the technologies of fabrication of advanced composites from both reinforcements and matrices aspects. Therefore, over this period there were developments in manufacturing methods, crucial studies of fracture mechanics and properties of composites. As a result of this interest, many modern composites were developed which were stronger and stiffer with more light-weight materials than before in important sectors like aerospace, construction, transportation and automobile applications [12].

2.1 Composite Material

A composite material, which is composed of two or more different phases that exist separately (the reinforcement and matrix phase), has unique properties that do not

exist in these phases separately [11], [15]. The phases, which should not dissolve into each other [9] and should be combined at a macroscopic scale [14], [16], [17] can be distinguished by the naked eye. There are of course other materials which are combined from different phases at a microscopic scale, but the resulting materials are not considered composites; these include metallic alloys [16] and polymers which sometimes contain dispersions in their structure.

Each phase, used in combination in composites, has its own role inside the material. Therefore, composite properties are primarily dependent on the properties of their component materials [12], [13] and proper control of the manufacturing process of composites leads to it being possible to achieve all of the aspects listed below [10], [13].

- Significant bonding between reinforcement and matrix
- The suitable orientation of the reinforcement, especially when it is a fiber
- Sufficient volume fraction of reinforcement
- Uniform distribution of reinforcement within the matrix material
- Proper curing or solidification of the resin, if used
- Elimination of voids and defects as far as possible

The structural properties of composites can make them attractive materials to utilise for many applications primarily to support load, but also where there is a functional requirement and the mechanical performance is secondary. Modern composite materials technology has continuously made efforts to obtain the optimum properties for this range of applications (to support load, different functional requirements and the mechanical performance) [17].

A- Matrix Phase

The matrix phase can be defined as a continuous phase in composite materials which is usually either polymer or metal, or sometimes ceramic. Each of these material classes has own characteristics. For example, polymers have low stiffness and strength, metals have medium stiffness and strength, but with high ductility, and ceramics have high stiffness and strength but with extreme brittleness [18]. The matrix serves many crucial roles in composites, such as holding the reinforcements together, transmission of load to and among the reinforcements, protection of the reinforcements from environmental effects and giving the final bulk form to the composites. The matrix also keeps the orientation and spacing of fibers in continuous reinforced composites [17], [18]. For metal matrix composites (MMCs) or ceramic matrix composites (CMCs) which are used at

elevated temperature, the matrix should be chosen in order to protect the fibers from oxidation [19].

B- Reinforcing Phase

The reinforcement can be defined as a second discontinuous constituent of composites which is surrounded by the matrix. Usually, it is stiffer, stronger, harder [17], [18], [20] and has lower thermal expansion [17], [20] than the matrix. Therefore, the high strength and stiffness of composites often derive primarily from this phase [18] which can exist in different forms (continuous fibers, discontinuous fibers, whiskers, particulates) and can be orientated or disorientated [20]. The kind and amount of the reinforcement are considered significant factors in the quality of the final composites [18].

There is another effective factor in the function of composites apart from the matrix and reinforcement, which could in some senses be considered as a third phase in structure of composite (although it does not take up any physical space), and that is the interface between these two phases [10]. It often plays an important role in determining mechanical properties of the composite [14]; for example the strength of the interface can affect the likelihood of crack deflection and the toughness of the overall composite.

2.2 Classification of Composites

There are several methods of classifying composite materials, which are based on different criteria such as material constituent type, forms and shape, applications, the bulk form of composites and constituent distribution [14]. However, the two most common classifications are based on the matrix materials and the reinforcement form [17]. This thesis will briefly discuss both classifications, and focus on the particulate reinforcement in this chapter. Strengthening mechanisms in composites and metal matrix composites will be discussed in more detail in the next chapter.

A- Classification Based on Matrix Material

This category of classification splits composites into polymer matrix composites (PMCs) which are sometimes called organic matrix composites to be more general and include carbon matrix composites, ceramic-matrix composites (CMCs), and metal-matrix composites (MMCs) [17]. The latter, which is the subject of this study, will be discussed later in this review.

B- Classification Based on Reinforcement Form

The second category of composites, which are classified by the reinforcement shape, could be further divided into two main common groups and some less common sub-groups. They will be briefly discussed in the following paragraphs and as shown in Figure (2-1) below:

2.2.1.1 Fibrous Composites

There are two types of fiber reinforced composites, continuous and discontinuous fiber reinforced composites. Generally, fibers can be defined as particles with an aspect ratio (length-to-diameter ratio) greater than 10:1 and length greater than 100 μm [14]. Continuous fiber has length very much larger than its cross- sectional area; if not it will be considered a discontinuous or short fiber. The properties of this kind of composites are strongly affected by fiber length, in general, increasing fiber length leads to enhancement in the elastic modulus and the strength of the composites [17]. Generally fiber reinforced composites are anisotropic, because their properties depend very strongly on the fiber orientation [9]. The continuous fiber reinforced composites are often fabricated to be a multi layered stack, every layer can having a particular fiber orientation. Such a stack is called a laminated stack or laminar composites [17]. Laminar composites need not be multi layers of fibrous composites only, sometimes they are fabricated from different layers of several materials such as polymer and metal and so on or from the same materials in different orientations [14].

2.2.1.2 Particulate Composites:

Particulate composites can be defined as materials with a matrix reinforced by particles. If all dimensions of the reinforcement phase are relatively equal, it will be termed a particle (as opposed to fibres discussed before), and a composite which contains such a phase is called a particulate composite. The particle geometry may be spheres, flakes, rods, or any other geometry, but should be relatively equiaxed [17]. Particles and whiskers with roughly 20-100 aspect ratio reinforcement are commonly used to strengthen MMCs. This type of reinforcement can be also classified as a discontinuous reinforcement [17]. Particulate composites have different properties in comparison with fibrous composites. For example, they are often isotropic due to the particles being randomly distributed and oriented, have high strength, elevated operating temperature and oxidation tolerance (though these latter come from the nature of the materials available in particle form, rather than any inherent behaviour of the particles themselves). Common examples of particulate

composites could include concrete, consisting of particles of gravel or sand, in a matrix of cement [9].

• **Flake composites** are composites containing flakes inside a matrix [14], [9]. A flake is a plate-like particle [14], and therefore, flakes can be difficult to have oriented and are also limited to a small number of materials for practical use [9].

• **Filled composites** are composites containing filler particles for filling purposes (e.g. cost reduction) rather than mechanical reinforcement [17]. Nevertheless, they are constituted of the main phase with a second material added. These composites cannot really be considered as particulate composites, even though sometimes the filler will also act as a reinforcement [17].

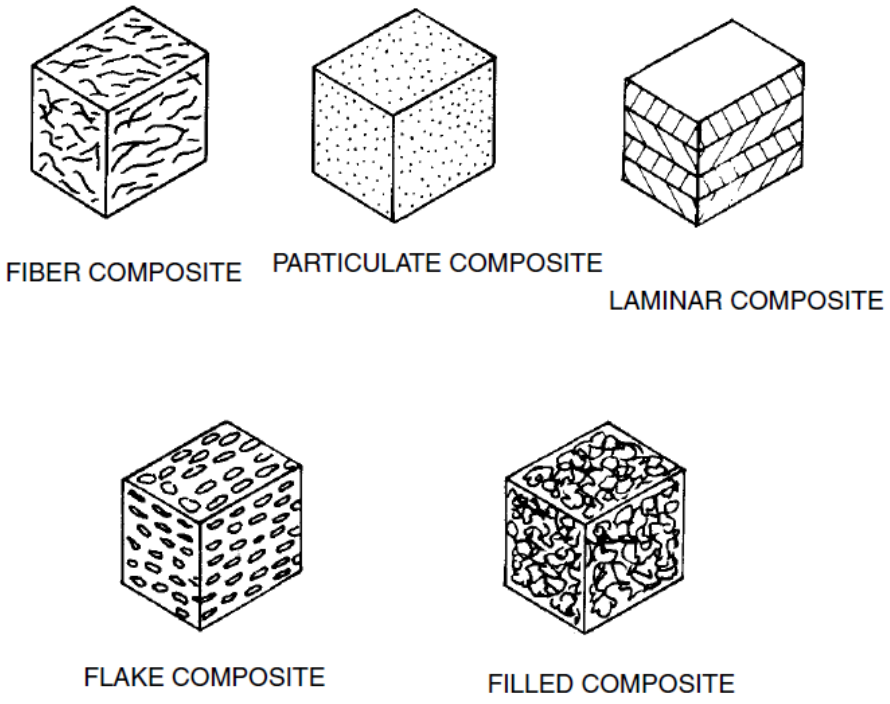

Figure (2-1): Composite classes depending on reinforcement form after [14].

2.3 Metal-Matrix Composite Materials (MMCs)

Metal Matrix Composites (MMCs) have attracted the interest of many researchers in recent years. They can be considered to some extent a product of the system of development of engineering materials for modern design applications [21], and first started as a viable technology when addressing the improved performance requirements of modern military

systems. In the era of the main developments, more economical and commercially viable production routes were introduced in order to serve these initial military applications. While some MMC applications were achieved in this period (1960s), the initial wave of development came to an end in the late 1970s, particularly when many developed nations carried out safety assessments on their military systems and began to emphasize risk criteria, along with an increasing focus on the importance of risk in civil applications (one of the drawbacks of at least the early MMCs was variable properties, which can lead to risk without good quality control and non-destructive testing). Also at that time (1970s) the focus moved to research directions which developed high performance composites [22]. However, the possibility for MMCs to serve in certain applications has not diminished, and they remain materials of interest for many uses, especially (as outlined later) those with demanding requirements that do not have to bear the load in safety-critical applications.

The Metal Matrix Composite concept in most cases is used to achieve the aim of lightweight or low density materials. In recent decades significant development has been achieved in light metal matrix composites. Therefore, this is where the most developed applications for MMCs are found, such as in the automotive industry, primarily in pistons and aluminium crank cases which are reinforced with ceramic fiber, and cylinder surface strengthening and brake disks which are strengthened with ceramic particles [23]. The developments in these materials have led to recognition in recent material science that MMCs can achieve the desired properties, and that the properties can be flexibly chosen for particular designs. They have potential, for example, in construction and as architectural materials, and where required properties are difficult to achieve with conventional materials.

Depending on reinforcement form, MMCs can be divided into two main types; discontinuously reinforced MMC (particle or short fibre reinforcement) and continuously reinforced MMC (long fibre reinforced) [21]. Particulate and discontinuous fiber reinforced MMCs are the most common; for example, these are used in automotive components, though they are still under development for aerospace components due to the higher design requirements [12]. Particulate composites have isotropic properties and mass production is relatively easily achieved in comparison with continuously reinforced MMCs, leading to a more reasonable cost [12].

The production methods of MMCs are normally extensions of conventional methods of material manufacture, such as powder metallurgy. They have to achieve acceptable cost and be capable of processing a combination of several material types together (e.g. metal – ceramic) [24]. However, net shape or near net shape processing methods would be preferred as MMCs generally have poor machinability [25].

2.4 Production Methods of MMCs:

The processing techniques, which have been applied over many years to manufacture MMCs are numerous. Selecting one of them depends on the types of constituents of composites, especially, reinforced constituent form in order to obtain suitable microstructure and mechanical properties for each particular requirement of the composite. Commonly, these processing methods could consist of two main steps which are obtaining the required material composition or blend of constituents and secondary densification and consolidation processes [26]. The application of secondary processes may sometimes be important to eliminate shrinkage and distortion of the products [27]. Molten metal infiltration methods can be applied to processing of MMCs, and can be used to produce MMCs with a high volume fraction of reinforcement [28], [29], especially diamond particles in the current focus. Spark Plasma Sintering (SPS) and Powder Metallurgy (PM) which can be used to produce Particulate Reinforced Metal Matrix Composites (PRMMCs), as can spray deposition, reactive processing [26] and vapour-state technology [27]. The production methods of MMCs can be classified depending on the status of the matrix material during manufacturing such as whether or not it is in the liquid state, as discussed below:

2.4.1 Liquid State Production of Metal Matrix Composites

There are many liquid state methods of manufacturing MMCs, the main examples of which are discussed below.

A- Molten Infiltration Techniques

Molten metal infiltration means a penetration of molten metal into a preform of fibre or particle reinforcement [30]. There are many types of molten infiltration techniques. Some of them use external pressure to push the molten metal to penetrate into the preform of

reinforcement, others depend on the capillary action of molten metal only [26], [31]. The external pressure is generated by either applying gas (gas pressure infiltration casting) or mechanical force (squeeze infiltration casting) which are shown schematically in Figure (2-2) and Figure (2-3) below. The present study will refer to the gas pressure infiltration method in detail and the attention will be focused on some previous studies which have been done to produce metal matrix composites with diamond particles. The gas infiltration technique can be defined as the infiltration method which applies an inert gas to push the molten metal into the preform reinforcement as shown in Figure (2-3). The method is characterized by its ability to produce relatively large parts of composites [26], suitable for mass production, relatively inexpensive equipment [32], and it can overcome a lack of wetting between the matrix and reinforcement and avoid the possible damage of reinforcement particles, which might be caused by squeeze casting [26]. Further, this technique has the potential to be the most suitable method for producing metal matrix-diamond composites with a high volume fraction of diamond particles at a level of nearly 50% or more [33].

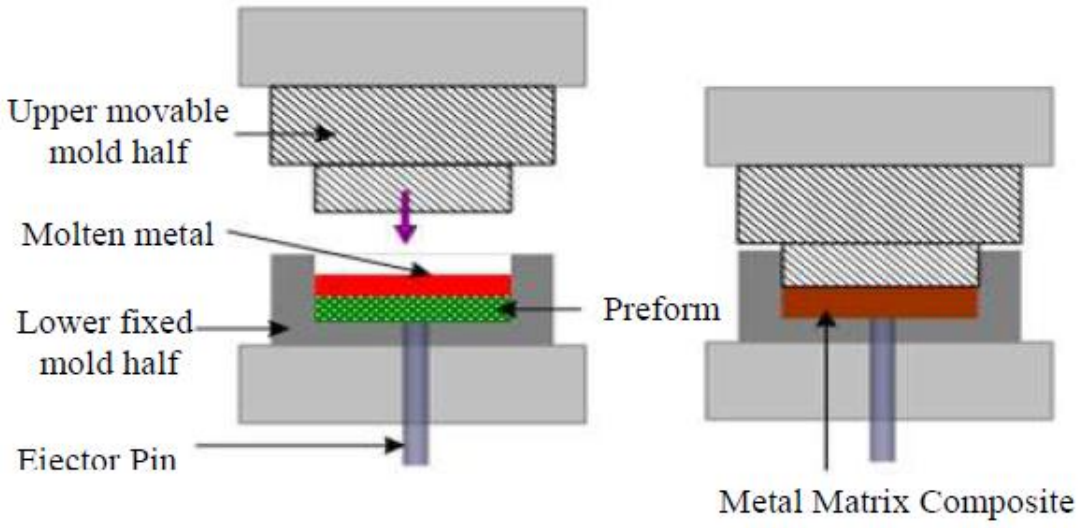

Figure (2-2): Schematic drawing of Squeeze infiltration Casting after [26].

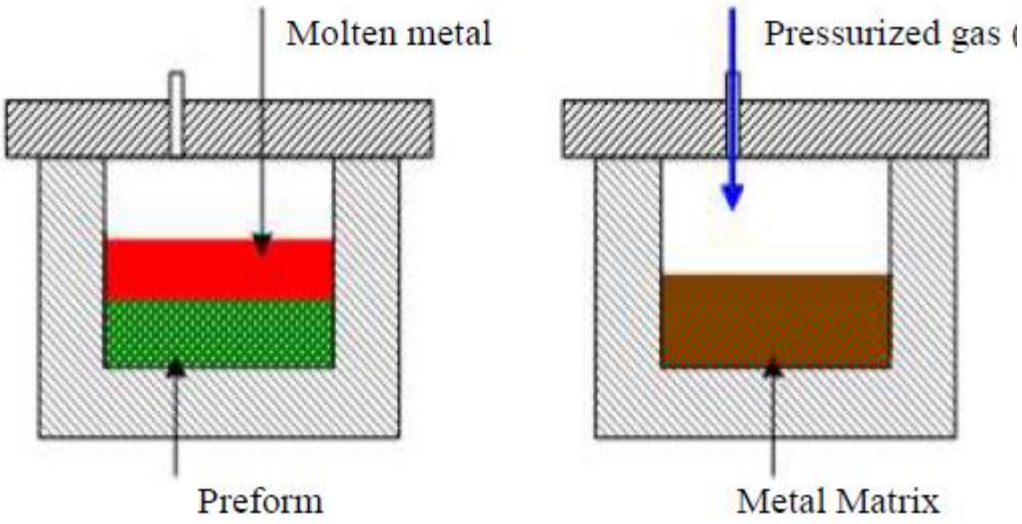

Figure (2-3): Schematic drawing of Gas Pressure infiltration Casting after [26].

2.4.1.1 Infiltration Mechanism

The capillary action and surface tension of molten metal play a crucial role in the wetting of reinforcement in addition to the surface and physical characteristics of the particles themselves [34]. These behaviours are governed by the Young- Dupre law for wetting in terms of contact angle and interfacial energies between solid, atmosphere (vapour or vacuum) and liquid phases. This equation was stated by Young in about 1805 for a system that contains solid and liquid phases [35], it was given in an equilibrium state of these phases as:

$$\gamma_{sv} = \gamma_{sl} + \gamma_{lv} * Cos\,\theta \quad \ldots\ldots\ldots\ldots \quad \textit{Equation 2-1}$$

where γ_{sv}, γ_{sl}, and γ_{lv} are the interfacial energy between solid-vapour, solid-liquid, and liquid-vapour respectively, and θ is the wetting angle, as shown in Figure (2-4).

Hence, effective wetting can be achieved when θ < 90 as shown in Figure (2-4 b) [34]–[36].

This equation was subsequently modified for practical use with molten metals by Cyril Stanley Smith [35] in 1948 with the interpretation that interfacial energies are crucial to determine the structure of solids, especially in the metallurgical process of casting when both phases (liquid and solid) coexist [35]. This modification has been considered as a foundation of metallurgists and ceramicists over the last half century [37]. He termed the

work which is required to obtain effective wetting of liquid on a solid phase, the work of spreading a liquid on the solid. Spreading work (W_s) was given as follows:

$$W_s = \gamma_{sv} - \gamma_{sl} - \gamma_{lv} \quad (By\ assuming\ \theta=0) \quad \text{Equation 22-2}$$

Here, the adhesion of liquid will not happen if the value of W_s is not positive, but the liquid will form as a drop on surfaces as shown in Figure (2-4 a) [35]. That work (W_s) is required to spread a drop of liquid on a solid surface, but when a solid particle is immersed in liquid there is another type of wetting that happens, which is called immersional wetting (W_i), and is given as:

$$W_i = (\gamma_{sl}-\gamma_{sv}) \quad \text{Equation 2-3}$$

Following these ideas, metallurgists who deal with molten metal infiltration have tried to utilize these wetting equations to estimate the pressure required to fully wet molten metals on solid surfaces, and hence give an effective infiltration. For example, Mortensen and Jin [36] assumed that the minimum pressure, which is required to achieve an infiltration of molten metal into preform reinforcement, should equal to the work of immersion with regard to the surface area of reinforcement particles [36].

Then:

$$P=\Delta P= S_F\ (\gamma_{sl}-\gamma_{sv}) \quad \text{Equation 2-4}$$

where S_f is the surface area of the interface

$(\gamma_{sl}-\gamma_{sv}) = W_i$

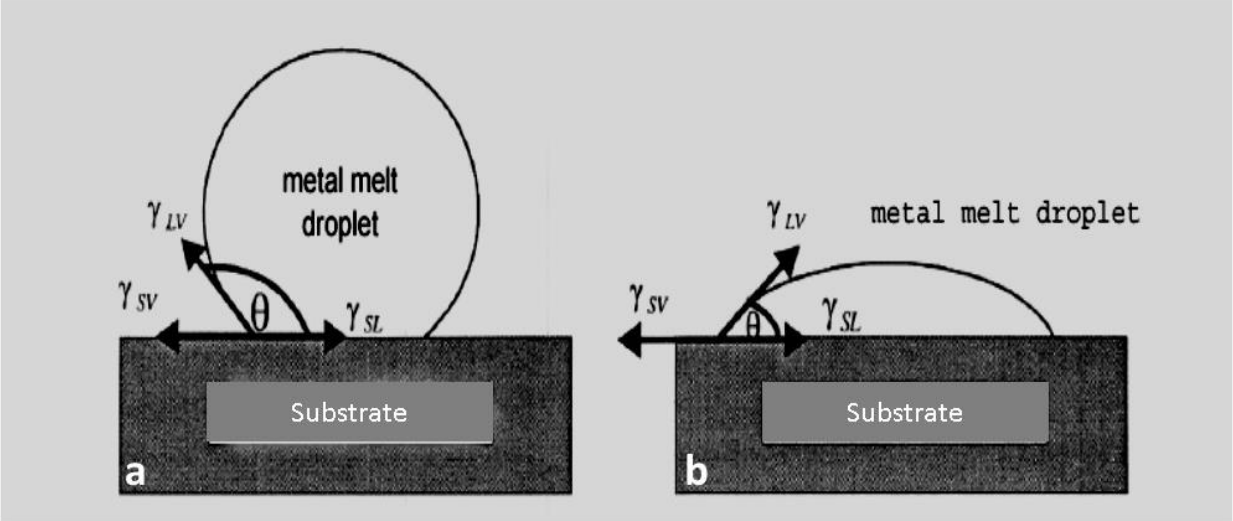

Figure (2-4) : Schematic diagram of a Molten metal droplet on a ceramic substrate a- θ > 90° b- θ < 90° after [34].

B- Stir Casting

Stir casting is considered one of the most important methods of manufacturing composite materials [38]. This is achieved by adding the reinforcement particles into the liquid metal with the aid of continuous stirring of molten metal prior to beginning solidification of the mixture, and after that leaving it to solidify [38][39]. The process can normally be achieved by simply available casting equipment supplied with a mechanical stirrer as that shown in Figure (2-5). Therefore, this technique can be considered relatively simple and low- cost.

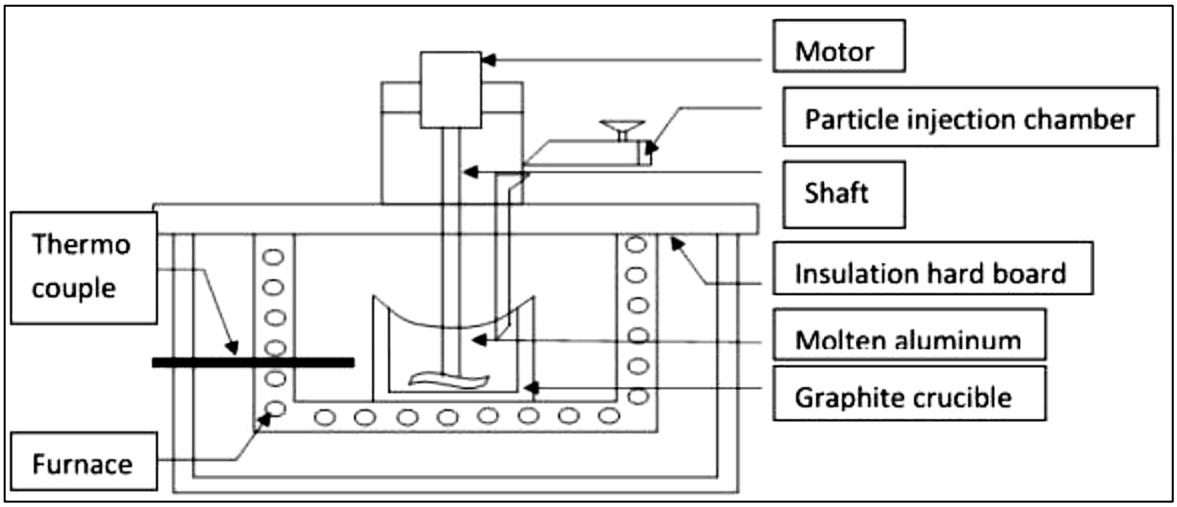

Figure (2-5): Schematic view of a stirring mechanism for the fabrication of composites *after* [38].

The common challenge of reinforcing metals with ceramic particles is difficulty of achieving suitable wetting between the liquid metal matrix and the reinforcement particles [38], [39]. This challenge can be generated from many factors, an important one of which is the liquid viscosity, which can be an obstacle to wet particles by liquid [38]. Therefore, the vortex technique, which is commonly called stir casting, has been applied by introducing the molten metal by a rotating impeller into a pre-treated reinforcement to promote wetting [39]. A further step may be encouraging the interfacial reactions by extending the contact time of liquid-ceramic at melting temperature before letting the composite cool down [38]. Other problems may occur during solidification, such as inhomogeneities due to segregation and accumulation of reinforcements in preferable areas due to directional solidification, which may push the reinforcement to these areas. These defects can in some cases be avoided by rapid solidification [38].

2.4.2 Solid State Production of Metal Matrix Composites

A- Conventional Powder Metallurgy (PM):

The powder metallurgy (PM) technique, has been developed to be applied in composite manufacturing in order to overcome the wettability obstacle between composite constituents in some composites when manufactured by routes involving matrix fusion [40]. In this method two or more different separated powders, which represent matrix and reinforcement, are mixed together in powder form [40], [41] followed by pressing and sintering process, which should be carried out in the solid state at about 85% of melting point of the lowest constituent melting temperature (which is normally that of the matrix), to achieve near-net-shape product of MMCs. There are different types of pressing which can be used according to the type of composite and its requirements, which are Hot Isostatic Pressing HIP, Cold Isostatic Pressing CIP, sometimes applied in combination as Cold and Hot Isostatic Pressing CHIP [41]. Sometimes the pressing stage is combined with the sintering stage so they are considered as one stage, especially when the vacuum hot press is utilised for consolidation. Through such routes, composites can achieve over 95% of theoretical density [40]. Some composites sintered at high temperature may go over the solidus line to generate a thin layer of liquid phase at composite interfaces. The densification kinetics of such composites, which involve liquid phase generation through sintering, especially in high amount and long contact time with reinforcement, have drawbacks. These include encouraging thermodynamic reactions to occur more easily

between the liquid phase and the reinforcement to create undesirable intermetallic compounds at the reinforcement particle- matrix interfaces and significant grain growth in the microstructure. Therefore, entirely solid state consolidation is preferred ,bringing about the emphasis, from the early stages of powder mixing on obtaining the right distribution of reinforcement in the matrix as this determines the initial homogeneity of the composite [40].

The powder metallurgy technique, like other techniques, has advantages and drawbacks:

1. MMC products, which are manufactured by the PM method, have good performance with good strength and stiffness, but the PM equipment is relatively expensive and such composites are associated with high costs [40], [41] and the production procedures are complex and limited in complexity of products which can be produced.
2. The PM method is capable of utilising a variety of matrix and reinforcements due to its ability to control the reactions between composite constituents by applying solid state sintering and controlled cooling rate.
3. Non-equilibrium solidification of alloys can be utilised to form the matrix by the use of rapidly solidified powders. This may be especially significant, when the composite is required for high tolerance strength applications [40] because some metastable phases are frequently desirable for strengthening, such as transitional precipitates (e.g. Guinier–Preston or G. P. zones), especially in Al-Mg and Al-Cu alloys, or martensite in steel. These precipitates are nonequilibrium phases, and require critical cooling rates from higher temperature phases to retain what is in these cases a desirable metastable structure [42].

B- Spark Plasma Sintering (SPS)

In this technique the powder, which is once again a mixture of powders of the matrix and reinforcement materials, is put into a special mould, which is designed for this purpose, and is made of an electrically conductive material. The mould with the mixture of powders in it is put inside a chamber and placed under vacuum. After achieving vacuum in the

mould environment, the sample is heated by alternating current that passes through the sample. At the same time a punch is used to compress the sample during the heating time and the force used and the temperature of heating can be chosen depending on the requirements of the product (although the temperature should obviously be less than the melting points of the powders), the sample can be held at this temperature for some time which also can be chosen by the user [43].

C- Diffusion Bonding

Diffusion bonding is another solid-state manufacturing method, which has been developed to produce metal matrix composite reinforced with fibres, and was originally utilised for joining metals. This fundamentally depends on atomic-thermodynamic behaviour, that contacting materials at high temperature, especially metals, exhibit atomic diffusion between clean surfaces. This inter-diffusion leads to surface bonding. Even though, this atomic diffusion can occur by different mechanisms, it requires two main factors to be applied which are elevated temperature and pressure, in addition to long contact time. There are different pressing configurations which can be used for this method, but Hot isostatic pressing (HIP) is preferred over uniaxial pressing because in HIP high gas pressure and temperature can be applied with different geometries. The MMC constituents can be arranged in preferable orientations as either composite wires (fibres wrapped with matrix alloy) or as laminar composites as shown in Figure (2-6). The diffusion bonding method also has good features such as its ability to process different metal matrices and control the orientation and volume fraction of reinforcement, but it has drawbacks as well, such as high processing pressure and temperature with long time that will increase the cost of the process, in addition to the limited shapes which can be manufactured [30].

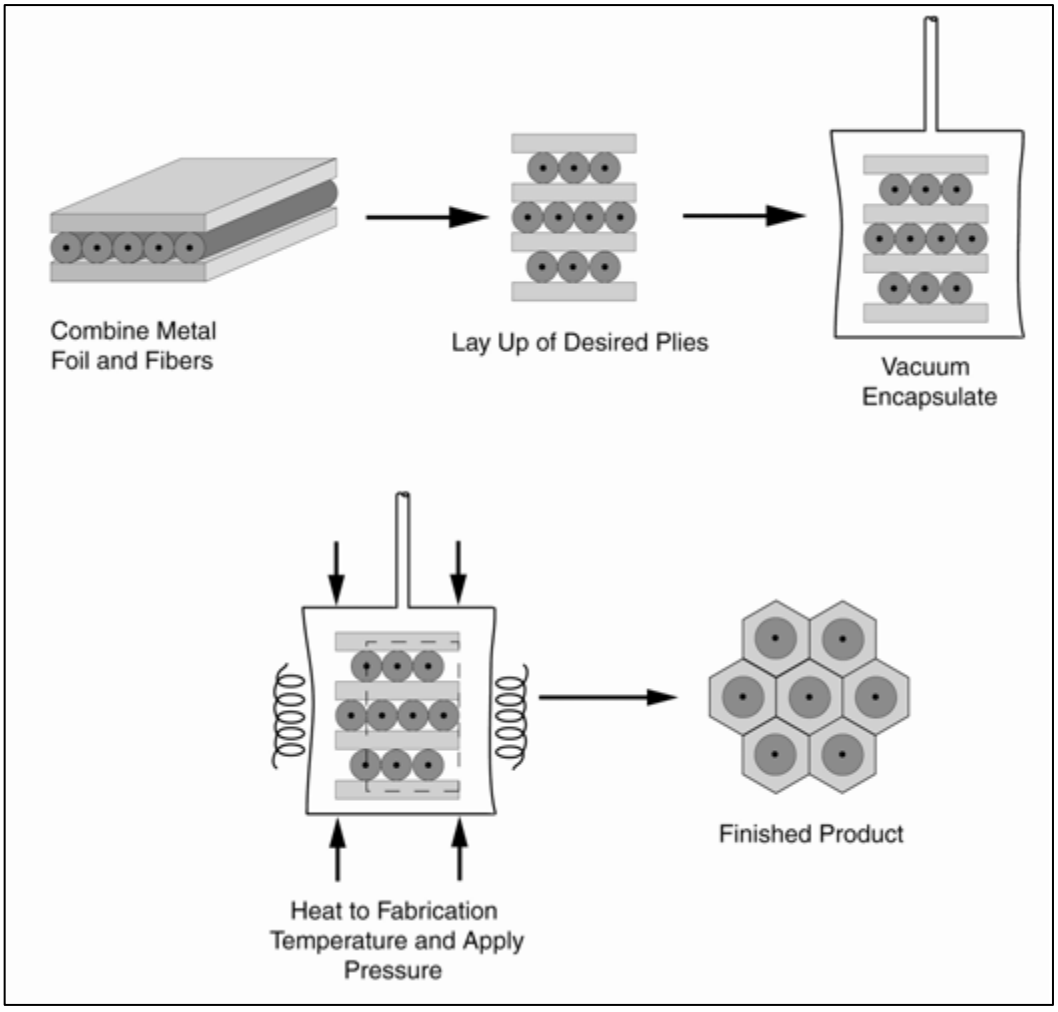

Figure (2-6): Schematically drawing of diffusion bonding method after [30].

2.4.3 Deposition Techniques

Deposition methods were originally coating processes for pre-coating reinforcements prior to consolidation of the composites by other techniques. Generally, in most MMCs, it is important to spread thin coating layer on the reinforcement surfaces prior to their being combined with a matrix to fabricate composites. This coating layer plays important roles in the composite process and performance as follows [44]:

1. Protect the reinforcements from reaction with the matrices or even diffusion by forming a diffusion barrier.
2. Keeping the individual reinforcement particles separate from each other and preventing a direct reinforcement- reinforcement contact.

3. Enhancing the bonding between composite constituents by eliminating interfacial reactions, preventing undesirable brittle intermetallic compounds from formation at interface.
4. Eliminates thermal and residual strain concentrations in between the composite constituents.
5. Offers handling protection to the reinforcement.

Recently, deposition processes have been integrated with extra procedures such as hot pressing or HIP to produce MMCs, especially those reinforced with fibres [38]. The most common deposition techniques, which are **Physical Vapour Deposition (PVD) and Chemical Vapour Deposition (CVD)**. In both techniques fibres are moved through highly active evaporated metal environments, which can be either deposited thermally or reacted with other media such as another vapour or plasma in order to encourage metal vapour to deposit on the fibres [21], [30], [38], [45]. The main difference between the two techniques is the way of generating the vapour phase. In the PVD technique physically activated evaporation is used such as high power or laser emission [38] while in CVD chemically activated reaction is employed to cause evaporation of matrix or reaction with another vapour [21]. Simply, PVD involves a vapour of atoms or atom clusters being condensed. This may either be ionized or normal vapour. Therefore, there are three common PVD sub-techniques, which may be distinguished by the mechanism of deposition; these are evaporation, sputtering, and ion plating.
CVD, which involves a reaction of evaporated components at the substrate surfaces inside reactor that contains the substrates, leads to deposit a solid surface layer on a substrate with other reaction products that can easily be removed. This reaction is governed by the thermodynamic conditions, which are the vapour pressure and temperature. CVD is mainly performed at higher vapour pressure and temperature than PVD, and so there are chemical reactions occurring at the substrate surface like atomic diffusion [46]. The rate of deposition in CVD can be lower than that in PVD in a single process [46]; PVD can reach 5-10 micrometers per minute while CVD will be slower [45]. However, CVD can be applied to achieve multilayer coatings, while PVD is limited to a single layer only. Finally, non-refractory metals and alloys can be processed with PVD only, because CVD has high range of temperature 850-1250°C in comparison with 200-600°C for PVD [46]. However, the deposition techniques in MMCs manufacturing are generally considered slow methods due to their low productivity and requirement of post-consolidation by diffusion bonding

to complete their net-structure (composite), but there are some advantages for these techniques such as that a good degree of interfacial bonding and controlled reinforcement orientation are easily achieved [30]. Additionally, there are many other less commonly used deposition techniques, which will be briefly discussed in this study as follows [30]:

Dipping or immersion plating: which is like infiltration casting apart from that fibres in the form of a net are continuously drawn through a bath of metal ions in solution while metal matrix is encouraged to precipitate from these ions by the help of electric current to form a coating layer on the reinforcement, which acts as a cathode. This method is characterised by moderate temperature, reducing the chances for damage to fibres. Nevertheless, the bonding is not as good as in PVD or CVD and this method exhibits voids between fibres layers and it has limitation in matrix alloys which can be processed.

Spray deposition: in this technique a drum coated with foil is used to spread winding fibres then a molten metal is sprayed onto them to create a coating layer. Plasma torch, arc or flame is used to melt the matrix metal, which is either wire feedstock or powder. This method allows a good fibre alignment control and quick consolidation of composite so the contact time between constituents will be reduced, consequently this leads to the elimination of interfacial reactions [30], [40].

2.5 Strengthening Mechanisms of Composites

The strengthening mechanisms of composite materials depend on the reinforcement form and its distribution in the matrix, either fibrous, particulate or another form [47]. As a result the failure mechanisms are still an open question for fracture mechanics; in other words, there is not a fixed criterion of fracture mechanics of all composites [9]. In this research attention will be focused on the strengthening mechanisms in particulate composites in more detail.

2.5.1 Strengthening Mechanisms of Particulate Composites and Equations for Properties

Generally, all composite materials will obey the limit of the Rule Of Mixtures (ROM) law, which can provide initial estimations of bounds for mechanical properties of composites, describing the general property of the composite as P_c. The overall value of P_c comes from

a contribution of the matrix and reinforcement properties, which are P_m and P_r, respectively:

$$P = P_m \times V_m + P_r \times V_r \quad \text{Equation 2-5}$$

where V_m and V_r are the volume fraction of matrix and reinforcement, respectively.

This law can be applied to all composites with some modifications, which are made to be more specific to particular types of composites, often depending on reinforcement geometry and distribution [14]. For example, in relating to particulate composites, many attempts have been made to modify the ROM to be appropriate to them taking into account the characteristics of particles. One of the most significant approximations for short fibres and particulate composites is the Eshelby model, which is considered a semi-empirical model. It assumes the inclusion (a single particle) has ellipsoidal geometry [48], [49]. The inclusion will cause a misfit strain field which will oppose the stress field which is applied. The stiffness tensor is used to explain the roles of matrix and inclusion inside the composites [20], [49], [50]. Other researchers have modified the ROM law to create another semi-empirical equation, which can be applied to particulate composites with a relatively high aspect ratio of reinforcements; the Halpin-Tsai equation [51]:

$$E_c = \frac{E_m(1+2\,s\,q\,V_p)}{1-q\,V_p} \quad \text{Equation 2-6}$$

where S is the particle aspect ratio and q is given by:

$$q = \frac{E_p/E_m - 1}{E_p/E_m + 2s}$$

All other terms are as defined previously.

2.6 Fracture Mechanisms in Particulate Composites

Generally, mechanical behaviour in particulate MMCs is determined by the microstructure of these composites, and the composite microstructure itself primarily depends on the form and properties of reinforcement particles [48], [52] in addition to the matrix behaviour [53]. Particle properties play an important role to enhance composite properties, and this enhancement is affected by different factors, such as; the particle sizes, the particle distributions and their relative content in the matrix, and the particle morphology [39], [53]. Other factors are the compatibility between the matrix and the particles [39], [53], which may depend on whether are there interactions between them. Where debonding at an interface governs mechanical properties in different MMCs, micro voids may form, and

contribute to plastic deformation of the matrix material until they eventually meet to form a crack [54], [55]. The experimental investigation of the interface in particulate MMCs to explore debonding defects is limited [53], [56]. Therefore, there are many prediction models (some of them numerical) for the interfacial fracture behaviour of PMMCs. One important foundation model of these prediction models, is the cohesive model [56], of Dugdale [57], [58]. This model is considered to be a good tool to simulate the interfacial decohesive progress in such composites. This model attributes the generation of stress to the interfacial displacement at interface when the strain is equal to the critical fracture energy, then a crack may initiate and damage occur, which can be controlled by the interfacial strength [53]. Many factors, such as if the particles are different sizes, irregularly distributed in the matrix [53], or variation in their volume fraction [53] and particle– matrix interfaces [39] all affect particulate MMC's behaviour; assessing only one factor will not allow the whole possible macroscopic mechanical behaviour of these complex composite morphology [53]. Therefore, further studies of the mechanical behaviour of particulate MMCs are required to achieve a comprehensive understanding of their design and industrial application [56]. In regard to the fracture mechanism in particle reinforced MMCs there are two main broad groups of mechanisms which have been reported, which are particle fracture and interfacial fracture (debonding failure) [59]. Babout et al. [59] studied the effect of plastic behavior of the matrix surrounding the reinforcement on the damage creation mode, and found a difference in fracture behavior between pure aluminum matrix and another with a higher yield stress (aluminium alloy 2124), where the fracture of particles dominated in the latter matrix, while in pure aluminium matrix the debonding fracture was dominant. This occurred even though both were reinforced with 4% vol. spherical zirconium and silica particles. This study stated that there are three possible modes of fracture in respect of the stress that cause particles fracture as described in Figure (2-7) [59].

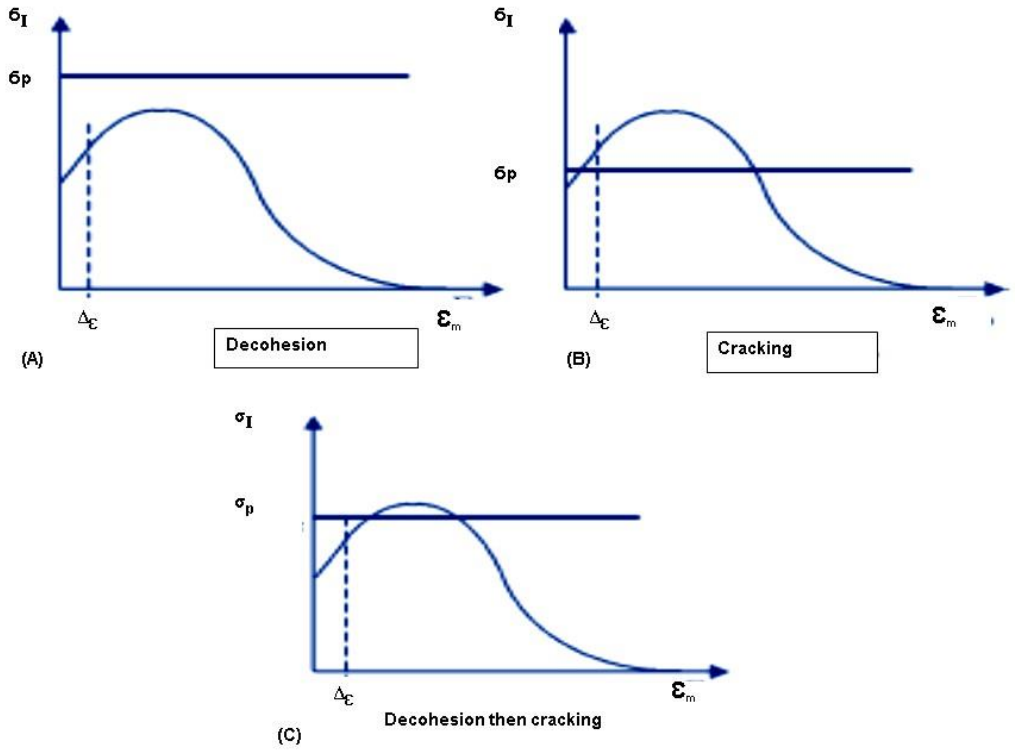

Figure (2-7): Possible fracture mechanisms in MMCs adapted from ref. [59] *with permission from Acta Materialia.*

Figure (2-7) shows the effects of stress-strain in particle depending on the fracture stress of inclusion and matrix, where in (A) interfacial fracture, (B) particle fracture, and (C) the interfacial crack followed by particle fracture. Finally this study concluded that larger size reinforcements should have less fracture strength than smaller ones [59].

2.7 Synthetic Diamond

When considering the reinforcement phase, materials that introduce desirable properties, such as high hardness, high thermal conductivity, etc., are often selected. For this reason, materials with extreme properties such as diamond are often attractive. However, naturally occurring diamond is subject to some degree of property variation, and more importantly is extremely high cost. Therefore, the advent of reliable methods for synthetic diamond production was a vital enabling technology for the advent of diamond-based MMCs.

Originally, the word ‘diamond’ is a derivative from the Greek word ‘adámas’, which means unbreakable or adamant in the English language. It is usually identified as the hardest material, with its hardness located at the top of Moh’s hardness scale (based on the relative measurement of materials’ ability to scratch each other), equalling 10 on the scale. Although some other mechanical properties of the diamond are not as good as its hardness (for example, diamond tends to be entirely brittle during fracture [60]) the Young’s modulus is also very high, about 1000-1075 GPa [60], [61]. These properties make diamond as a theoretical engineering material potentially suitable for a wide range of applications, although for cost and processing reasons the actual applications are more limited. For example, one area of use is where there is a demand for high hardness and high abrasive resistance such as grinding wheels and cutting tools and so on. Diamond applications in different fields can be simply shown in Figure (2-8).

Furthermore, diamond has particular optical properties such as its unique luminescence; its ability to absorb and reflect light with several colours. These give it a particular visual appearance which make it attractive for jewellery [62]. Although mechanically resistant, diamond is thermally degradable into graphite or oxidized form at elevated temperature, around 700℃ and above, especially in the presence of oxygen [32], [60].

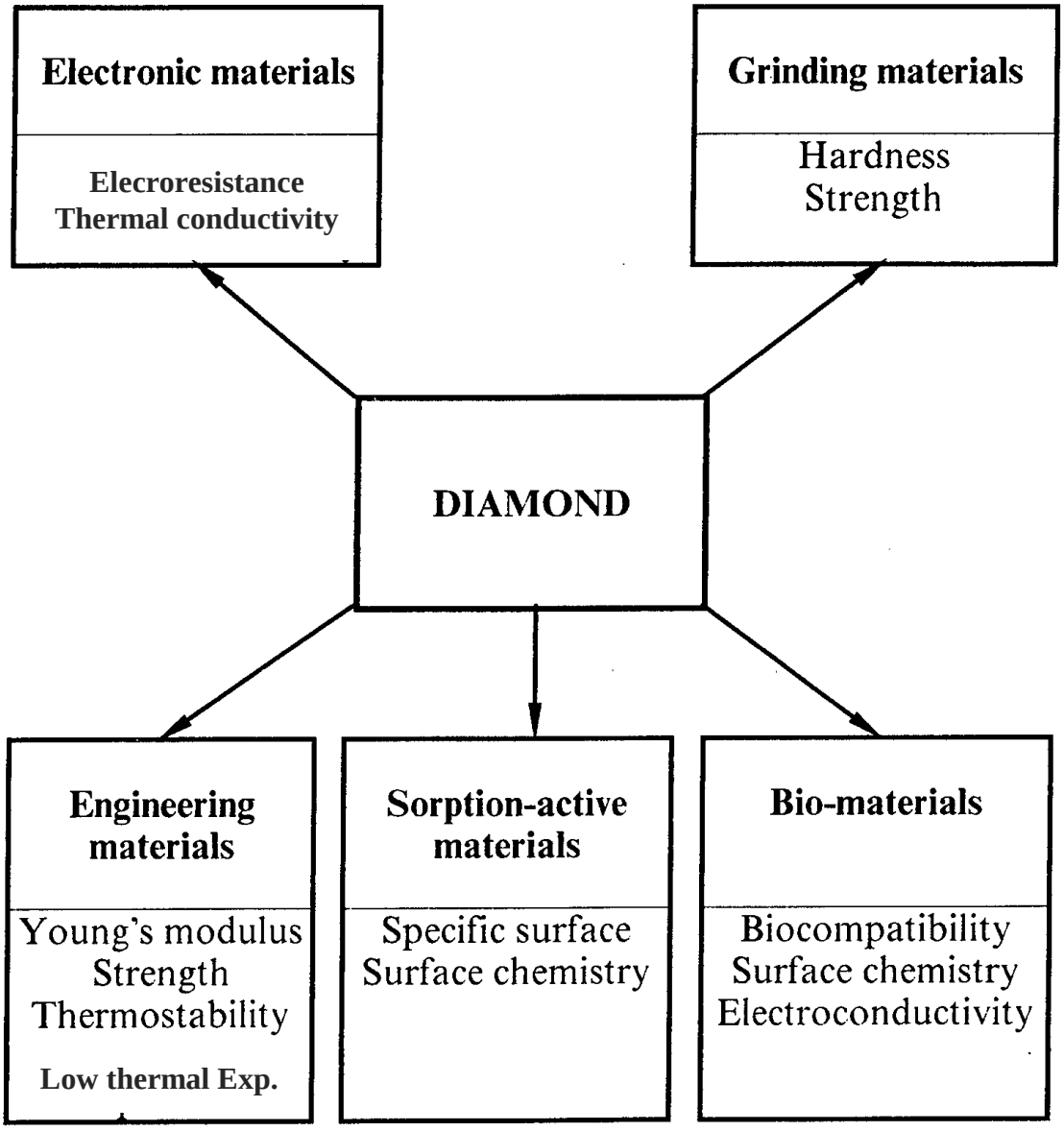

Figure (2-8): The general areas of application for diamond applications [61].

There are two main classes of diamond, which are natural and synthetic. Natural diamond forms naturally from carbon in the mantle of the earth under very high pressure and temperatures [62], while the synthetic diamond is a man-made product which is produced during exposure of carbon to similarly extreme conditions of temperatures and pressure. Diamond can be classified depending on impurities into two main types which are type I and type II. Then these types are also classified into sub-types according to the co-existence of atoms of impurities inside the crystal structure [63] as shown in Figure (2-9) below, which represents the two dimensional drawing of tetrahedral bonding of carbon

atoms in the diamond structure. Where either nitrogen or boron atoms replace the C atoms the diamond types are delineated [63].

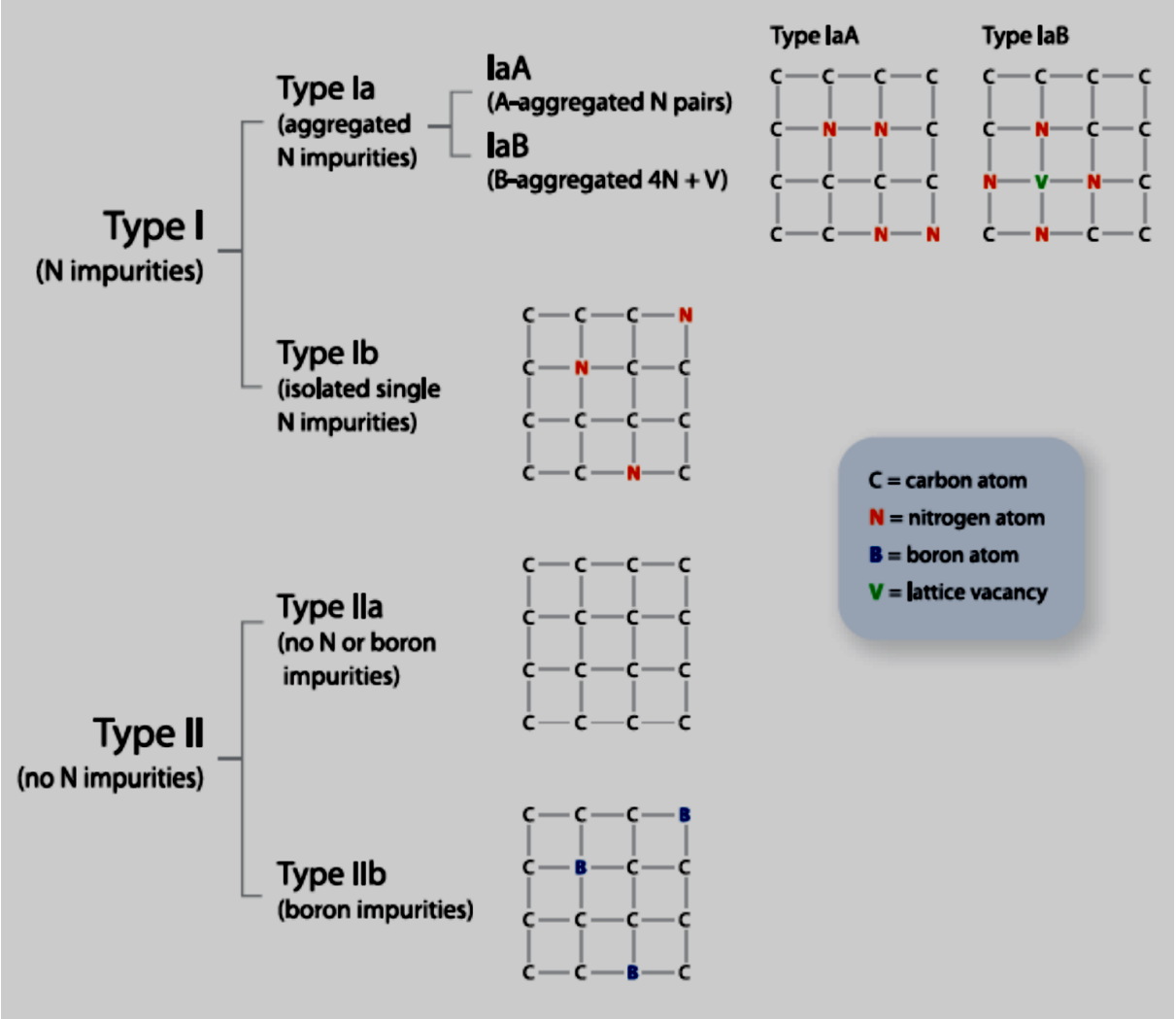

Figure (2-9): Diamond types and classification depending on impurities occupying carbon atom sites [63].

The existence of defects and impurities in the crystal lattice of diamond is a significant factor in the change of the diamond colour as shown in Figure (2-10). Therefore, many attempts have been made to recognize the diamond type from observation of its colour [63]. But these efforts have not succeeded, because the colour of diamond is derived from the elements present, while the position of these atoms relative to the carbon atoms determines the diamond type.

Figure (2-10) : Colour variety of diamonds depending on impurities [63].

Manufacturing of synthetic diamond started in the late 1950s when the first successful synthetic diamond was made [60]. The manufacturing processes of synthetic diamond can be divided into two main production technologies which are the High Pressure- High Temperature process (HPHT) and Chemical Vapour Deposition (CVD) [64].

Diamond production was started by Swedish and American scientists using HPHT. In this technique, a carbon substrate is exposed to temperature of about 1300 – 1800°C and 50 to 70 kbar pressure with some molten metals as a catalyst to obtain an effective growth of diamond [65]. Suitable catalysts include iron, nickel [60], FeCo, FeNi or Al, Ti, Zr for getting nitrogen free diamond [65]. The HPHT process, which is schematically shown in Figure (2-11 a), is considered quite expensive because it requires high pressure and temperature, which makes the equipment costly.

In contrast the CVD technique Figure (2-11 B) requires less demanding conditions. Typically in this method CH4 gas is passed through a plasma at about 10-200 Torr pressure and 700 -1000°C temperature [65]. In CVD the diamond produced is often polycrystalline and much purer than the HPHT diamond because the latter often contains some inclusion or residual metal from the metal catalysis as shown in Figure (2-11 C). Another important aspect to mention is that both techniques have to use a diamond seed to grow a new diamond from graphite as shown in Figure (2-11 D) [65].

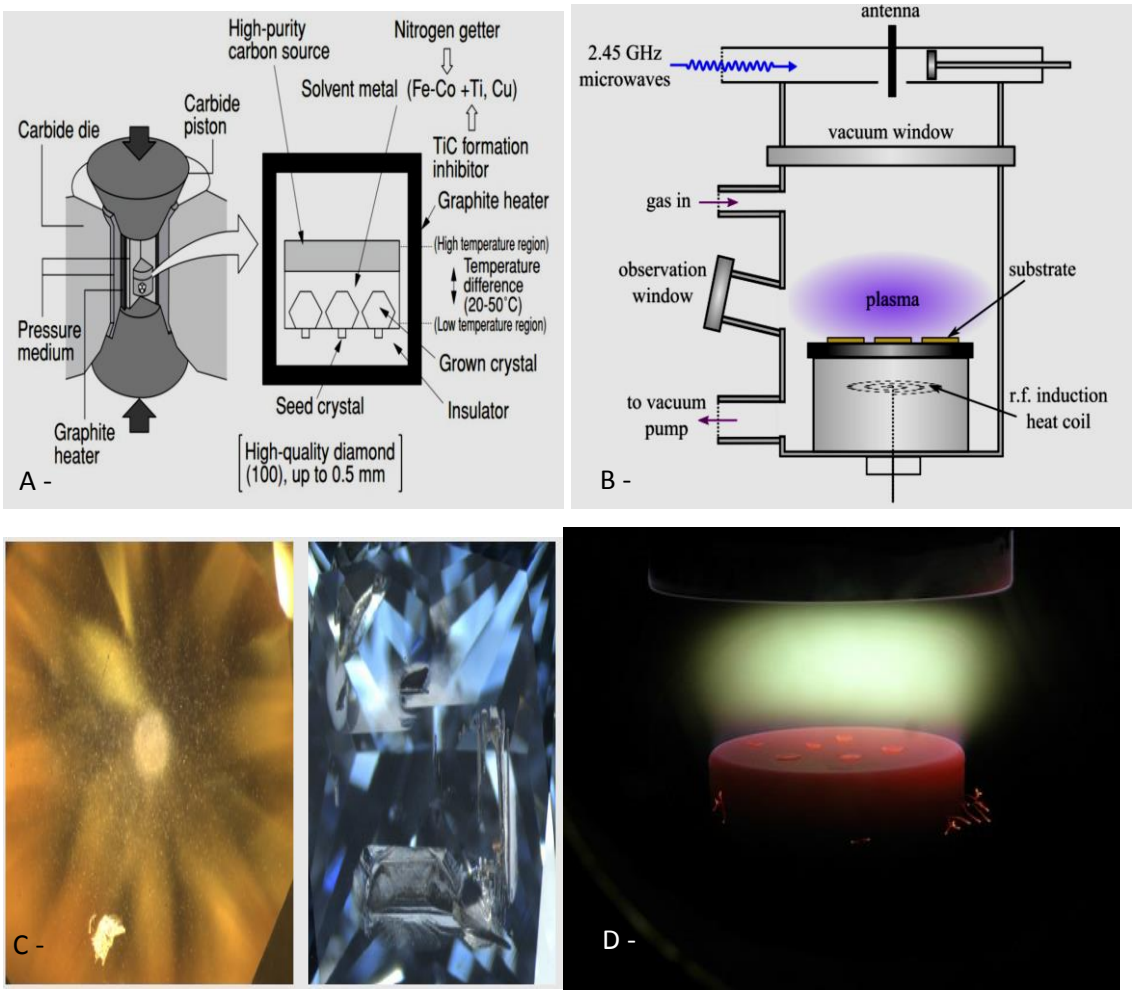

Figure (2-11) : A, B schematic drawings of HPHT and CVD techniques, respectively, C- inclusion and metallic resides in HPHT diamond, and D- growth of diamond on seed plates [65].

Chapter 3 Metal Matrix-Diamond Composites (MMDCs)

Should a diamond-reinforced MMC be desired, the choice of which metal to select as the matrix remains. There are many metals which have been used as matrices for MMCs in general, including aluminium (Al), titanium (Ti), magnesium (Mg), copper (Cu), silver (Ag), lead (Pb), iron (Fe), zinc (Zn), tin (Sn) and nickel (Ni) [12]. These metals have been used with different kinds of reinforcement. Especially, silver, copper and aluminium as a matrix are reported where diamond is used as reinforcement phase [66]. This is particularly the case for thermal management applications such as high heat flux conductors and heat sinks in electronic devices [67], [68]. The selection of these metals has evidently been made from the point of view of maximizing the overall conductivity, with the ease of processing a secondary consideration.

These classes of composites are attractive for use with microelectronics and semiconductors because of their exceptional thermal properties (their thermal conductivity reaches up to 900 W m^{-1} K^{-1} and they have very low thermal expansion [69]). There are many studies which have dealt with these elements as metal matrices with diamond particle reinforcement for thermal applications, and some of these studies have measured their mechanical properties, which will be discussed in the sections below.

3.1 Thermal Properties of Metal -Diamond Composites

The unique thermal and optical properties of diamond have been deeply studied. Diamond-metal composites have been used as heat dissipation materials in electronic devices or in X-ray and infrared transmission components. Seal [70] reviewed the use of CVD diamond wide plate for thermal management of semiconductor pieces in electronic devices and he concluded that the commercial need for CVD diamond thin films for the electronic industry will be highly important as heat spreading components and infrared transmission plates within this currently fast developing industry [70], with the need to eliminate the high cost of diamond. Therefore, some studies have suggested that metal-ceramic composites are suitable in applications where their priority is high thermal conductivity requirements compared with quite low electrical conductivities. For example, Al_2O_3 and SiC with metals are widely used [71].

Beyond these, improvements in industrial technologies lead to the need to explore and look to unique composites with very high thermal conductivity. These composites would

probably be produced from diamond reinforcement with different metal matrices [66], [72], particularly matrices from Cu, Al, Ag, and their alloys [66] though some researchers have studied thermal properties of diamond with other matrices such as Ti, Ni, and Fe. Most of these studies are focused on the interaction between diamond/metal interfaces because of their effects in different applications.

However, good bonding between matrix and reinforcement is required to enhance thermal conductivity. This depends on the Maxwell equation which assumes that there is a perfect bonding when applied to calculate theoretical thermal conductivity of metal-diamond. For example, when this is applied to calculate theoretical thermal conductivity for Cu-diamond composites it is found to be theoretically equal to 842.1 W. m^{-1}. K^{-1} for a 1:1 Cu: diamond ratio using the Maxwell equation with λ_{Cu}= 400 W. m^{-1}. K^{-1} and $\lambda_{Diamond}$=1800 W. m^{-1}. K^{-1}. Nevertheless, there have not yet been any composites reported that can reach this theoretical value due to defects and weak bonding between phases, in addition to the diamond shape being variable. The researchers who are interested in this aspect have often tried to achieve as much as possible from the Maxwell's theoretical thermal conductivity of Metal-diamond composites [73]. Another challenge, which has faced researchers in this field of composites, is the high cost of manufacturing associated with them. Therefore, the major materials, which are used industrially for heat transfer and dissipation, are high thermal conductivity (TC) metals such as copper and aluminum with (TC) about 400 W. m^{-1}. K^{-1} and 250 W. m^{-1}. K^{-1}, respectively. However, the thermal expansion coefficient of these metals is somewhat high and needs to be reduced without affecting the thermal conductivity [71].

Copper-diamond composites could be promising materials for many engineering and industrial applications. Copper has the highest thermal conductivity among all metals [74] except silver. Therefore, it seems to be the optimum choice for the applications with high heat flux and thermal conductivity demands, such as in connection to laser emission, high brightness LEDs, power switching connectors and transistors in electronic devices [75]. But the Coefficient of Thermal Expansion (CTE) of copper alone is not able to achieve the demands of the recent generation of semiconductor components [74], particularly those containing P-N junctions which form laser diodes [76], [77]. Therefore, it has become important to develop new materials to perform well under such demands. These materials should have a combination of good thermal conductivity and low CTE [73], [76], [78] . One material that could potentially obtain this combination of properties is diamond-Cu composites [75] if they can be optimized for manufacturing processes and costs.

Many attempts have been made to overcome obstacles such as poor bonding, using different fabrication techniques and coated surface of diamond particles [79] or even using some active elements as alloying elements in order to increase the bonding between diamond particles and matrix by carbide formation at the interface [73], [80]. Ren et al. [81] report that, the coating of diamond particles by a Ti or Cr layer to a limited thickness before fabricating with Cu as composites by powder metallurgy, leads to a significant decrease of thermal resistance at the interface between diamond and Cu in composites.

There are many researchers who state that the thermal conductivity of the interfacial layer plays a crucial role in the whole thermal conductivity of the diamond composites [82]. Ren et al. [81] have found Cr coating more effective than Ti coating in reducing interfacial thermal resistance between Cu and diamond [81] which may be because the thermal conductivity of Cr (94 W. m^{-1}. K^{-1}) is higher than for Ti (22 W. m^{-1}. K^{-1}) . Also Xia et al. [82] have reported that the Cu-diamond composites, which have achieved relatively higher interfacial thermal conductivity than those which are fabricated with coated Cu-1 %Cr diamond particles, are fabricated by PM with coated Cu- 0.5%B diamond particles. The thermal conductivity reaches 300 W. m^{-1}. K^{-1} for the composites with coated Cu-0.5%B diamond particles. The researchers state that the thermal conductivity of the interfacial layer plays a crucial role in the whole thermal conductivity of the diamond composites [82].

Lee et al. [83] have achieved as high a thermal conductivity as 719 W. m^{-1}. K^{-1} in 50% Diamond/Ag with 2 at. % of Ti additives for the Ag matrix by using the simple transient liquid stage sintering technique with low cost. They proved that the Ti additives may enhance the fluidity of melting through the formation of a transient liquid state in addition to forming some carbides at diamond/Ag interfaces by finding that Ti and TiC coexist at product interfaces [83].

Yupeng et al. [84] have studied a diamond-copper joint in a light emitting diode (LED) where the diamond is used as a heat sink. Al-Ni multilayers were utilized in this research as high thermally conductive materials to replace solder layers between each two layers to promote a self-propagation of joint between copper and diamond. They found that the thermal conductivity and shear stress of multilayers formed with bonding from nano particles of Ni-Al, which have been used, have greater thermal conductivity and shear stress than the alternative silver adhesive [84].

Silver-diamond composites can also be a good choice of materials for high thermal conductivity applications, in addition to many other engineering and industrial applications.

Heat sink components in electronic devices have been made from a limited number of metals and alloys, such as magnesium and aluminium; both metals have a good combination of high thermal conductivity and relatively low density, then they may be suitable for lightweight electronic packages, but with the developments in the electronic industry and emergence of new generations of electronic devices that require high heat thermal conductivity [60], [85] passive materials [60] [86], and materials with a high melting point which can be fabricated into complex shapes [60] [85], it has become important to use new materials to meet these demands. Silver-diamond composites offer these properties [60], [85], [86]. In addition to that, silver has the highest thermal conductivity among all metals and diamond has the highest thermal conductivity among all conventional materials, as shown in Table (3-1) [87]. Therefore, many researchers have recently focussed their attentions on silver-diamond composites for thermal management and electronic applications such as heat sinks in computers, diodes and laser power devices [86]. The thermal performance of these composites varies according to many factors, such as chemical matrix composition, diamond types and particle size of the diamond.

Tavangar et al. [64] have assessed the thermal conductivity of silver-11 at. % silicon - diamond by using two different particle sizes of diamond. They found that the thermal conductivity changes between (410 and 780 W. m^{-1}. K^{-1} depending on the particle size variation of diamond reinforcement between grit limits 70/80 and 270/325 (212-180), (53-45) µm, respectively [88]. Abyzov et al. [68] have also achieved a high thermal conductivity of silver-diamond composite, reaching about 900 W. m^{-1}. K^{-1} by using diamond particles in the size range between 430 to 180 µm which were coated with tungsten and infiltration cast without any gas pressure (meaning that the particles were wetted by the liquid metal). The coating layers were checked by SEM, XRD, XR spectral analysis and Atomic Force Microscopy to know their structure and chemical composition, and they were found to contain W, W_2C, and WC. This high conductivity might come from these components, which tend to make strong bonds with a matrix [68].

Mizuuchi et al. [89] have also produced silver-diamond composites from powder mixtures of diamond, Ag and Si by using a Spark Plasma Sintering (SPS) method. They obtained 717 W. m^{-1}. K^{-1} thermal conductivity at 50 Vol% diamond which is about 80% of the theoretical thermal conductivity according to Maxwell-Eucken's formula. That is because of the existence of Si which might help to form some compounds at the interface between diamond and silver, in addition to the production method where solid-liquid interfaces exist during the densification stage under SPS [89].

Table (3-1): The thermal conductivity of some common engineering materials [87].

Materials	**Thermal conductivity (W. m^{-1}. K^{-1})**
Diamond	2000
Graphite	80-~2000
Carbon	350-900
Silver	427
Copper	398
Silicon Carbide	350
Aluminium	237
Beryllium	218
Magnesium	156
Silicon	149
Brass	109
Nickel	91
Steel (316 S. S)	13.5
Water	0.66
CO_2 (gas)	0.015

Additionally, Aluminium Matrix Composites (AMCs), have become a very important material contributing to different industries such as aerospace, automobile, and electronic devices [20]. The next paragraphs will discuss AMCs with diamond reinforcement from thermal perspectives.

Aluminium matrix with diamond composites are an important material for heat dissipation in electronic devices because they achieve excellent thermal conductivity with relatively low thermal expansion [90]. These composites could be a better choice for heat transfer layers than silver or copper with diamond because of the density of these elements, shown in Table **(**3-2) [87]. This is particularly the case for weight-critical electronic equipment, such as microprocessors of laptops and diodes [90], [85], and even in some military applications [91].

Table (3-2) : Density of some common engineering materials[87].

Materials	**Density (at room Temp.) g/ cm^3**
Co^2 (gas)	0.0018
Water	1
Magnesium	1.746
Beryllium	1.85
Carbon	2
Graphite	2.25
Silicon	2.33
Aluminium	2.71
Silicon Carbide	3.1
Diamond	3.52
Steel (316 S. S)	8
Brass	8.4
Nickel	8.9
Copper	8.945
Silver	10.52

Several studies have been undertaken in the last two decades on aluminium matrix with diamond composites for thermal management applications [86]. Supan et al. [92] were among the first and made an important breakthrough in manufacturing of aluminium-diamond composites for heat sinks and thermal management when they obtained a thermal conductivity of about 240 W. m^{-1}. K^{-1} in Al-13 Vol. % Si- 40 Vol. % diamond composites at 175 ℃ , which were produced by mixing the powder and pressing it under a specific

pressure and temperature until the compacted ingot was melted, staying at this condition for 15 minutes after which it was cooled [92]. The investigations have been continued on these promising composites. Ruch et al. [93] have achieved as high as 670 W. m^{-1}. K^{-1} thermal conductivity in aluminum- 7 wt. % silicon- about 60 wt. % diamond composites. They also showed that there are preferable planes in the diamond crystal which tend to react with molten aluminium more than others from SEM images such as those in Figure (3-1 a and b), where the bonding of matrix with a diamond on the (100) planes was clearer than other planes. The researchers suggest that thermal conductivity might be significantly affected by the microstructure at the interface between diamond and aluminium matrix as they observed a wide variation in thermal conductivity, dropping as low as 130 W. m^{-1}. K^{-1} in some samples [93].

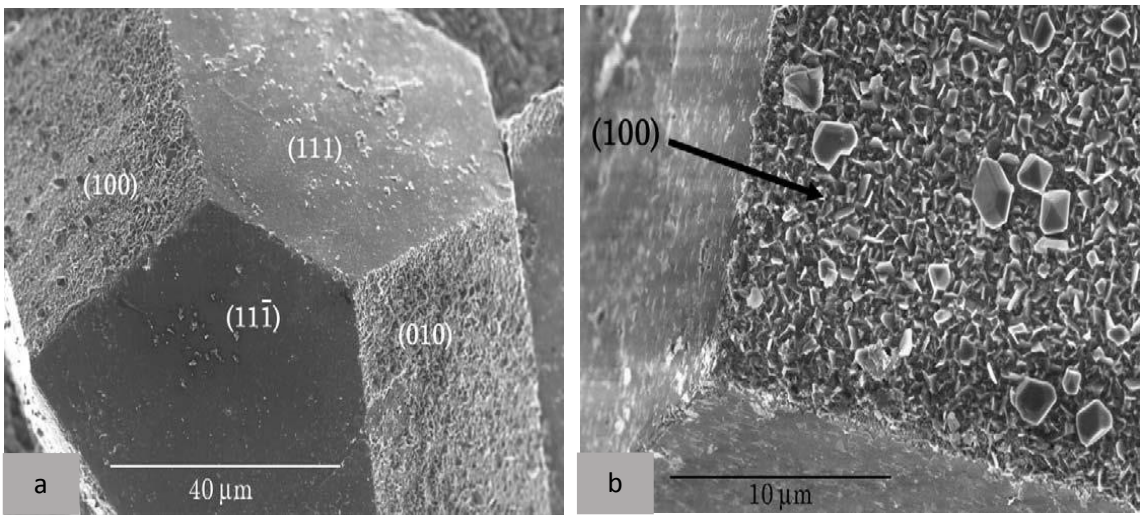

Figure (3-1) : SEM micrograph of a- {100} Diamond faces covered by Al matrix, b- interfacial reaction components on (100) surface reproduced with permission of the publisher [93].

Monje et al. [94] have also investigated the interfacial microstructure of aluminium-diamond composites. They proved that an interfacial microstructure can be a crucial factor to determine the final properties of composites by their examinations on the interface and its effects on the interfacial bonding. Also, they revealed that there is selectivity in the reaction between the matrix and diamond crystal on specific planes; {100} in contrast to {111} crystal planes, where carbides were observed on {100} planes and {111} were free of carbides. These authors stated that the {111} planes require increased contact time

between molten aluminium and diamond to react. In contrast the quick reaction was on the {100} planes that leads to a significant contribution in bonding between matrix and diamond [94].

Monje et al.[95] have done further investigation of the effects of aluminium carbide formation at the interface and manufacturing conditions on the thermal conductivity (TC) of aluminium-diamond composites. They achieved thermal conductivity up to 670 W. m^{-1}. K^{-1} by doing some surface modification of diamond particles when using a variety of contact times of molten aluminium with diamond to generate controlled layers of Al_4C_3 on the diamond surface. Also, the researchers stated during their investigations on aluminium-diamond composites that the {100} faces are responsible for strong bonding between aluminium and diamond because these faces tend to react with molten aluminium more easily than other faces of the crystal. They suggested that this happened because the double bonds of carbon atoms on the {100} planes are easily broken to form aluminium carbide at the interface, whereas the bonding of carbon atoms is strong on the {111} crystal faces [95].

Another modification of diamond surface has been made by Caccia et al. [2] when they exposed the diamond to oxygen atmosphere under controlled conditions of pressure and temperature in order to generate a thin layer of graphite on the diamond surface which can easily release carbon atoms; these atoms contribute to aluminium carbides formation at the interface that lead to increased interfacial thermal conductivity [2].

So the modification and morphology of the diamond surface can be considered an important aspect for thermal conductivity enhancement of diamond aluminium composites. Therefore Tan et al [96] examined some carbide-forming metallic elements as coating layers of diamond particles to enhance TC, which are Cr, Ti, W, Mo, and compared those with diamond coated with non-carbide forming metallic elements (Ag, Ni, and Cu). They obtained a high TC of aluminium-diamond composites with diamond coated by the first group of elements where the authors achieved a high TC above 600 $W.m.^{-1}K^{-1}$ with these elements whereas with the latter group the TC was even less than uncoated diamond reinforcement [96].

Other studies have modified the matrix itself to enhance its wettability for the reinforcement by decreasing the surface tension of molten metal. Milliere and Suery [97]

have shown that the addition of 1 wt.% Mg to an aluminium alloy can reduce the surface tension of molten aluminium from 860 dyne/cm (0.86 N/m) to 650 dyne/cm (0.65 N/m) at the melting temperature of aluminum [97]. The addition of Mg at this limit (≤1%) can avoid the formation of intermetallic compounds and obtain a solid solution of Al-Mg, as shown in the phase diagram of Al-Mg alloy, Figure (3-2) [98]. Because of their effects on mechanical and conductive properties, intermetallic compounds may be undesired in some applications. Kimura [99] also stated that the addition of 3 wt. % of magnesium to molten aluminium can reduce its surface tension from 0.76 to 0.62 Nm at 720℃ [15], [99].

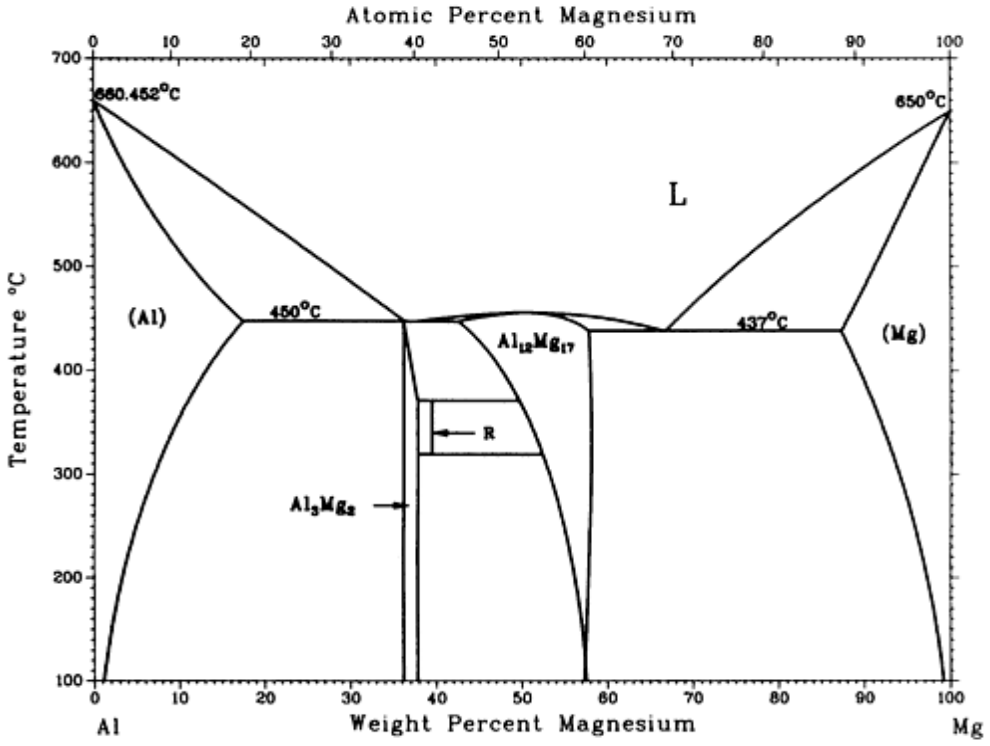

Figure (3-2) : Phase diagram of Al-Mg alloy reproduced with permission of the publisher [98].

3.2 Mechanical Properties of Metal -Diamond Composites

Diamond's mechanical properties are outstanding, especially the hardness, which is a dominant property of diamond in many mechanical applications. This leads to the idea to study the possibility of utilising the diamond in tribological applications. But its fracture strength and cost are accounted as limitations. Therefore, some studies have been done to apply the outstanding hardness of diamond in composite materials by using a wide range of different matrices. Boland and Li [100] first looked deeply into tribological and wear

properties of thermally stable diamond composites (TSDCs) over 15 years leading up to 2010 at the Commonwealth Scientific and Industrial Research Organisation (CSIRO) in Australia. They applied this composite as cutting elements. The TSDCs have been produced by compacting 80% diamond with 20% silicon under High Pressure and High Temperature (HPHT) conditions which reach about 2-2.5 GPa at 1500 ° C. The Si will be melted and penetrate into the diamond grit interfaces under these conditions, then it reacts with diamond to create SiC. At this point the matrix will be almost entirely formed from SiC, which bonds the diamond grains together by strong bonds. When this stage is completed, fast quenching is applied to prevent the diamond from converting to graphite. Boland and Li modified the Pin on Disc technique to do wear tests by using an alumina grinding disc and TSDC samples as a machining tool in their study, because the standard wear test would be ineffective with this kind of super hard material. No measurable loss in weight or other wear indicators were found, even though the authors focused more on microstructure observation than tribological and wear measurements. The authors have stated a relative estimation of wear resistance for a comparable purpose of conventional hard tungsten carbide WC with their superhard materials. The wear rate of WC was found to be between 0.01 to 0.12×10^3 (Material cut (wt%)/ Tool loss (wt%)) and the wear rate of different produced TSDC was found to be between 0.3 to 818.9×10^3 (Material cut (wt%)/ Tool loss (wt%)) [100].

Larsson et al. [101] have studied the abrasion and erosion wear resistances of diamond-silicon carbide composites, which have been fabricated by penetration of molten silicon at 1550 ℃ into pre-compact 60 Vol.% diamond-10 Vol.% carbon and sort of volume is porosities under a vacuum, Their abrasion rates were about half that of most commercial engineering ceramics such as cutting tools of polycrystalline diamond (PCD) with 5 wt. % Cobalt bonding, tungsten carbide and 6 wt. % cobalt bonding, alumina and SiC. These materials have been used as comparable references of erosion and abrasion resistances materials.

Nickel as well has widely been utilised as a matrix in metal-diamond composites like other metallic elements such as Al, Ti, Cu, Fe, and Sn. These elements have all been applied alone or as part of an alloy.

Michalski and Cymerman [102] have applied Ni and aluminium together to obtain Ni_3Al as a matrix during the process. The Plus Plasma Sintering (PPS) technique has been used for 5 min at 1000℃ to manufacture Ni_3Al and Ni_3Al/diamond composites, in order to

compare the hardness and observe the interfacial bonding phase in case of diamond. The hardness of Ni_3Al-30% diamond composites was more than double the Ni_3Al hardness, being about 650 HV in comparison with 305 HV of Ni_3Al. Nickel carbide (Ni_3C) was formed at the interfaces of Ni_3Al/diamond composites, leading to bonding between phases in the composite.

Wang et al. [103] compared wear behaviour between microcrystalline Nickel (m-Ni) and nanocrystalline Nickel (n-Ni), both with and without nano sized diamond particle reinforcement. These material matrices and composites were precipitated on a pure Ni plate by the conventional electrodeposition technique of coating. The microcrystalline matrix with nano diamond was found to have the highest wear resistance among the both pure nickel coating and nano nickel reinforced with nano diamond, which showed even less wear resistance than pure matrix. The composites and the different worn surfaces are shown in Figure (3-3).

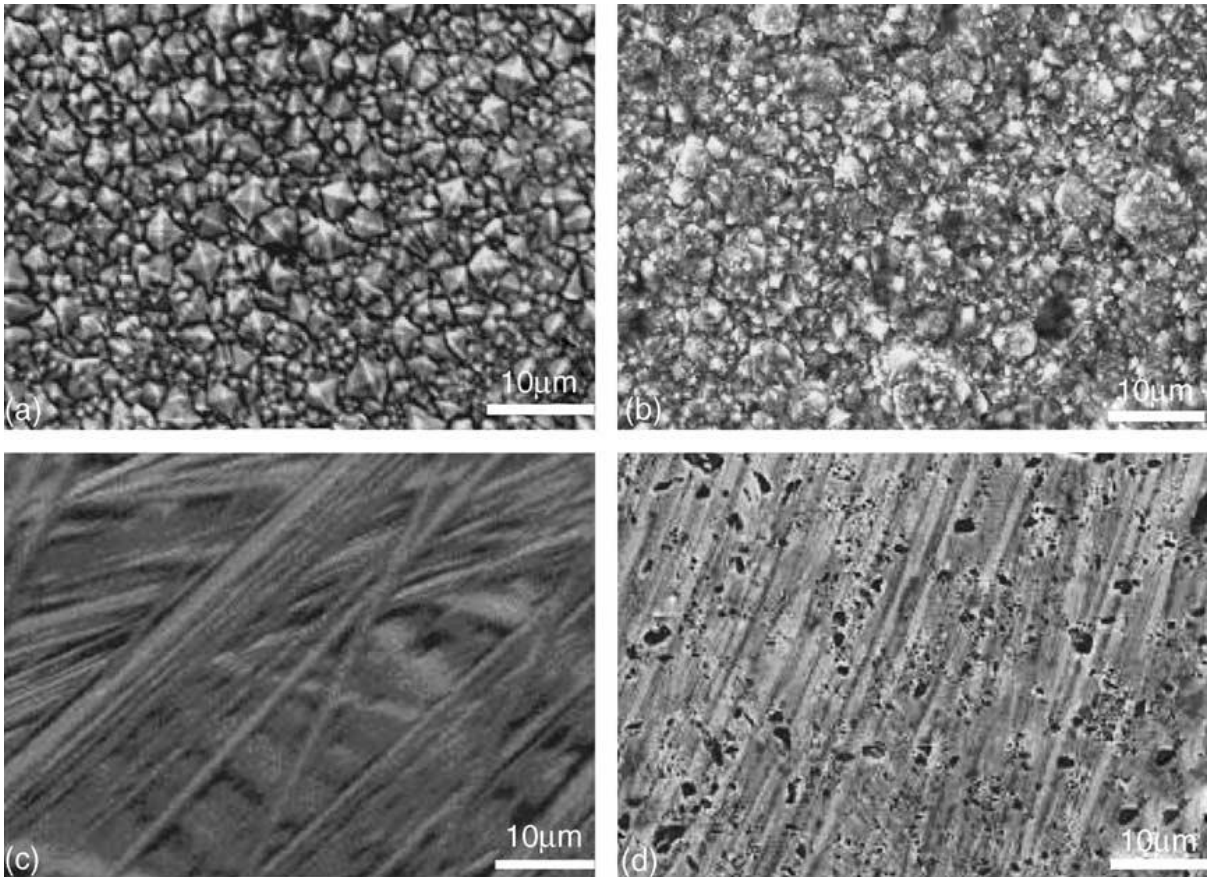

Figure (3-3): SEM worn surface of (a) micro-Ni, (b) micro-Ni/diamond, (c) nano-Ni and (d) nano-Ni/diamond reproduced with permission of the publisher [103].

Twomey et al. [104] also did a comparative study of different manufacturing processes where they utilised two different procedures, tube furnace and rapid discharge plasma

sintering (RDS) techniques. In both paths 80% Ni-20% diamond powder was compacted into 20mm diameter pellets at various pressures, of 100, 200 and 300 MPa and sintered at two different temperatures (850 and 1000℃) under inert gas atmosphere to produce composites. The results showed that using RDS to manufacture Ni-diamond composites was better than using a furnace because the RDS samples, which had less graphitization of the diamond than furnace samples (even though an atmosphere of 3 to 1 H_2/N_2 was used in both techniques), lead to higher hardness and abrasive wear resistances, especially for 850 ℃.

Mechnik [105] utilised a complex metals binder as a matrix to produce cutting element metal-diamond composites, where a 51 vol.% of Iron (Fe)–32 vol.% of Copper (Cu)–9 vol.% Nickel (Ni)–8 vol.% Tin (Sn) mixture was mixed with 35 vol.% of 302-455 µm diamond particles. 800 ℃ sintering temperature for 1 hour was used before different hot compacting pressures were applied to find the behaviour of these composites, especially the interfacial phases in the diamond-matrix interface. The solid solution was found to contain iron, copper, $NiSn_3$ and Cu_9NiSn_3. The hot compaction method does not affect the existence of the solid solution, but it can alter the interfacial structure. When a pressure less than 200 MPa was applied for less than 3 min, the nanoscale interfacial phases were composed of graphite embedded in γ-Cu and Ni_3Sn. Otherwise, the high hot compaction pressure, which lasts for more than 3 min, causes the graphitised surface of diamond to react with α-Fe to form a 5-40 nm layer of Fe_3C at the interface, as shown in Figure (3-4). Wear resistance can be enhanced by the formation of this layer because it helps to prevent pulling the diamond particles out from the matrix during abrasion.

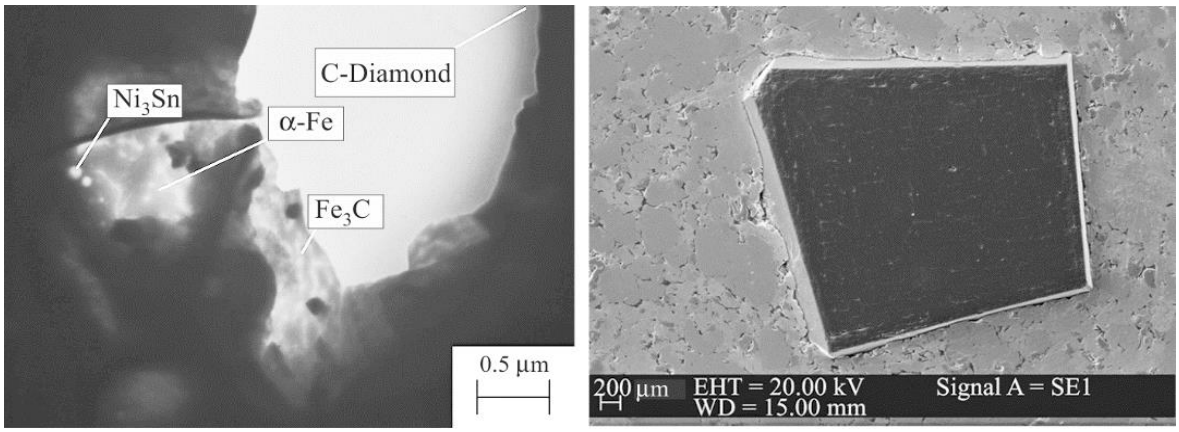

Figure (3-4): The diamond-matrix transition zone and Fe_3C layers at interface reproduced with permission of the publisher [105].

Copper is primarily employed for its excellent electrical and thermal characteristics, and ductility, but the main weak point of this metal and its alloys is a low hardness. This prevents its use in some applications which demand a high stiffness or strength. In order to address these weaknesses, copper has been reinforced with different reinforcement materials [4], such as short fibres, whiskers, ceramic particles and diamond particles, including nano-diamond particles [57], [74]. Diamond is particularly favoured as it can assist the thermal conductivity of the copper.

Metals have been fabricated as nanostructures and nanocomposites, these are considered significant ways to improve hardness through grain size reduction. However, small particles have a large surface area, or interface area in a composite, which implies a high energy. Therefore, it is important that thermal stability of these nanomaterials are taken into account during manufacturing and practical applications [22]. One of the significant nanomaterials to have a high thermal stability is nano-diamond particles.

Nunes et al. [106] have fabricated Cu- nanodiamond by two approaches which are hot extrusion and spark plasma sintering (SPS) after mechanical alloying (MA) of the powder when they mixed the powder of copper and 20 at. % nanodiamond. The mechanical and physical properties were evaluated for materials as a mixed powder and both production routes. The hardness showed a relative decrease for the products in comparison with milled powder and the extruded sample was lower than that in the SPS method. The hardness was lower at the prior particle boundaries (PPB) than in the particles for SPS production. The density of the material has been reported to depend on production approach as well; it has been found that the extrusion produces a denser product than the SPS approach.
TEM images show clear bonding at nanodiamond-Cu interfaces and the nanodiamond particles often locate on the grain boundary of the matrix, although they occasionally exist inside grains (shown by arrows in Figure (3-5 a) while the BSE images show a thin layer of pure copper at the boundaries as is shown by arrows in Figure (3-5 b). This shows that Cu- nanodiamond segregation occurred in SPS products [106].

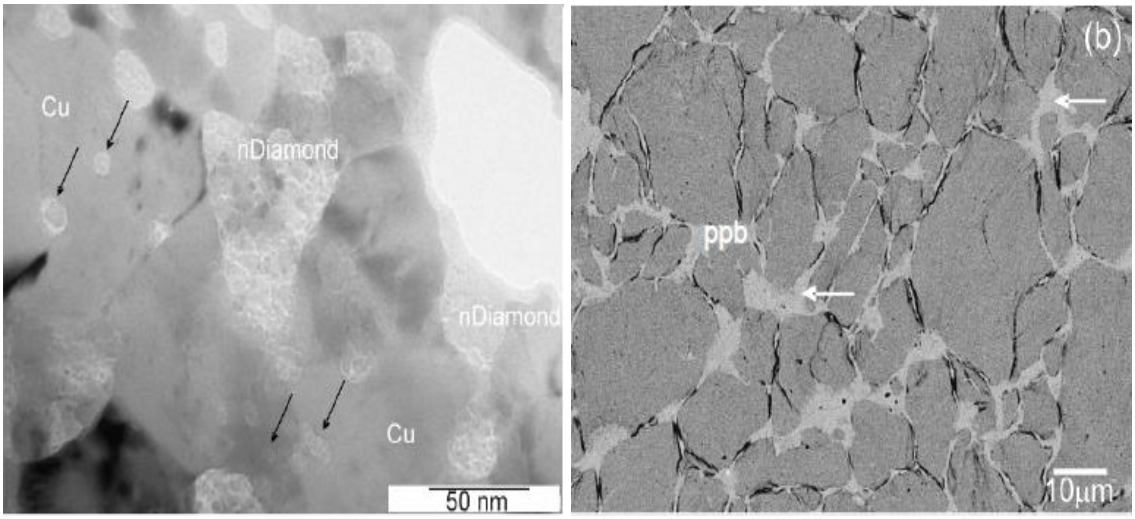

Figure (3-5) : a- TEM image of microstructure of extrusion product b-BSE image of the SPS product reproduced with permission of the publisher [106].

Correia et al.[4] also used an extrusion technique to fabricate Cu-nanodiamond composites after they had mechanically alloyed the powder components. The nano-diamond powder was used in a different atomic percent (5, 10, 15, 20 and 30 at % carbon) with copper powder to produce the copper-nano-diamond composite. Hardness tests showed that there is a decrease in the hardness below the mixture powder hardness before extrusion. The hardness was enhanced with increasing volume fraction of nano-diamond. SEM imaging showed a uniform distribution of nano-diamond in the matrix, as shown in Figure (3-6) [4].

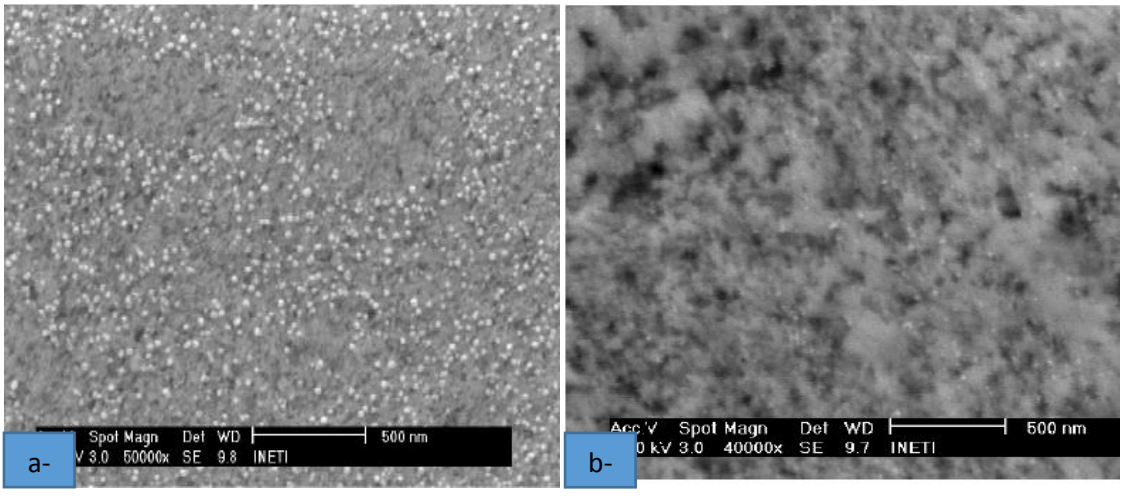

Figure (3-6) : SEM pictures of the internal microstructure a: of mechanically alloyed Cu-30at% nano-diamond as powder b: for extruded product Cu-30% nano-diamond reproduced with permission of the publisher [4].

The authors have, as they described, clearly observed bonding between the matrix and reinforcement by TEM imaging as shown in Figure (3-7) (taken from their work). The researchers also suggested that these particles might act as pinning points for the grain growth of the matrix during the progress of hot extrusion (the effect is marked by arrows in Figure (3-7) [4]. This effect would also lead to a strength enhancement.

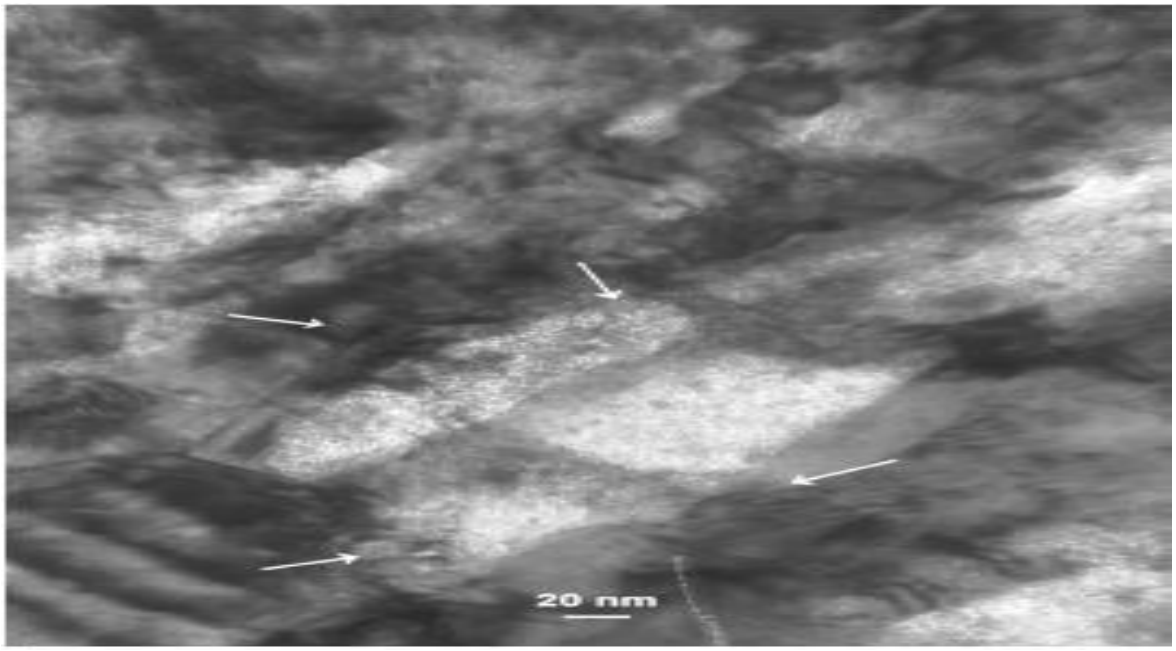

Figure (3-7) : TEM image of extruded Cu-30at%C nano-diamond reproduced with permission of the publisher [4].

Weidenmann et al. [90] have studied certain mechanical features for Cu–2.5 at. % B alloys which are reinforced with 55–60 vol. % different grit size diamond particles (500/600 grit (35-30 µm), 140/170 grit (106-190 µm), 325/400 grit (45-38 µm), 230/270 grit (63-53 µm)), and compared their features with other composites. These composites were produced by the infiltration casting method. The mechanical properties achieved were a Young's modulus of 150 GPa and Ultimate Tensile Strength (UTS) below 50 MPa for the Cu–2.5 at. % B matrix. This matrix may be chosen to encourage boron carbide formation at the interface to improve bonding and to see how it will affect the composite properties. Therefore, these composites tended to fail under the loading that was necessary to induce a small amount of deformation, required to measure the Young's modulus. Also the authors concluded that there is no significant influence of particle size variation on Young's modulus. SEM observation of the fracture surface indicated that there is very weak wetting between molten Cu and diamond particles as shown in Figure (3-8) where

diamond surfaces were found to be free from metal. That was concluded to be the main reason for failure under a very small deformation [90].

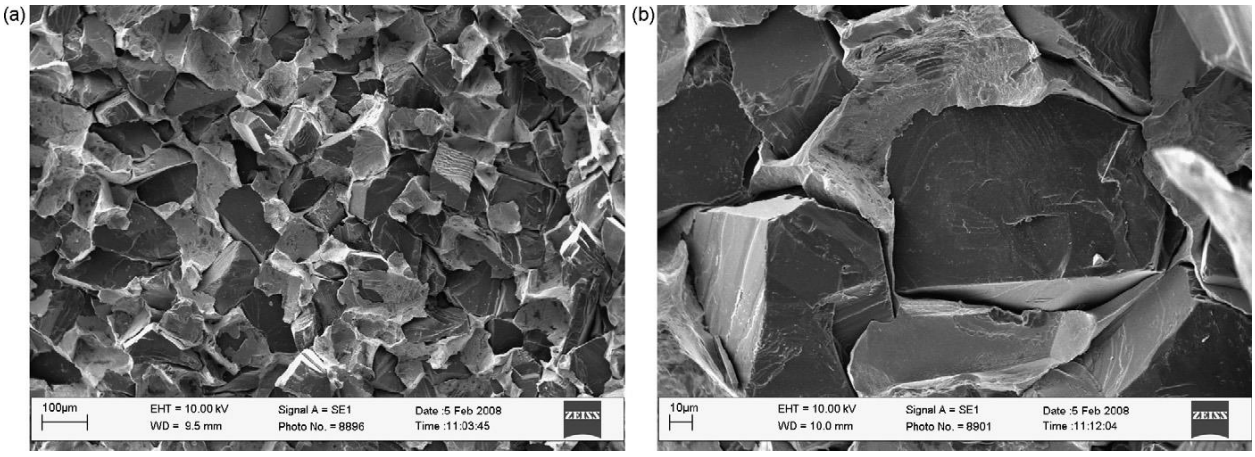

Figure (3-8) : SEM images of a Cu–2.5 at.% B + 140/170 (106-190 µm) composite at different magnifications reproduced with permission of the publisher [90].

Silver-diamond micro-composites (particle size of reinforcement at the micro scale) are commonly used as electrical contact materials because the silver is able to transfer high electrical currents without extreme heating, due to its low resistance. Therefore, there are many electrical contact applications for silver as a pure metal or a matrix composite, the latter particularly where they demand high tribological resistance and surface properties. Electrical contact materials are exposed to extreme conditions during service, these conditions require materials to combine suitable mechanical and electrical properties and service life. Silver-diamond composites are the best materials able to work under these conditions in different contact applications [107].

Weidenmann et al. [90] also have measured some mechanical properties for Ag–11 at. % Si alloys reinforced with 55–60 Vol. % by the same method as for their study of Cu alloys, discussed above. They achieved Young's modulus (E) of 300 GPa and UTS of 314 MPa for the Ag–11 at. % Si matrix alloys with the smallest particle size (22 µm) of diamond reinforcement while the UTS was lower (214 MPa) for those with the largest particle size (106-190 µm). SEM observation of the fracture surface revealed poorer wetting of matrix to the coarser diamond surfaces. However, there was some matrix material which covered some of the diamond particle faces. Also some dark spots appeared in the matrix, which could be a result of the ductile behavior during strain, as shown in Figure (3-9) below. It was predicted that the high tensile strength for these composites arose as a result of crack

progression passing through the diamond particles instead of only through the matrix material [90].

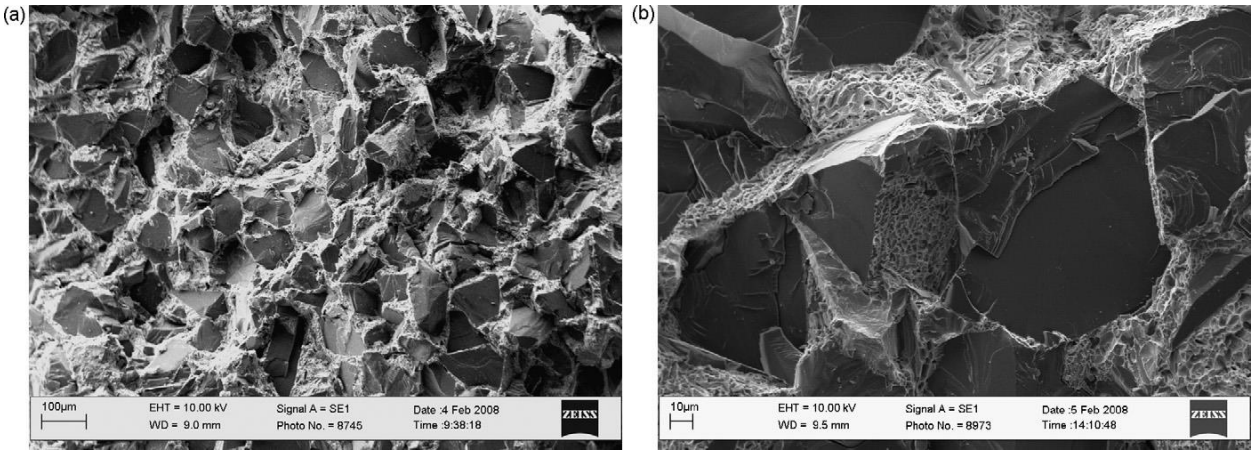

Figure (3-9) : SEM images of an Ag–11 at-% Si + 140/170 composite at different magnifications reproduced with permission of the publisher [90].

Rigou et al.[107] have estimated the effects of variation of the diamond particle sizes on the wear properties of silver-diamond composites when the coating layer was made by electroplating silver with different particle sizes of diamond as reinforcement to coat a copper substance. Three different particle sizes of diamond (1, 0.25 and 0.1 µm) were used. SEM imaging showed that the increasing particle size of the reinforcement phase leads to an increase in layer thickness, and for all particle sizes there is a good adherence between the composite layer and Cu metal as shown in Figure (3-10) [107].

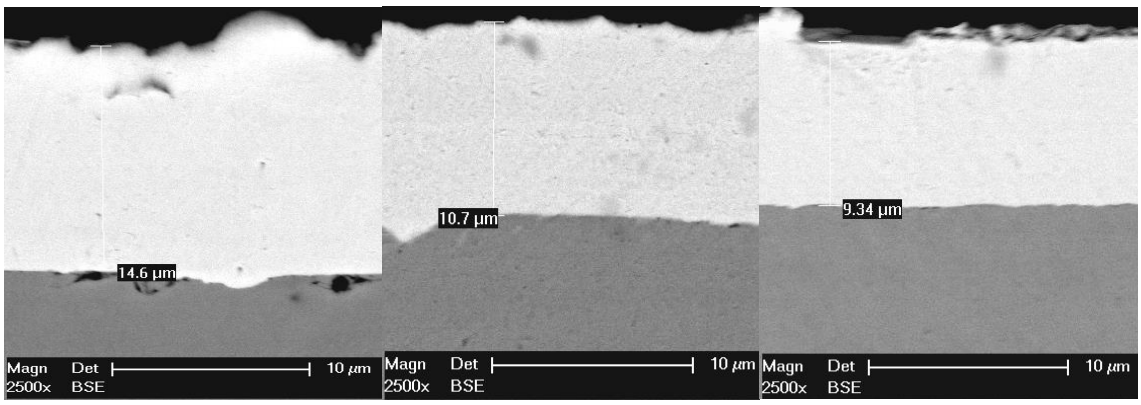

a – 1 µm; b – 0.25 µm; c – 0.1 µm

Figure (3-10) : SEM images of silver/diamond dispersion layers with different diamond particle size reproduced with permission of the publisher [107].

Wear resistance tests by a pin-on disk technique with a ball made from chromium steel 100Cr6 proved that the smallest diamond particle size reinforcement has the highest wear resistance. Digital micrographs showed that there are obvious scratch lines aligned with the direction of motion over the composite layers that were reinforced with 0.25 μm and 1 μm particle size diamond (Figure (3-11 a and b), due to abrasive wear, while the specimen reinforced with 0.1 μm particle size has fewer scratch lines (Figure (3-11 c) [107]. That behaviour from an engineering point of view seems to be a logical result of the abrasion process, because the hard particles after removal from the matrix will act as additional milling powder on the surface. Therefore, the coarser particles will have a larger effect on the wearing surface.

a – 1 μm, b – 0.25 μm, c – 0.1 μm

Figure (3-11) : Digital microscopic images of the Surface of the silver/diamond Dispersion layers with different diamond particles size after wear tests reproduced with permission of the publisher [107].

Aluminium also has a significant importance as a choice for lightweight designs, but its stiffness is still relatively low. Therefore, much effort has been made to enhance these properties [108]. For example, fabricating Aluminium Matrix Composites (AMC) in order to improve stiffness and other properties; these include aluminium-diamond composites. There are several recent published works which have assessed the thermal properties of such materials. However, their mechanical properties and behaviour data have not been covered in detail. Such data are crucial to assess their performance under different mechanical circumstances for instance, their response under thermal cycling [90], cutting forces, wear and abrasive forces.

Sugishita et al. [109] compared grinding performance of an aluminium bonded diamond wheel with commercial bronze bonded and resin bonded wheels. They have performed

grinding tests for three types of wheels, aluminium bonded diamond composites, resin bonded diamond, and a commercial bronze wheel. Two thicknesses of wheels were used for the tests, 3 mm (T3) and 6 mm (T6). The aluminium bonded wheel proved to have the best balance between grinding performance (G_r, volume of material removed from sample/ material removed from wheel)) and power consumption, especially in the grinding of Al_2O_3 substrate. The grinding of a silicon nitride specimen was slightly different due to the diamond particles becoming cutting edges for the hard material Si_3N_4. Therefore, the abrasive damage of diamond composite layers is rapid. Nevertheless, when the T3 wheel was used, the stock removal rates were increased, as shown in Figure (3-12). The researchers concluded from these tests that the grinding performance of an aluminium bonded diamond wheel was better than the grinding performance of bronze bonded diamond wheel [109]. This can be related to formation of thin bonding layer of $TiAl_3$ and TiC intermetallic compounds at interfaces as a result of the presence of trace amounts of Ti during the manufacturing of the aluminium bonded wheel, which leads to better bonding between aluminium and the diamond.

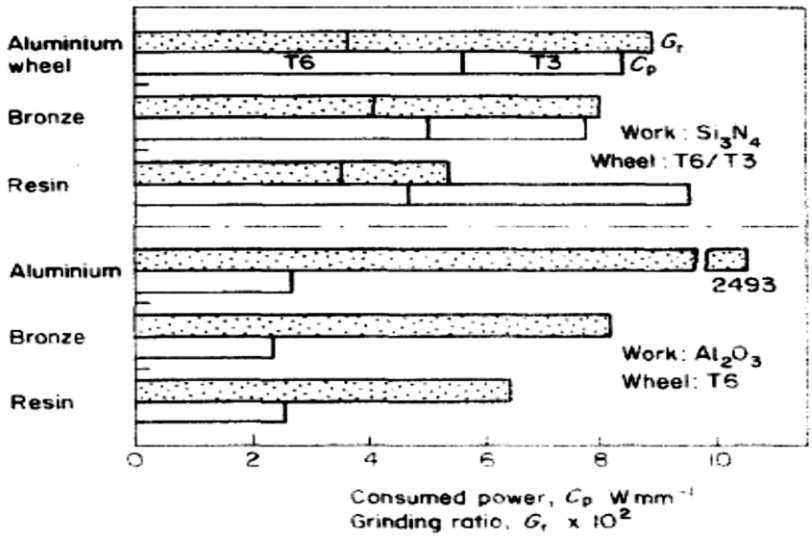

Figure (3-12) : The comparison of the grinding ratio and consumed power of three kinds of wheel during machining of two specimens which are silicon nitride and 96% alumina reproduced with permission of the publisher [109].

Holloway & Paul [91] have successfully manufactured aluminium-diamond composites for a gun barrel and they suggest that these composites may have sufficient properties to perform as rocket nozzles, cookware, heat dissipation, and automobile components especially, with volume fraction of diamond reinforcement between 30-40 % in order to

offer good balance of high strength and stiffness, sufficient thermal conductivity, and low coefficient of thermal expansion.

Weidenmann et al. [90] evaluated some mechanical features for two metal matrices, pure Al and Al–2 wt.% Cu alloy, produced as described before. They have obtained a Young's modulus of 240 and 250 GPa for Al 99.99% and Al–2 wt. % Cu matrix respectively, and an ultimate tensile strength (UTS) is 90 and 124 MPa for Al 99.99% strengthened with 500/600 grits (35-30µm) and 140/170 grits (106-190µm) respectively, 149, 137, 132, and 131 MPa for Al–2 wt. % Cu matrix strengthened with 500/600, 325/400 (45-38µm), 230/270 (63-53µm) and 140/170 grits respectively. These results were found from chevron notch and tensile tests. The authors have also reported that the diamond particle size has no significant effect on the stiffness of the samples, but the fracture toughness was increased with increasing particle size. The large particle sizes of diamond have high UTS in the pure Al matrix composite samples, but the behaviour was opposite for the Al–2 wt. % Cu-matrix composites, which may be related to the formation of a wide area of intermetallic compound on the surface of large particles. Even though composites show little influence of diamond particle size on strength, particle size increase leads to considerable increases in plastic strain to failure, and generally the composites that are reinforced with 140/170 diamond grit (106-90 µm) have the largest ductility. The maximum properties of fracture toughness were obtained with 40 µm particle size of reinforcement for the Al–2 wt. % Cu matrix. The fractured areas were observed by SEM, as shown in Figure (3-13) and Figure (3-14) both exhibiting ductile deformation, and they clearly show the platelet-like structure of Al_4C_3 [90].

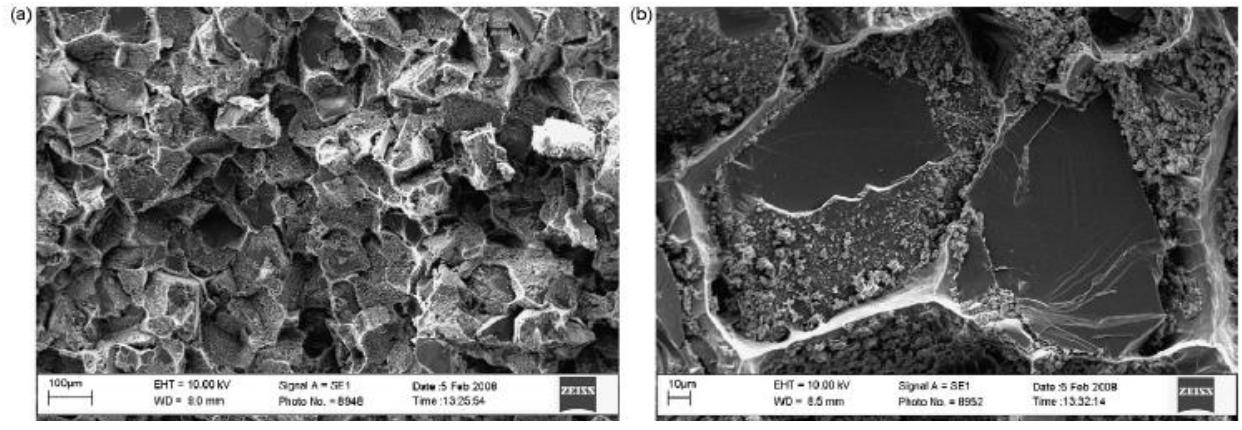

Figure (3-13) : SEM images of an Al99.99 + 140/170 (106-90 µm) composite at different magnifications reproduced with permission of the publisher [90].

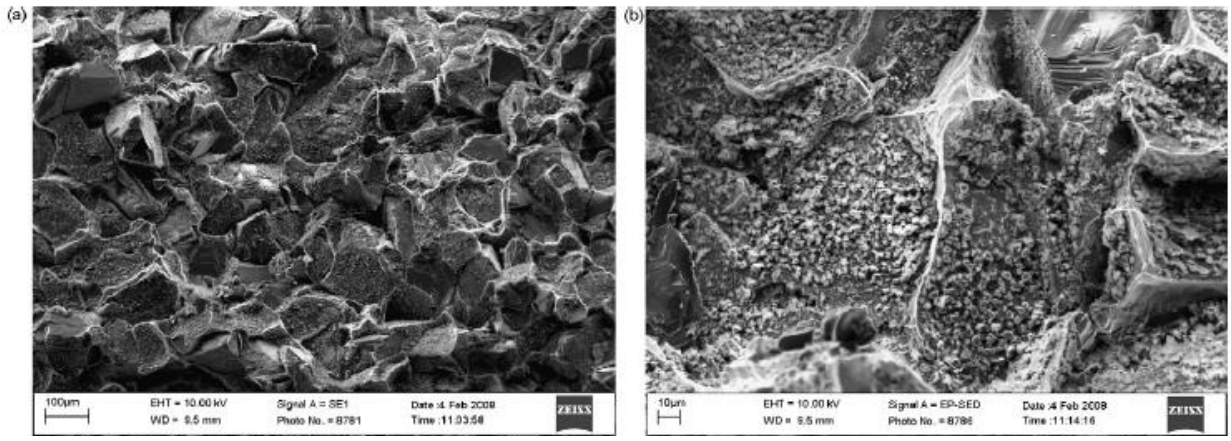

Figure (3-14) : SEM images of an Al–2 wt-% Cu + 140/170 (106-90 µm) composite at different magnifications reproduced with permission of the publisher [90].

3.3 Summary

To sum up, from the previous studies that have been reported concerning diamond/metal composites, it can be said that most work has concentrated on the thermal management properties more than mechanical and tribological properties. Even so, there are some researchers who have reported some of these properties, but these data are still not sufficient to allow comparison with the requirements of the diamond/metal composite in such applications as of interest here, especially in grinding and machining tools.

Therefore, this study will be focused on these composites from processing aspects to enhance their performance under tribological conditions where it will exploit the combination of excellent hardness of diamond and its cutting features with good ductility of metal to fabricate composites which can resist the abrasive cutting forces and which tend to cause high wear rates in the opposite abrasive cutting wheel.

These composites could, for example, be suitable for use in security locks. The studies which have been reported concerning metal/diamond composites have concluded that the interface between metal matrix and diamond reinforcement is a crucial factor in determining the final properties of the composites. Therefore, in this study addressing the issue of weak interfacial bonding is the one of the priorities. This will be done by seeking processing steps to offer good bonding between phases, for example by using diamond with surface modifications (a coating), using different carbide-forming elements as a matrix or adding different alloying elements to the matrix. In addition, the abrasive cutting

of these materials is not a well-studied area, and indeed the test methods for this property, as would be important for a security lock, are not well-known. Therefore, there is likely to be the need to additionally develop a bespoke test protocol for this work.

Chapter 4 Wear

Wear can be defined as the damage of a solid surface due to the relative movement between that surface and another surface or material in contact with it. This normally leads to the loss of materials from one or both contacting surfaces. There is no single, standard data which can describe the effect of the full range of mechanical stresses and chemical environments to which materials can be exposed; wear phenomena occur in a varied range of real work conditions in applications so there are a variety of wear types and mechanisms [110]. However, there is valuable information about the wear behaviour of materials in certain practical environments [111]. Many attempts have been made to predict wear according to essential material characteristics. One particular example is Archard's Equation [112], which considers hardness one of the primary factors to determine wear of materials, and ignores asperity contacts between surfaces [113], [114]. Asperity contact can become an important factor in wear, but its role is not taken into account in deriving the equation. Nevertheless, there are many types of wear which can be described by the Archard equation [113], [115] (see Eq. 4-1),

$$V = K \times F \times S / H \quad \text{..... Equation (4-1)}$$

where V = Volume of wear (mm^3) , F = the normal load (N), S = sliding distance (m),

K = wear coefficient ($mm^3/N^{-1}.m^{-1}$), and H = hardness of the softer surface (MPa) [114].

4.1 Wear Types

Wear classification is considered to be arbitrary and deciding which type(s) of wear might be encountered in an application is possibly the most significant challenge. Removal of material from any solid surface can occur in only three ways; by melting, chemical decomposition and mechanical separation of particles from contacted surfaces. The latter could be associated with a high strain to separate atomic layers or by cyclic lower strain to separate these layers by fatigue. In some cases chemical and physical effects may work together, such as in abrasive wear within a chemically aggressive environment [111]. Drawing more distinctions than in these three mechanism types, there are several wear types which have been reported; abrasive, adhesive (attrition), fretting, fatigue, erosion, oxidation and corrosion [110], [111], [116]–[118] which can be summarised into the main mechanisms given in Table (4-1), along with the types of motion that cause them [119].

These will be discussed in more detail in the following sections. Additionally, Farrow [120] introduced the possible interactive processes and parameters influencing wear in relevant schematic manner,Figure (4-1). Generally, the nature of wear generation could belong to two main causes which are mechanical and chemical. The latter (corrosion and oxidation forms) [12], are not discussed further here where the focus is on solid surface wear (mechanical wear). This forms a high percentage of industrial losses to wear, about 95%, further broken down to 50% abrasion, 15% adhesion, 8% erosion and 8% fretting while the chemical wear accounts for about 5% [121], [122], [120] with the remaining 5-8% due to fatigue wear [116], [122]. Even so, wear does not usually occur by just one mechanism at a worn surface, therefore it is important to study each type of wear and possible mechanisms by which it may happen [123].

Table (4-1): Summarised the types of wear and their mechanism [110],[119],[124].

Wear Type	**Contact Type**	**Movement Type**	**Wear Mechanism**
Abrasive	Elastic-plastic	Sliding	Abrasion
Adhesive	Elastic-plastic	Sliding	Adhesion
Erosive	Elastic-plastic	Impact-sliding	Abrasion
Fretting	Elastic-plastic	Oscillating	Adhesion- abrasion
Fatigue	Elastic-plastic	Rolling	Fatigue
Tribo-Chemical	Electrolytic	Electrochemical	Chemical reaction
Impact	Elastic-plastic	Impact	Solid-particle crushing

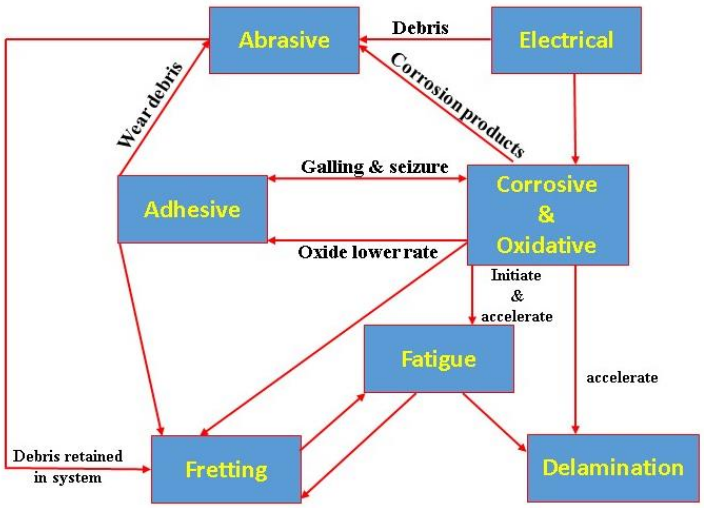

Figure (4-1): summery of possible interaction among wear types, re-produced from Farrow[120] after farrow and Gleave [122].

4.1.1 Abrasive Wear

Abrasive wear is considered one of the most dominant wear mechanisms [116],[125]. It can be defined as when wear is caused by forcing hard asperities or particles to move along solid surfaces. As a consequence, these hard objects create wear in the contacting surfaces and lead to progressive loss of material.

It has been reported that the hardness of most metals has a crucial role in controlling their abrasive wear properties and metal with high hardness exhibits a lower wear rate as shown in Figure (4-2). Khruschov [126],[127] stated that the method of hardening determines the increase in wear resistance and can even lead to a deterioration in some cases when it is abrasive wear. Other properties, such as Young's modulus, also have important effects on wear, for both metallic and non-metallic materials [125], [128], [129], [130]. Oberle [129] studied the effect of elastic modulus on wear properties and showed that, when the elastic modulus of material is low, the total deformation in the contacted surface will increase, increasing the contact radius [129]. This was demonstrated practically in ball on flat wear test configurations. Leyland and Matthews [130] developed these ideas to use the hardness to elastic modulus ratio as a more important parameter than the hardness alone in assessing the wear resistance of materials [130]

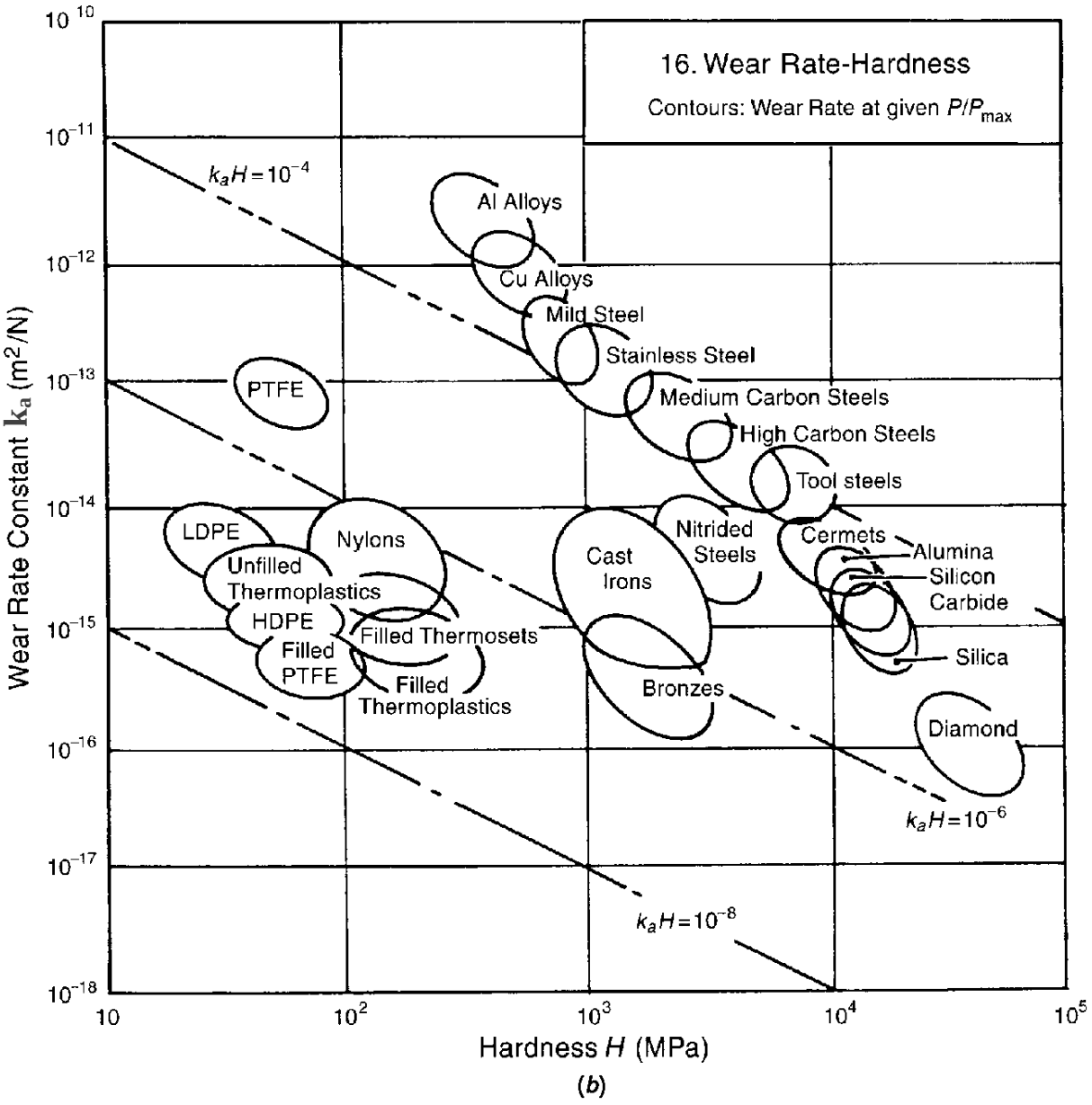

Figure (4-2): Chart of wear rate constant (k_a) against materials hardness (H) for common engineering materials after [131].

The chart in Figure (4-2) can be used as a guide of material selection for the requirement of high wear resistance. Diamond would clearly be a suitable material for wear resistance requirements, but the high cost may be an obstacle. Therefore, silicon carbide and alumina will be the second-best choices if eliminating silica due to its uncertain wettability with molten metals, especially aluminum [132]. Even so, there are other materials not shown on this chart, such as tungsten carbide and silicon nitride, which may also have suitable properties [127].

The classification of abrasive wear is normally according on the nature of contacting surfaces. The nature of contacting surfaces and their circumstances can determine the type of abrasive wear. Two main types of abrasive wear are encountered, two-body and three-body abrasion wear. Two-body abrasion wear happens if the asperities or hard particles wear the opposite surface by removing material, such as in free-flow ore or machining. Three-body wear happens if the asperities or hard particles are surrounded by another two bodies, such as jaw crusher or a plow in a sandy soil [111], [133]. Consequently, this type of wear itself can be divided into four sub-types depending on how many bodies coexist and their position relative to each other, which can be summarised in Figure (4-3) [111].

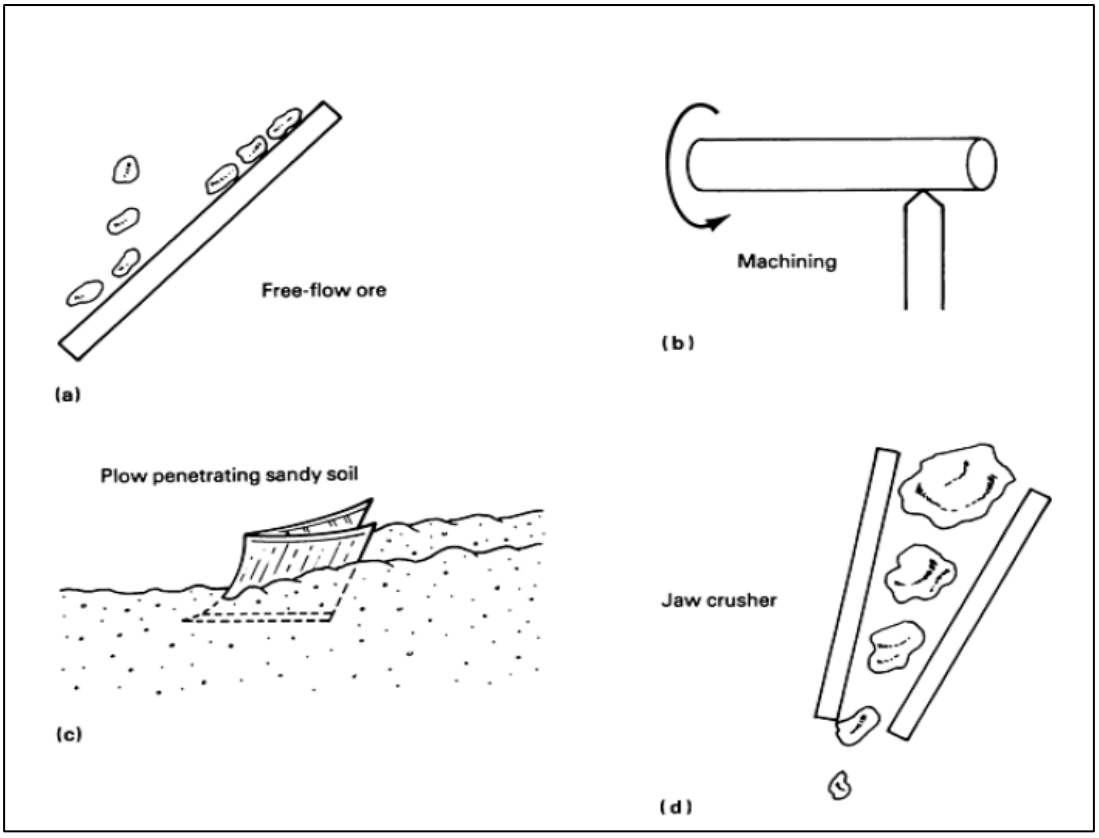

Figure (4-3): Types of abrasive wear. (a) Open two-body. (b) Closed two-body. (c) Open three-body. (d) Closed three-body reproduced with permission of the publisher [111].

Almost all abrasion wear occurs where there are hard particles or asperities. There are many factors which can affect the manner of abrasive wear and in which mechanism the material can be removed [133], [134] There are four different mechanisms which have been reported as shown in Figure (4-4) [134], [135]. These mechanisms act separately or simultaneously during abrasive wear according to the surface conditions and abrasive

particles where the abrasive wear is come from sliding hard particles or asperities on the worn surface. The mechanisms are discussed below:

Cutting: when the counter surface (the worn surface) is soft, the hard particles sliding over the surface will cut a thin layer from surface, forming wear debris, as shown in Figure (4-4 a).

Fracture: when the worn surface is brittle (such as ceramics), fracture normally takes place gradually because of the propagation of micro-cracks through the surface and the wear debris will be in the form of fragments due to cracks crossing, as shown in Figure (4-4 b).

Fatigue: When the abrasive particles or asperities have rounded edges or are not sharp enough to scratch a softer material, these edges will be aggressive to ductile materials with load/unload effects through continuous sliding, which leads to fatigue failure of affected surface, as Figure (4-4 c) shows. This mechanism may be useful when the surface deformation is repeated to form a smooth surface, as in polishing to remove asperities, by fracturing due to repeated load cycles.

Grain Pull out: materials with weak bonding at grain boundaries or interphase boundaries, such as ceramics, can be worn by pulling grains out from the structure [133]–[135]

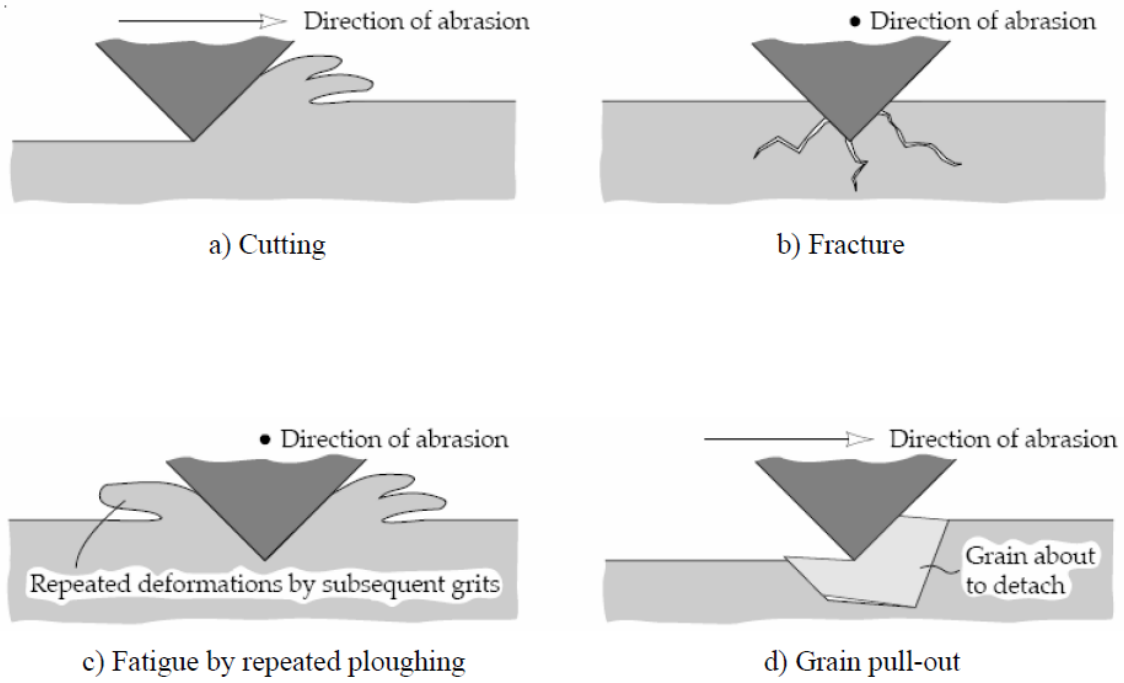

Figure (4-4): Abrasion wear mechanisms: a) micro-cutting, b) fracture, c) fatigue, and d) grain pull out [134], [135].

4.1.2 Adhesive Wear (Attrition)

Adhesive wear, sometimes called attrition wear [118], is normally caused by local melting of the asperities and adhering to the opposite contacting surface. These will then be sheared off as a result of the relative motion between the contacting surfaces [136]. The adhering asperities often lead to transfer of materials between two contacted surfaces [13], especially when the two surfaces entirely contact together, which is one of main conditions for attrition wear. Therefore, a lubricating film is one important solution to prevent or reduce the attrition wear by isolating two contact surfaces from being entirely direct contact [13]. Adhesive wear and tribofilm formation can be associated with other types of wear in sliding or relative movement of solid surfaces. These two mechanisms often occur during most sliding wear between two contacting solid surfaces [137]. Figure (4-5) describes the adhesive wear mechanism when there is sufficient degree of bonding by adhesion at the interface between two plastically deforming surfaces. This bonding, which is able to resist the relative motion between contacting surfaces, leads to pull out of some of the plastically deformed layers from one or both surfaces. Micro-cracks will initiate and propagate in the contact area to form the fracture mode combined from shear and tension.

At this stage some material transfer may occur at the contact interface before wear debris is formed when the cracks meet [123].

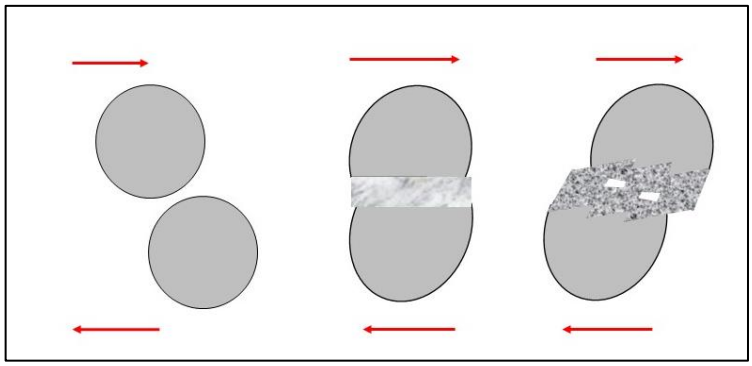

Figure (4-5): Schematic description of adhesive wear mechanism.

There is some similarity between abrasive wear and adhesive wear, particularly at low applied load and fine abrasive particle size. Therefore, some interaction in wear mechanism may exist during the abrasive wear process, and it becomes difficult to recognise which type or mechanism of wear either takes place at subsurface and worn surface regions [138].

4.1.3 Erosive Wear

There are some cases of wear, where surface wear occurs due to a shell or thin layer of worn surface. When this surface is exposed to a jet of solid particles with specific impact angle and velocity, these particles will move over the surface for some distance, then change their direction. The contact and movement of these particles will leave grooves and scratches on the surface, and consequently lead to the formation of wear debris. This type of wear can be called erosion wear [116]. The erosive wear rate depends on particle impact angle [127] and erosive wear becomes significant at a specific value of this angle, which varies according to the properties of the surface material. Thus, there are different effective erosion angles between brittle and ductile materials, and the erosion rate is higher in brittle materials when the hard particles perpendicularly impact the surface, such as tool steel and glass, while in ductile materials the wear rate is greater when the particles are incident at a narrow impact angle, such as in mild steel or aluminium. This is shown in Figure (4-6), which displays the erosion rate as the removed surface mass divided by the mass of hitting particles, with a variety in impact angle for brittle and ductile materials [139].

Initiation and propagation of micro-cracks is the dominant mechanism in erosive wear, which leads to remove materials from the surface ether at a relatively high wear rate (high-speed wear) or relatively low wear rate (low-speed process). Therefore, it is thought to be that volumetric material removal corresponds to the particle speed [116], [127].

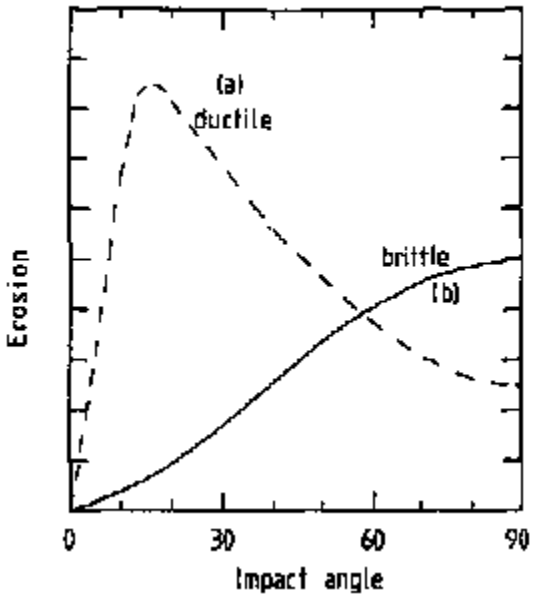

Figure (4-6): The relationship between erosion and impact angle a) for ductile material and b) for a brittle material after [139].

4.1.4 Fretting wear

Fretting wear can be defined as that the wear that is caused by the existence of low-amplitude oscillatory motion between contacting bodies, which are supposed to be under static conditions [111], [140], [141]. Therefore, it is considered one sub-type of fluctuating reversed sliding wear, when there is a very narrow clearance contact (about 50 - 150 µm) [136]. There are two main mechanisms of fretting wear, starting with adhesive impression at the contact area between the contacting surfaces, occurring due to the tightening up of the clearance between them. This area begins to be oxidized, often as a result of the high residual energy stored in the worn contacting area [142]. Hence, this type of wear is sometimes named "fretting corrosion", and the wear debris is normally in the form of oxides [111]. The other mechanism is called "fretting fatigue'' and occurs where there are cyclic loads [143]. Fastening machinery elements, jointing structures and rivets are likely places to create fretting phenomena. For example, in aircraft structures there are many parts containing steel and aluminium components assembled by rivets or joined by fastener

bolts. In some of these combined parts, even those attached with the same materials like rivet assemblies, there are three main contact places which may be exposed to fretting phenomena as shown in Figure (4-7) [111].

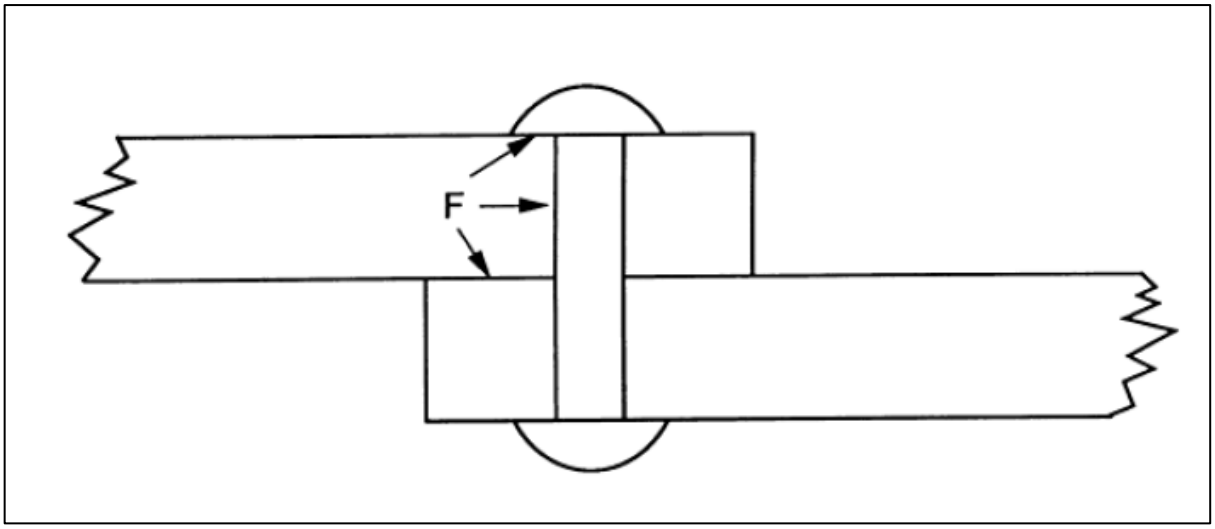

Figure (4-7): An aluminium-steel joint by rivet indicates the possible fretting areas reproduced with permission of the publisher [111].

4.1.5 Fatigue Wear

Fatigue wear is when the surface damage comes from fracture of the materials surface due to fatigue by cyclic load [142], which can occur in ether sliding or rolling movement patterns surfaces [123], [134] The main expected mechanism of this type is that a fatigue fracture occurs due to crack propagation on the surface or in the subsurface. The surface cracks can penetrate further and interact with the subsurface cracks, or the latter may propagate out and connect with the surface cracks, then many pits or voids form on the surfaces with continued cyclic load. The development of those cracks is affected by many factors, especially moisture in the atmosphere which will lead to faster development of in comparison to dry atmosphere [134], [142]. Also there is a critical number of load cycles that has to be achieved to produce fatigue wear [134]. This number of cycles can be predicted, particularly for rolling cycles, by equation (4-2) below[123]:

$N_f \, \alpha \, \frac{1}{w^n}$ ..... Equation (4-2)

where:

N_f: is the critical number of rolling cycles required to generate wear particles.

W^n: is the normal load applied with constant n, which refers to the shape of rolling components, will be equal to 3 in case of bearing for example.

4.2 Wear Measurement

Generally, wear rate, which is the term used to quantify wear of materials, refers to the volume loss, mass loss or dimension loss due to removed materials per sliding distance or unit time [142]. The selection of measuring units for stating wear or wear rates is made according to the wear type to be measured (the test type configuration, shape and size of the testing samples etc) [136]. Wear testing devices, which can be also utilised to measure frictional properties of materials, may be a standard or customized equipment.

During experimental measuring of wear it is important to note if an initial wear stage can be detected. This is characterised by rapid breakage of particles in the worn surface, and is often ignored leading to emphasis on the more stable steady state stage of wear [144], but the full description is needed to accurately calculate wear rates [136].

The most common way of reporting a wear measurement is the volumetric removal amount of material divided by sliding distance [144]. There are many findings that report wear measurements, express wear quantity by volumetric measurement units (mm^3) because this expression can be more accurate when describing comparable wear for different materials with a different densities [111].

Therefore, many standard wear tests recommend reporting volume units of wear for comparison of materials. Occasionally, worn areas can be directly measured even if they are complex in geometry, especially if a highly accurate result is required. In this case the direct measurement of volume loss would be done to calculate wear but like this measurements will take long time to obtain [111].

Otherwise when volume or mass loss of wear cannot be accurately measured in the worn area, visual inspection or shape of wear debris is applied to estimate wear performance. There are alternative methods for wear assessment, which include the surface roughness of the worn bodies in comparison with a reference material (benchmark), which has been experimentally tested under the same conditions. Other criteria, based on the wear values of reference materials, are applied to find the relative wear enhancement of the testing materials. In other words, in sliding or erosion wear test for example, the wear factor will be a result of mass/volume loss of the interested materials for the test per unit sliding

distance over the mass/volume loss of the reference materials per unit sliding distance. Theoretically, wear rates either in terms of contacting time or sliding distance, is normally been assumed to be linear [136].

Nevertheless, there is deviation in some cases of wear from this assumption, such as in erosive wear and sliding wear, where they do not have a completely linear trend over all their wear life cycle. An practical example of this is the initial running wear, which may take place in new bearings, and is higher than the wear rate at the steady-state stage [136].

Finally, wear is classified according to the worn surface features and wear debris sizes into mild wear and severe wear. Wear with smoother worn surface and smaller wear debris (between 0.01μm to 1μm in size) is a mild wear while the wear with a rougher worn surface which can be visually inspect by the naked eye and larger wear debris (20 μm to 200 μm in size) is a severe wear. The determination of material wear behavior is considered crucial in tribology with regard to considerations such as frictional force [142].

4.3 Grinding Wheel Wear

Researchers in tribological properties of engineering materials began with investigation of abrasion, and the polishing and cutting mechanisms of metals. Hence the majority of cutting theories and equations have been derived to be applied to metals first, and then have been modified to be suitable for other engineering materials, such as rock, abradable and polishing materials. A variety of abrasive particles, especially diamond and SiC have been utilised for cutting or grinding and polishing operations. Therefore, distinguishing between cutting, grinding and polishing operations became important for tribology, because these operations can be distinguished by the wear type caused; by factors like surface morphology, operation speed and debris size and shape [145]. The wear of a grinding wheel has been frequently studied, finding it is a very complex phenomenon, combining many wear mechanisms due to contact between individual abrasive particles and the work piece [146], [147], [148]. Malkin and Cook [148], [149] addressed the grinding wheel wear in two separate papers, and classified the wear occurring into three main types; attrition wear, particle fracture, and bond-particle fracture, Figure (4-8). Attrition wear is determined by how much each abrasive particle has dulled as a result of sliding over the surface of the workpiece. The flattened area of active abrasive particles is the origin of particles dulling [148]. Wear intensity occurs by abrasive particle fracture and bond-particle fracture during wheel wear processes depending on the amount of

removal of grains from the wheel. They used a model to analyse grain size distribution, removed as a wear debris, to estimate the proportion of each type of wear (abrasive particle fracture, particle-bond fracture, and attrition wear). Wear debris was sieved into fractions corresponding to grit sizes of wheels to separate the accumulated wear swarf from the grinding wheel from the metal debris from worn workpiece, using dissolution with aqua regia (1/3 molar ratio of nitric to hydrochloric acid, which does not attack alumina) [149]. They found the attrition wear forms about 4 percent of total wheel wear [149] which corresponds with Jagdeesha [150].

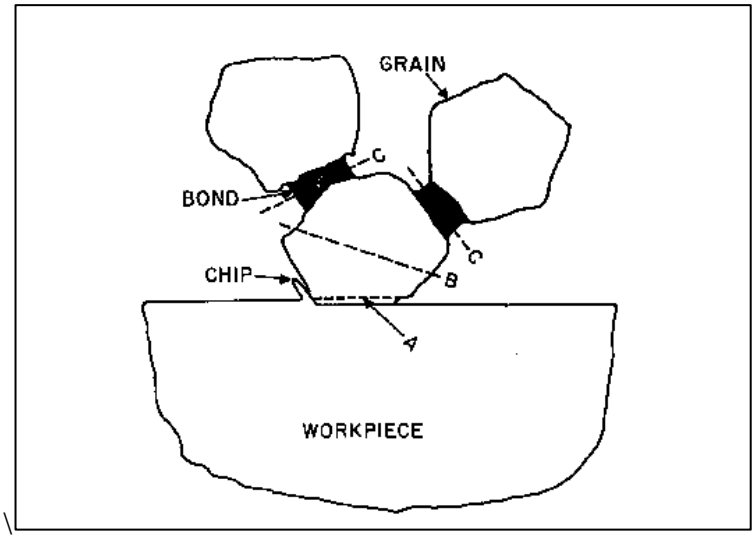

Figure (4-8): The three possible type of wear in grinding wheel: A) attrition (adhesion) wear, B) particle fracture and C) bond-particle fracture (particles pulling out) reproduced with permission of the ASME publisher [148].

During their study of wear rate of the wheel they found (especially for the finest dressed wheel) that the wear generally occurs in three stages, as shown in Figure(4-9) [147], [149], as for single-point cutting tools [150], [151], while in coarse dressed wheels, the third stage disappears. The first stage, which is characterized by a high initial run-in wear, is followed by the linear steady state wear stage, which is the second stage. The last stage, which is the third stage of wheel wear, shows a rise in wear rate [152], This increased wear rate in the third stage is attributed to grinding burn [149][151], which leads to an increase in grinding forces [149].

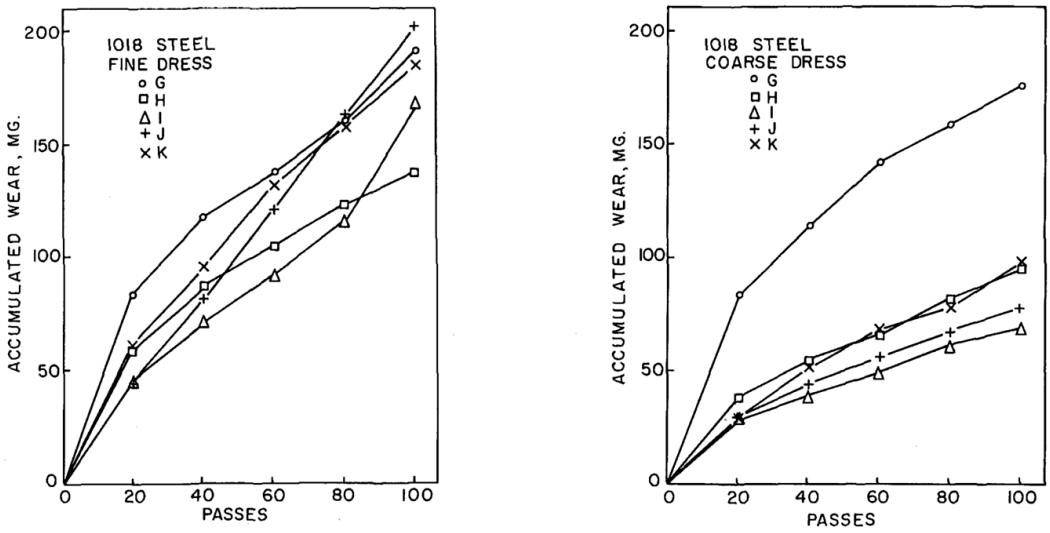

Figure(4-9): Accumulated wear against number of grinding wheel passes, the left figure shows wear behaviour of fine wheel dressing (the three wear stages are seen) while the right figure shows coarse wheel dressing (the third wear stage disappears) reproduced with permission of the ASME publisher [149].

Jackson attributed each wear stage to the domination of a specific wear mechanism domination and stated that there is a general similarity between the wheel wear curve and other general wear process curves, such as those for a single point cutting tool. As shown in Figure (4-10), the high initial wear at the first stage relates to breaking of the matrix-abrasive grain bonding (grain pull out). The second wear stage, is related to more slow fracture of the particles themselves, and the third accelerating wear stage, is characterised by severe wear and the wheel losing bond strength as a result of thermal damage, which is normally combined with wear at this stage, and may affect the workpiece as well [151].

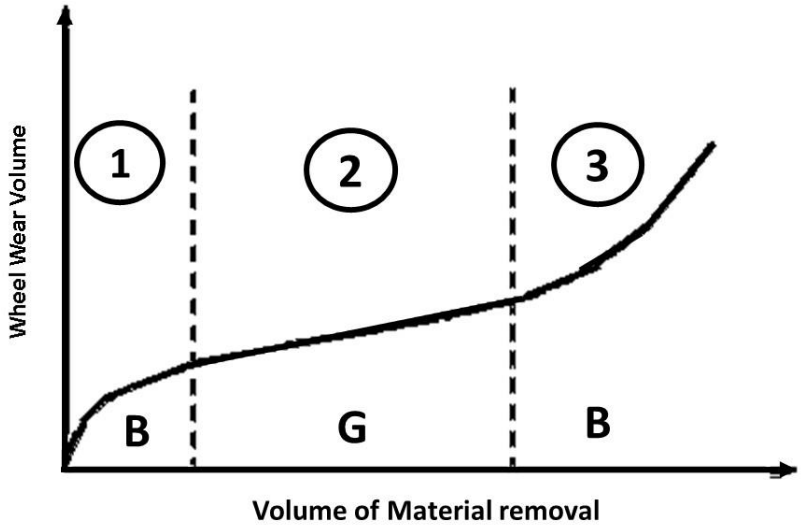

Figure (4-10): Three regimes of grinding wheel wear indicated each area with most dominant wear mechanism, where B refers to bond fracture and G refers to grain fracture [151].

Generally, the grinding process is combined with wheel wear, and the rate of this wear is a crucial parameter, which can be used as an indication of the grinding wheel performance, the efficiency and quality of overall grinding operation and workpiece [151]. There is a specific performance criterion or index of the wear resistance of the grinding wheel, which is called the grinding ratio (G-ratio). This is practically expressed as proportional volume loss between removed materials from the workpiece to removed materials from the grinding wheel as shown in equation (4-3) below [147], [151]–[153].

$G=\frac{Vw}{Vs}$ ……Equation (4-3)

where V_w and V_s are the removed volume of workpiece and wheel, respectively.

Even so, the grinding ratio is not truly an expression of grinding wheel wear in all cases [149] because abrasive wear can occur in a grinding wheel by pulling out whole abrasive grains, where the diameter of these grains is greater than the depth of total wear, which is the measured parameter used to calculate the volume removed from the wheel [154]. In this situation, any variations in grinding conditions cause unexplained changes in the grinding ratio [149]. Michele et al. [153] applied the G-ratio as a criterion to assess

segmented grinding wheel wear in their study of intermittent grinding. Liao et al. [147] stated that the wear of grinding wheel should be measured as material circumferentially removed from the wheel during grinding, applying a formula to calculate radial wear of a grinding wheel, V_s, which is presented in equation (4-4) below:

$$V_s = \pi \times d_s \times \Delta r_s \times b \quad \text{Equation (4-4)}$$

where, d_s is the average diameter of the wheel before and after wear, Δr_s is the radius reduction of grinding wheel, And b is the grinding wheel thickness.

These workers recognised that the volumetric wear calculations are not sufficient to establish a clear idea concerning the wear mechanisms that occur in a grinding wheel. Hence, microscopic investigations are a crucial technique to analyse the worn wheel surface [147].

4.4 Wear of Composite Materials

After the wear of the grinding wheel has been discussed, now it can said that the wear of composite materials is probably somewhat similar to the wear of such a grinding wheel, especially in the case of particulate reinforced composites. This can be concluded from the similarity in the nature and structure of a grinding wheel and its wear mechanism in comparison to the structure of particulate reinforced composites. Both of these materials consist of hard (brittle) particles embedded in a relatively softer (ductile) bonding matrix, with a different amount of reinforcement according to their application requirements. The wear of composite materials has been assumed to be sliding wear in the relatively ductile matrix and abrasive wear in the reinforcement. The hard particles of reinforcement are exposed to the three main types of wear mechanism as for the abrasive grains in a grinding wheel. These three mechanisms are pulling out of particles, ploughing and crack propagation at reinforcement particles or at the particle/matrix interface [155]. Jian-min et al. [156] stated that the wear mechanism in composite alloys depends on the wear type (whether two or three-body wear configuration), with the assumption of a combination of micro-cutting and ploughing in case of two-body wear, but in case of three-body wear the mechanism will be pull out or break down of the particles [156]. Das et al [138] also attributed abrasive wear of MMCs-SiC reinforcement to cutting and ploughing, but they noted that SiC grains extrude to form a thin layer on the contact surface which tends to prevent matrix wear. With high applied load or long sliding distance this layer starts to

crack and break down, leading to increased wear rate by converting to fine abrasive particles. In addition, investigation of the sub-surface found that the wear mechanism formed a layer, in either alloy or composite, as a result of plastic deformation at the contacting surfaces. This layer also becomes cracked and removed by introducing cracking at the interface between this layer and the plastically deformed face of the worn surface with continous wear operation [138]. This is in agreement with other researchers studying combined wear mechanism [137]. With this complexity in wear behavior and mechanisms in composite materials, it became important to find a model or equation to describe the wear behavior of a composite for greater understanding. Two such models of abrasive wear of composites have been developed according to the rule of mixtures.

The first equation, Khruschov's rule, applied the inverse rule of mixtures to calculate abrasive wear in two-phase composites [157], equation (4-5) below.

$$\frac{1}{W_c} = \frac{V_m}{W_m} + \frac{V_r}{W_r} \quad \text{..... Equation (4-5)}$$

where, W and V: refer to the wear rates and volume fractions , respectively. Subscript *m*, *r and c*: refer to the matrix, reinforcement and composite, respectively. The wear resistance, R, in Khruschov's model is represented by the inverse of the wear rate, R = 1/W.

Khruschov built his model (Eq. (4-5)) according to the assumption that the constituents of the composite wear concurrently at the same rate. As long as this model is the inverse rule of mixtures, then the wear rate of composites will be a nonlinear relationship with the volume of reinforcement as shown in Figure (4-11). This equation reveals that the abrasive wear behavior of a composite will be controlled mainly by the reinforcement, as the actual wear rate of the matrix is normally much higher than that of the hard reinforcement [126], [128], [157], [158].

The second wear equation for composite materials, applied by Zum-Gahr [159] to interpret practical wear results of multi phase materials, is completely linear, as it folows the regular rule of mixtures. This model implies that the wear trend of composite materials is not governed by a particular constituent, but rather each constituent contributes in proportion with its volume fraction in the composite, equation (4-6) below and Figure (4-11)

$$W_c = V_m \cdot W_m + V_r \cdot W_r \quad \text{.....Equation (4-6)}$$

In this equation, increasing volume fraction of reinforcement will linearly reduce the abrasive wear rate of the composite because this model neglets the role of interfaces [158], [159].

However, Eqs. (4-5) and (4-6) are intended to indicate upper and lower possible rate limits for abrasive wear in a composite, and these limits may not be experimentally encountered because the equations are simplified and non-physically founded. This can clearly be seen in Figure (4-11), as both equations depend on an assumption that all constistuents wear at the same time by the same mechanism, as if they were in bulk form. These two models ignore the contributions of other factors, such as interfacial properties between the phases, their relative sizes, and the fracture toughness of the components; all of these factors can have a significant impact on abrasion performance in composites [160]–[162]. Therefore, the failure to account for such effects in predictions is considered the main limitation of current abrasive wear models of composites [155].

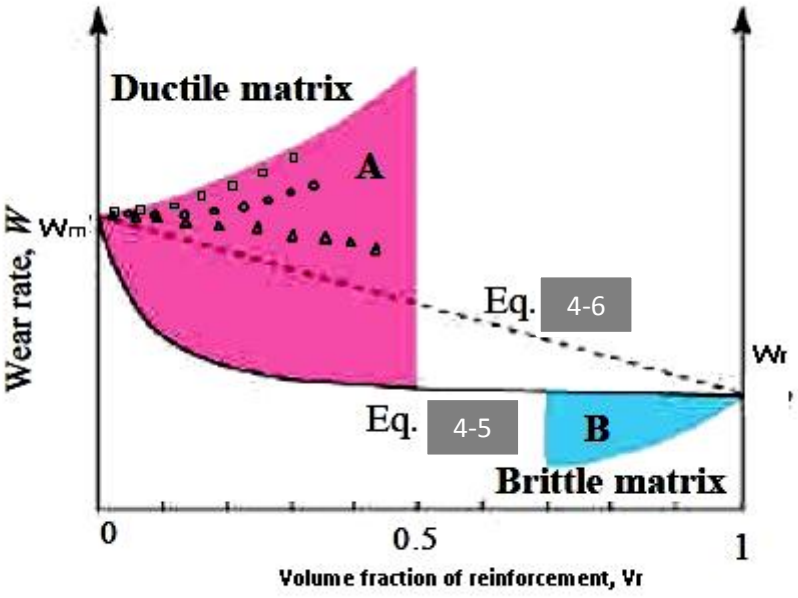

Figure (4-11): Abrasive wear models in composite materials.

Generally, there are two important, but opposing properties which govern the sliding of abrasives on a solid surface in a manner which results in volume removal; the hardness and toughness. For example, in ductile materials, the primary wear mechanism is attrition

wear, related to plastic deformation, and therefore, the material hardness will be an important factor in controlling the amount of material removal. Meanwhile, the governing mechanism in a brittle material depends on fracture at, or near, the surface, and so the key property will be the toughness of the material. However, the abrasive wear of composites models show that the existence of reinforcement improves the wear rate, but in the area denoted A in Figure (4-11) the experimental data for a ductile matrix exceeds the upper limits of the abrasive composites model, which indicates a negative effect from reinforcement, which also cannot be described by these models [155].

Unfortunately, until now a comprehensive model for abrasive wear of composites has not been developed, and the existing models for composites are highly inaccurate and do not take into account the role of the composite microstructure [155]. Therefore, this scope of materials science is still open for new approaches. Recent studies have achieved a progression in their investigations of how other factors can impact wear resistance of composite materials in addition to volume fraction of reinforcement, such as the nature of the reinforcement materials, the applied load, relative sizes of the abrasive particles of both contacting surfaces, size of reinforcement and interfacial bonding between matrix and reinforcement. This is especially true in metal matrix composites, which is our target in this study.

Rao [163] found that the wear rate of Al7075 AMCs reinforced by SiC decreases with increasing the volume fraction or particle size of reinforcement [163]. Pradhan [164] also concluded that the wear resistance of AMCs reinforced by SiC increases with the amount of SiC reinforcement, due to reductions in the coefficient of friction with this increase, in addition to the formation of an oxide layer. Furthermore, there are many types of wear that take place in AMCs, adhesive, abrasive and corrosive [164]. Ahmad [165] stated that increasing applied load during the wear testing of AMCs with alumina reinforcement leads to rise in wear rate, while the coefficient of friction was constant up to 50 N and began to decrease at 75 N and 100 N load. At different load conditions the AMCs suffered from combinations of many types of wear, abrasive, adhesive and fatigue. At high load even the roughness of the worn surface of the AMCs increased, while the coefficient of friction continued to decrease. Ahmed attributes this to pull out of alumina particles from the surface of AMCs throughout the wear test [165]. Das et al.[138] and Hutchings [166] compared relative sizes of abrasive grains between worn surfaces and causes of wear body at high stress in abrasive wear of composites. They found that, when the size of the

abrasive that causes the wear is smaller than the size of particle reinforcements and they have homogeneous distribution in the matrix, the wear resistance of composite will be very high, and vice versa. This is because if the abrasive particles are coarse that will lead to pull out or cracking and then removal of the reinforcement more quickly, especially under high applied load. In addition to the important function of particle size in wear resistance Hutchings [166] also suggested that composites which have good interfacial bonding and sufficiently tough particle reinforcement to resist a fragmentation then scooping out from the worn surface of composite, can achieve high wear resistance. Even so, no one has investigated the subsurface region, as it may be effected by wear; this may help to understand how the early stages of material removal begin, and consequently find solutions to eliminate the material removal through high stress abrasive wear [138][166]. Harti et al. [162] have suggested that applying a high load in wear tests results in severe wear in Al2219-TiC composite, which is normally combined with vibration, high noise and a rise in the worn surface temperature. They introduce solution for enhancing the wear resistance of composites by increasing the amount of TiC particle reinforcements, which can contribute to increasing the hardness of composites, and consequently improve overall wear resistance [162].

Chapter 5 Experimental Work and Research Program

This section shows the details of materials, experimental methods, and equipment or devices that are used to produce and investigate the metal matrix-diamond composites explored here. This comprises a number of investigations, starting with a study of the effect of particle sizes and surface condition of reinforcement particles and ending with the influence of different matrices on the abrasive and tribological properties of MMDCs and MMCCs. In creating the samples for these trials, different manufacturing techniques have been applied.

The plan of this work is summarised in Figure (5-1) showing the tasks completed and how they relate to each other, (see the figures below).

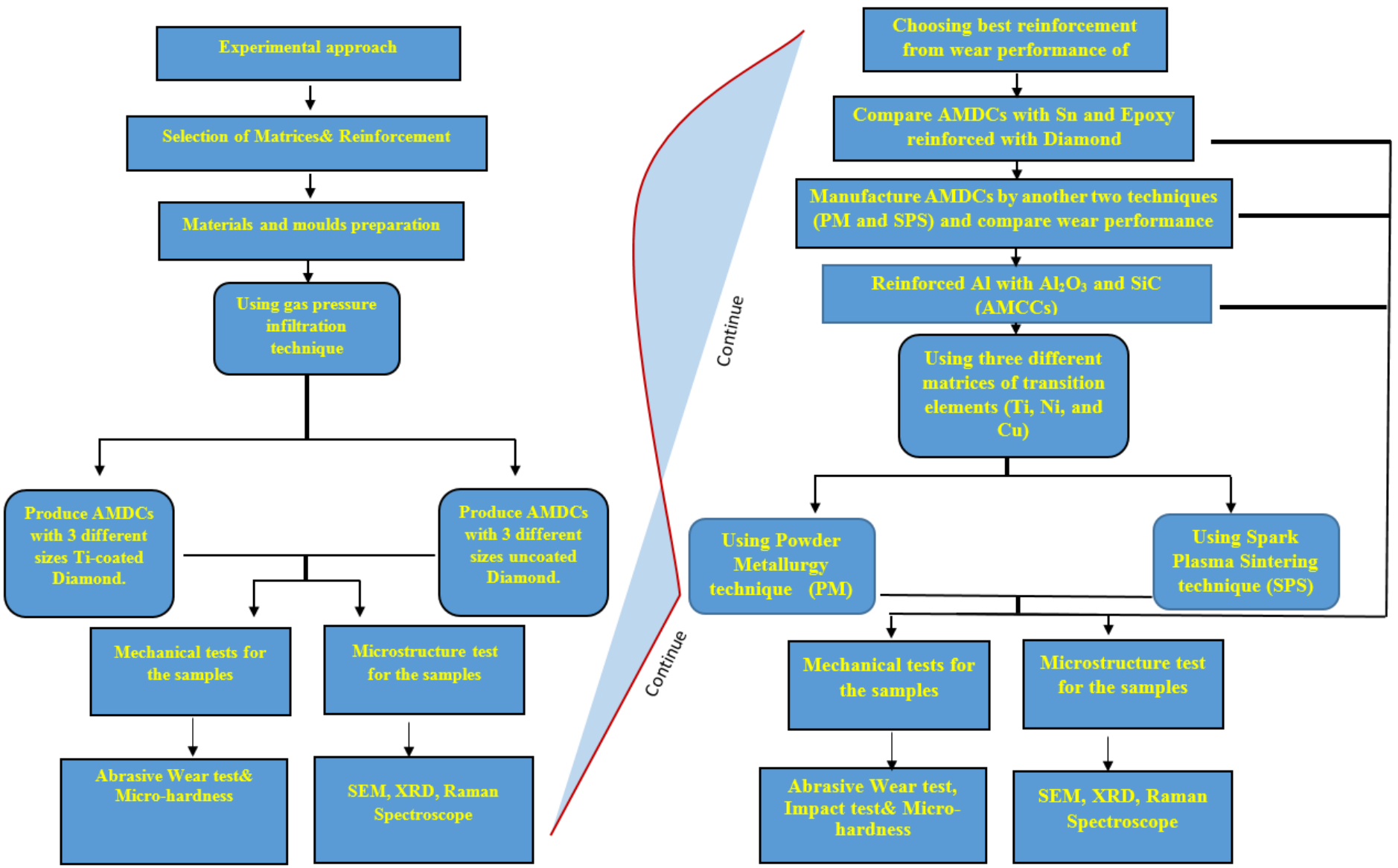

Figure (5-1): Flow charts of the summary experimental program.

5.1 Materials Used

In the current work, initially materials were used to produce aluminium matrix – diamond composites, employing two kinds of diamond powder (uncoated diamond and titanium-coated diamond), they were brought from **HX** Zhecheng Hongxiang Super Hard Material of Research institution Compony, Zhengzhou-Henan, China with three different particle sizes (75-63 , 250-212, 500-420) μm and a metal matrix (Al-1wt.%Mg alloy) One size, the largest particle size (among the three sizes) used in this work, was in Ti-coated condition only. This was used after observing the results from the previous three particle sizes. In addition to another large particle size (840-710 μm), which was used later to confirm effects of particle size on wear behaviour, as summarised in Table (5-1). The matrix alloy was prepared by casting a master alloy, which has a chemical composition Al-5wt.%Mg, with an appropriate quantity of pure aluminium, using one part of master alloy with four parts of pure aluminium to achieve Al-1wt.%Mg. Figure (5-2a) shows its microstructure, with diamond particles separated into three different particle sizes (by sieving) for both forms (coated and uncoated), as shown in Figure (5-2 b and c) for example.

Table (5-1) : Sizes (grit and dimensions) of diamond particles used for both coated/uncoated diamond[167]–[169].

No	**Grit (US)**	**Particle size** μm
1	35/40	500-420
2	60/70	250-212
3	200/230	75-63
4	20/25	840-710

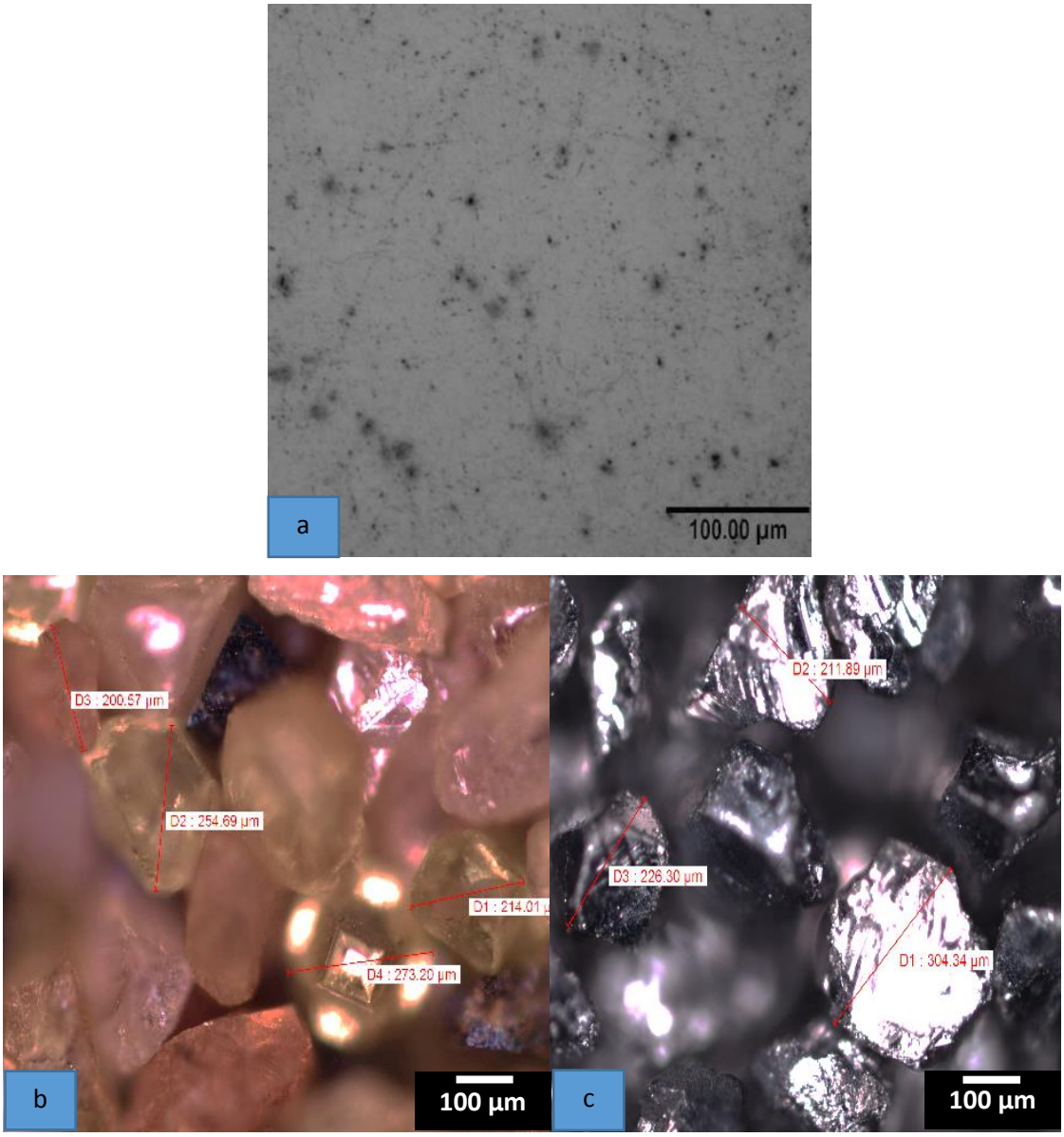

Figure (5-2): Optical microscope images of a- the microstructure of Al-1 wt.% Mg, (b- and c-) 60/70 diamond particles (250-212) µm uncoated and coated ,respectively.

5.2 Gas Infiltration Processing (GI):

In the current work the experimental gas pressure infiltration rig has been designed to provide a controlled chamber suitable to make a variety of samples, including the abrasive test samples and Charpy impact test samples which will be discussed in more detail in chapter 6. The manufacturing of MMDCs, which has been performed over the duration of this study, has been undertaken with two main phases. The first phase used the metal matrix as Al-1 vol. % Mg Alloy with reinforcement of two types of surface condition (Ti-coated/uncoated) and different particle sizes of diamond particles, and in addition, ceramic

reinforcements, such as Al_2O_3 (Metal Finishing Supplies, Bridgtown/UK) and SiC (Alfa Aesar Scientific, Heysham, Lancashire/ United Kingdom). Three different manufacturing methods were utilised. That are introduced in more detail in next chapters as well. The next phase used different transition metals as matrices such as Ti, Ni and Cu, which were used as a powder with 5-35 µm particle size, apart from Ti which was 15-45 µm, mixed with diamond particles having the same particle size as those used with the Al-alloy that achieved good abrasive wear performance, in order to compare the performance of different composites and different manufacturing techniques.

Table (5-2): Al-diamond composites and the symbols used to describe them in this work.

Matrix	50-55 vol. % Diamond particle size (coated/uncoated) µm	Symbol of Composite with Ti-coated particles	Symbol of Composite with uncoated particles
Al- 1wt. %Mg	500-420	A_1	A
Al- 1wt. %Mg	250-212	B_1	B
Al- 1wt. %Mg	75-63	C_1	C
Al- 1wt. %Mg	710-840	AB_1	

From the results obtained from AMDCs with different particle sizes and surface conditions of diamond we chose Ti coated 420-500 µm diamond as the reinforcement for the next series of MMDCs. Different metal matrices (Sn, Ni, Cu, Ti) as well as epoxy. were utilised to fabricate composites reinforced with Ti coated (420-500) µm diamond to see which of them performed well under abrasive cutting conditions. All metal powders have at least 99.7 % purity, and were bought from Alfa Aesar Scientific, Heysham, United Kingdom.

5.2.1 Set up of a Rig for GI Processes:

The key part of the infiltration casting rig, which was built by the author of this thesis, a chamber made from 304 stainless steel alloy, this designed to achieve molten metal penetration into the reinforcement particle preform. It has a cylindrical geometry with 120 mm height and starts with a larger diameter on the gas pressure supply side and narrows on the other side where the preform is placed. This mould, used either for cutting samples or impact samples, is shown in Figure (5-3 a). This cylinder should be closed from both sides with two steel plates that are designed to tighten with four screws as shown in Figure

(5-3 b). Initially the cylindrical mould was made as a tube with a different wall thickness, starting at 5.5 mm for 40 mm depth, and after that changing to be 11.5 mm thick at the bottom where the diamond preform is held. This design however did not achieve complete infiltration, which was thought to be because the molten aluminium, and the preform it would enter, did not reach enough superheat. Then some of the thickness (about 6.5 mm) was removed to enhance the thermal transfer into the mould according to Fourier's equation of heat conductivity ($\Delta H \propto 1/\Delta t$) where H= heat quantity, t= thickness (as shown in Figure (5-3 c)). This rig contains a small pipe, which passes through the top plate to the chamber, which does two jobs. One of them is to allow extraction of the gas to form a vacuum in the chamber during the melting process; another is supplying a gas pressure in the chamber to push the molten aluminium to penetrate the diamond preform at the end of the melting process. This pipe is connected to the gas supply and the vacuum pump through a valve cross linking system, which was designed for controlling the vacuum and gas pressure at the same time. The main system was developed and used by Elizondo [170] and is shown in Figure (6-5**c**) in the next chapter. The infiltration process was done by packing the diamond particles at the bottom of the mould, packing at a density of between 50-55 Vol. %, then a piece of aluminium alloy was put in the upper wide part of the mould. This upper part can be considered as a pouring basin or cup and riser at the same time, and it helps ensuring the molten metal flows and penetrates into the preform after the melting process is completed. All the materials inside the chamber were heated up to 780℃ together for 2 hours under vacuum atmosphere (ultimate pressure 7.5 x 10^{-4} Torr ($1x10^{-3}$ mbar)). Then argon gas was supplied through the upper steel plate after the vacuum was isolated, by closing valve (1) and opening the valve (2) shown in Figure (6-5 c), and the composites were held under 5 bar pressure for 15 minutes. Finally, the composite ingot was left to cool under argon gas atmosphere to prevent diamond oxidation or graphitization.

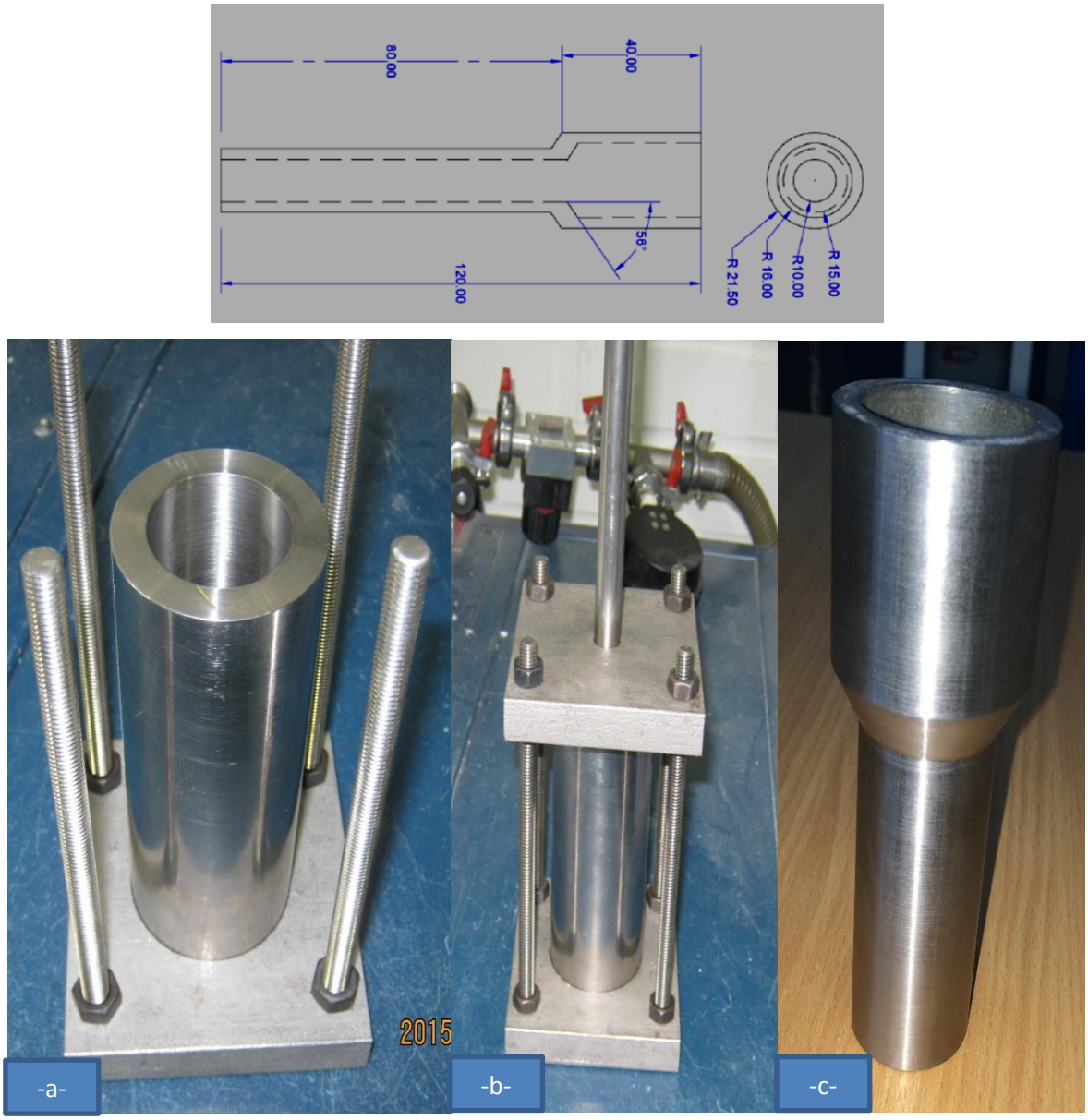

Figure (5-3): (–a-), (-b-) and (-c-) Steps of rig design for the infiltration system.

5.3 Production of MMDCs by Sintering

Unlike aluminium processing, composites made with relatively high melting temperature elements such as Ti, Ni and Cu in addition to Al, were produced by two manufacturing techniques, which are Powder Metallurgy (PM) sintering and Spark Plasma Sintering (SPS) techniques in the same ranges of temperature (950℃ for the Ti matrix with 800℃ used for Ni, 700℃ for Cu and 550℃ for Al) , which will be discussed in more detail in the next chapter. Weighing materials (matrix and reinforcement) according to their density was used to achieve the required volume fraction of reinforcement with weights calculated by applying equation 5-1 below.

$\boldsymbol{\rho}=\frac{\boldsymbol{M}}{\boldsymbol{V}}$ …….. Equation 5-1

where: $\boldsymbol{\rho}$ is the density of material (g/cm^3)

M: mass (g)

V: volume (cm^3)

The diamond/metal powder mixtures were created using a centrifugal mixer with 250 rpms revolution speed for 10 min for both SPS and PM methods and compacted prior to sintering by using a Specac manual hydraulic press as shown in Figure (5-4 a), but the compaction pressure of samples pre-sintering was different because in the case of SPS the mould was graphite, Figure (5-4 b), so more limited in maximum load, while in the PM case it was steel, Figure (5-4 c). The latter was carried out under a load of about 70 MPa while for SPS the pressure was 50 MPa. In addition to pre-sintering pressing pressure was applied in the SPS during sintering, which was keeping the materials under 50 MPa for 10 minutes (sintering time). AMDCs were produced in both techniques in order to compare results. Both techniques utilised the same temperatures for each matrix element for 1 hour for 10 min, in the cases of PM and SPS, respectively, as is mentioned in more detail in chapter 6. Both processes are schematically depicted in Figure (5-5). AMDCs and AMCCs were produced in these two techniques as shown in Table (5-3), Table (5-4) and Table (5-5), where the X letter in the tables indicates composite production.

Figure (5-4): a) Press used to compact powder, b) SPS graphite mould and punches and c) PM mild steel mould and punches.

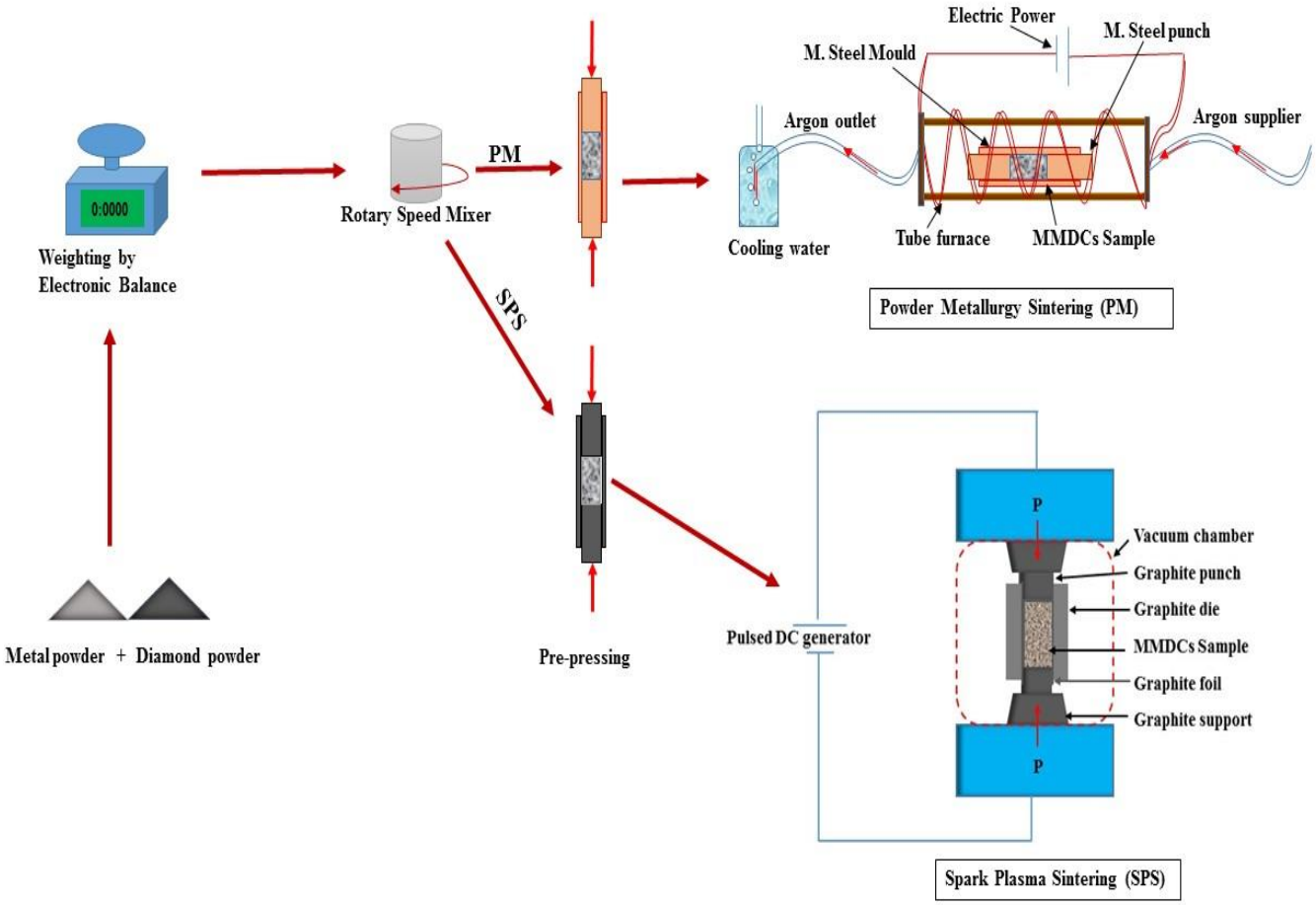

Figure (5-5): Schematic drawing of sintering processes showing PM and SPS routes of MMDCs production.

*Table (5-3): MMDCs reinforced with (500-420) diamond particles produced by the **SPS** technique.*

Reinforcement / Matrices	0% Dia. reinforcement	5% Dia. reinforcement	15% Dia. reinforcement	30% Dia. reinforcement	50% Dia. reinforcement
Al	--	--	--	--	X
Ni	--	--	--	--	X
Cu	--	--	--	--	X
Ti	-X-	X	X	X	X

Table (5-4): MMDCs reinforced with (500-420) diamond particles by conventional PM under Argon.

Reinforcement **Matrices**	**0% Dia. reinforcement**	**5% Dia. reinforcement**	**15% Dia. reinforcement**	**30% Dia. reinforcement**	**50% Dia. reinforcement**
Al	-x-	--	--	--	x
Ni	-x-	--	--	--	x
Cu	-x-	--	--	--	x
Ti	-x-	x	x	x	x

Table (5-5): MMCCs reinforced with (35/40)-(500-420) microns of SiC and Al_2O_3 particles by different techniques (GI and PM).

Reinforcement **Matrices**	**50% SiC reinforcement**	**50% Al_2O_3 reinforcement**	**30% SiC-20% Dia. reinforcement**	**30% Al_2O_3-20% Dia. reinforcement**
Al GI	-x-	-x-	-x-	-x-
Ti PM	-x-	x		

5.4 Microstructural Tests:

The microstructure imaging was achieved by Scanning Electron Microscope (SEM) for all composites as ingots because there are difficulties associated with sample preparation for optical microscopy, due to the diamond particles which have the highest hardness among engineering materials. Even though, several attempts were made to prepare samples for optical microscopic imaging, unfortunately they failed to achieve a flat and smooth surface by conventional grinding and polishing methods, especially those made with high hardness matrices, while only some composites that made with Al matrices achieved acceptable level of preparation (some optical microscope images shown in chapter 6). The results of SEM images are discussed in the results and discussion sections. Two instruments were used for secondary electron imaging (SE) and Energy Dispersive of X-Ray Spectrum

(EDX); inspect-F and inspect-F50 both manufactured by the FEI company. For SE images 20 kV and 30 kV electron voltages were applied.

5.5 X-Ray Diffraction Tests (XRD)

X-Ray Diffraction was carried out on composites reinforced with coated and uncoated diamond to observe the major different phases that may be present. The X-Ray Diffraction test was performed using a Siemens D5000 (Cu, GAXRD) diffractometer. This diffractometer is equipped with Cu source which generates an X-ray beam with 1.5417 °A radiation wavelength using 40 kV as a voltage. The detector is moved through an angle of two theta between 20 to 100 degrees. Eva-Bruker diffraction and PDF-4 software were used to analyse obtained X-Ray diffraction patterns.

5.6 Raman Spectroscopy

The Raman spectroscopy was utilised at the current work in order to explore if there is any evidence of formation intermetallic compounds in the composites, especially at interfaces, and if there is any conversion of diamond to graphite. This instrument has been used in studying carbon bonding particularly, graphene layers, carbon nanotubes and sometimes diamond deposition for machining tools. The technique fundamentally depends on carbon atom bonding vibrations; as shown in Figure (5-6) this displays three possible types of photon scattered emissions when the excited laser hits the molecule (carbon in the current case) in addition to absorbed infrared ray. These types are Rayleigh scattering (C) which is where the photon keeps the same energy and returns from the virtual energy level to its own original energy level or Stokes Raman scattering (d) this occurs when the photon loses energy during its return from the virtual energy level which will cause vibration of bonds in molecules or anti-Stokes Raman scattering (e) when the photon gains another energy level during its return from the virtual energy level, which will also cause a vibration in atomic bonds in different modes.

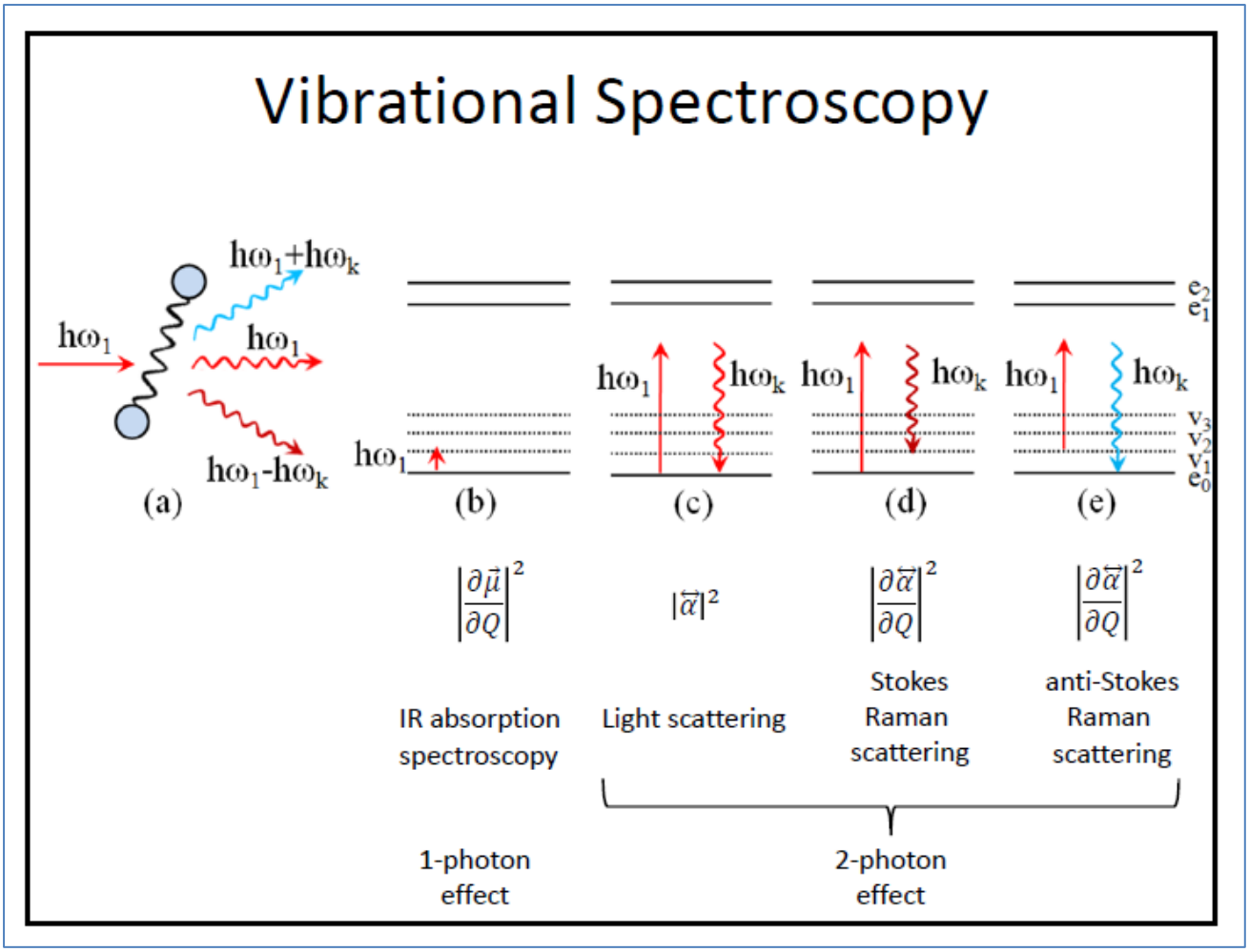

Figure (5-6): Three possible types of photon scattered emissions when the excited laser in a Raman microscope hits molecules [171].

There are two main modes of band vibration which are identified as D and G vibration modes and are shown in Figure (*5-7*) which displays schematically the differences between those modes and where they make Raman shifts. Most researchers agree that the D band, which exhibits Raman shifting between (1310-1360 cm^{-1}), is related to a high type of disorder. This disorder sometimes is called breathing mode vibrations (A_{1g} symmetry, where the subscript notation is used by chemists as symbols referring to specific configurations of electrons in orbitals) and occurs in aromatic ring structures and does not appear in graphite [172], [173], while the G band, which normally exhibits Raman shifting between 1500-1600 cm^{-1}, is related to the stretching vibration plane of the sp^2 orbital in carbon where there is an aromatic chain (E_{2g} symmetry) [174]. There are second order Raman shifts which may appear such as the D' band at about 1620 cm^{-1}, which is also related to disorder, normally found in nano-crystalline graphite [173], [175] and the other

two secondary Raman shifts, which are indicated at 2700 and 2900 cm^{-1}, and are marked as the 2D and D+G bands [173].

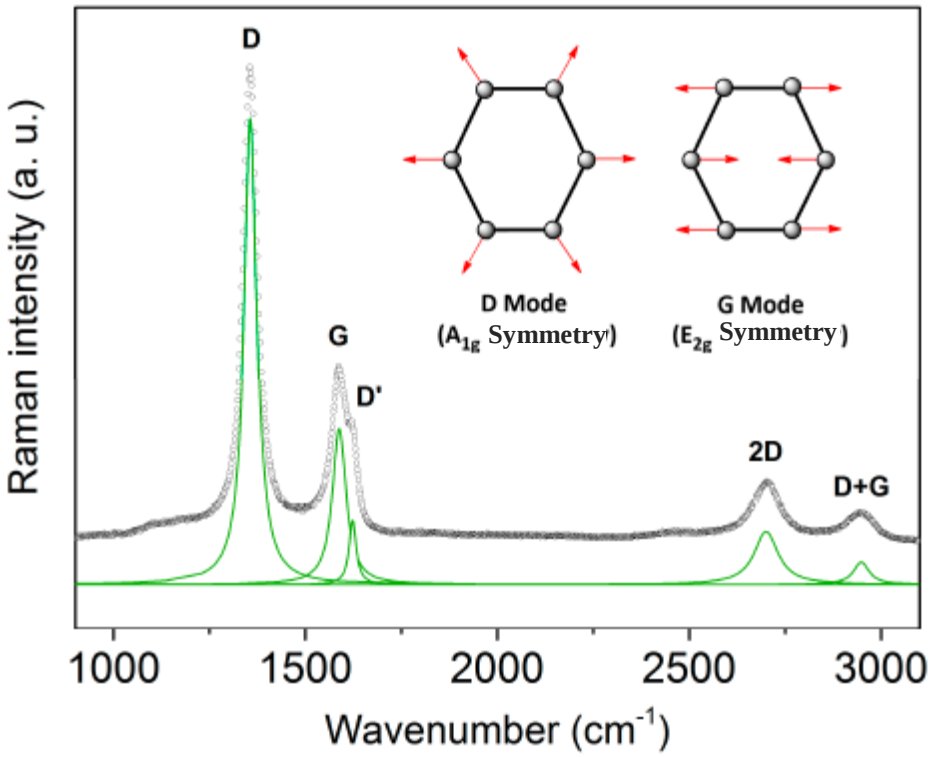

Figure (5-7): The differences between D and G modes in Raman scattering reproduced according to (CC BY 4.0) [173].

This instrument is very useful to study diamond structure changes, diamond bonding with different matrices, graphite formation at the diamond surface and intermetallic compound formation at the diamond-matrix interfaces as will be shown in chapter six. The instrument used, is a Renishaw inVia Raman Microscope, which can generate a green laser (514.5nm), would penetrate less than 0.7 μm into a material (according to [176], the beam penetration of a laser is 0.7 μm at 532 nm), and this device is located in the Department of Materials Science and Engineering at the University of Sheffield. Either bulk or fine powdered samples can be tested in this instrument [177], though the MMDCs samples were used as bulk materials after flattening their surface to avoid any reflection or distortion which may occur of the excited laser that hits the sample surface.

5.7 Abrasive Resistance Tests

The specimens for the abrasion resistance tests were produced in special moulds from mild steel which were designed to fit into the specimen holder in a bespoke grinding device set up for these tests; their dimensions are shown in Figure (6-6) in Chapter 6 later on. These moulds were put inside the chamber below a piece of aluminium alloy after it was filled with diamond and then the same process (gas infiltration method), which will be discussed later in section 6.3 in Chapter 6 as well, was used to fabricate these samples inside the mild steel moulds. For the other two methods a mild steel tube was used as a sample holder to cover and hold the MMC samples during the cutting process in the case of SPS samples and this tube was already utilised as a mould in the powder metallurgy route.

The abrasive resistance tests were made by cutting the MMCs samples by using commercial cut-off discs (Kennedy 230-4430K, supplied by Cromwell Industrial Tools, UK). The discs being 115 mm in diameter and 1 mm thick and contain aluminium oxide-60 micron abrasive particles [178] as shown in Figure (5-8). The estimation of abrasion resistance of the composite samples was achieved by comparing the reduction in diameter of the cut-off blade with the rate of cutting through the material during the cutting process. These tests have been done by a special mounted grinding device which has been designed for this purpose (Figure (7-7), where it is equipped with a camera and ruler in front of the disc to record how the disc diameter has reduced during the cutting process as will be discussed in more detail in Chapter 7. Three cutting tests were made on each sample and the recorded videos were made by other camera for each test have been divided into several images when one image was obtained every second by using (MATLAB R2014a) software in order to get a ruler reading every second in addition to photos which were taken by the camera.

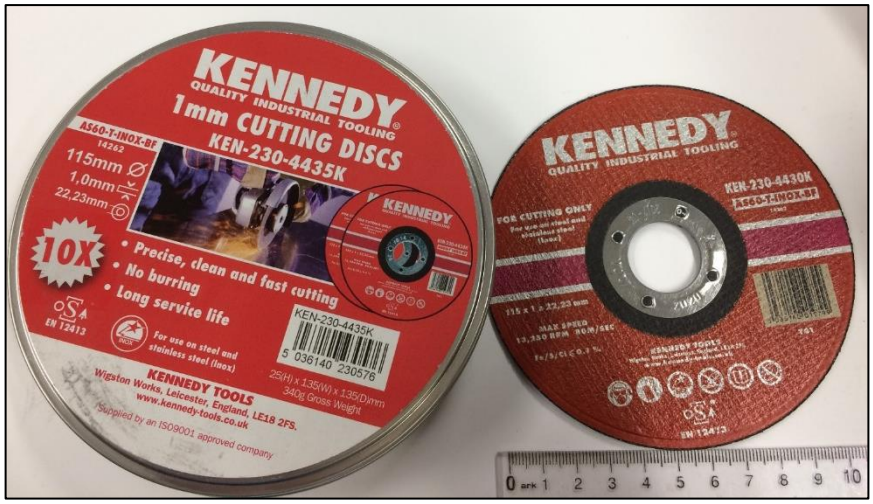

Figure (5-8): The abrasive cut-off discs used.

5.8 Temperature Measurement

A Dodocool GM300 laser infrared thermometer gun, which has measurement range of temperature: -50°C to 380°C, 0.1°C resolution, ± 1.5% accuracy at 0.12-1 m distance, was used to check temperature level achieved during the cutting process, as shown in Figure (5-9).

Figure (5-9): The laser infrared thermometer gun used in the experiments.

Chapter 6 Development of Methods to Produce MMCs

Security is an important issue in many contexts throughout the world. One particular set of examples comes from the use of portable angle grinders to overcome locks, barriers and physical security protection in areas such as banks, ATMs, jewellery stores and for theft of bicycles. The low cost and portability of these devices, combined with the speed at which they can cut through many materials used in these applications (such as high strength steels) has proliferated their use by criminals as was mentioned in more detail in the introduction chapter. It is therefore timely to focus on security obstacles to prevent thieves from holding these advantages, and this project attempts to do this by innovating new metallic matrix diamond composites, which could be an excellent solution. These materials are considered for manufacturability and performance, and for the industrial and commercial aspects.

Processing investigations proceeded by experimenting with three different production methods, which are now described, along with their results and processing development.

6.1 Particle Size and Chemical Analysis of Diamond

The particle size analysis has been done with one group of diamond particles to find the true size of the diamond particles and to be sure that it corresponds to the sieving analysis of particles, as shown in Figure (6-1) displays the distribution of the mean particle sizes (red curve peak) corresponding to about 400 µm or a bit more on x-axis of the graph (size classes), which is compatible with the range of the coarsest group, 35/40 grit (500-420 µm). Energy dispersive X-Ray spectroscopy (EDX) was applied to both diamond particles (coated/uncoated titanium) to verify impurity levels and the presence of the coated layer where needed. Examples are shown below in Figure (6-2 a and b). The chemical composition of the cut-off discs used was found by the EDX technique as well, as shown in Figure (6-3). This chemical composition was assessed to distinguish some of the elements which may be transferred to the cut composite surface during the cutting process.

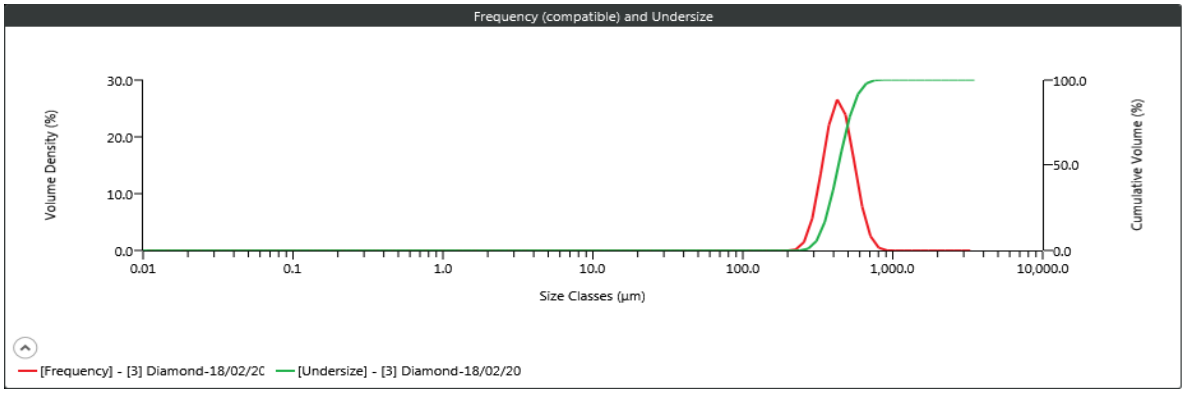

Figure (6-1): Particle size analysis of 35/40 grit (500-420) µ, performed with the Malvern Mastersizer.

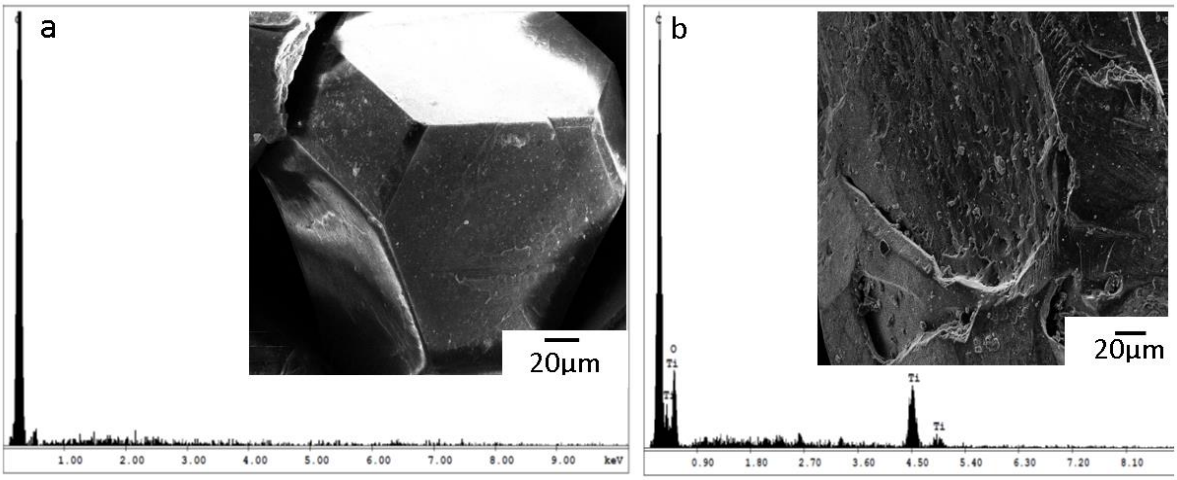

Figure (6-2): EDX analysis and SEM images of diamond particle surface for a) Uncoated Diamond b) coated Ti-Diamond.

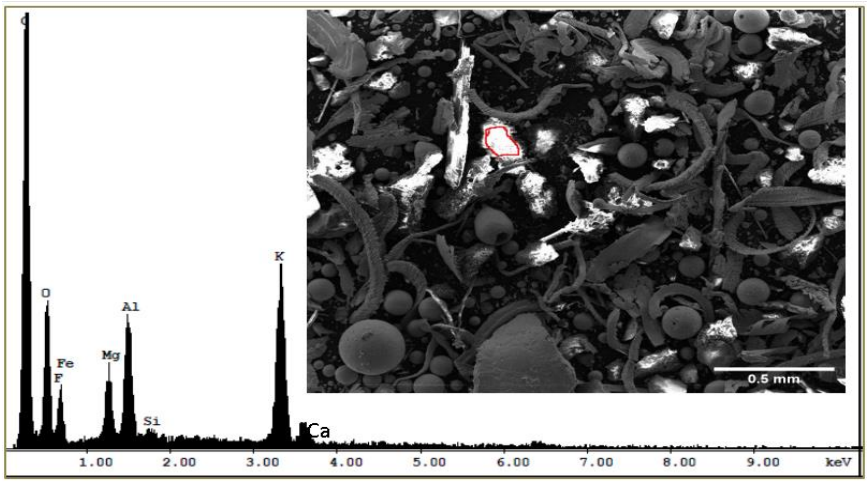

Figure (6-3): Cut-off Disc Composition determined by EDX analysis of the area highlighted with red in the inset SEM image.

6.2 Sample Design

All composites prepared for the abrasive cutting were fabricated in a mild steel cylinder in which they were retained after processing for testing. This eased fabrication in some cases, as there was no need to remove the material from a mould, and more importantly, acts as a simulation for a real application in security applications, where the material may be used as an infill. In some cases these consumable mild steel cylinders were utilized as a mould for production, particularly in the GI and PM routes, while in others the cylinder was added later, such as for the SPS route of production, as discussed in more detail in the earlier experimental chapter.

For reasons of availability of different materials three different sample diameters were employed. The differences in sample diameter depended on the production route; GI samples have a diameter of 7.7 mm, the diameter is 11mm for SPS samples and 8.6mm for PM samples. These sizes were firstly chosen to be as close as possible to the real diameter of security locks and secondarily due to mould design limitations.

6.3 Gas Infiltration (GI)

Diamond is a very attractive material in terms of many of its properties, but like other materials it has some limitations. One of these is poor performance in the air at higher temperatures, where diamond may become active either by oxidation or by conversion to its more stable form (graphite), which can also be promoted by the presence of oxygen [179]. Initial experiments used for manufacturing AMDCs were melted aluminium without an isolated atmosphere (in an open environment under air) before closing the system and applying the argon gas used to cause molten aluminium to penetrate in between diamond particles, which were already heated in the mould to the processing temperature (740˚C). These trials resulted in almost all of the diamond being converted to graphite. Figure (6-4) shows the sample produced, with almost all diamond lost by oxidation or conversion.

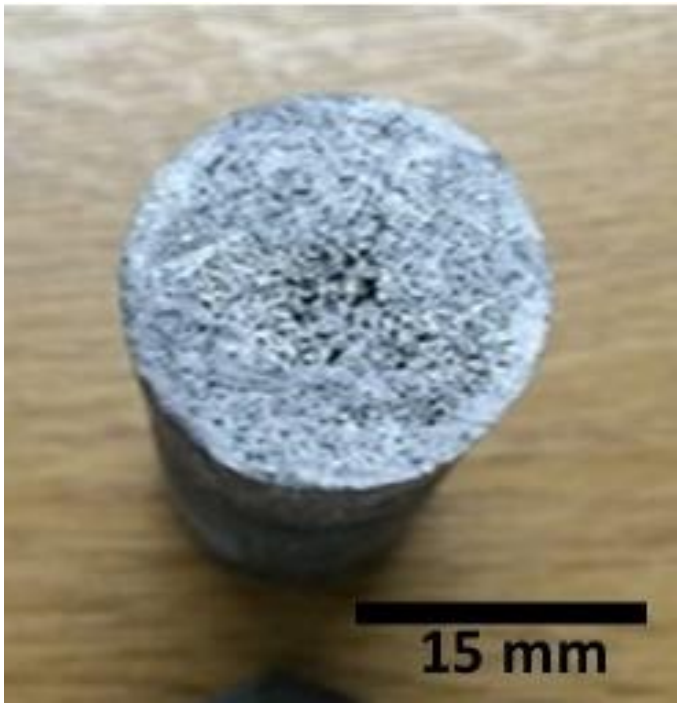

Figure (6-4): Failed Sample from an initial GI trial under air.

To overcome this problem an isolated chamber was used with vacuum and argon gas regulation capability. The pump to create vacuum was left running throughout the melting process, until the infiltration of molten metal, which is done by opening a valve to permit ingress of argon gas; this in turn pressurises the molten metal which penetrates the bed of diamond particles.

This infiltration rig, shown in Figure (6-5), was connected to the vacuum-argon gas system, and is made from a 304 stainless steel alloy cylinder fitting into flanges on stainless steel end plates with carbon paper gaskets. This is considered to be an isolated chamber to process the composites in. The cylinder was 120 mm height and starts with a larger diameter on the gas pressure supply side where the piece of metal to be infiltrated is placed. The other side the (bottom side) is narrower, and this is where the shaped mould (for a cutting test sample or Charpy impact sample) was placed. The chamber was designed in this configuration to achieve better penetration of molten metal into the diamond particle preform.

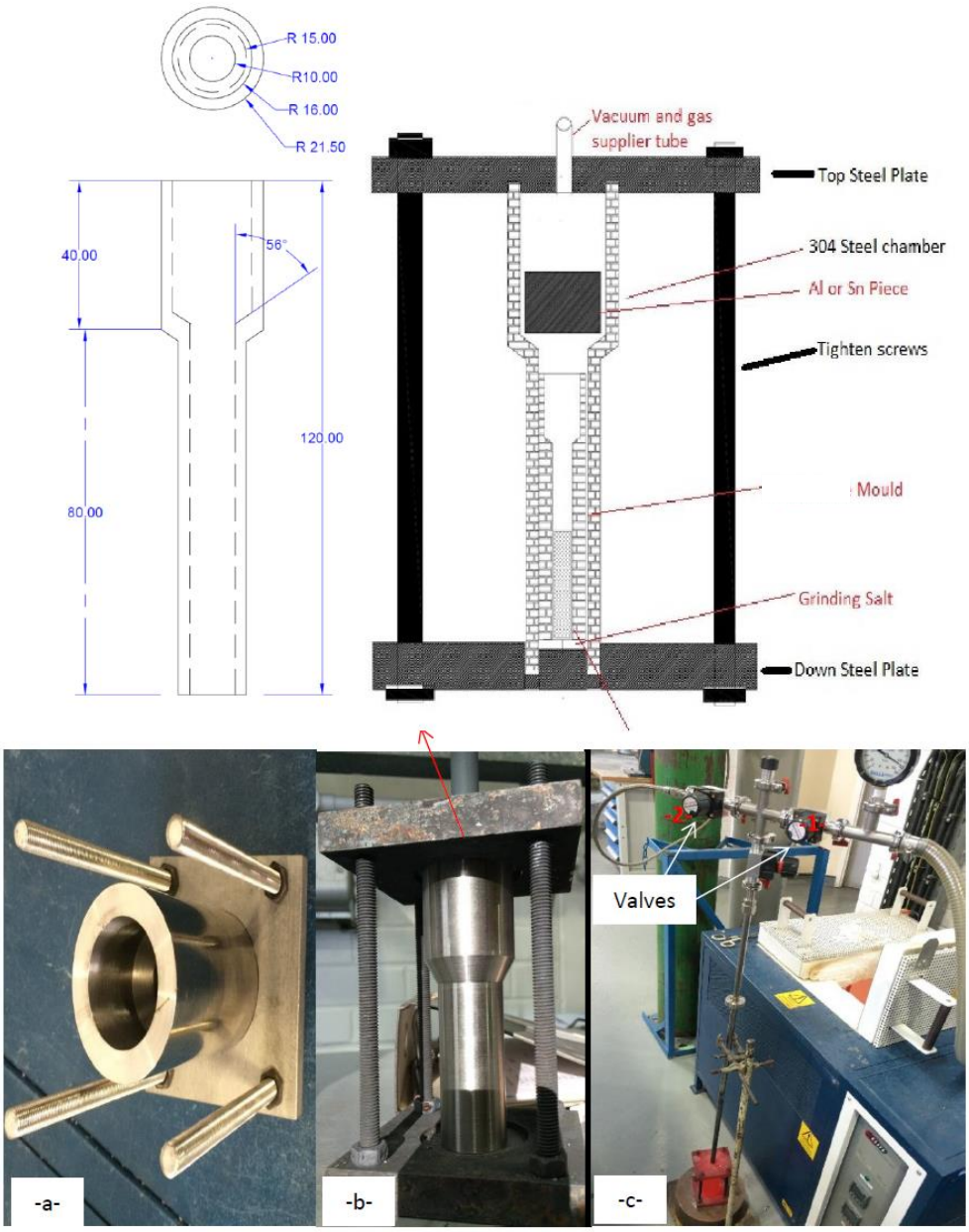

Figure (6-5): (-a-), (-b-) Steps of GI rig design and (-c-) Infiltration system.

The cutting test mould was compacted with preformed reinforcement particles (diamond or ceramic, which was used for comparison) and designed to fit inside the chamber during the casting process. The moulds are designed to help molten metal to penetrate to preformed particles by changing their diameter from the wide upper to narrow bottom part as shown in Figure (6-6). The widest upper part will help to collect and accommodate molten metal at top of the preform and give good enough contact with the edge of the mould such that gas pressure applied will push liquid metal into the narrow end part of the

mould. The shape change also has the advantage that it reduces the wastage of the diamond particles, and post manufacture machining, by making the net shape required for testing. All these moulds and the infiltration rig, apart from the vacuum-gas valve system, were ordered and designed the authour of this thesis and machined in the workshop of Electrical and Electronic Engineering, The University of Sheffield.

Figure (6-6): Machined moulds used for GI processing of cutting test samples.

For the impact test a special mould was designed to make Charpy impact sample. The idea of setting up this mould was derived in the same way as for the cutting test moulds, and it has the same outer dimensions. The mould consisted of two main pieces as shown in Figure

(6-7), which were fabricated to attach together in the chamber to form the Charpy impact sample in. These were made from 304 stainless steel to retain dimensional accuracy under infiltration processing temperature. After attaching the two parts into the chamber, the reinforcement diamond particles were compacted in, to prepare the preform for infiltration by putting the piece of metal which will become the matrix above the preform at the top of the chamber. All other procedures were kept the same as for making the cutting test samples.

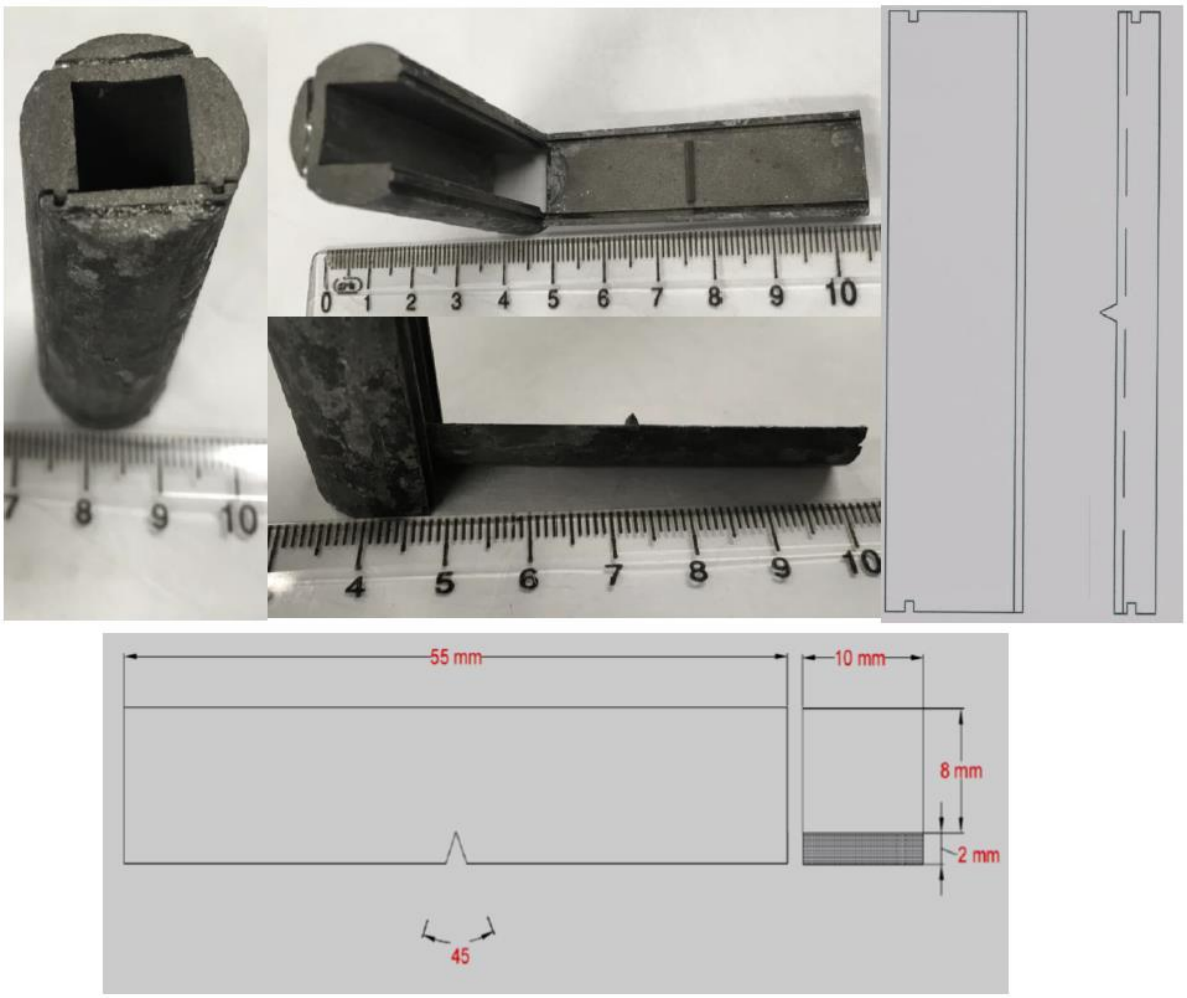

Figure (6-7): The design of Charpy impact mould and resulting sample.

6.3.1 Infiltration Processes

All the infiltration process steps are described in the schematic diagram in Figure (6-8).

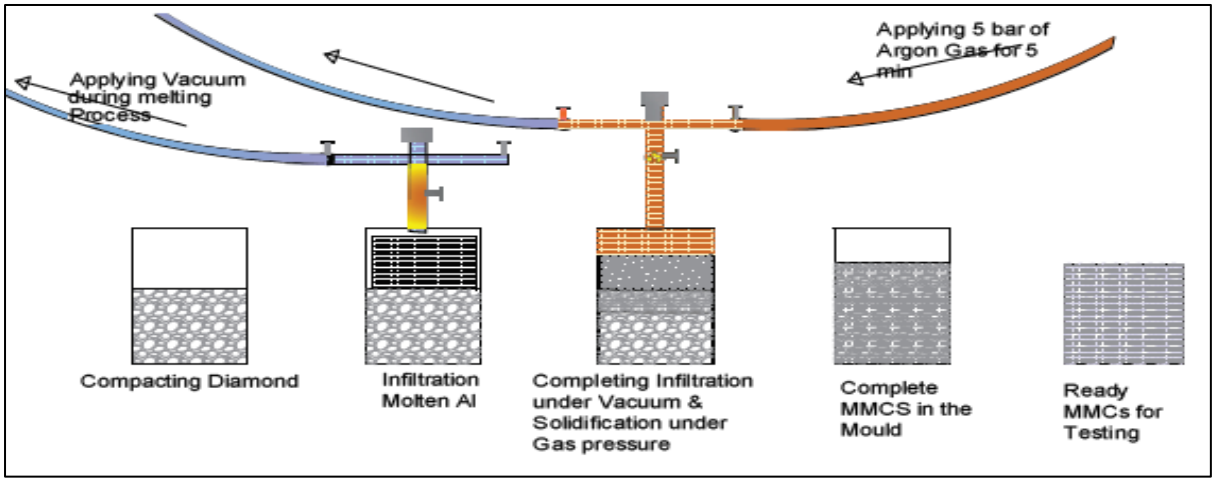

Figure (6-8): Schematic diagram showing infiltration process steps.

The gas pressure was estimated depending on capillarity and the Young equation for molten metal wettability of ceramics.

$$P_i = 2\gamma \frac{\cos\theta}{r\,\rho\,g} \quad \text{.....Equation (6-1)}$$

where P_i is the infiltration pressure, γ is the surface tension of the molten aluminum (0.86 Nm [180], ɵ is the contact angle between the molten aluminum and the moulded compact material (this value is not widely reported, but has been measured for carbon as about 79°[181]), r is the radius of pores, ρ the liquid density and g is the acceleration due to gravity. To find the possible pore size (r), which can be formed between compacted reinforcement particles in the current work the 40/35 grade particle was taken, which has 420-500µm particle size, to calculate the possible pore size, as this grade was used to reinforce most of the produced composites. The pore size can be approximately calculated if the reinforcement particles are assumed to be spherical in shape and if three of them would meet to form the hole, shown by the auto CAD drawing in Figure (6-9) where the particles with 420 µm diameter (0.42 mm) have been drawn in two dimensions. Where these three circles meet there is space for a small circle, which represents the pore size in the powder bed. Other triangular spaces around this circle have been neglected because the diamond particles are not perfectly uniform spheres, and such spaces will not be precise.

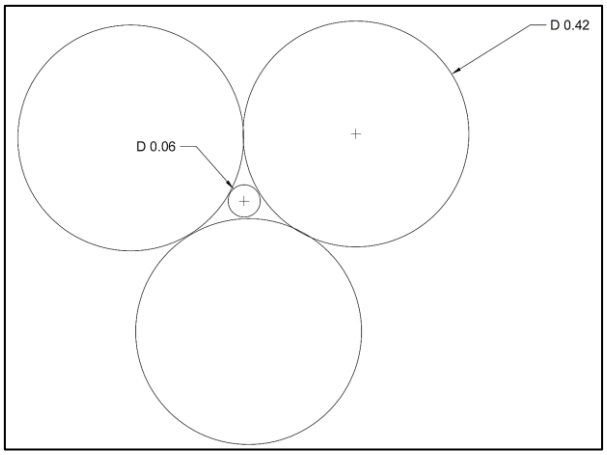

Figure (6-9): Auto CAD diagram showing the possible porosity size between diamond particles, assuming they have a spherical form.

6.4 Spark Plasma Sintering (SPS)

To explore additional elements and alloys with higher melting points as matrices it was important to find a processing method that would not affect the diamond structure itself (the instability of diamond at high temperature was one crucial challenge for this work). To address this, powder metallurgy technique, Spark Plasma Sintering (SPS), was chosen as another production method as this exposes the mixture for a relatively short time to high temperatures, and the metal remains in the solid state. The technique can operate for high melting point elements which would not have been possible in GI such as Ti, Ni and Cu, and in addition can be used for Al itself. The melting point of these elements is higher than the decomposition range or graphitisation limit of the diamond, which is started at above about 700 ℃ in an oxygen environment [32], [60] and a little higher in isolated environment either vacuumed or with inert gas. In these experiments the sintering temperatures were allocated for each element separately to allow sufficient temperature for bonding particles while minimizing the risk of oxidizing or converting diamond to graphite. Suitable sintering temperatures were in the range 57-83% of the melting point of the matrices, which means the sensitivity of diamond to high temperature was the main limitation in setting these temperatures and a balance was made between this limitation and obtaining a composite with acceptable interfacial bonding. The maximum sintering temperature reached was 950℃ for the Ti matrix with 800℃ used for Ni, 700℃ for Cu and 550℃ for Al. These temperature limits were kept the same in the PM production method, which is described later in the next section of this chapter. Special SPS moulds were designed for this purpose, as shown in Figure (6-10). Figure (6-11) shows the SPS

machine, which was used to produce samples, more details about it and the SPS processes were previously discussed in the experimental chapter (section 5.3).

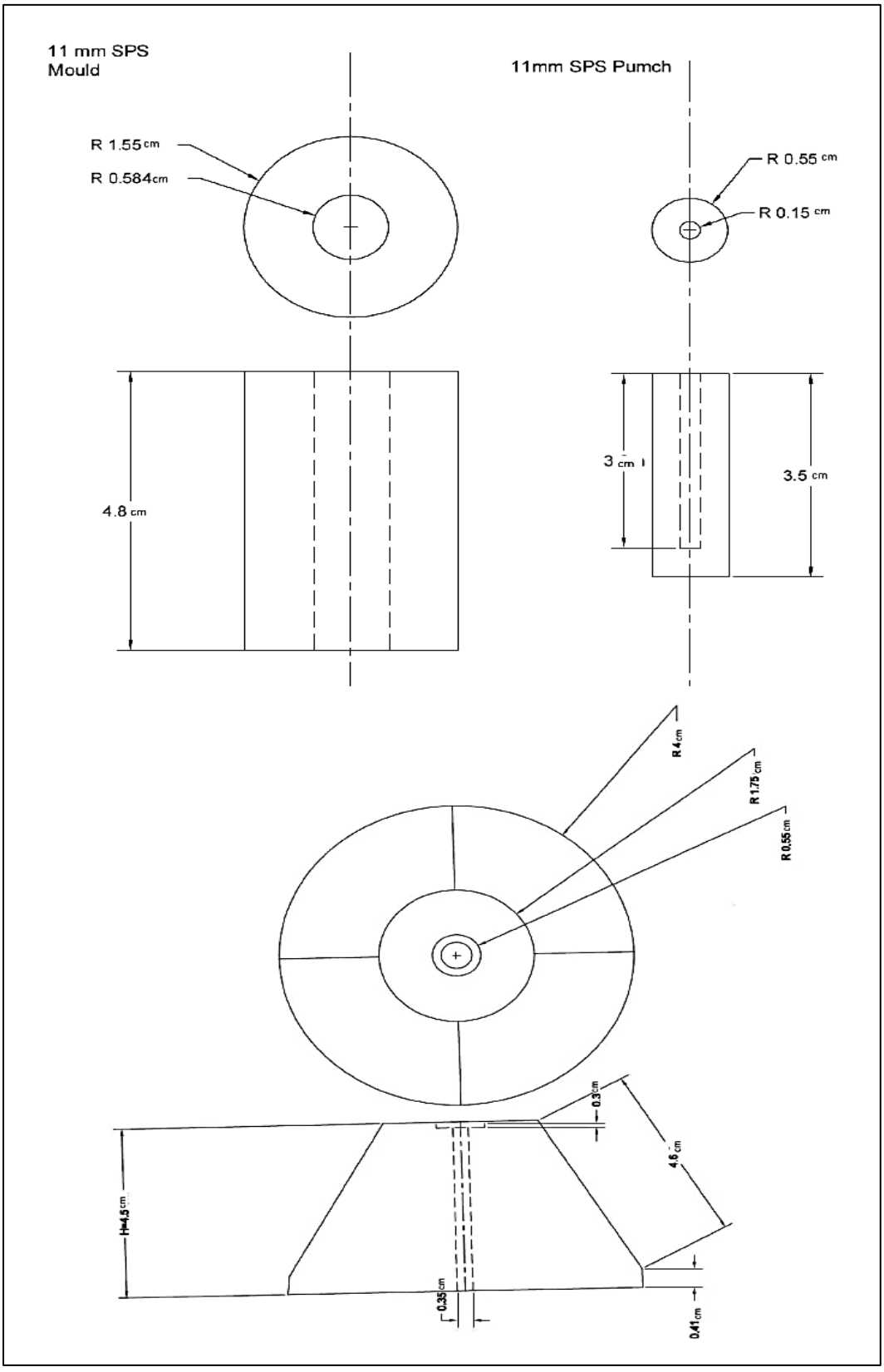

Figure (6-10): SPS mould designed by Auto CAD.

Figure (6-11): The SPS machine which was used for SPS sintering.

6.5 Conventional Powder Metallurgy (PM)

The powder metallurgy technique, with sintering under argon flow, was applied to create samples allowing comparison of the techniques discussed before with more conventional methods. This technique uses a significantly longer dwell time when compared with SPS, and this allows the creation of bonds between different particles which make up the mixture. Where there is a reinforcement, as in this case, and multiple phases present, either this bonding occurs by particular chemical interfacial reactions or mechanical fixation (perfectly surrounding the reinforcement by matrix) which may be aided by differential contraction due to thermal effects. Mild steel tube moulds were utilized with 14.2 mm outer diameter and 8.6 mm inner diameter to manufacture PM samples, as shown in Figure (6-12) below.

Figure (6-12): PM moulds and punches.

The powder, which would become the matrix, was mixed with diamond particles at 50 Vol% (calculated depending on the real density of the composite).

We may, for example, wish to produce Ti reinforced with 50 vol. % of diamond (diamond density is 3.55 g/cm^3 and Ti density is 4.5 g/cm^3), in the form of a rod 30 mm in length and 8.6 mm in diameter. We can find the required volume of both matrix and reinforcement by applying equation (5-1) pp. 80, after calculating the volume of the tube to be filled as follows:

V of 30 mm long 8.6 mm diameter tube = $3.14 \times (0.43)^2 \times 3 = 1.74$ cm^3

This volume of tube × 50% (filled volume required for each component)

= 0.87 cm^3. Applying this value in equation (5-1) to find the mass of each component in grams

$M_{Dia} = \rho_{Dia} \times V_{Dia} = 3.55 \times 0.871 = 3.10$ g of diamond

$M_{Ti} = \rho_{Ti} \times V_{Ti} = 4.5 \times 0.871 = 3.92$ g of titanium

The same procedures were applied to calculate all materials volume fractions in both methods of production (PM and SPS)**.** Then, the mixture was compacted and pressed inside the mould by applying 70 MPa compacting pressure from both sides of the tube

mould using two steel punches to improve the homogeneity of the compaction. This is shown in Figure (6-12). Those compacted composites were put in a Lenton tube furnace (Leicestershire, England) with max. operation temp. 1600°C Figure (6-13) for sintering under argon flow, using a heating rate of 10℃/min, with all materials held at their respective sintering temperatures for 1 hour. The temperature was chosen depending on matrices (950°C for Ti, 800°C for Ni, 700°C for Cu and 550°C for Al, the same range of temperatures which were applied with SPS) then left to cool inside the furnace. The samples were used to compare PM products with other products, which have been made by other techniques.

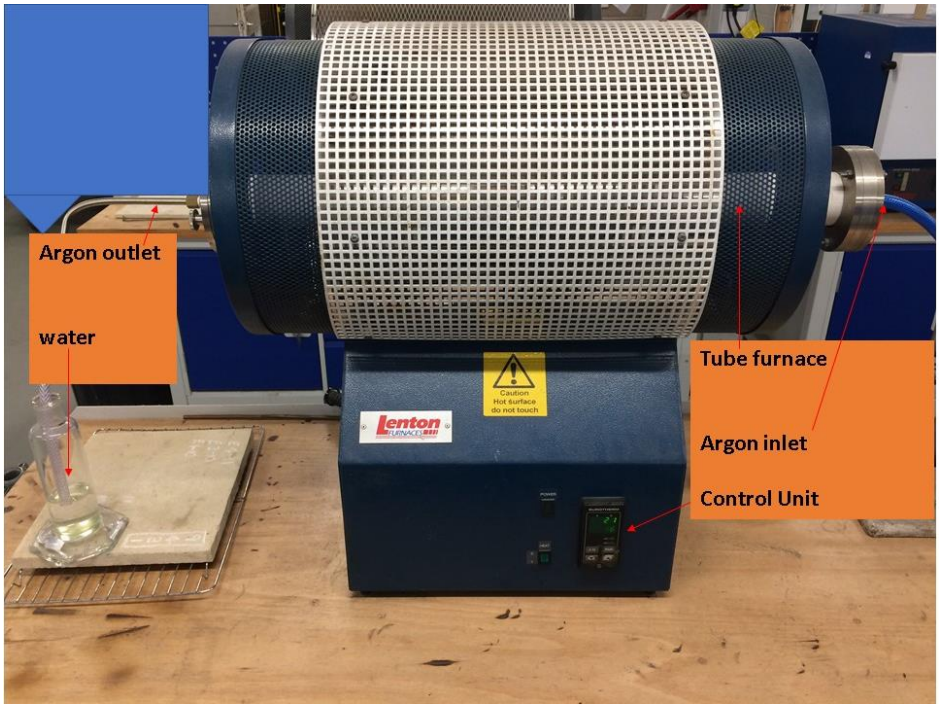

Figure (6-13): Tube furnace used for PM sintering.

6.6 Mechanical Properties of Produced Composites

The experimental results obtained during this study and their discussion will be shown and analysed in this section**.** These results can be divided into two groups which are microstructural results such as SEM imaging and X-Ray diffraction, and mechanical such as impact, hardness and abrasion resistance results (cutting results). The results for both groups of composites, which are reinforced with coated/uncoated diamond, will be included in this section. In addition, the analysis of particle size and purity for the diamond particles is reported, which was done at the beginning of the experimental work.

6.6.1 Hardness

The hardness of all produced composites was measured using a Vicker's micro indentation hardness device, where a load is applied via a diamond pyramid indenter with 136˚ angle and 0.3 kg load for 15 sec, on the surface of the composite sample. The hardness measurement was carefully done to prevent the indenter impacting the diamond particles and keeping measurement in the central region of the matrices, at least 5 readings about 5 indent diameters a way from a particle. The hardness results, which are shown in Table (6-1), reveal that the hardness of the matrix is not a crucial property governing the wear properties, as will be shown in chapters 8 and 9, where, for example Ti, Ni, and Cu do not have wear properties in proportion to their hardness values.

Table (6-1): Hardness of MMDCs and MMCCs.

Composites	Vickers hardness (kg/mm^2) GI	Vickers hardness (kg/mm^2) SPS	Vickers hardness (kg/mm^2) PM
Al-50%Dia.	105.3	143.2	134.5
Sn-50%Dia.	11.2	--	--
Ni-50%Dia.	--	122.5	106.6
Cu-50%Dia.	--	125.4	114.6
Ti-50%Dia.	--	325.7	375
Al-20%Dia.-30%SiC	115.25	--	--
Al-20%-30% Al_2O_3	114.7	--	--
Al-50% Al_2O_3	103.25	--	--
Al-50%SiC	106.6	--	--
Ti-50% Al_2O_3			260
Ti-50%SiC			283
Epoxy50% (Gravity Infiltration)	16.25	--	--

In addition to the hardness test, Charpy impact testing was also performed on the GI produced composites (Al and Sn based composites), and the results show that the impact energy of GI AMDCs was about 8.6 J, while the impact energy of Sn-base GI SMDCs was about 2.6 J. Both were required to break $1cm^2$ cross section with 45° notched Charpy impact samples (see Figure (6-7), three samples were tested from each composite.

6.7 Structure Investigation of Produced MMCs

All composites produced were investigated to make sure they had the imtended volume reinforcement after exposure to the processing conditions such as pressure, temperature and possible chemical reactions that may occur between composite constituents. These conditions may affect the relative volume fraction of reinforcement. The measurement of volume fraction was done by analysing selected SEM images of composites with Image J software to calculate the percentage area of matrix to whole image area. As an example of the measurement, one process is shown in Figure (6-14). Table (6-2) displays the measured volume fraction of reinforcement and matrix for all composites.

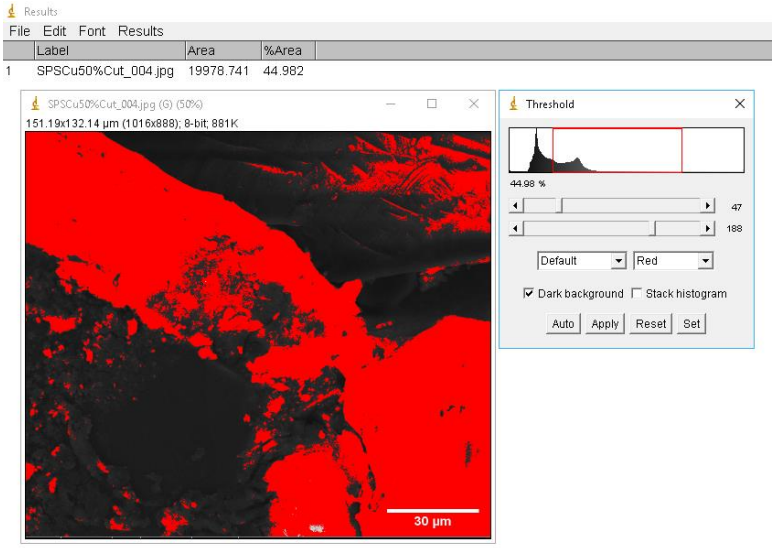

Figure (6-14): Example of measurement of volume fraction of reinforcement of SPS Cu–50%Diamond, reinforced with 420-500 µm diamond particle size.

Table (6-2): Volume fraction of reinforcement and matrix in various MMDCs and MMCCs.

Composites	Matrix vol. %	Reinforcement vol. %
GI Al-50%Dia.	50.0	50.0
PM Al-50%Dia.	50.7	49.3
SPS Al-50%Dia.	47.1	51.9
Sn-50%Dia.	52.4	47.6
SPS Ni-50%Dia.	47.8	52.2

PM Ni-50%Dia.	47.6	52.4
SPS Cu-50%Dia.	45.0	55.0
PM Cu-50%Dia.	51.3	48.7
SPS Ti-5%Dia.	93.5	6.5
SPS Ti-15%Dia.	84.3	15.7
SPS Ti-30%Dia.	71	29
SPS Ti-50%Dia.	47.4	52.6
PM Ti-5%Dia.	94.6	5.4
PM Ti-15%Dia.	84.7	15.3
PM Ti-30%Dia.	69.3	30.7
PM Ti-50%Dia.	48.0	52.0
Epoxy	51.0	49.0
Al20-30 % Sic	53.1	46.9
Al20-30% Al_2O_3	51.2	48.8
Al-50% Al_2O_3	51.4	48.6
Al-50%Sic	48.0	52.0
Ti-50% Al_2O_3	52.9	47.1
Ti-50%Sic	47.5	52.5

6.7.1 Structure of AMDC Produced by GI

In the current study, most microstructural observations for metal-diamond composites were made under a Scanning Electron Microscope (SEM) because the preparation of samples for optical microscopy required a flat and smooth surface. It was attempted to achieve these surface conditions by conventional procedures of preparation and finishing samples, but this was not found to be possible, particularly with the existence of diamond particles in relatively hard matrices like Ti, Ni and Cu or even with less hard matrices like Al it was not easy to get high quality smooth surfaces, as is clear in optical images of AMDCs, Figure (6-15) and Figure (6-16). Other authors have made efforts on this aspect before and have reported the same difficulties [93], [94].

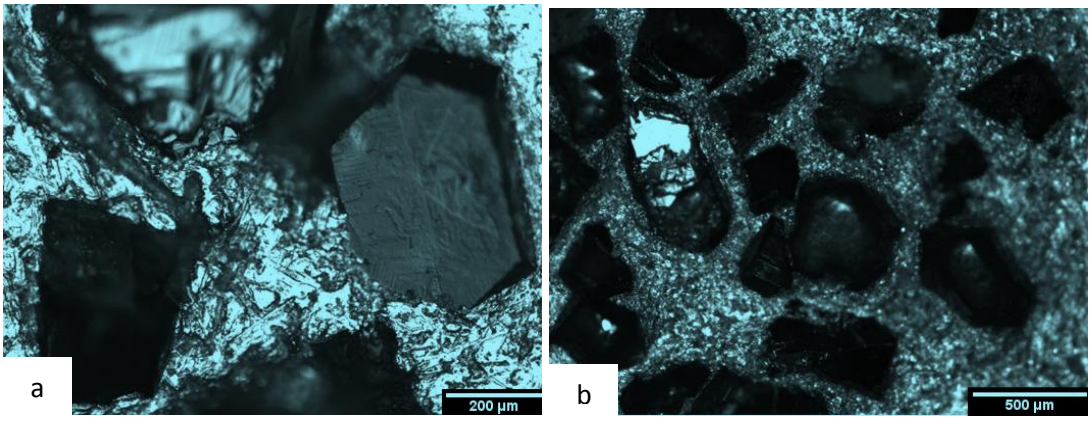

Figure (6-15): Optical microscopic images a- A_1 sample (AMDCs reinforced with Ti-coated 35/40 grit (420-500 µm) diamond particles) and b-A sample (AMDCs reinforced with uncoated 35/40 grit (420-500 µm) diamond particles).

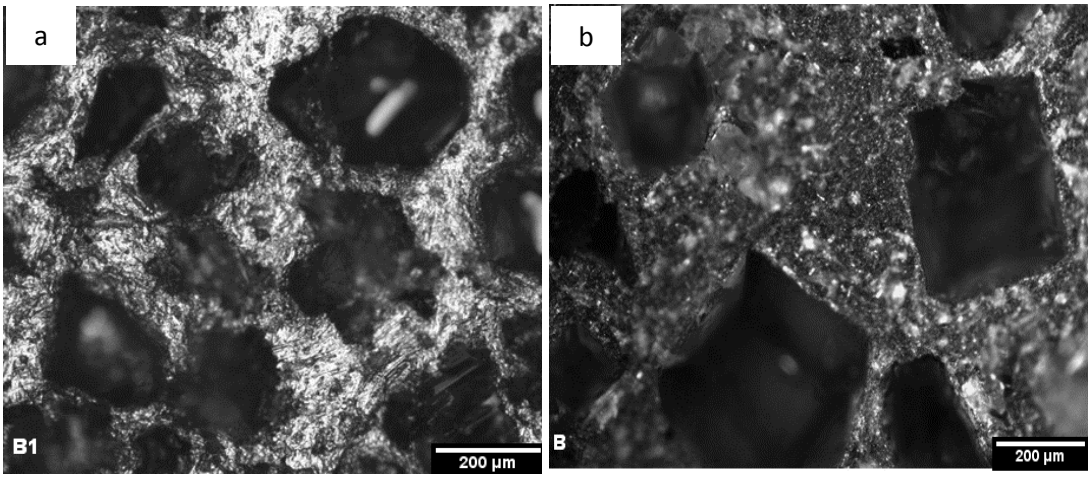

Figure (6-16): Optical microscopic image of B_1 sample (AMDCs reinforced with Ti-coated 60/70 grit(212-250 µm) diamond particles) and b) B sample (AMDCs reinforced with uncoated 60/70 grit(212-250 µm) diamond particles).

In AMDCs, SEM inspection appears to show preferable planes for the bonding between aluminium matrix and diamond for both groups (coated/uncoated) of reinforcement. These planes may be cubic {100} planes in the diamond crystal, whereas others are not preferable for bonding which are octahedron {111} planes. This conclusion corresponds with other suggestions that are reported in literature [93]–[95] as shown in Figure (6-18 a and b). Nevertheless, exploring preferable differences between {100} and {101} planes could be

beneficial for future work, because there is no clear evidence; previous authors have suggested that the {100} have preferential interaction.

Also the selective planes for interaction of matrix-reinforcement were clear for 250-212 µm (uncoated B, coated B_1) as shown Figure (6-19), but they were difficult to recognize among cubic {100} or rhombic dodecahedron {101} or octahedron {111} for 75-63 µm (uncoated C, coated C_1) because the particle size was very small as shown in Figure (6-20).

Another important observation noticed that with the coated Ti diamond particles SEM imaging suggested better bonding and interaction with the aluminium matrix at the interface than uncoated diamond, as shown in Figure (6-21 a) and b) for aluminium-diamond with particle size 500-420 µm (uncoated A, coated A_1). This interaction can be related to the Ti active element present at the surface of the diamond. The Ti at the diamond surface is expected to interact with molten aluminium by dissolving and forming either solid solution when the interaction has excess aluminium, that the face of coated layer in contact with matrix over 665 °C [182] (less than the processing temperature 780 °C) or create some intermetallic compound at the interfaces not in direct contact with matrix, which will be enriched by Ti (over 24 at. % Ti) as shown in phase diagram Figure (6-17), apart from Al_4C_3 which may also be found at this interface, although the amount is less than at uncoated diamond-aluminium interface as shown in the Raman spectrum Figure (6-27) and will be revealed in more detail in the next section by XRD Figure (6-28), pp. 115 and 117, respectively.

In another two composites with smaller particle sizes (250-212 and 75-63 µm) there also appeared under SEM inspection differences in interfacial bonding between reinforcement and matrices for coated and uncoated diamond, where there is a clear interaction at the interface of coated diamond with matrix in Figure (6-22) and Figure (6-23).

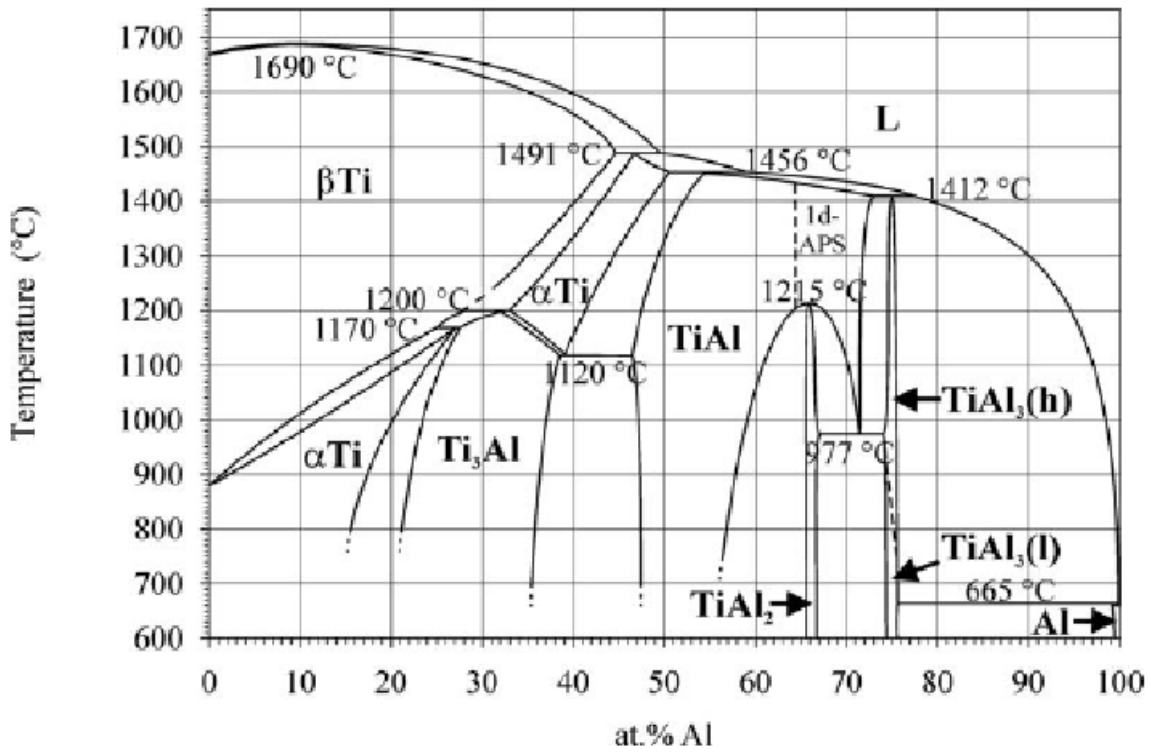

Figure (6-17): Phase diagram of Al-Ti [182].

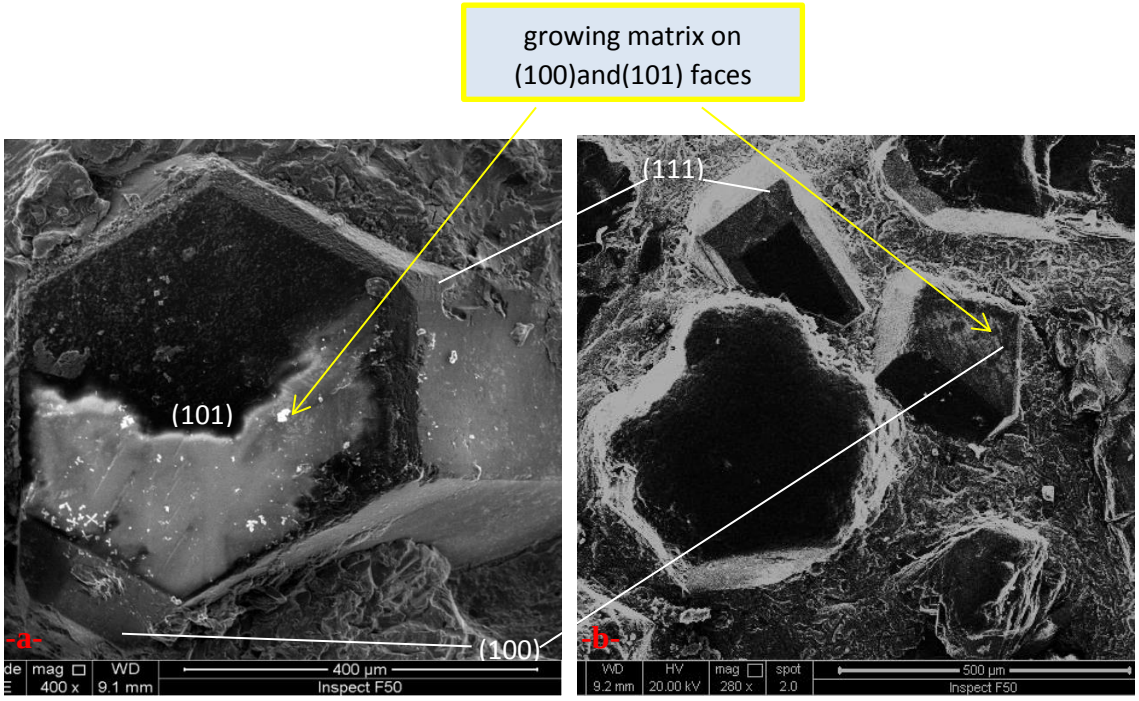

Figure (6-18) : a- Al- uncoated diamond composite with particle size (550-425) µm (Sample A) and b- Al- coated diamond composite with particle size (550-425) µm (Sample A_1).

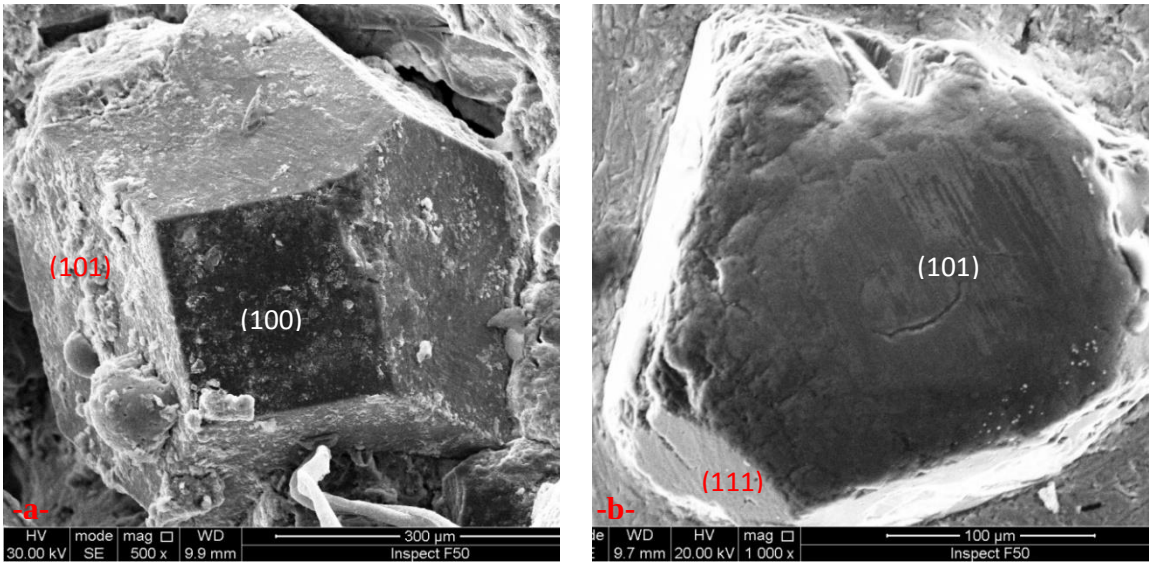

Figure (6-19) : a- Al- uncoated diamond composite with particle size (250-212) µm (Sample B) and b- Al- coated diamond composite with particle size (250-212) µm (Sample B_1).

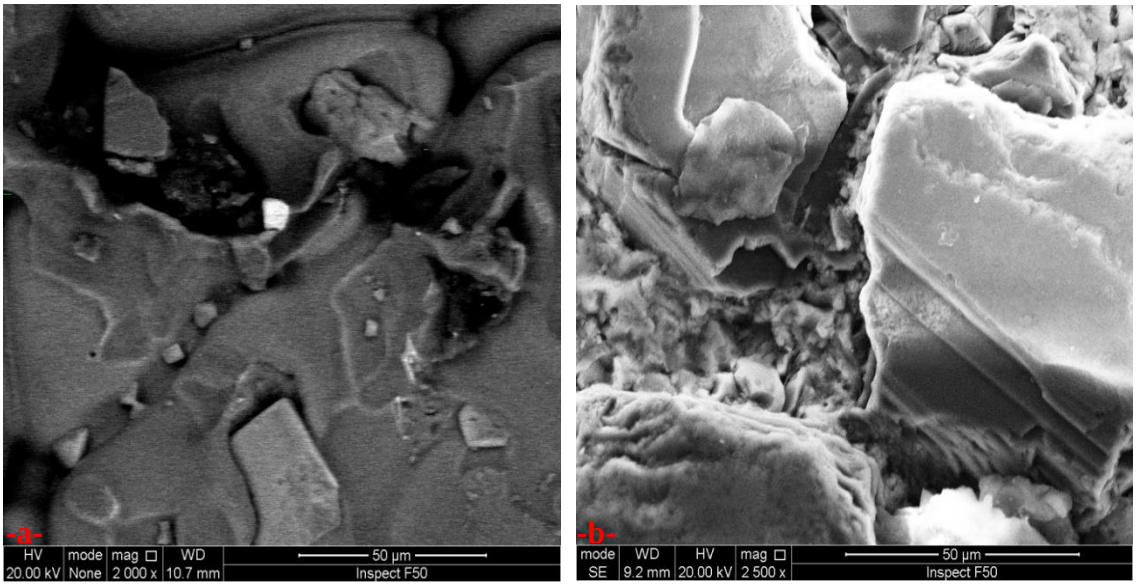

Figure (6-20): a- Al- uncoated diamond composite with particle size (75-63) µm (Sample C) and b- Al- coated diamond composite with particle size (75-63) µm (Sample C_1).

The SEM images of fracture surfaces reveal that the carbide layer which is formed on the surface of Ti-coated diamond is more adhesively homogenous on the surface. This is probably related to the presence of the Ti layer which is likely to react directly with the aluminium matrix by forming a thin layer of titanium aluminide. Other alternatives are that the bonding occurs by Van der Waals bonding with the aluminium or by the formation of aluminium carbides. However, in this case the thickness and configuration of the

interfacial compound was more homogenous and thinner than in the case of uncoated diamond. In particular the observations suggest that the brittle form of carbide (Al_4C_3) may be prevented from forming due to the Ti layer, or at least be very limited in extent as was shown in XRD patterns and Raman spectroscopic shift, Figure (6-28) and Figure (6-27). The optical microscope images, Figure (6-15 a and b), show differences at the interfaces in the interaction shape of coated and uncoated diamond with the aluminium matrix. The interface in the A_1 sample appears rougher with more interaction in comparison with the A sample, as a result of the coated layer. In the A sample there is an interfacial layer formed, possibly from reaction between the diamond surface and aluminium to form Al_4C_3. This carbide may coexist with graphitised diamond at the surface, which would be supported by the Raman spectrum analysis Figure (6-27).

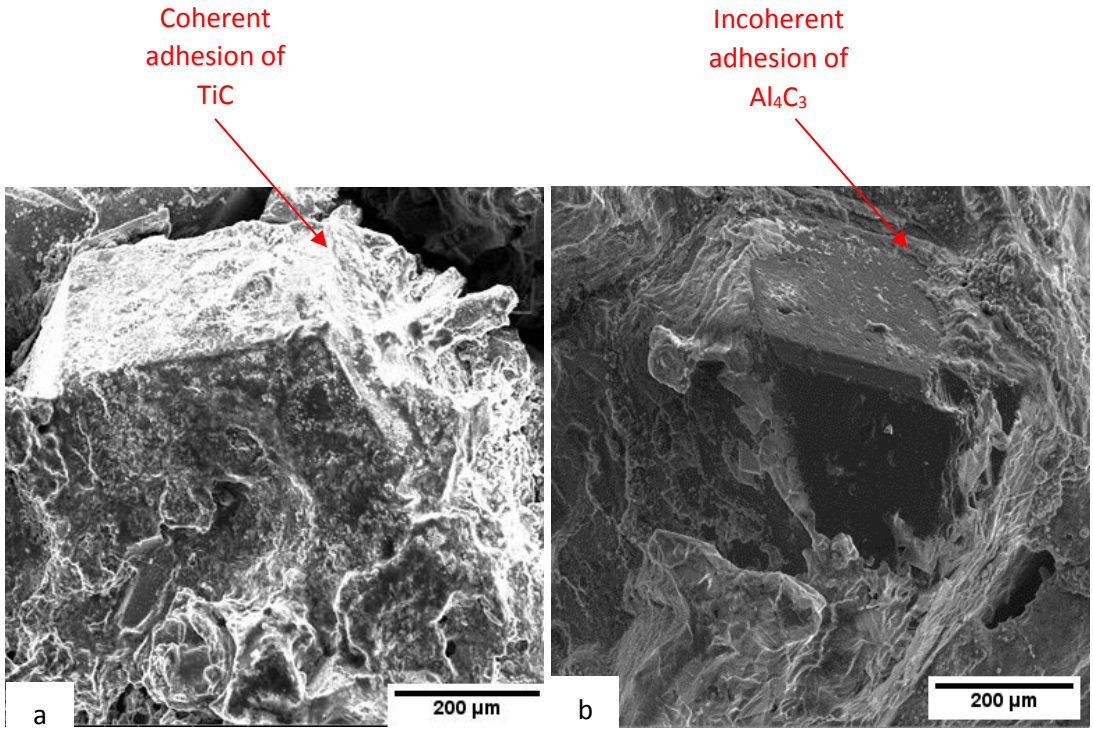

Figure (6-21): SEM images of fracture surface a- A_1 sample (AMDCs reinforced with Ti-coated 35/40 grit(420-500 µm) diamond particles) and b-A sample(AMDCs reinforced with uncoated 35/40 grit(420-500 µm) diamond particles).

The Ti layer coating leads to a decrease in interfacial energy for bonding by decreasing the contact angle between molten Al and diamond from 79˚ to about 60˚ [183] and that can prevent formation of aluminium carbides especially (Al_4C_3) which is considered a brittle form of carbides [184], [185], as its peaks appear more clearly with uncoated

diamond reinforcement from the Raman spectrum Figure (6-27) and XRD pattern Figure (6-28). All these reasons lead to sufficient interfacial bonding, which can prevent easily pulling out of reinforcement particles from the matrix, this would happen in uncoated reinforced composites due to the layer of brittle carbides at the interface as clearly revealed by SEM shown in Figure **(**6-21).

Some cracks, which possibly come from growth of existing cracks through the particles as well during the process are seen in the microscopic images Figure (6-16). This shows that the interfaces in B and B_1 are different, where the interface in B_1 is thinner and tends to adopt a zigzag bonding shape, while the interface in B was thicker and more linear and smooth. The SEM images in Figure (6-22) clearly reveal that the micro cracks in coated particles (Figure (6-22 a)) lead to the platelets of carbide formed at the reaction layer to be homogenously distributed, with a snowflake-like appearance on the coated surface. Meanwhile the uncoated particles show an interfacial compound which is inhomogenously distributed and even indicates some areas of diamond surface which do not have any impression of adherent matrix, (Figure (6-22 b)).

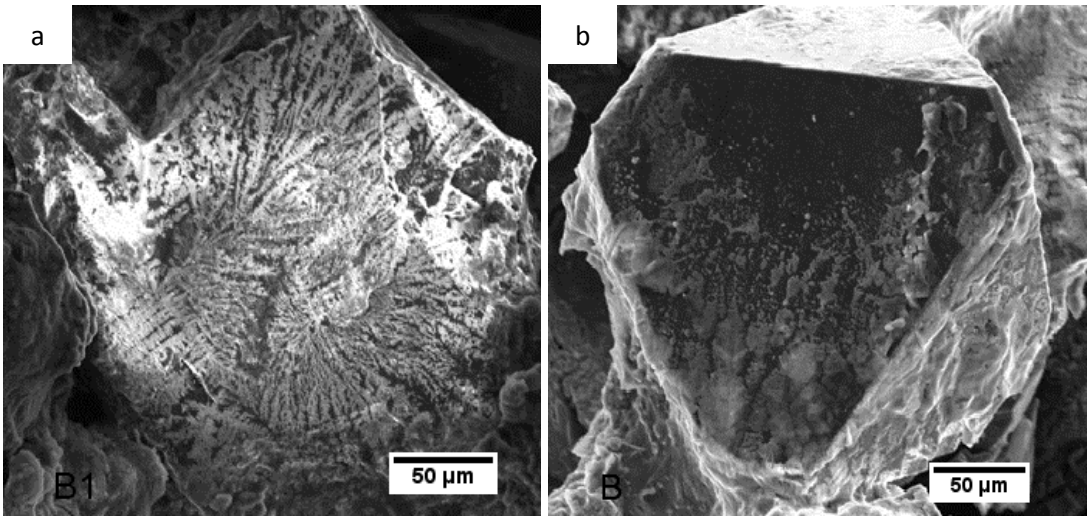

Figure (6-22): SEM images of broken surfaces of a) B_1 sample (AMDCs reinforced with Ti- coated 60/70 grit(212-250 µm) diamond particles) and b) B sample(AMDCs reinforced with uncoated 60/70 grit(212-250 µm) diamond particles).

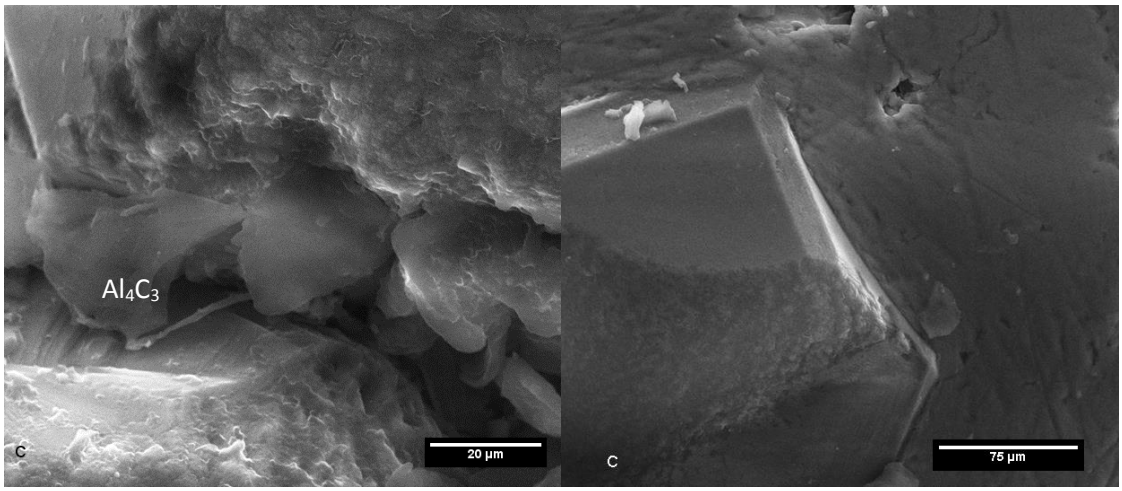

Figure (6-23): SEM images of C sample (AMDCs reinforced with uncoated 200/230 grit (75-63 µm) diamond particles). The images show clean and smooth interfaces with some platelet-shaped compound which is thought to be Al_4C_3.

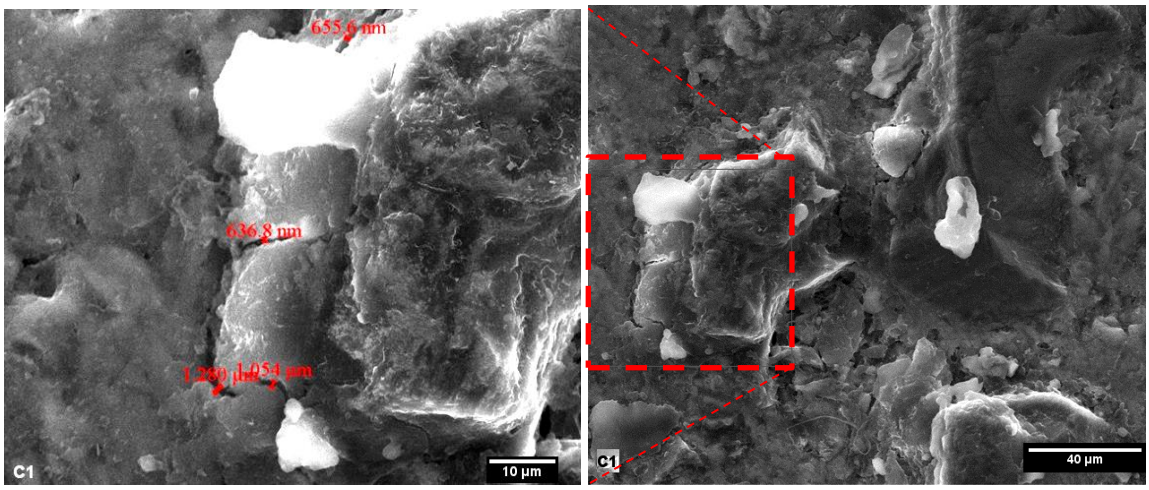

Figure (6-24): SEM images of C_1 sample (AMDCs reinforced with Ti-coated 230/200 grit(63-75 µm) diamond particles) shows some particles has been cracked during the casting process.

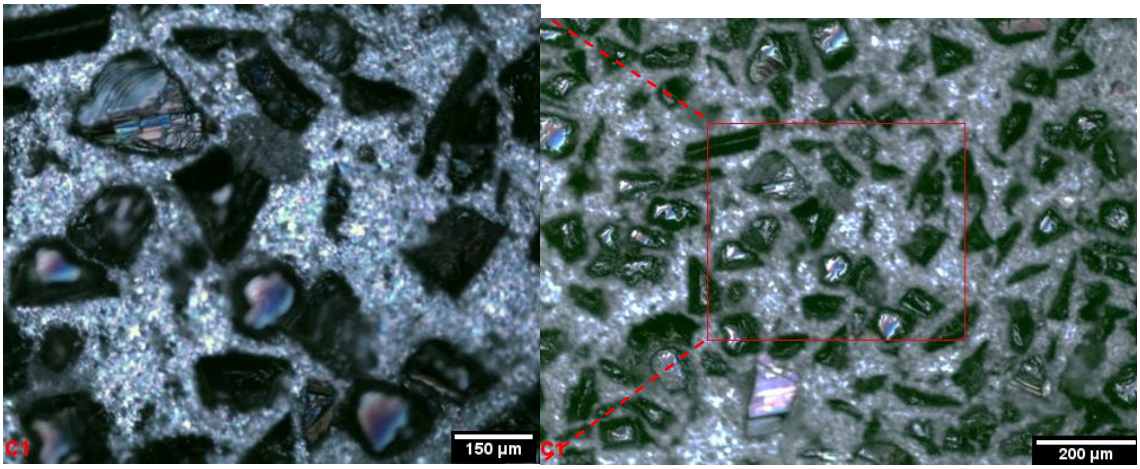

Figure (6-25): Optical microscopic images of the C_1 sample (AMDCs reinforced with Ti-coated 230/200 grit(63-75 µm) diamond particles)showing some cracked particles.

The cracks in the Ti-coated layer, that appear in Figure (6-24) and Figure (6-25), may have been generated during manufacture because the Ti coated diamond particles experience heating from room temperature until 780˚C. This will generate thermal stresses between the diamond particles and the coated Ti layer because of the differences in thermal expansion between coating and particles [186]. Tensile and compressive stresses may be generated in the coated layer as a result of the restriction of the low thermal expansion coefficient of the diamond, while the diamond itself could experience some small degree of tensile stress as a result of higher Ti thermal expansion, recognizing that the amount of coating (Ti coating thickness is about 2 µm only) is very much less than the diamond, with generated stresses correspondingly lower. Tensile stresses developing into compression stresses have been reported before in MMCs with rising processing temperature [187]. To explore this further, we can calculate the thermal stress that can be induced in an individual coated particle during heating to the process temperature of 780˚C, ignoring the aluminium matrix effects and dealing with the coating as a uniform, well-adhered layer around particle. The expected stress behavior of Ti-coated diamond particle is explained schematically in Figure (6-26). Equations 6-1 and 6-2 were applied to evaluate thermal stresses, which could be generated in one direction (as an assumption to simplify the calculation).

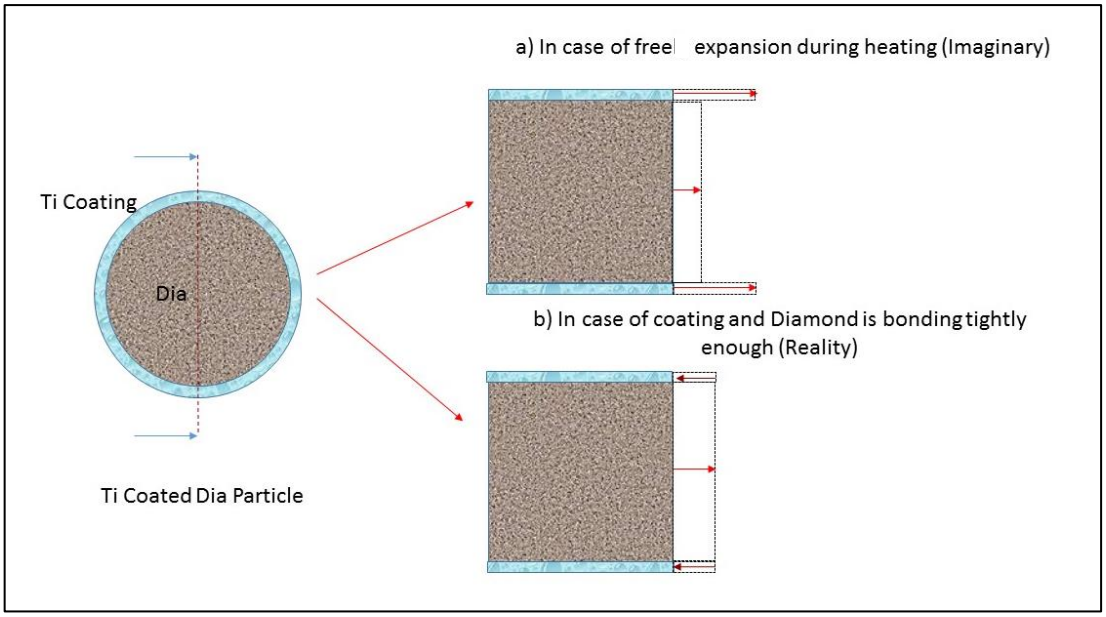

Figure (6-26): Schematic illustration of possible thermal stresses in Ti-coated diamond particles.

From the Figure (6-26) and applying the thermal strain equation at equilibrium we can get

$\Delta L_{Dia} + \Delta L_{Ti} = (\propto Ti - \propto Dia) \times L \times T$

$$\frac{\sigma Dia \times L}{EDia} + \frac{\sigma Ti \times L}{ETi} = (\propto Ti - \propto Dia) \times L \times T \text{ (at T=780 °C)} \quad \textit{.....Equation (6-2)}$$

At equilibrium should $F_{Ti}=F_{Dia}$

Then,

$$\sigma_{Dia} \times A_{Dia} = \sigma_{Ti} \times A_{Ti} \quad \textit{.....Equation (6-3)}$$

Thermal expantion $\propto Ti = 8.41\times10^{-6}$ m/C°[188], $\propto Di = 1\times10^{-6}$ m/C°[189], [190], [191]

E_{Ti} =103 GPa, E_{Dia}= 1020-1220 GPa [60],[190],[192] assumed to be = 1050 GPa, L=D=0.06mm, $t=2\times10^{-3}$

Then, can get

σ_{Dia}=58.725 MPa, σ_{Ti}= 536.282 MPa

that means σ_{Ti} is predicted to exceed the Ti tolerance of compressive stress, which is about 170 MPa [193] at maximum, while the generated stress in the diamond was less than the maximum tensile stress of diamond which can reach about 1200 MPa [190]. It is thus feasible that thermal stresses from processing could lead to failure of the coating.

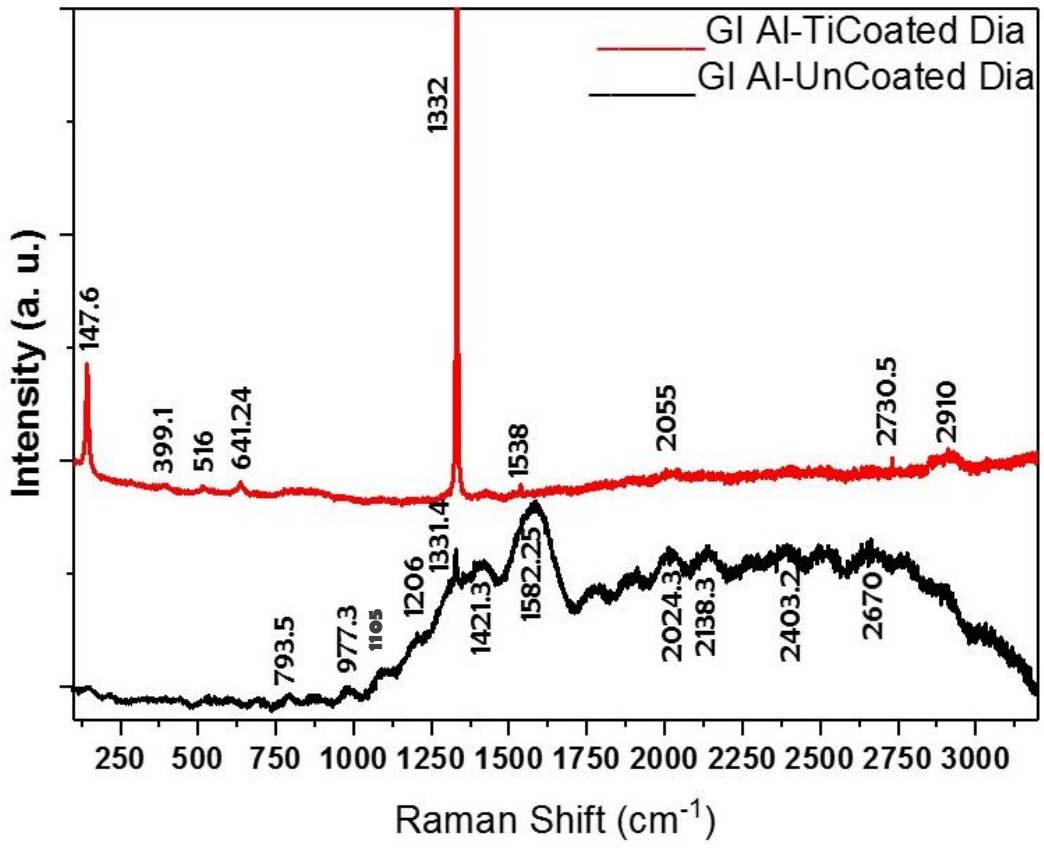

Figure (6-27): Raman spectra of AMDCs reinforced with Ti- coated diamond particles (red colour)) and AMDCs reinforced with uncoated diamond particles(black colour).

The Raman spectra, Figure (6-27), shows that there are appreciable differences between coated and uncoated diamond reinforcement. The AMDCs reinforced by uncoated diamond particles reveal many peaks related to graphite [194], which are present at shifts between 1400 to 3000 cm^{-1}. These in particular can be identified as a first order of disorder carbon atomic band vibrations (G band) at about 1421.3 and 1582.25 cm^{-1} as well the second order peaks appearing at about 2024.4, 2138.3, 2403.2 and 2670.0 cm^{-1} [195]. D band, which has been reported to be corresponding to the diamond [100], [115], [194]–[196] revealed a peak at about 1331.4 cm^{-1} with relatively low intensity, probably affected by Raman reflection from surrounding graphite. Therefore, it appeared connected as a shoulder to the main graphite peaks. Even so, most of these peaks exhibited some additional backward or upward displacements from their standard locations, possibly due

to existence of some carbides and oxides [197]; for example the Raman excitation peaks at about 793.5 cm^{-1} probably relates to Al_4C_3 [198][199] and the two peaks appearing at around 1105 and 1206 cm^{-1} probably refer to Al_2O_3 [200]. There is in addition the possibilty of other θ-Al_2O_3 peaks which are difficult to identify because their excitation often corresponds with Raman excitation of carbon peaks [200].

The peak appearing at around 977.3 cm^{-1} probably does not relate to the composite structure, but relates to SiC, present from the SiC grinding paper which was used to polish the sample's surface for Raman spectrographic analysis. While in the AMDCs that were reinforced with Ti-coated diamond the situation was different where the peaks corresponding to graphite and amorphous carbon reflect a very low intensity the first order (G band) at around 1425 and 1538 cm^{-1} and the second order graphite peaks at around 2055, 2730.5 and 2910 cm^{-1}. The diamond peak here (D band) reflects a very high intensity of Raman excitation at around 1332 cm^{-1}, whereas other peaks, such as those related to aluminum carbides or oxides seen with the uncoated reinforcement, are absent. Other components are seen, possibly produced from oxidation of the Ti coated layer to form TiO_2 at around 147.0, 516.0 and 641.2 [201], [202] while 399.1 related to TiC [204].

- **X-ray Diffraction of AMDCs with (coated/uncoated) Reinforcement**

The X-ray diffraction examinations identified that there are differences in some of the phases present, depending on the type of diamond particles which are used, either Ti coated or uncoated diamond. There are some intermetallic components which clearly appear under the X-Ray diffractometer in composites with Ti coated diamond, whereas they do not appear at all or appear with a lower intensity with uncoated material, such as TiC, Al_4C_3, Al_2O_3 in addition to some theta shifting in some main peaks of matrix and reinforcement, as shown in Figure (6-28).

These differences resulting from shifting of some positions of the peaks could be related to the carbide formation and matrix elements on the surface of particles in the case of coated diamond, in addition to Mg existing in the matrix already. This carbide formation may lead to better bonding at the interface. This may help explain the differences in wear behavior between specimens with coated/uncoated reinforcement, as will be shown in the next sections.

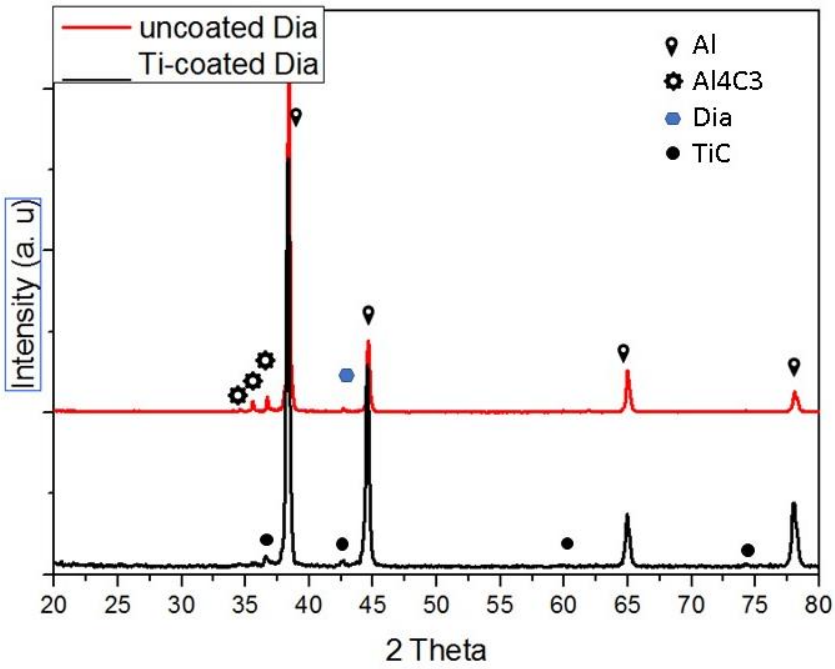

Figure (6-28): XRD patterns for both composites with coated/uncoated diamond.

6.7.2 Study Effects of Different Manufacturing Routes on AMDCs Structure

SEM imaging and EDX showed clusters of intermetallic compounds at a micro scale at interfaces, especially on the Ti coated diamond surface as that clearly shown in Figure (6-29). EDX indicates there is aluminum present, which may refer to the possibility of formation Al_3Ti. This may help in holding reinforcement particles in place, in addition to the mechanical support from the matrix by surrounding the reinforcement. The small difference between PM product and SPS may related to the sintering time where in PM the time was enough to bond the aluminum powder particles together to hold the diamond reinforcement while the short time (10 min) in SPS was not enough to make a good bonding at matrix rather than with reinforcement, as can be seen in the SEM images Figure (6-29 a and b) of PM and SPS, respectively. Nevertheless, compared to the accuracy of the measurements the difference between these two processes was not significant.

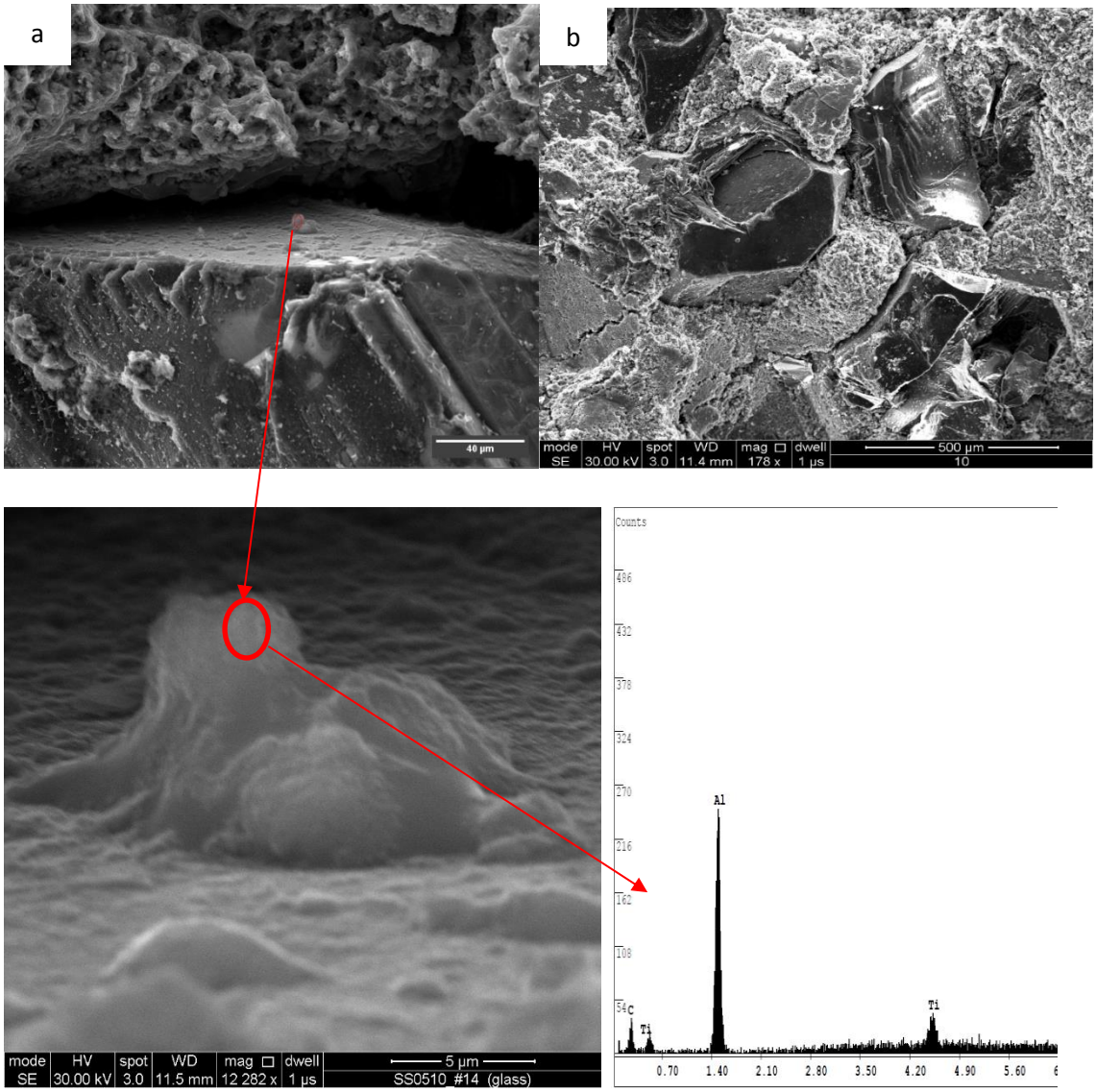

Figure (6-29): SEM images of Al-diamond a)(SPS) showing a cluster of TiC on the diamond surface of SPS product, and b)(PM) showing some micro cracks in the composite passing through interfaces.

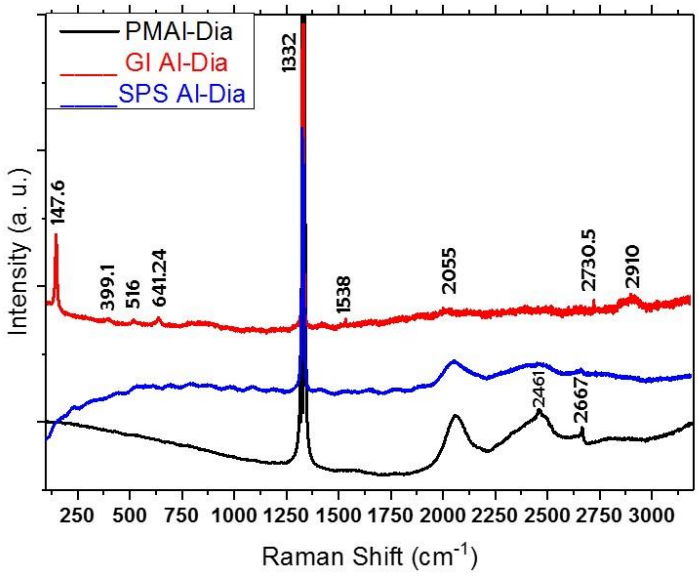

Figure (6-30): Raman spectra of AMDCs of the three different manufacturing processes (SPS, PM and GI).

Figure (6-30) shows Raman spectra of different AMDCs manufactured by different manufacturing methods, where red, blue and black curves represent GI, SPS and PM methods, respectively. The Raman spectrum reveals different interfacial compounds and carbon forms that may be created during processing by the different production methods and temperature ranges used in the process. There is a clear and high intensity D peak (diamond band) appearing at around 1332 cm^{-1} [100], [194] in all AMDCs, but there are differences in other carbon peaks, such as the G peak (graphite band). This disappears in PM and SPS composites while it appeared at 1538 cm^{-1} [194], [203], [204] in GI composites, along with other early peaks, which are thought to be related to TiO_2, appearing at 147.6, 516 and 641.24 cm^{-1} [201], [202], [205] and 399.1 related to TiC [206]**.** This formation was probably due to the relatively high temperature (780°C) used in the GI process, which consequently led to oxidation of the Ti coated layer and graphitisation of the diamond surface in contact with the molten aluminum. The second order Raman peaks of carbon were clearly present at about 2055, 2461 and 2667 cm^{-1} [195], [203] in PM and SPS composites, while some of those appeared at around 2730.5 and 2910 cm^{-1} in GI product. Some shifting of peaks from their known locations may occur as a result of existence of Ti at the interface [207] or some oxidation occurring in the one of composites

constituents [197]. as their shifting compared with known reported peaks is shown in Table (6-3).

Table (6-3): Summary of Raman peak locations in Al-Dia. according to the reported references.

Diamond Raman shift		2^{nd} order Graphite Raman shift		TiC Raman shift		Anatas TiO_2 Raman shift		Rutile TiO_2 Raman shift	
current study	Ref.	current study	Ref.	current study	Ref.	current study	Ref.	current study	Ref.
1332 In all three routes of production	1332 [100], [194], [196], [208]	1538 in GI 2055, 2461 and 2667 In SPS and PM 2730.5 and 2910 In GI	1591[204] 1580 [194], [203] 2670, 2690 [204] 2400, 2700, 3100 [204], [208]	399.1,	407, [206]	147.6, 516 and 641.24	146[205] 513, 639 [201], [202]	240, 820	236, 826 [202]

6.7.3 Study Structure of AMCCs

The microstructure investigations of pure AMCCs Figure (6-31) and Figure (6-32) or that are loaded with diamond Figure (6-33) and Figure (6-34) may not approve a clear difference in composite structure apart from that is the interfacial bonding was better in case of using SiC as reinforcement rather than alumina. This difference, that was found in bonding between aluminium as a matrix from one side and SiC or alumina as reinforcement from the other side, may be related to the nature of the reinforcement morphology and its compatibility with aluminium. There is the appearance of a light contrast layer covering the alumina reinforcement in examination of composites under SEM, Figure (6-32), which may result from some interaction at interface to create extra aluminum oxides, especially with existence of oxygen in alumina molecular or trapped from atmosphere. This oxide probably prevents wetting of the original reinforcement.

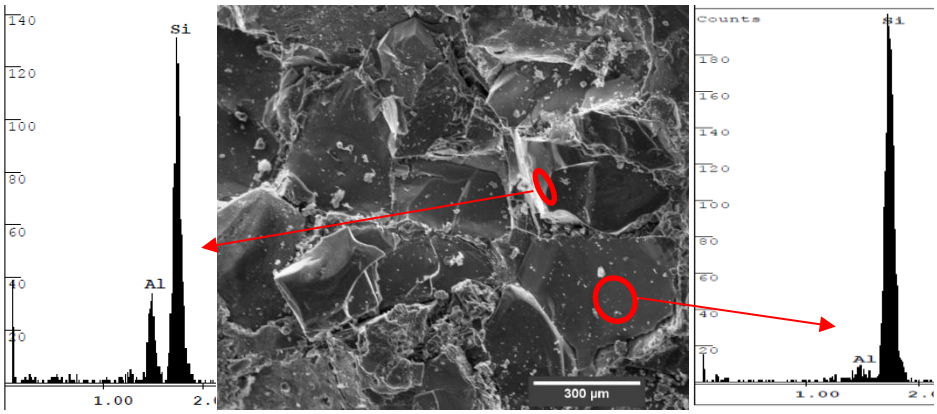

Figure (6-31): SEM image and EDX of fracture surface of GIAl-SiC composites reveals that the break occurred at interface.

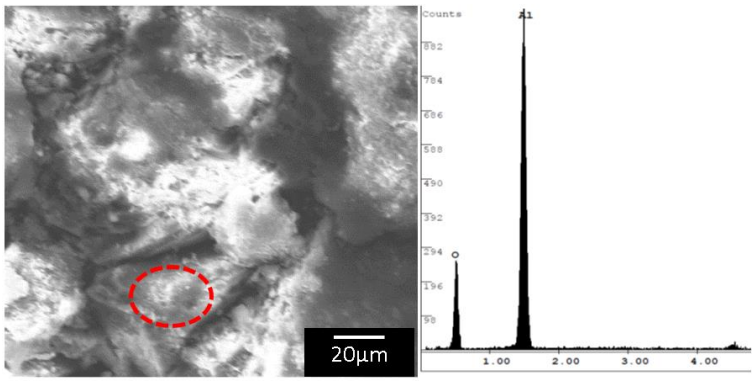

Figure (6-32): SEM image of fracture surface of GIAl- Al_2O_3 shows the interfacial bonding is not as good as in GIAl-SiC.

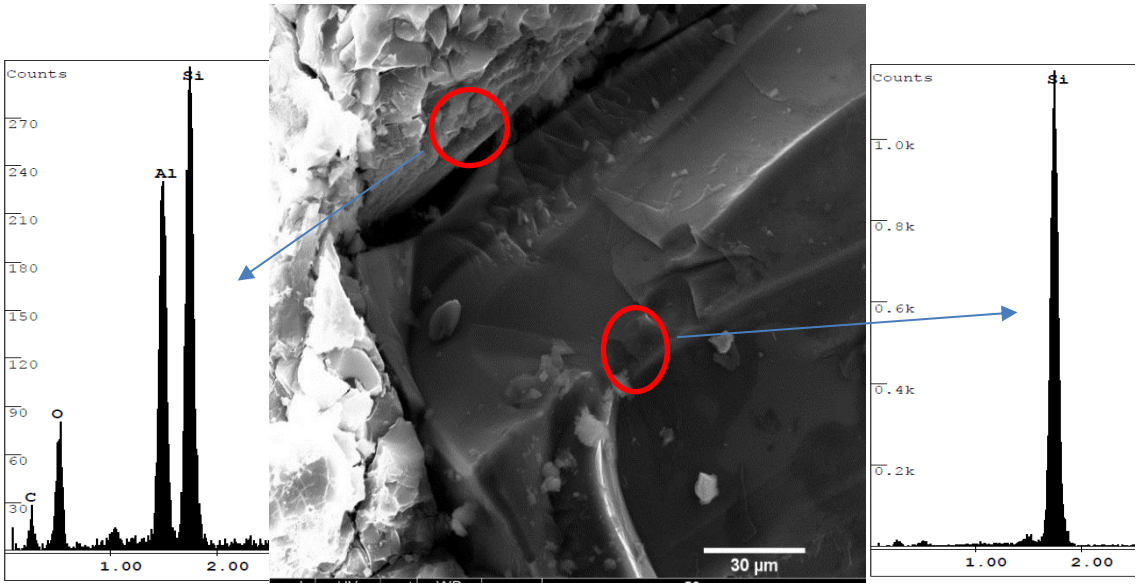

Figure (6-33): SEM image of GIAl50%20 Dia.-30SiC broken surface reveals that there is apparently sufficient bonding with the matrix as shown by fracture of the SiC particles.

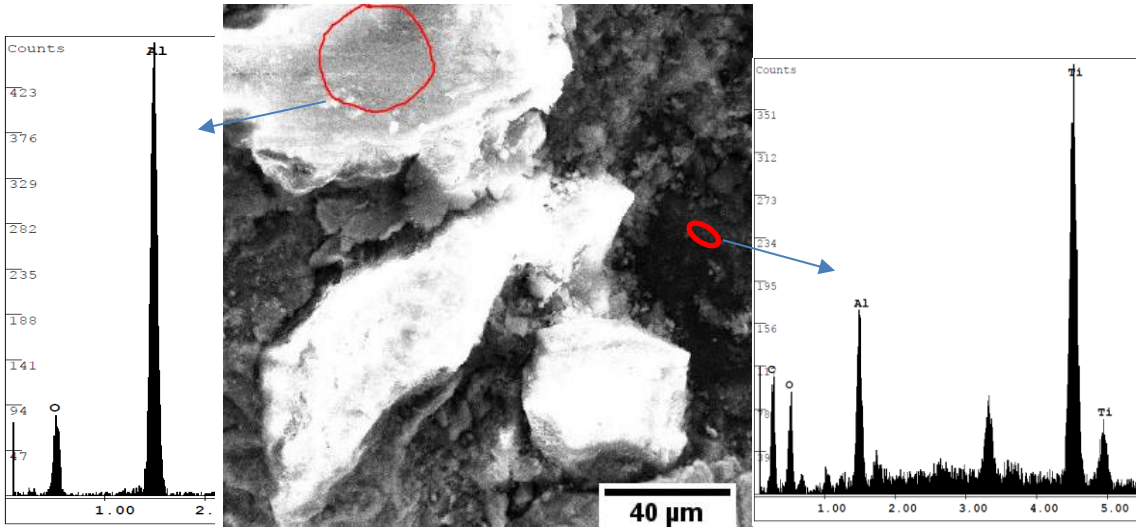

Figure (6-34): SEM image of GIAl50-20Dia.-30 Al_2O_3 *broken surface reveals that there is weak bonding and the break passes along the interfaces.*

6.8 Structure of Transition Metals- Diamond Composites

6.8.1 Ti-Diamond Composites

Figure (6-35 a) and b) display phase diagrams of Ti-C and Ti-O, respectively. This figure gives an idea about what possible types of compound that can be formed by interfacial reaction of Ti-diamond composite's constituents [98]. There is a possibility of carbide or oxide formation at the interface between matrix and coated Ti-diamond particles, and Figure (6-35 a) displays the possible formation of TiC, in addition to graphite which would

be more stable than the diamond, especially when the carbon percentage exceeds 16 wt. % at about 500 °C, close to the processing temperature of the composites. Figure (6-35 b) displays the possibility of formation of Ti_3O even at a percentage of oxygen below 4 wt. %. If the level rises to about 10 wt. % it can coexist with Ti_2O, until 15 wt.% O_2 at about 400 °C, which is about the processing temperature of composites.

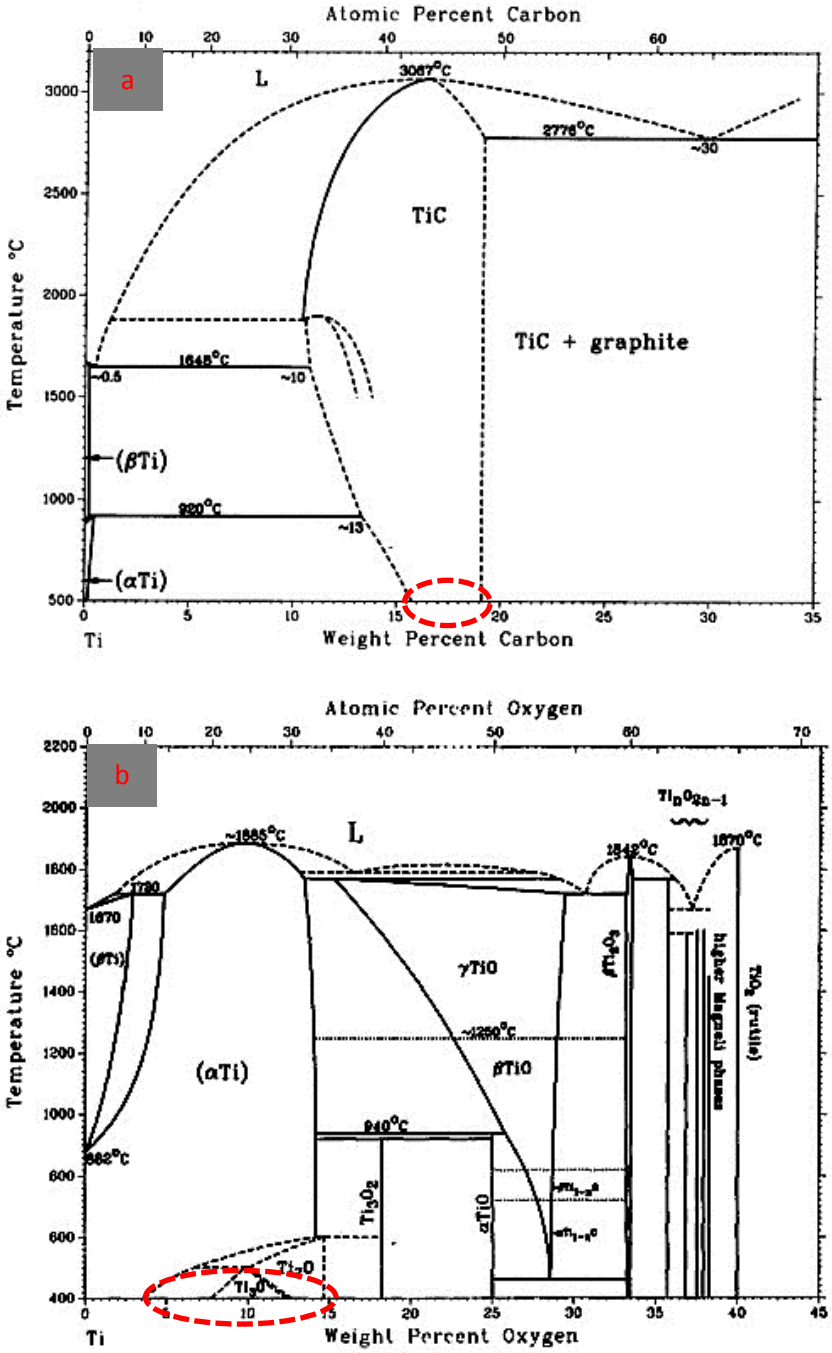

Figure (6-35): a) Phase diagram of Ti-C and b) Phase diagram of Ti-O after reproduced with permission of the publisher [98].

Therefore, some measurements were made on composites by Raman spectroscopy to investigate whether there is graphitization of diamond reinforcement or if any intermediate compounds formed as a result of interaction between the composite constituents at interface. Figure (6-36) displays the Raman spectrum of Ti-diamond composites manufactured by SPS (black curve) and PM (red curve). The Raman spectrum curves reveal in both cases (PM & SPS) that there are relatively high intensity Raman peaks, which represent a sp2 crystalline structure of diamond (D peak)) [194], [196], [208], but with different shifts and sharpness. The D peak in SPS composites exhibits a band at 1335 cm^{-1}, which is about ~3 cm^{-1} forward shift from the standard D peak (1332 cm^{-1}) and clear sharper peak than an equivalent peak in PM composites, which appears as a band at about 1310 cm^{-1}, which is around ~22 cm^{-1} backward shift. Meanwhile the sp3 crystalline structure, which corresponds with the G band (C–C stretching, which is called the graphite peak) [194], [208] does not exhibit any peak in its known place (1582 cm^{-1}) [196] or nearby in either composite. There are however, Raman peaks at about (2064.1 cm^{-1}) and (3783.3 cm^{-1}) in SPS Ti-diamond composite, which probably represent the second order of amorphous carbon or graphite, while the second order peaks, which appear in PM composites at 2458, 2669 and 2924.6 cm^{-1} [195], [204], seem to be corresponding to second order graphite bands. It is common that the graphite exhibits two 2D peaks, which are 2D1 and 2D2 bands and here possibly are 2458 and 2669 cm^{-1} [204], with 2924.6 cm^{-1} probably corresponding to the 2G peak. The existence of the 2D peak in the form of two sub peaks [204], [208] in addition to the shifting of the Raman peaks indicate that graphitization and oxidation have occurred during the sintering process, as these peaks are very sensitive to carbon structure configuration [195], [197]. This conclusion has been confirmed by analysing other Raman peaks, which appeared at an early shift in PM composites, corresponding to other bands apart from the diamond or graphite bands, at different intensity. These peaks are related to intermetallic compounds generated at the interface or matrix due to interaction between the constituent phases, especially with oxygen. The Raman peaks at 495 and 655 cm^{-1}, may relate to anatase bonding vibrations in titanium dioxide [201], [202] and those at 240 and 820 cm^{-1} may relate to rutile bonding vibrations in titanium dioxide [202], while the peaks at 224.3 [208], 282.3, 402 and 605 cm^{-1} [206] correspond to titanium carbide (TiC). These peaks and their related locations are summarised in Table (6-4). All these intermediate compounds and Raman peaks forward/backward displacement indicate that both Ti-diamond composites were exposed to oxidation and graphitization, but at different levels. This was clear from the differences

in Raman peaks, which were almost in agreement with the XRD patterns of these composites, Figure (6-37), and SEM, Figure (6-38) and Figure (6-39).

Table (6-4): Summary of Raman peak locations in Ti-Dia. according to the reported references.

TiC Raman shift		Anatas TiO_2 Raman shift		Rutile TiO_2 Raman shift		Diamond Raman shift		2^{nd} order Graphite Raman shift	
current study	Ref.	current study	Ref.	current study	Ref.	current study	Ref.	current study	Ref.
224.3 282.3, 402, 605	221 [208] 255, 407, 603 [206]	495, 655	513 639 [201], [202]	240, 820	236, 826 [202]	1335 (SPS) 1310 (PM)	1332 [194], [196], [208]	(2064.1), 3783.3) (SPS) and (2458, 2669, 2924.6) (PM)	2670, 2690 [204] 2400, 2700, 3100 [204] [208]

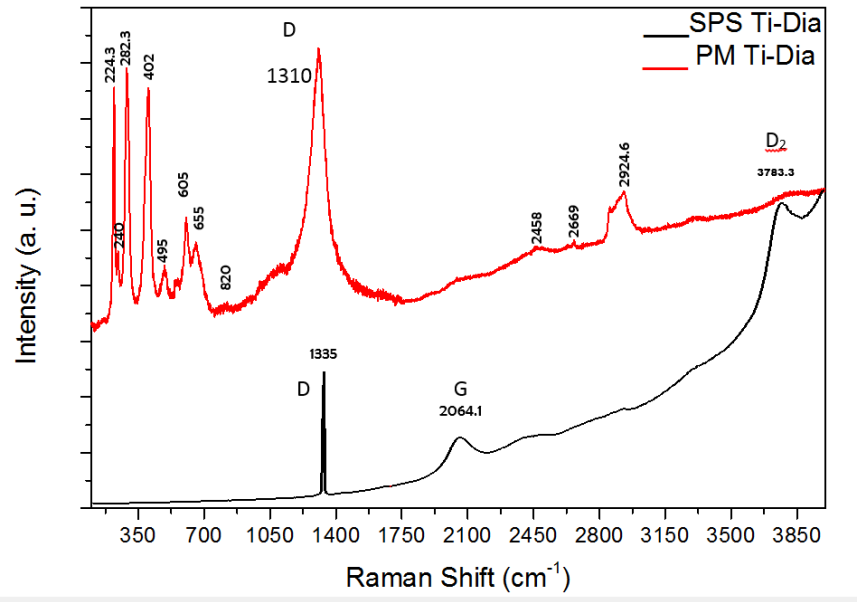

Figure (6-36): Raman spectrum of SPS and PM Ti-diamond.

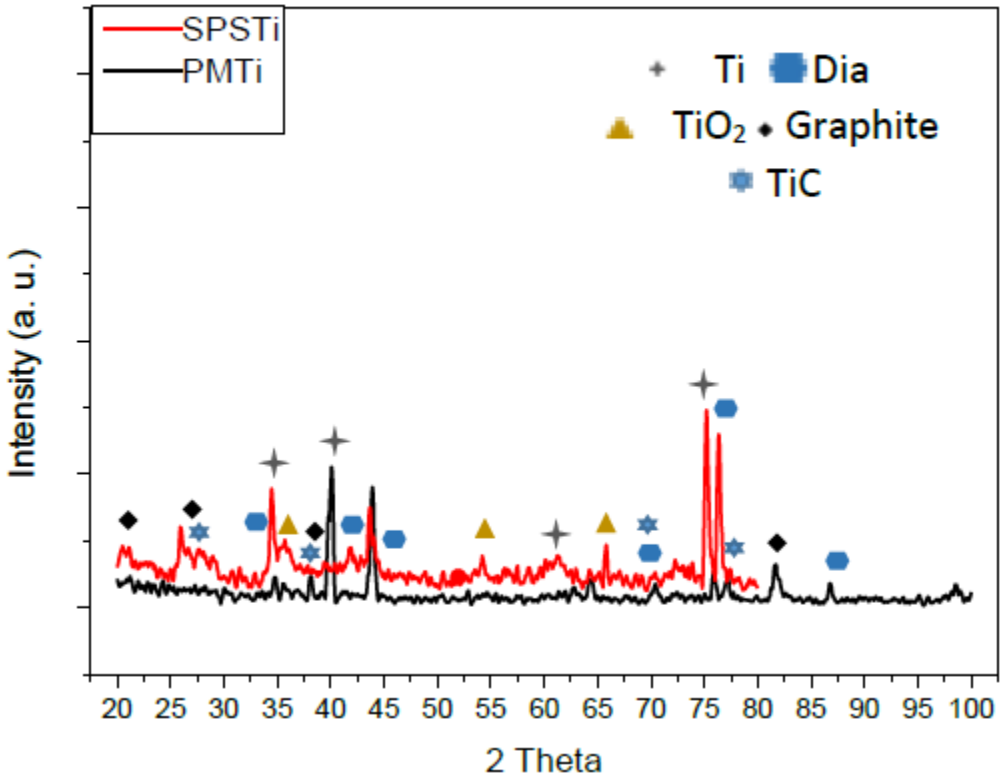

Figure (6-37): XRD pattern of PM & SPS Ti-diamond.

The SEM imaging and EDX of the fracture surface, shown in Figure (6-38) and Figure (6-39), reveals the role of Ti at the interface. The effect was clear in case of PM Ti composite Figure (6-39), which strongly bonds to the Ti or TiC on the surface of the coated diamond, leading to cleavage of the diamond particle during fracture of the specimen. The fracture of diamond particles may be related to defects in the diamond structure which may caused by graphitization [209] the same behaviour was seen in the SPS case as shown in Figure (6-38).

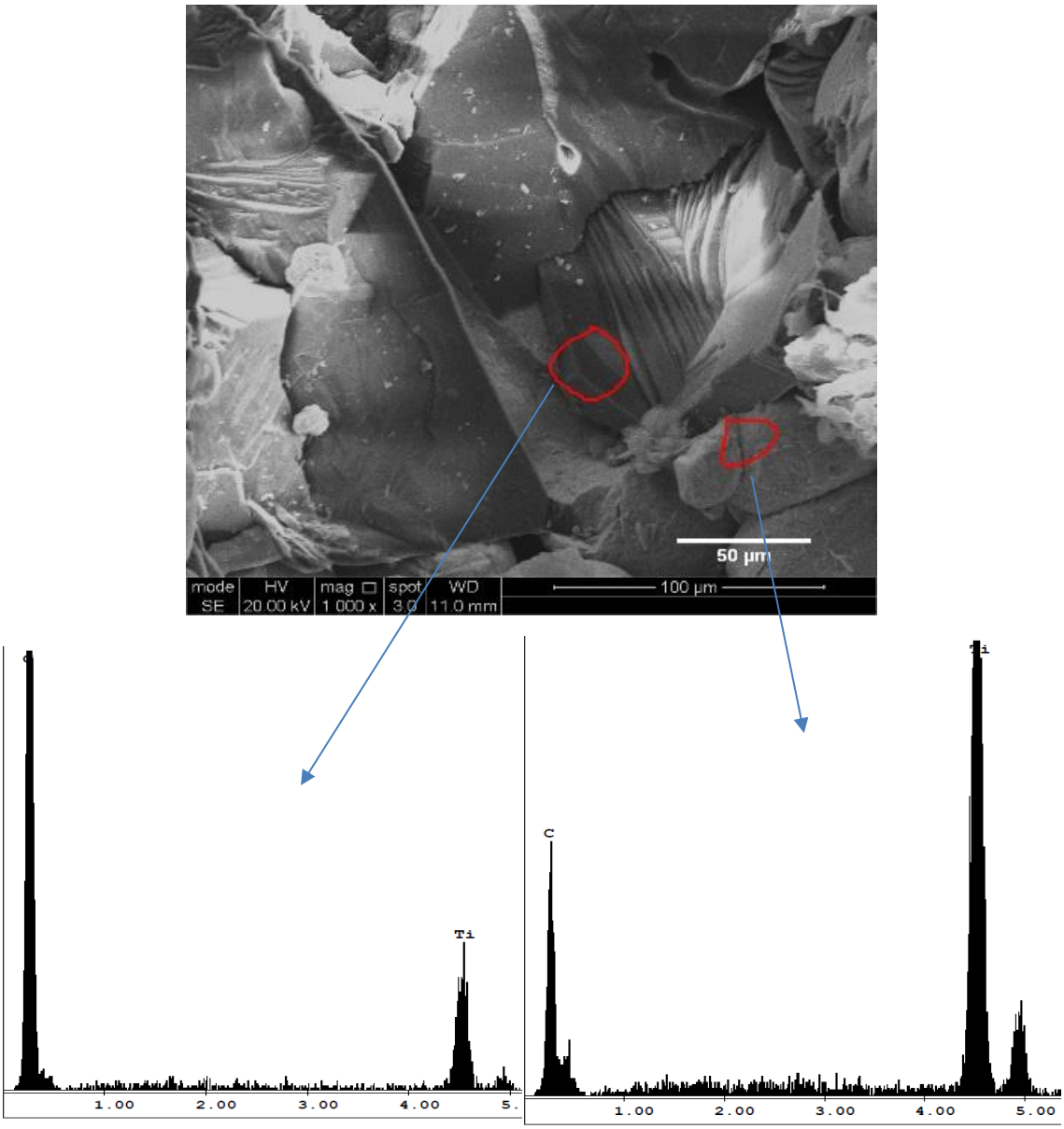

Figure (6-38): SEM image and EDX of SPS Ti50%-Dia. broken surface shows that the diamond particle was breakage and some carbon has diffused to Ti matrix (right).

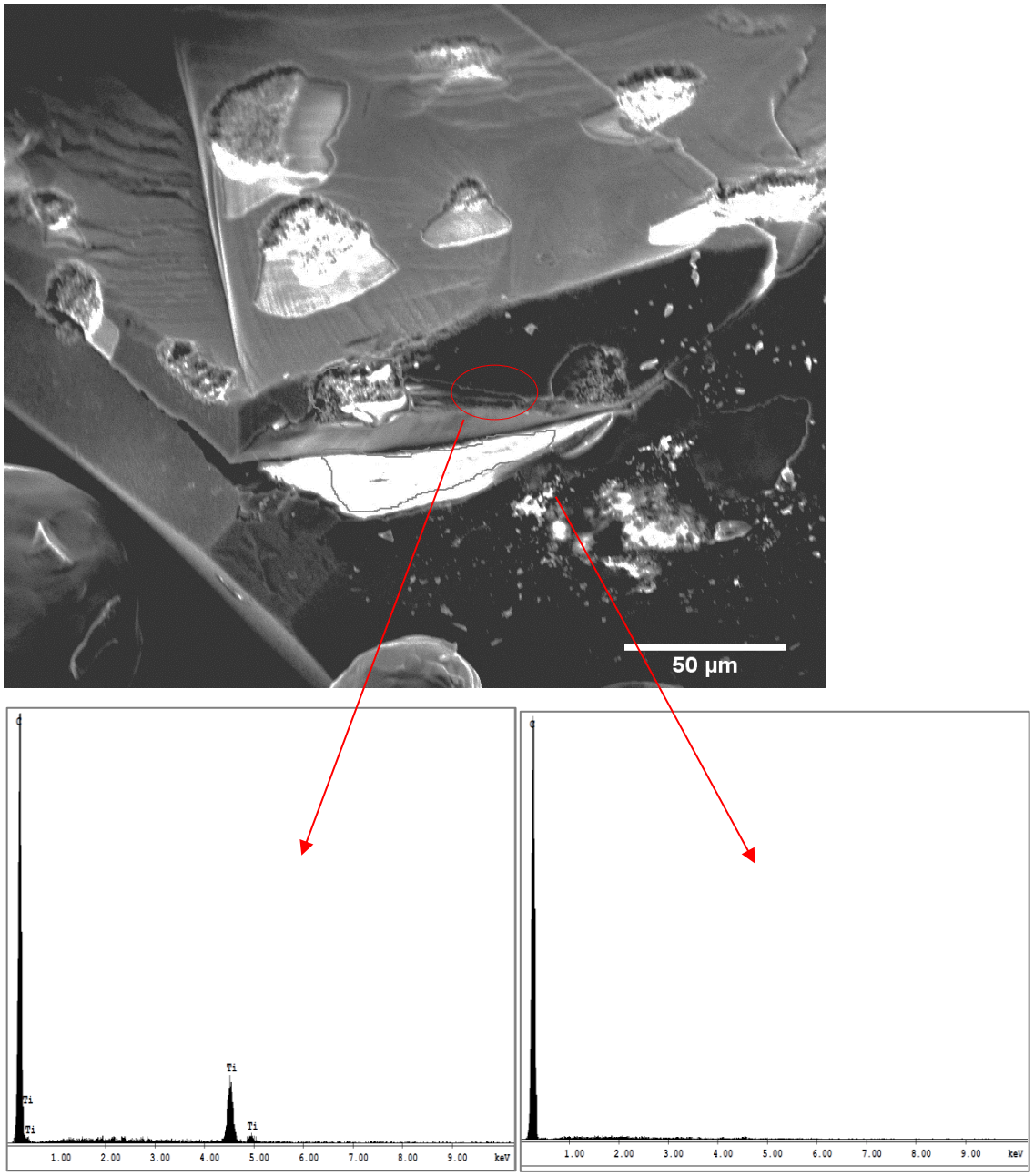

Figure (6-39): SEM image and EDX of PM Ti-diamond fracture surface shows impression of partially bonding with Ti particles and cleavage of diamond particles prior the fracture.

6.8.2 Ni-Diamond

In the Ni-diamond composite the situation at the interface was different. The Ti layer at the diamond surface may react with the Ni matrix to create an intermetallic compound, Ni_3Ti or NiTi, which clearly appears in the fracture surface of the PM product as shown in Figure (6-40). This area is enriched by Ni which has good diffusivity in Ti, especially at temperatures above 500 °C, this diffusion mobility may lead to some Ni atoms being dissolved in the Ti, and reacting to form compounds [210].

Some other features were revealed under SEM images as clusters with a size of some microns on the surface of diamond particles as, shown in Figure (6-41). Such clusters were not seen by SEM in the case of SPS products, Figure (6-42). The clusters were examined by EDX to see if they contain elements known to form intermetallic compounds in Ni-diamond composites. The EDX examination found the features were rich in Ni in addition to Ti, carbon and oxygen, which is considered to be the indication of the existence of nickel carbides and oxides. Then these clusters are confirmed with Raman peaks to be nickel oxide in addition to TiC, Figure (6-45), pp. 135.

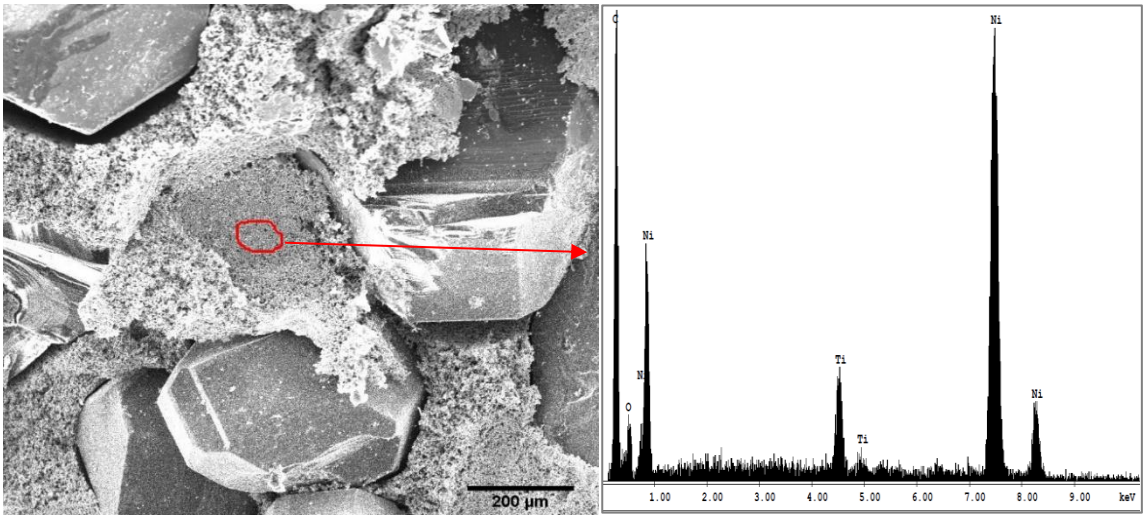

Figure (6-40): SEM of PM Ni-diamond fracture surface shows some impression of pulling out particles in fracture plane and EDX show there are existence of Ni-C-O-Ti at the interface.

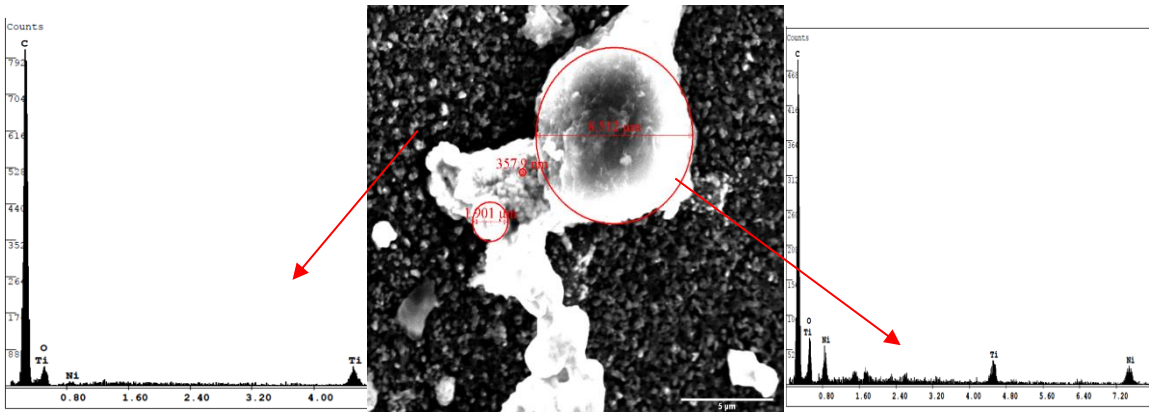

Figure (6-41): SEM image and EDX of TiC cluster growth on diamond surface in PM Ni-Dia. interface.

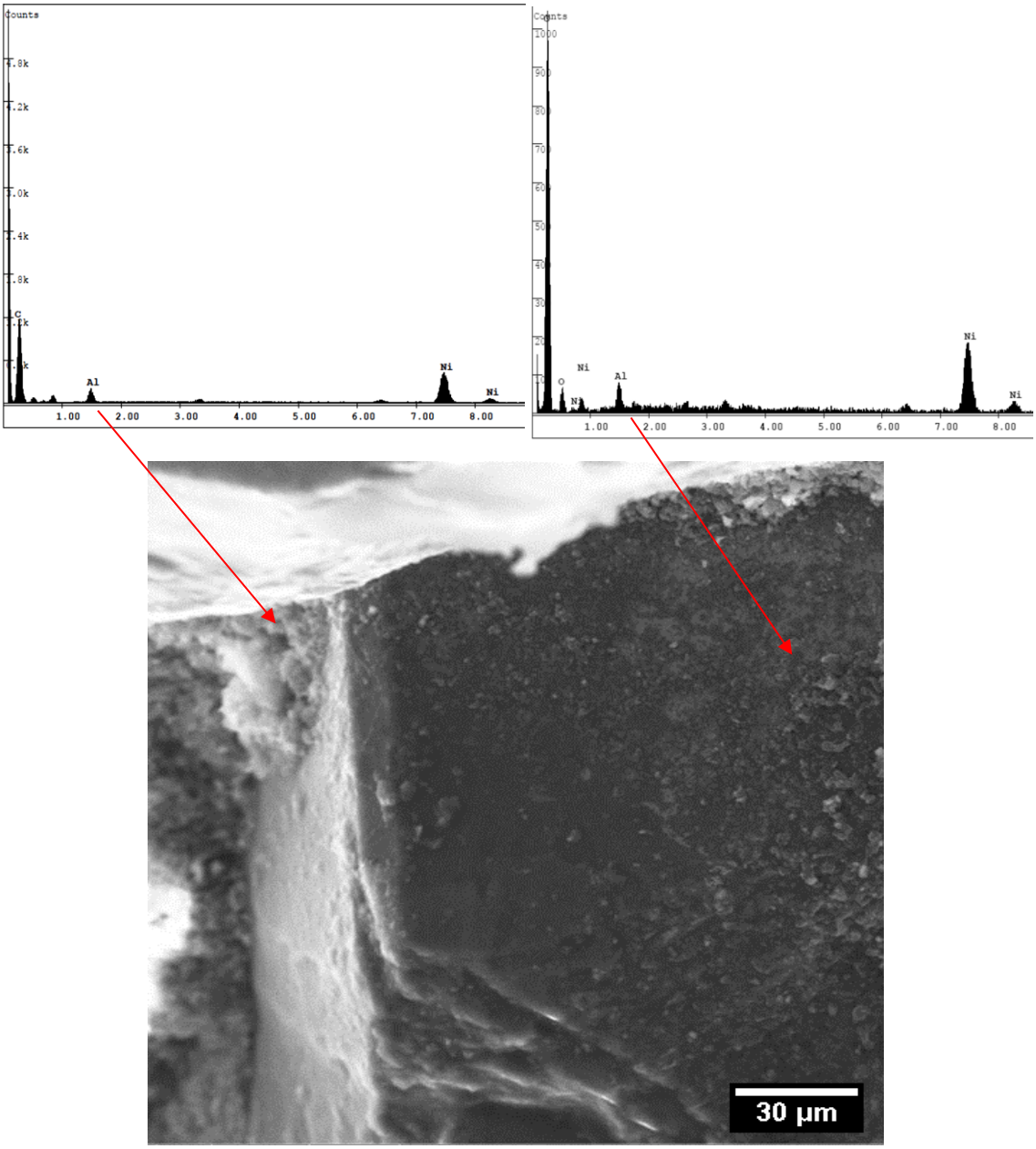

Figure (6-42): SEM image of SPS Ni-diamond shows limited interaction of Ni-C at diamond surface.

The indication of forming interfacial compound in composites produced by PM suggests further investigations into the differences in interfacial bonding mechanism would be needed to determine the dominant mechanism at the interface of composites, in SPS and PM routes of Ni-diamond composites production. Therefore, it is important to understand the possible reactivity of Ni toward carbon and oxygen at the range of processing temperature (800˚C). This can be shown for equilibrium by Figure (6-43) , the phase diagram of Ni-C, showing the solubility of carbon in Ni at 800°C is very limited (<0.6wt.% C, which is the maximum solubility limit at 1326.5°C [98]). This solubility decreases with

reducing temperature to a minimum limit at room temperature, though residual carbon can make a metastable Ni_3C phase [98], [211], [212], which also encourages more carbon to later diffuse out of Ni [211]. In regard to the oxidation of metals at elevated temperature, different metals will be oxidized at different rates. For example, Ni is more stable against oxidation than Cu; Figure (6-44) displays the initial stage of metal oxidation with time and temperature, including Ni and Cu.

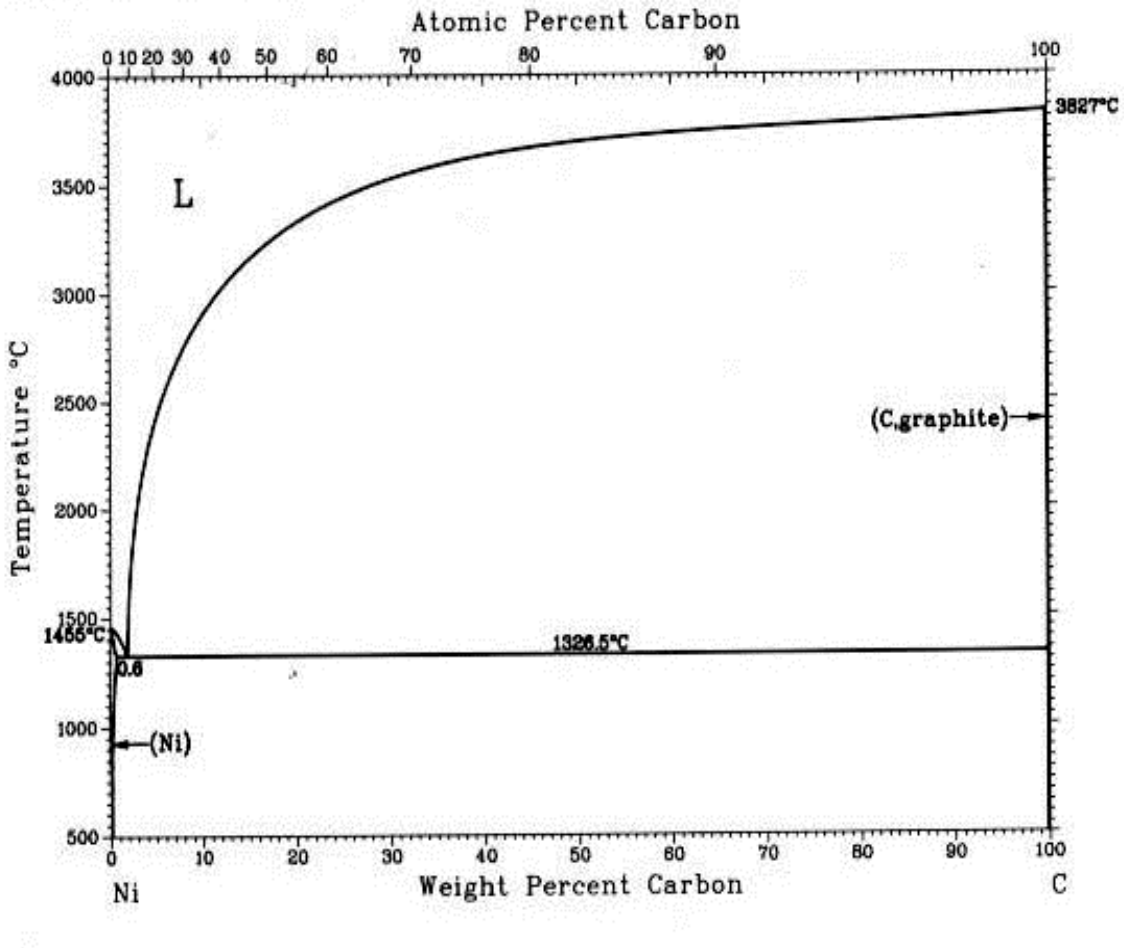

Figure (6-43): Phase diagram of Ni-C reproduced with permission of the publisher [98].

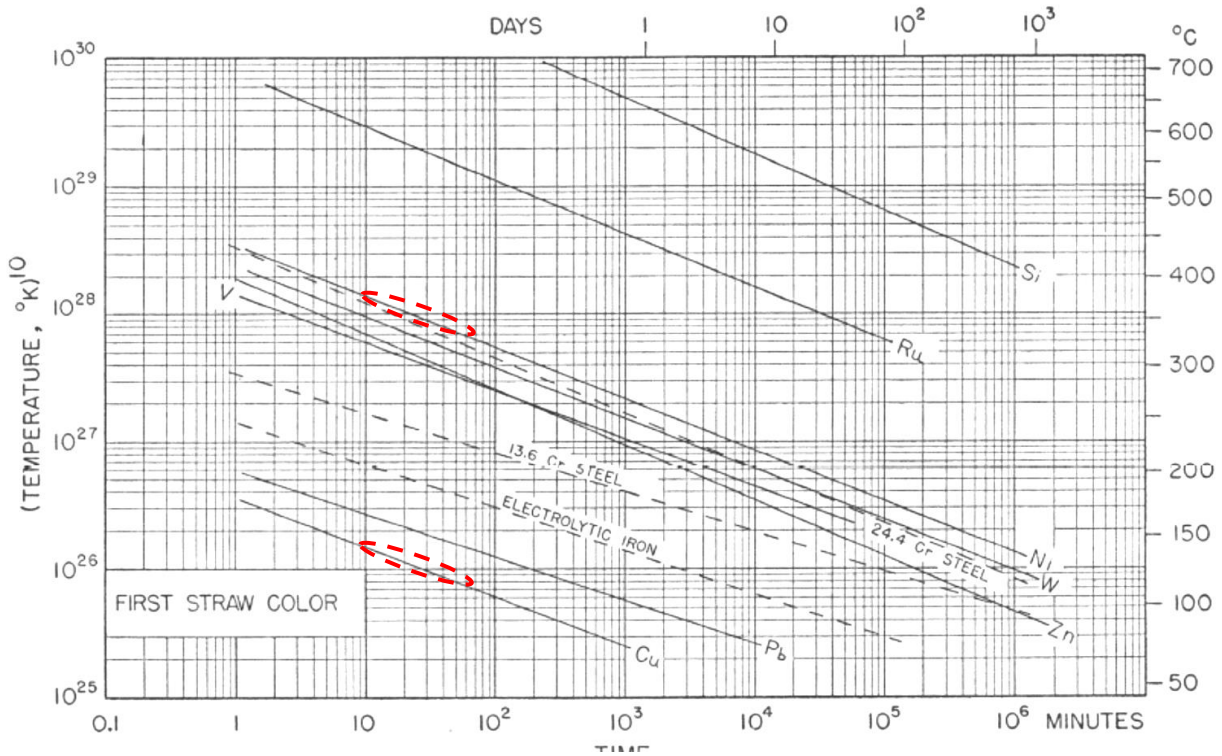

Figure (6-44): Effects of rising temperature on the first order straw color oxides of different materials [213].

XRD analysis and Raman spectroscopy were the main techniques applied to identify whether there is a real compound (a reaction phase) of these elements (Ni, C, O, Ti) or if these elements existed in free form in the clusters examined by EDX.

Raman spectra peaks, Figure (6-45) may answer these concerns and identify either these clusters, in Figure (6-41), wear a third phase or not, by showing Raman peaks which correspond to carbides or oxides, or by showing shifts in the peaks of diamond and graphite [197], [214].

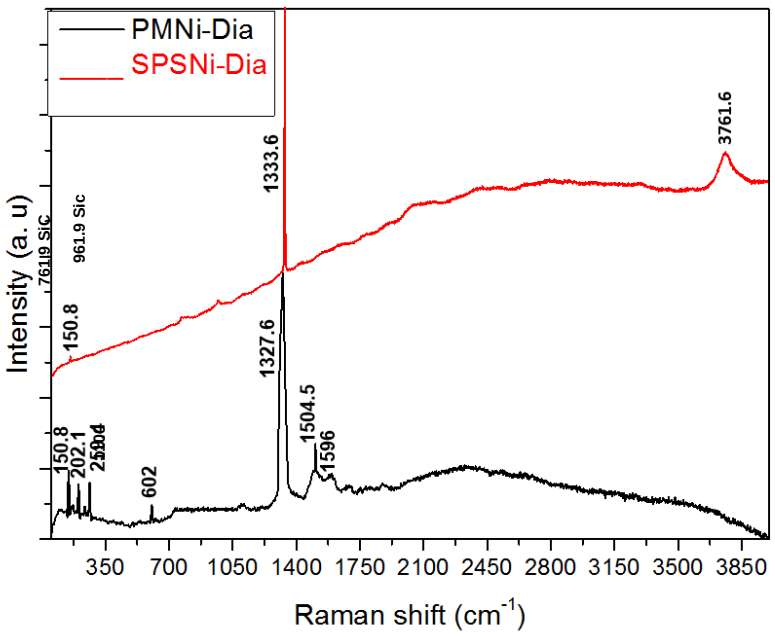

Figure (6-45): Raman spectrum of Ni-diamond composites of different production methods (PM- black curve and SPS- red curve).

The Raman peaks of the Ni-diamond composites reveal that there are differences in interfacial compounds formed in both manufacturing methods. The Raman spectra curve of PM composites exhibited a backward shifting of a D band about (~4.4 cm^{-1}) from the standard D band, which should appear at 1332 cm^{-1}[214], where it was at 1327.6 cm^{-1} and a G band, which corresponds to vibration of sp2 bonding at carbon structure (graphite), splits into two neighbored peaks at 1504.5 and 1596 cm^{-1}. In SPS composites the D band peak, which was shifted about 1.6 toward, appeared at 1333.6 cm^{-1}, but the G band peak (graphite) was disappeared here and the second order Raman peaks appeared at about 3761.6 cm^{-1}. These displacements and changing in intensity or disappearing at all for some peaks are indications of the formation of oxides in composites [197]. Early Raman peaks (low wave number) were especially present in PM composites, at about 150.8, 202,1 and 259.4 cm^{-1}. These peaks seem to be corresponding to TiC and TiO_2 [201], [205] may come from the oxidation of the Ti layer which exposed to oxygen ether from content within the argon or trapped in powder through handling or processing. The Ti-coating face which is in contact with the surface of diamond particles may create TiC at 602 cm^{-1} [206] while a small peak at 1100 cm^{-1} is related to NiO [215], [216] all detected Raman peaks and a comparison with reported known peak locations are shown in Table (6-5). These indications are almost in agreement with SEM and EDX observation, Figure (6-40) and Figure (6-41).

Table (6-5): Summary of Raman peak locations in Ni-Dia. according to the reported references.

NiO Raman shift		TiC Raman shift		Anatas TiO_2 Raman shift		Diamond Raman shift		2^{nd} order Graphite Raman shift	
current study	Ref.	current study	Ref.	current study	Ref.	current study	Ref.	current study	Ref.
1100	1100 [215], [216]	202 259.4 and 602	221 [208] 255 and 603 [206]	150.8	146 [205]	1327.6(PM) and 1333.6 (SPS)	1332 [194], [196], [208]	3761.6 (SPS) and 1504.5 and 1596 (PM)	3100 [204] [208] And 1591[204] 1580 [194], [203]

The XRD pattern, Figure (6-46), shows some unexpected peaks for PM samples, which were different from SPS samples. This corresponded to NiO in PM products while in SPS products there is a new difraction peak, which corresponds to graphite, that may come from the diffusion of carbon at the relatively high SPS processing temperture (800°C) from the graphite foil lining the graphite moulds [217]. The other cause is the formation of oxides, that may lead to weak bonding between composite constituents in the case of PM, that may come from the long holding time at elevated temperature in this non perfectly isolated atmosphere in the tube furnace, compared to the perfectly sealed vacuum chamber in the SPS method. It may also be that existing graphite in the SPS products may work as solid lubricant at this stuation especially at the intial stage of wear, Figure (9-17 b), because the diffusion of carbon in the composite structure does not exceed a few microns in Ni-diamond from outer diameter which is in contact with graphite foil which is lining the graphite mould at these tempertures (800°C) [217].

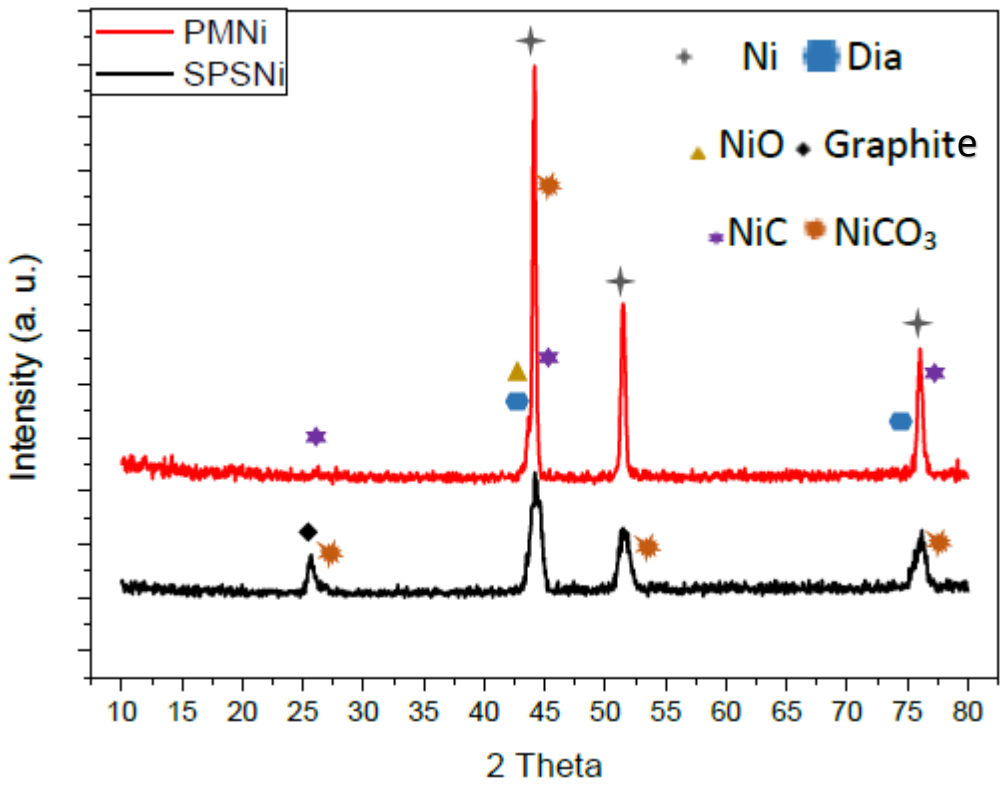

Figure (6-46): XRD pattern of Ni-diamond composites (PM and SPS).

6.8.3 Cu-Diamond Structure

The manufacturing methods have an important role on the composite structure and phase bonding, which finally may impact the wear behavior even with the lower tendency of Cu to react with carbon than other matrices, according to the phase diagram of Cu-C, Figure (6-47 a) [98], but its ability for absorbing oxygen may be the one important issue that should be taken into account when comparing how the processing methods affect performance. Different processes may exclude oxygen more or less effectively, and this oxygen can be trapped by the matrix or reinforcement during materials handling or processing. For example, the PM sintering was done under argon flow in tube furnace, and standard grade argon contains some oxygen as an impurity [218]. These trace amounts either dissolve in Cu or tend to form oxides as shown in the solubility of O in Cu diagram, Figure (6-47 b). Only 8 ppm oxygen would dissolve at 850°C (the process temperature is 700°C) while the exceeding this limit will react with Cu to form Cu_2O [219] and this limit of solubility will reduce with temperature so more oxides can precipitate.

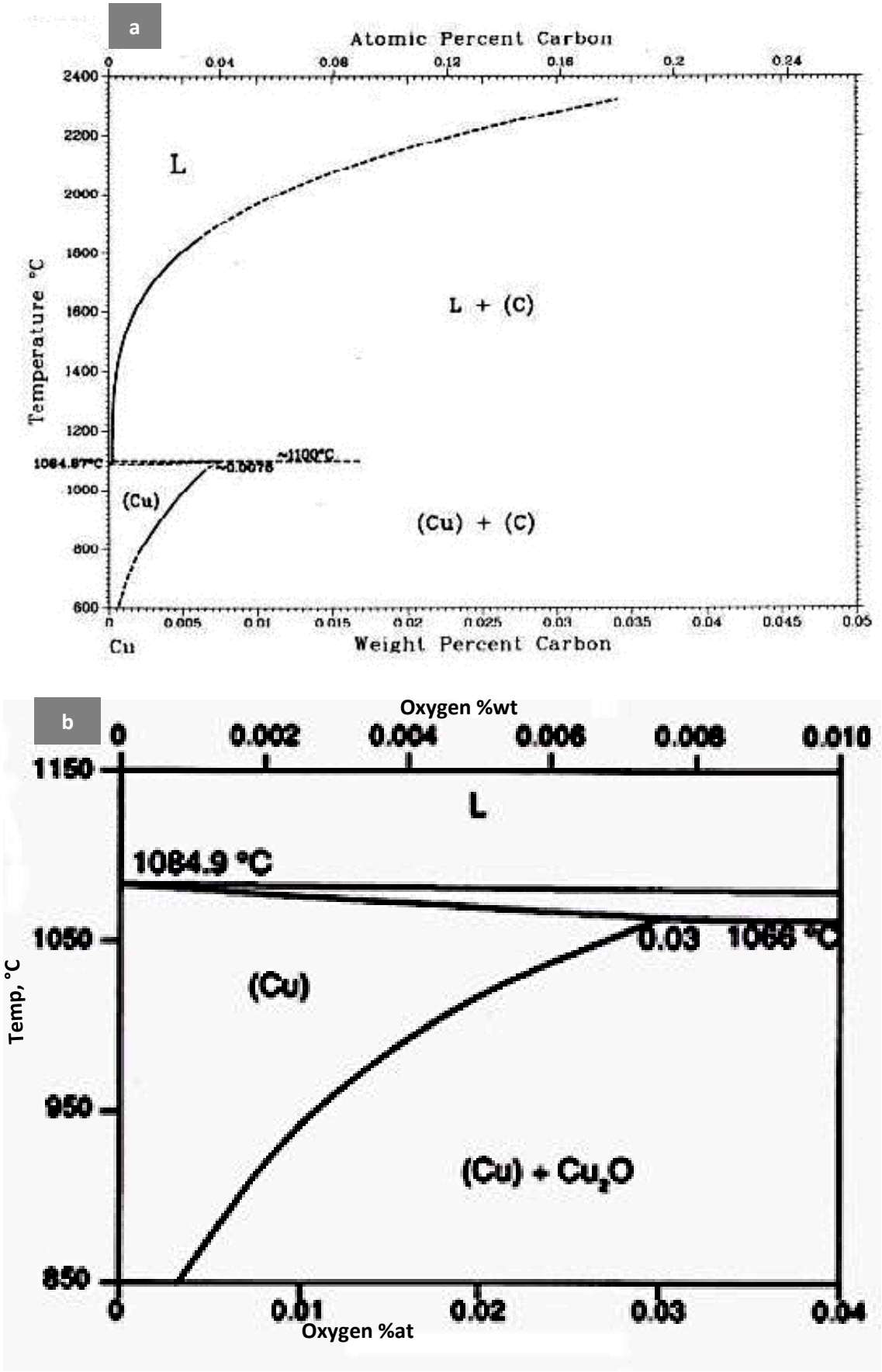

Figure (6-47): Parts of phase diagrams a) Cu-C and b) Cu-O.

To find out the possible compounds which may form in the Cu-diamond composites. The fracture surfaces of these composites were investigated with SEM imaging and EDX analysis, Figure (6-48), Figure (6-49), to observe if there are some compounds (carbides or oxides) at the interface, which may promote or weaken the interfacial bonding, and consequently affect the wear properties. The fracture surface of Cu-diamond composites has shown the existence of some intermetallic compounds at the Cu-diamond interface, as shown in Figure (6-48) by EDX, which shows some Ti and oxygen present at the interface, which is further investigated by Raman spectrometry Figure (6-50). These elements existing with Cu may indicate CuTi intermetallic compounds and copper oxides. While in the SPS case the pulling out the coated layer from the diamond surface confirm that there is a good interaction achieved between Cu matrix and Ti coated layer as shown in SEM and EDX, Figure (6-48).

Additionally, the fracture surface of PM Cu-diamond composites has shown some intermetallic compounds at the Cu-diamond interface, while these kinds of compounds are not found elsewhere. Figure (6-48) shows EDX results, indicating some Ti at the interface. This Ti with Cu may refer to CuTi intermetallic compounds [220].

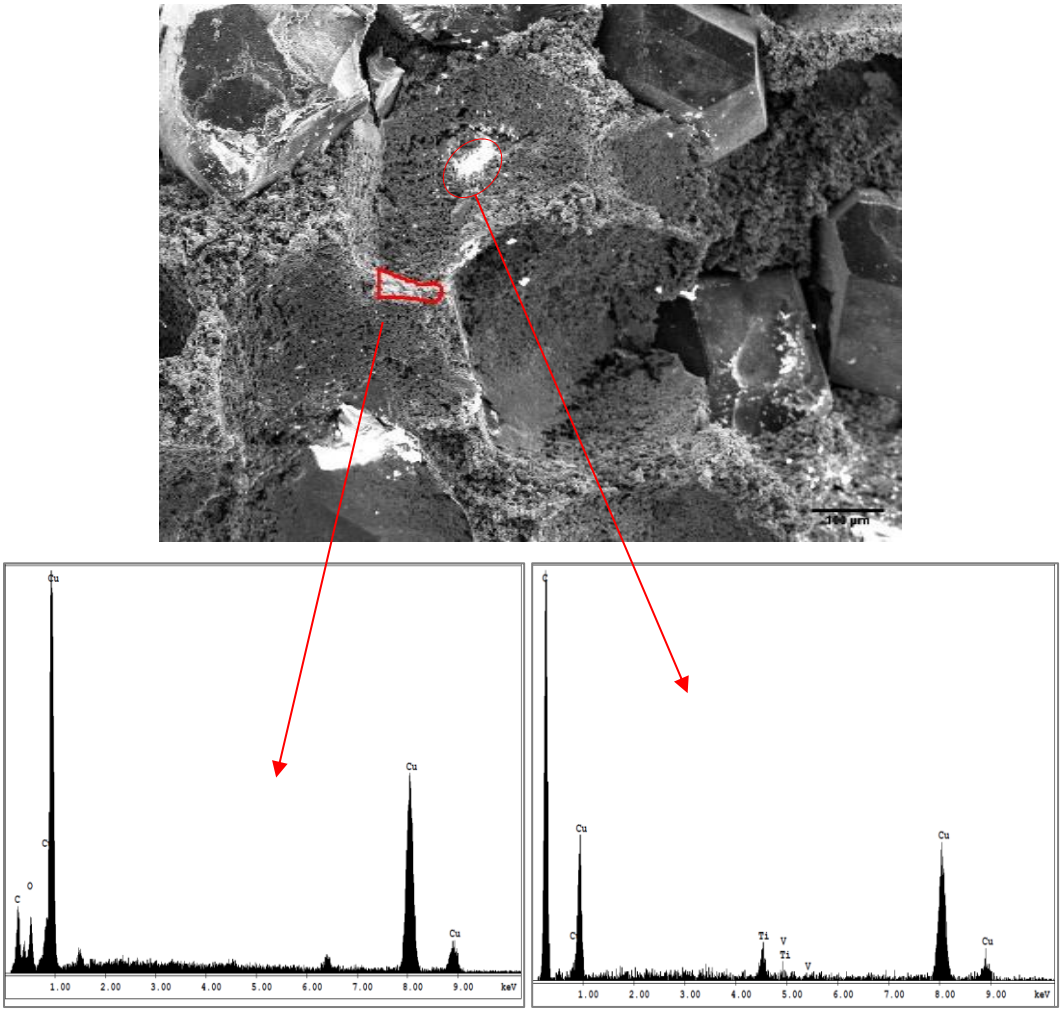

Figure (6-48): SEM image of PM Cu-diamond fracture surface, showing some Ti and C left on the matrix after pulling out diamond particles.

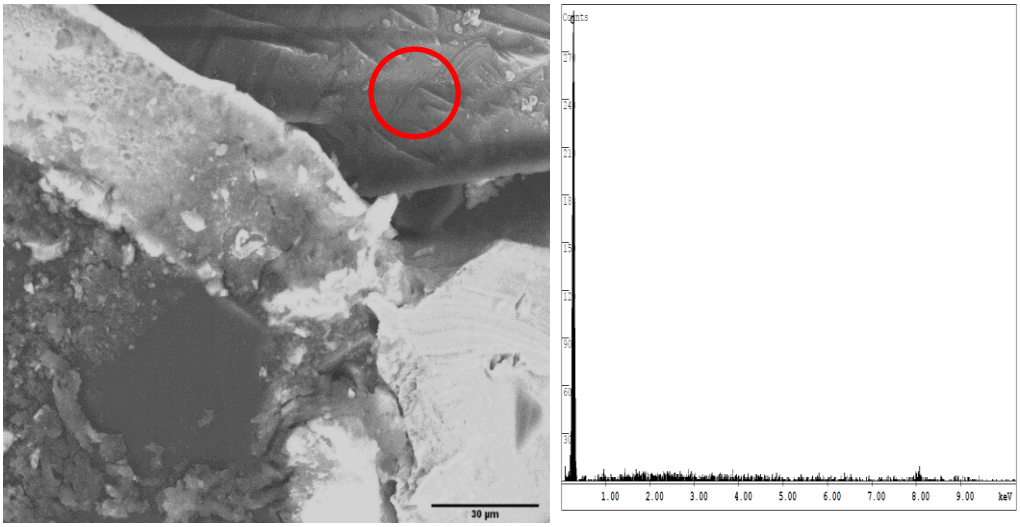

Figure (6-49): SEM image and EDX of fracture surface of SPS Cu-diamond composite showing there is a pulling out of coated layer from diamond particles.

Therefore, in order to further confirm there are some of these trace elements forming interfacial compounds the Raman spectrometer has been used to investigate the bonding of these compounds according on the band vibration of oxides or carbides, Figure (6-50) displays the Raman spectra of Cu-diamond processed by PM and SPS, respectively. The Raman peaks, which appear at 99.56 and 236.3 cm^{-1} may correspond to Cu_2O [221] and 344.8 cm^{-1} and a small peak at around 297 cm^{-1} corresponds to CuO [215] [221]. These peaks indicate there are some interfacial compounds present in PM processed composites. Even though those peaks are shifted by small distances from the known standard places of Raman shift, this shifting is probably as a result of some Ti at the reactive area (the diamond surface) [207]. The peak that represents the diamond (D Peak) appeared at 1327.6 cm^{-1} in both composites produced by SPS and PM in addition to relatively low intensity graphite peak (G Peak) which appears at about 1573.8 cm^{-1} [100], [195], [197], [203] in the PM product, but disappears in the SPS product, which has instead the second order carbon peaks at about 2053.2 and 3766.7 cm^{-1} [195]. The disappearance of the graphite peak and exhibiting of the peaks of copper oxides probably gives an indication that the oxidation that may occur during the sintering process in a tube furnace was higher in PM than SPS. This will affect the interfacial bonding of the composite constituents, and consequently reduce the wear resistance of the PM product. Even though, the D peak is shifted some distance about 5 cm^{-1} backward in both (SPS and PM) from its standard Raman shift which should be around 1332 cm^{-1} [195] this small shift may be related to the formation of some oxides [197] even they probably were in a very small amount in SPS composites in comparison to PM composites. The XRD pattern, Figure (6-51), shows there are some peaks of intermetallic compound which correspond with what Raman spectrum has shown as TiC and graphite, especially in the PM composite.

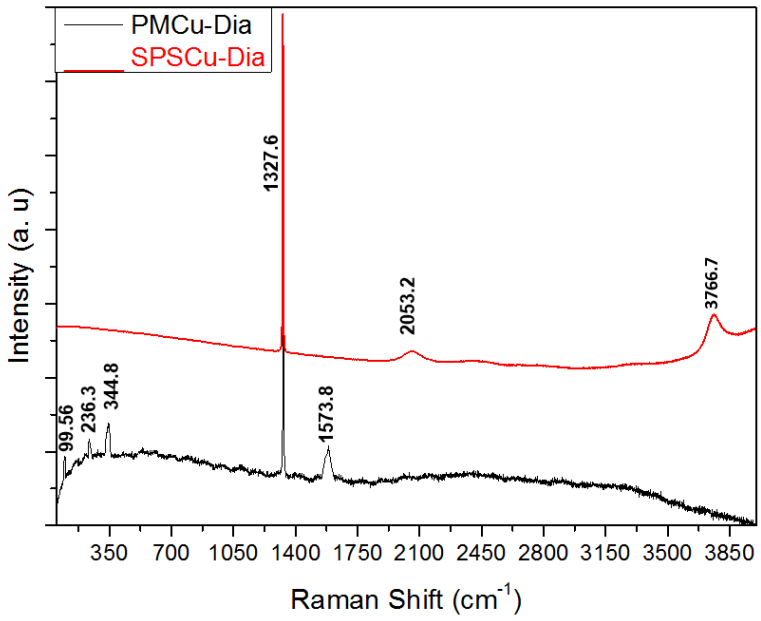

Figure (6-50): Raman spectrum of Cu-diamond composites (PM and SPS).

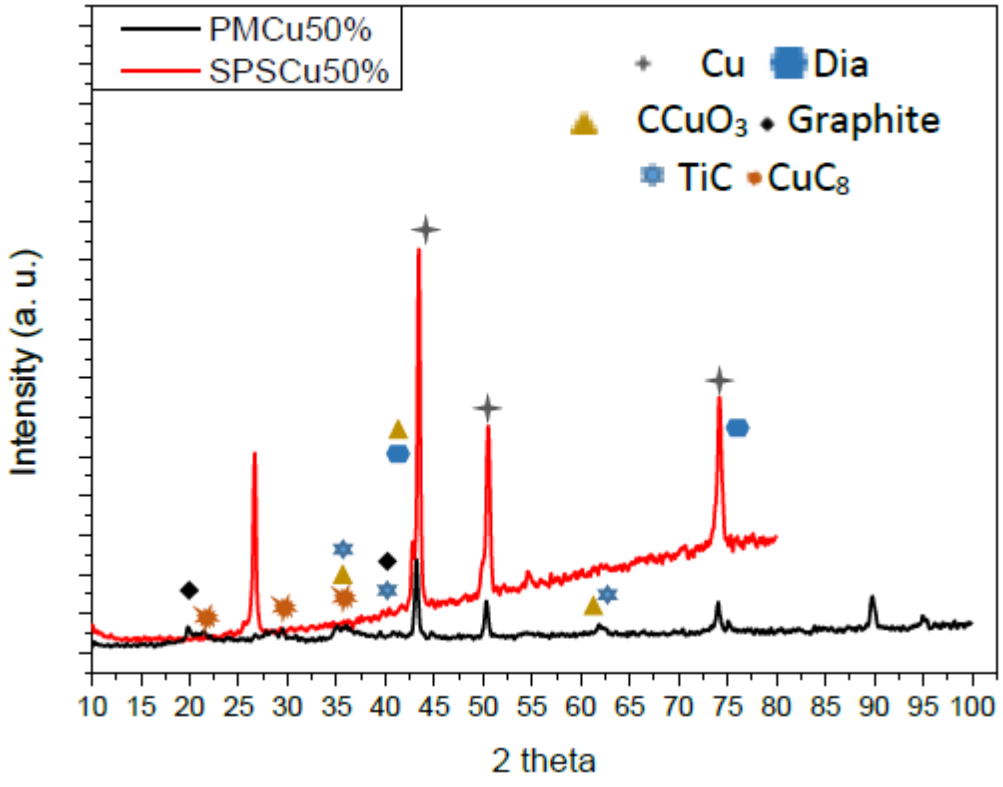

Figure (6-51): XRD pattern of Cu-diamond composites diamond composites (PM and SPS).

Chapter 7 Developing an Abrasion Test Method

This chapter deals with developing a novel device which has been designed to generate significant abrasive wear in a material developed to have extreme abrasion resistance, and allow characterisation of the wear behaviour. The development of a bespoke device for this was required after many attempts to use traditional methods for wear testing, such as tribometers, and finding that measurable wear did not occur. The description of this rig presented here will start with detailing the final configuration used for later experiments in this work, and describing its demonstration on standard test material, and how it can be used for assessment of abrasion resistance of materials. At the beginning of the work consideration was given to gathering data from high abrasive wear resistance materials, corresponding to the terms in the Archard Wear Equation (volume lost behavior during the test). The development and configuration of the device is explained below.

7.1 Constituent Parts

A. Steel Table

A heavy steel table was used with a top area of 60×60 cm and 80cm height to support the stand of an angle grinder. The table was chosen to be sufficiently high mass to be stable under the vibration of the angle grinder and cutting process to help the camera to capture the cutting process and ruler reading clearly.

B. Angle grinder stand

A specific mounted stand (TS 125/115 Trennständer Cutting Stand), which was designed for holding an angle grinder with 115- or 125-mm abrasive disc specification, was utilised. This was fastened by four fixation screws to the steel table before the angle grinder was mounted, as that shown in Figure (7-1) below.

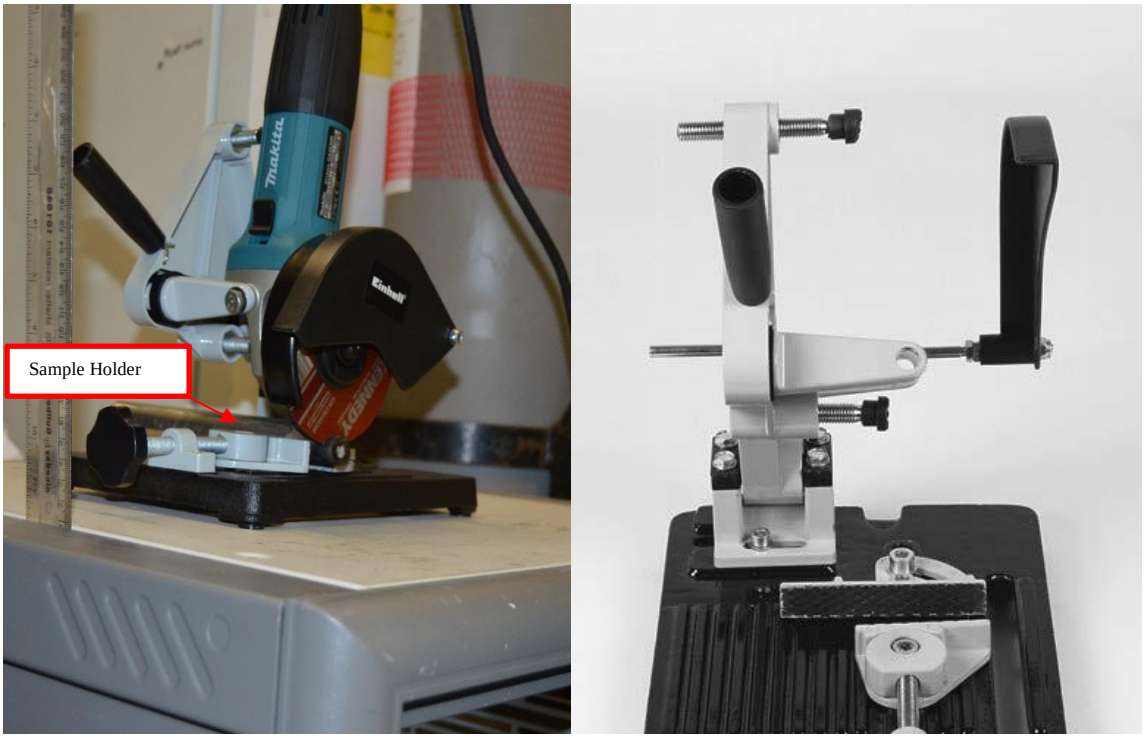

Figure (7-1): The angle grinder stand, in positioning fixed to the table.

C. Angle grinder

Figure (7-2) shows an angle grinder (Makita GA4530R 230-240V), fastened to the stand on the steel table. This angle grinder uses 115 mm disc diameter at speeds of 11,000 RPM. For the test desired, steady, constant pressure on the angle grinder was required, and to achieve this a specific dead weight was applied to the handle of angle grinder stand to maintain a fixed pressure. This weight was a 1.6 kg steel ring, which acts in addition to the weight of the angle grinder and stand arm, which was assessed as 2.9 kg. Thus, the weight applied during the tests was 3.5 kg.

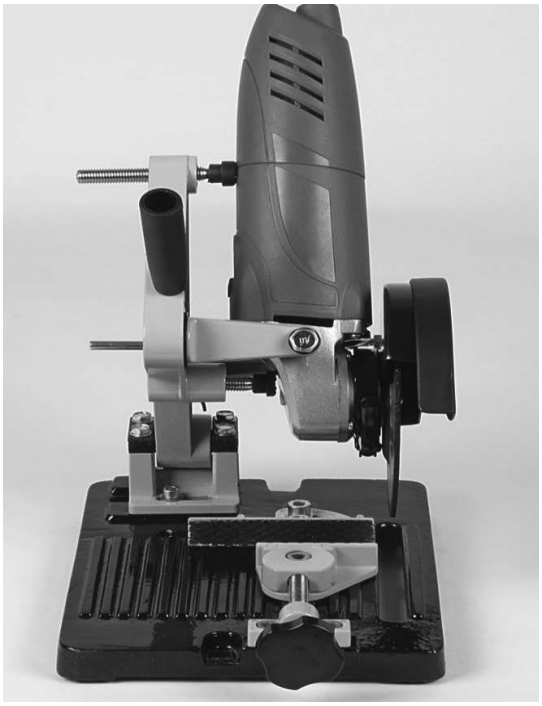

Figure (7-2): Angle grinder fastened to support stand.

D. Sample Holder

A stainless-steel sample holder was machined from mild steel tube with dimensions shown in Figure (7-3). This holder, which helps to fix the sample tightly with two holding screws and prevent movement during the test, is sufficiently long to be held on the stand clamp, to which the angle grinder stand is attached as shown in Figure (7-1) above.

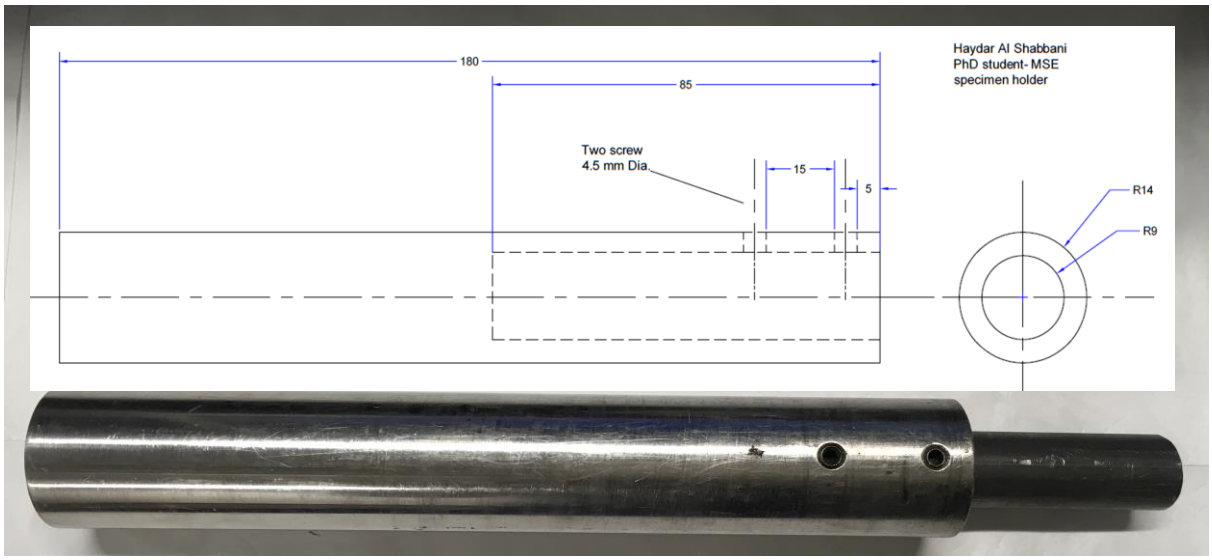

Figure (7-3): Machined sample holder.

E. Camera and Ruler

As well as cutting the sample, the rig must also record the progress of the cutting operation with time. The camera is therefore a very important part of this equipment, as this captures both the change in wheel dimensions (as the wheel itself is abraded) and cutting depth in the tested sample (as it is abrasively cut), with the cutting time. The changes in these distances can be quantified with the aid of a ruler, placed between the camera and the test (wheel and sample) during the test. The ruler was placed as close to the test as possible (around 3 cm distant) to avoid perspective errors and to allow the greatest resolution in the images possible (changes taking place on cutting were of the scale of millimetres). These can be derived later by analysing the dimension changes recorded by the ruler reading. Following this, the actual lost volume of material can be obtained from the dimensional changes by calculations (as discussed in detail in the next section). The camera and ruler position relative to the test is shown in Figure (7-4).

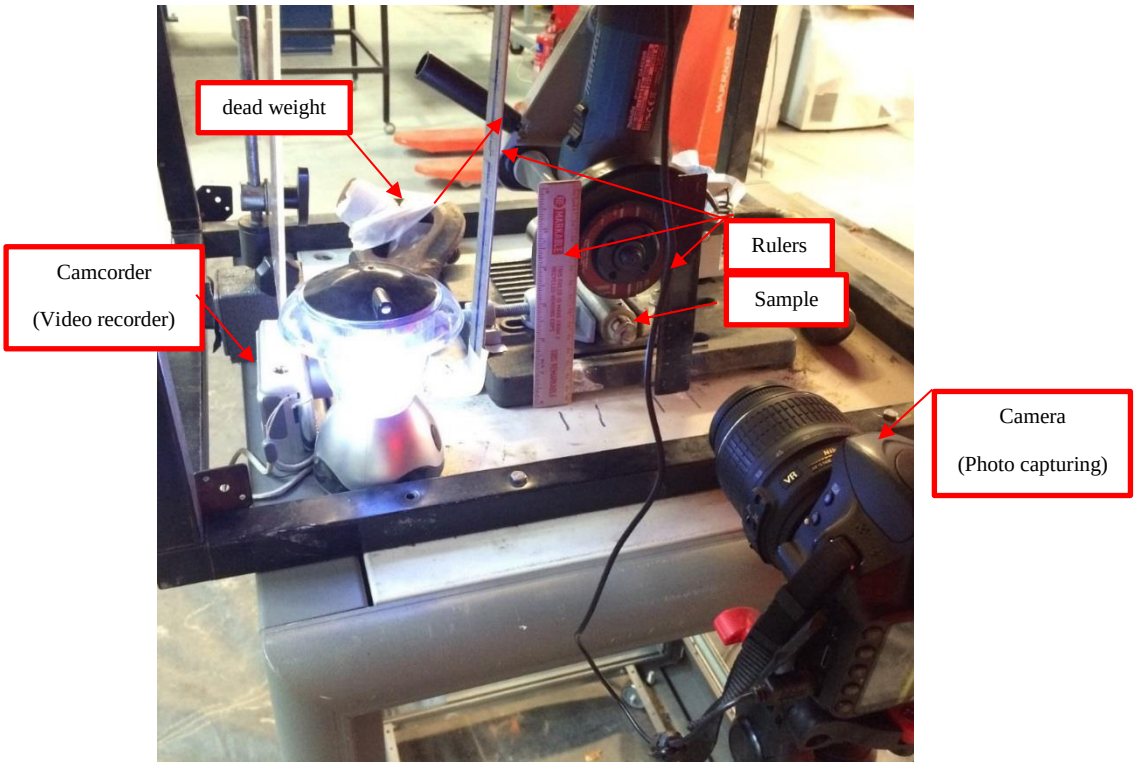

Figure (7-4): The position of the camera and ruler in the test configuration.

7.2 Mathematical Formulas and Assumptions Made in Calculations

The equations and formulae which were applied to calculate the lost volume from both sides in the test (the wheel and the sample), are derived from mathematical calculation of volumes. In doing these some assumptions are made, namely:

i) the wheel thickness is considered to be unchanging throughout the test; some rounding at the cutting face may occur, but cut sides were observed to be parallel in samples.

ii) the contact line at the cutting interface was considered to be a straight line contact, not a curve which it actually will be, although the relative radii of the wheel and the sample (57.4 mm and 4 mm, respectively) mean that this is not a significant difference. The intersection of the circles was represented by an auto CAD drawing shown in Figure (7-5) with the arc of a large circle (the wheel) cutting a small circle (the sample) to a depth of 0.5 mm (a typical depth achieved in most tests). This shows the true arc length is 3.7614 mm, while the linear distance at the same depth is 3.7607 mm, a difference of only 0.0007mm (a difference of <0.02%). The greatest difference possible, when the 8 mm diameter sample is cut halfway, is 0.0033mm (0.04%).

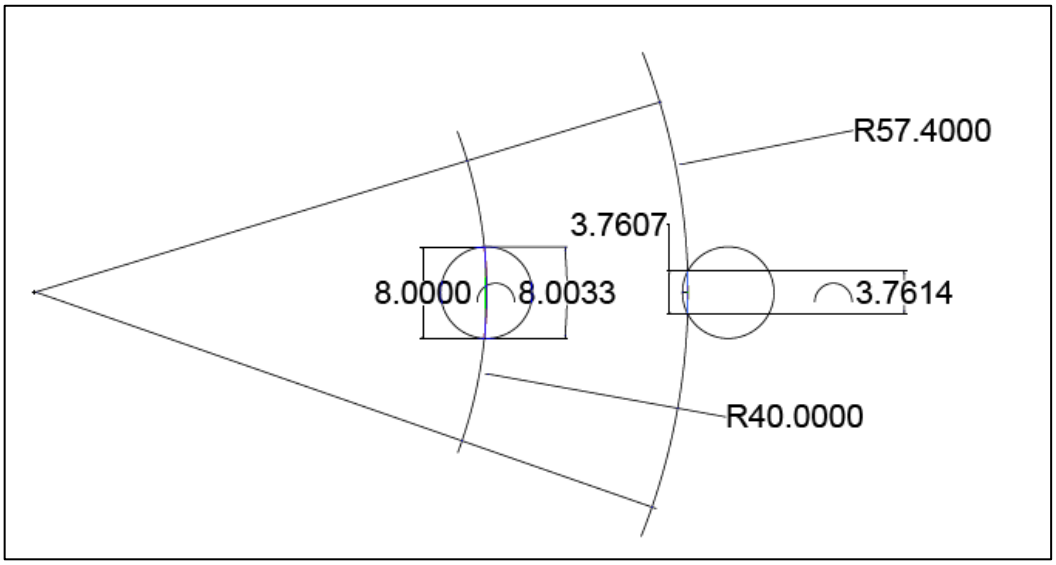

Figure (7-5): Auto CAD drawing showing the intersection of different circles representing the different geometry created during cutting test.

Following tests, the sample volume loss (the cut volume) was calculated from the segment of a circle corresponding to the penetration depth of the wheel as that shown in Figure (7-6)

$$Segment\ volume = \frac{1}{2} \times R^2 \times \left(\frac{\pi}{180} * \theta\right) - (Sin\theta) \times t \quad \text{Equation 7-1}$$

where the angle θ, which should increase with progression in cutting depth, can be found with the assumption that the contact arc at cutting contact is linear from:

$$\theta = (Cos^{-1}(\frac{R-Di}{R})) \times 2 \quad \text{Equation 7-2}$$

where R is the radius of the sample and Di is the depth of cut at specific time, *i*.

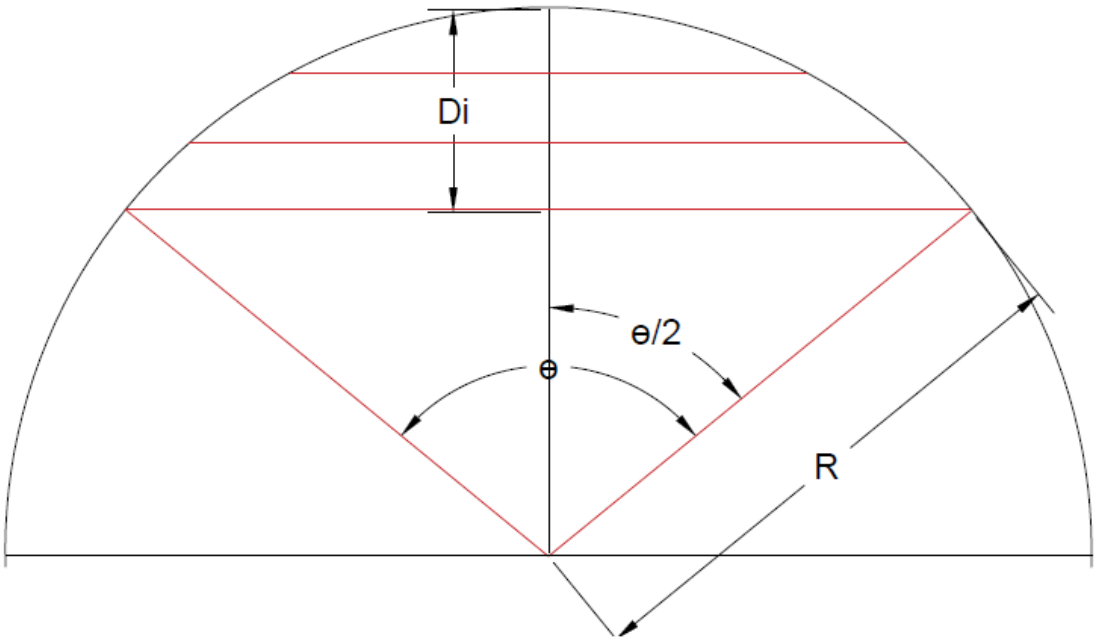

Figure (7-6): Auto CAD drawing showing the calculation of sample wear.

From this, the loss of volume from the wheel by wear is the difference between the volume at a particular time and the original volume of the wheel.

$$V_{Los} = \pi \times R_1^2 \times t - \pi \times R_i^2 \times t \quad \text{Equation 7-3}$$

where R_1 and R_i are the radius of the wheel at specific cutting times (1 at the beginning and *i* at a time during the test), respectively, and t is the wheel thickness, which is assumed not to change during the cutting process.

7.3 Running the Test

To obtain as precise as possible a result the test must run under video recording or with a camera with the capability of capturing at least 2 images per second. While the cutting wheel is running, a Digital Single-Lens Reflex Camera (DSLR) (Nikon D3200 Camera) was used. All samples were tested at the same controlled conditions of holding weight, rotational cutting speed and grade of cut-off wheels (alumina reinforced resin bonding cut-off wheel, Kennedy 230-4430K, supplied by Cromwell Industrial Tools UK - Sheffield) were used. The photos taken during the cutting process were used to measure ruler reading and hence the volume lost, which was plotted with cutting time to represent the abrasive wear of each sample. The overall rig is schematically shown with relevant dimensions in Figure (7-7).

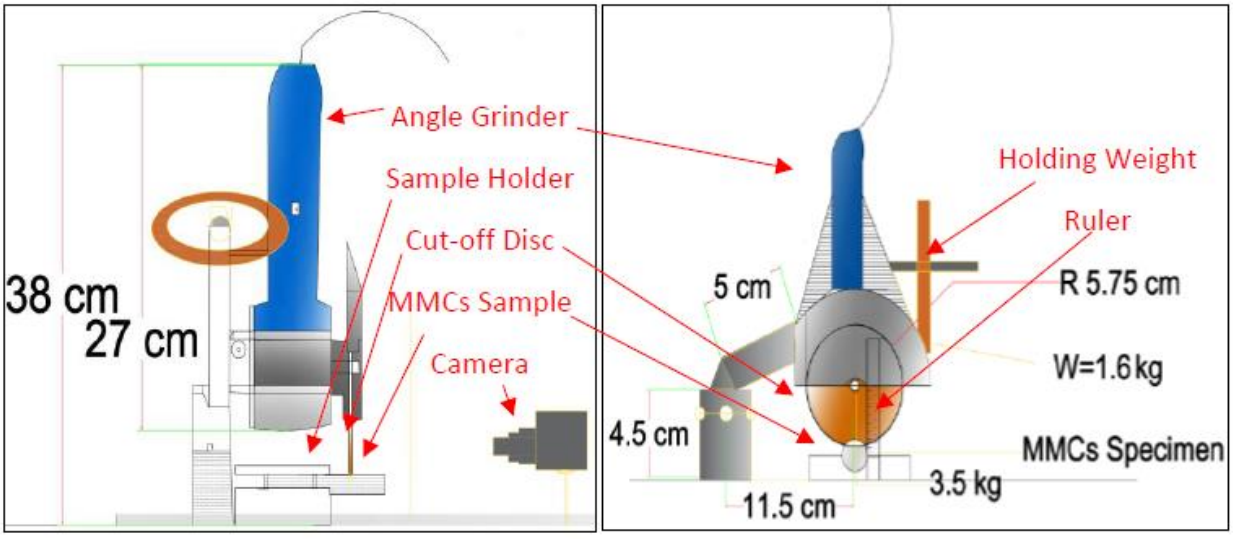

Figure (7-7): Schematic diagram of the configuration of the test rig.

7.4 Validation Test and Processing Results

The cutting rig was previously discussed in the above sections. The device generates abrasive wear by cutting samples (including the composites produced here) and comparing how much of the cutting blade volume was lost against the volume of material removed from the sample in cutting into it. The same type and dimensions of the wheel was utilized for all experiments to give an accurate comparison of the abrasive effects the composite materials had on the cutting wheel.

The standard Archard equation, which is widely used for assessing wear, was discussed earlier in chapter 4. This requires an accurate value for the contact distance for the blade with the workpiece during cutting in the current case. Therefore, this equation cannot be applied because the contact distance cannot be obtained as it changes throughout the cutting process in a way that is difficult to measure and account for. To deal with this, some previous researchers have taken the approach of defining a parameter representing a wheel wear resistance, which is called the G ratio. This is the material removal volume divided by volume worn of wheel, so a high G ratio indicates a minimum amount of wheel lost, and vice versa [147], [149], [151], [152], in the current work the wheel wear is very high, meaning there should be very low values of the G ratio for tests on MMDCs. We apply calculations depending on volume lost to represent the wear in both parts of the wear test (sample and wheel), with the results plotted with a cutting time. The high reduction seen in the wheel radius in comparison with much lower depth of cut of the sample can be considered as an indicator of the amount of abrasive wear (proportional wear) of the cut-off blade; at the same time, it refers to the degree to which the specimen is strong enough to resist the cutting process.

Another important point to note in the plots (and the majority of the other results recorded in the thesis) is the linear trend of wear, which corresponds to Archard's equation. Even though there is radial reduction in the wheel dimensions throughout test, the increasing frequency with which a particular point on the wheel arrives at the cutting surface (dependant on $v/2\pi r$) is compensated for by the decreasing linear velocity of the cutting blade (dependant on $\pi.r$); i.e. the angular velocity is held constant. This keeps the trend linear.

When wear curves are analysed in more detail, it is seen that the wheel wear often occurs in three stages, as in a conventional grinding process Figure (4-10); first a rapid initial wear stage, second steady state wear stage and then more rapid or final failure wear [147], [151], [152]. These are comparable to the three wear stages in flank wear curve in machining tools [222] Figure (7-8). In these moderate grinding processes the grinding trends in the first and third rapid stages have been reported to be unstable as a result of the highly abrasive wear rate. Furthermore, in the present case the mechanism linking grinding with radial wear of a wheel is still not sufficiently clear, because irregularly in configuration and distribution of the abrasive grains through grinding process [152]. Therefore, in the experiments here abrasive cutting of the unreinforced matrices (Ni, Ti, and Cu), that were produced using the same PM techniques employed to make MMDCs, behaviour similar to the conventional grinding curve and flank wear curve, is seen. In these descriptions abrasive wear exhibits three wear stages with time as shown in Figure (7-9), Figure (7-10), and Figure (7-11), display wear curves of the unreinforced matrices (Ni, Ti, and Cu respectively) and the abrasive wheels which cut them. Such behaviour has been studied by Mlikin [149] Figure(4-9). The estimated relative wear values of these materials were found by linear regression of the wear curve in the second stage. This method for estimation of relative wear was used for all results in this study and is discussed mathematically in the next section. The relative wear values, which were estimated from Figure (7-9), Figure (7-10), and Figure (7-11) are 2.5, 1.3 and 0.4 for Ni, Ti, and Cu respectively, while the aluminium matrix did not cause noticeable wear in the wheel.

The slope of the near-linear stage of the wear curve has been reported to represent in service wear in machining tools and for estimating tool life. Koren [223] derived a wear equation (equation 7-4 below) at this stage from the flank wear curve (a typical wear curve), Figure (7-8), to evaluate wear over time in machining tools.

$$W(t)=B+Aat \qquad \textit{Equation 7-4}$$

Where, W is wear at any specific time (mm), Aa is slope of curve in near-linear stage, and B is imaginary intersection with wear-axis at fixed value of time (0) [223].

To show the wear behaviour in an appropriate and comparable way, most of the results will be displayed by scatter plots, which show the material lost against cutting time for both samples and the cut-off wheel and comparing the result. Then, the slope of the secondary stage wear (the steady stage) for the composites, where distinguishable wear

stages are seen as pure matrices below (Figure (7-9), Figure (7-10), and Figure (7-11)), or the slope of entire curve for samples which show above 85% linearity (R^2) (in some composite in next chapters for example) of the material removal curve are found as characteristic values of the material behaviour. These slopes represent removal of material with time, of the samples and the wheel. The wear resistance for each material is interpreted in the form of relative wear, which was determined by dividing the slope of removed material from wheel by slope of removed material from samples. In addition to test matrices without reinforcement a conventional padlock with a similar diameter to the samples. A 7mm diameter steel padlock was cut in 1.5 seconds with about 75 micrometres worn from the cutting disc radius, meaning the relative wear was about 1.4. Cutting of a mild steel tube with 2.5 mm wall thickness (the same type as was used to contain the MMDCs), does not affect the cutting wheel at all (relative wear=0).

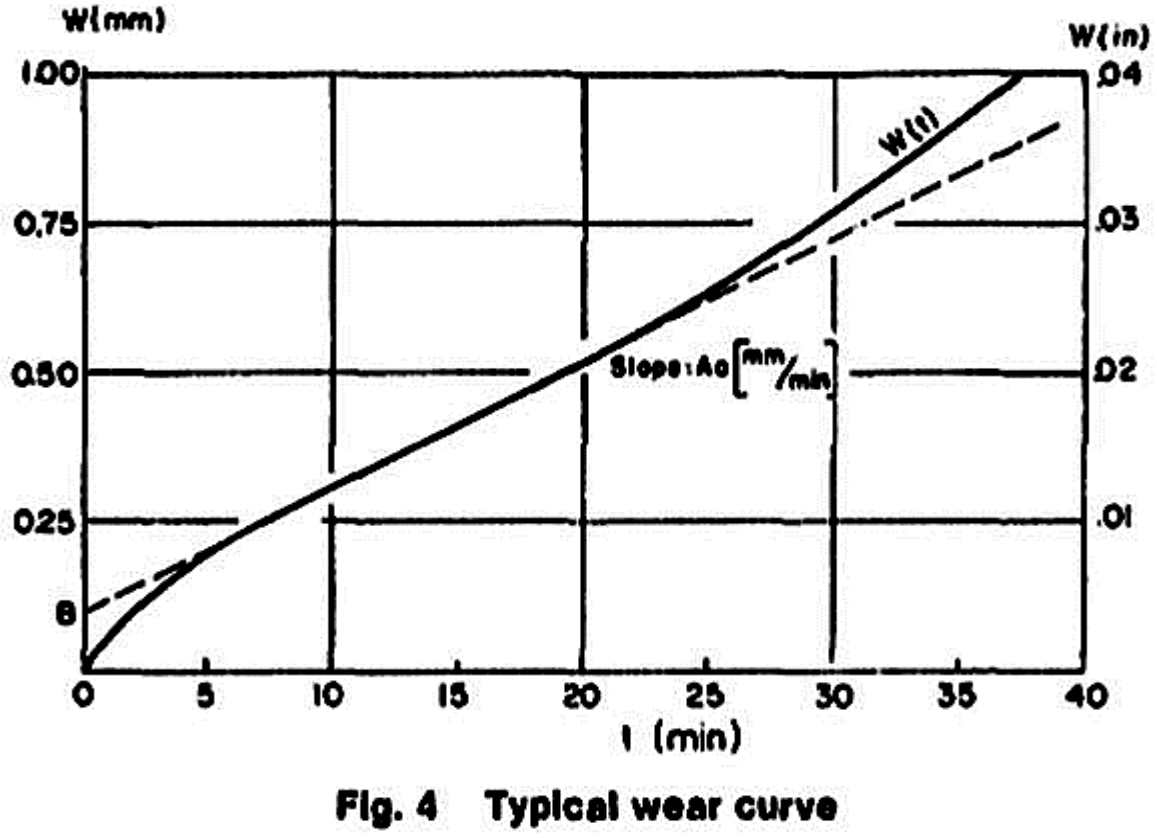

Fig. 4 Typical wear curve

Figure (7-8): Flank wear curve or as called typical wear curve by ref. [223].

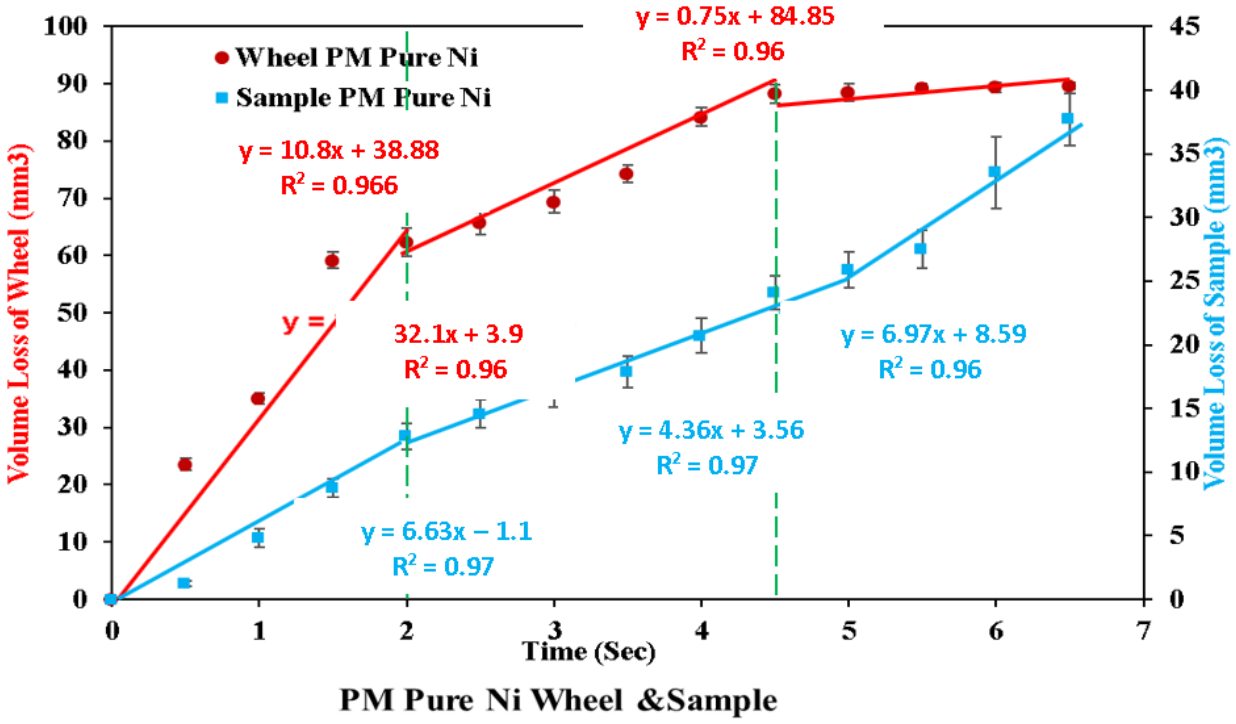

Figure (7-9): Volume loss against cutting time of PM-pure Ni samples and wheels cut them.

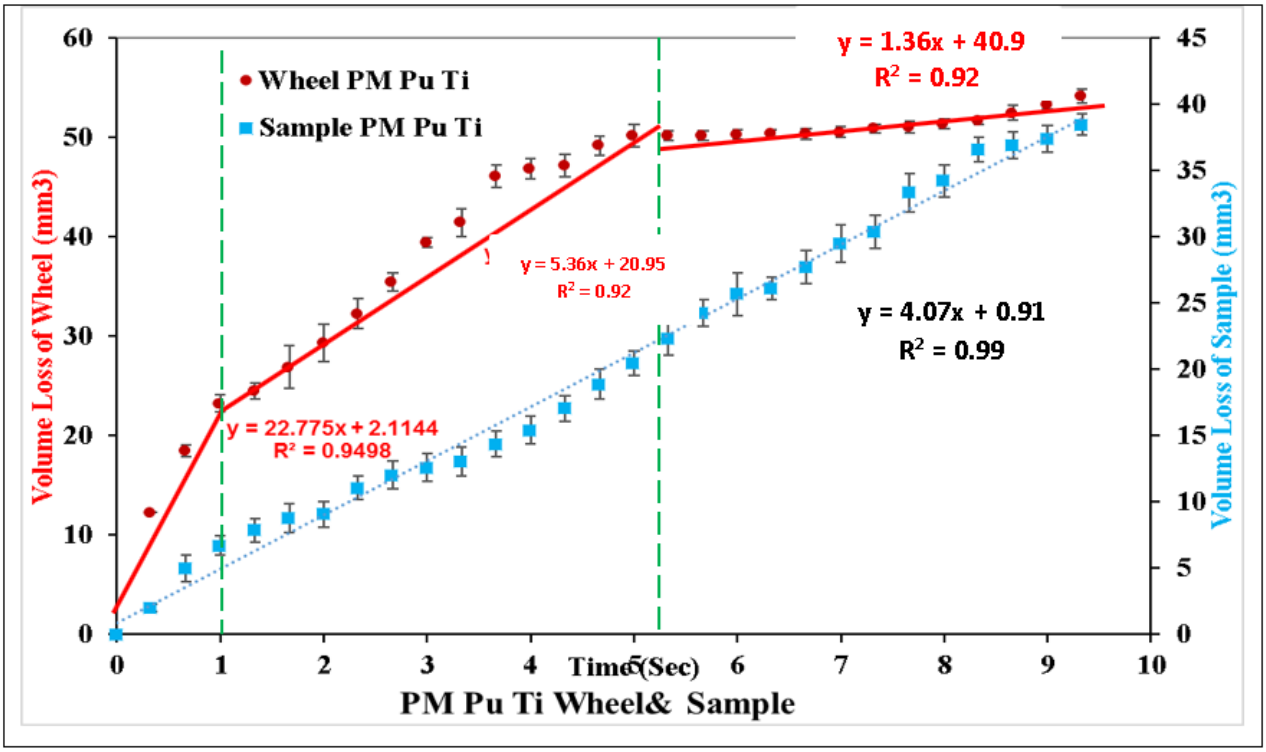

Figure (7-10): Volume loss against cutting time of PM-pure Ti samples and wheels cut them.

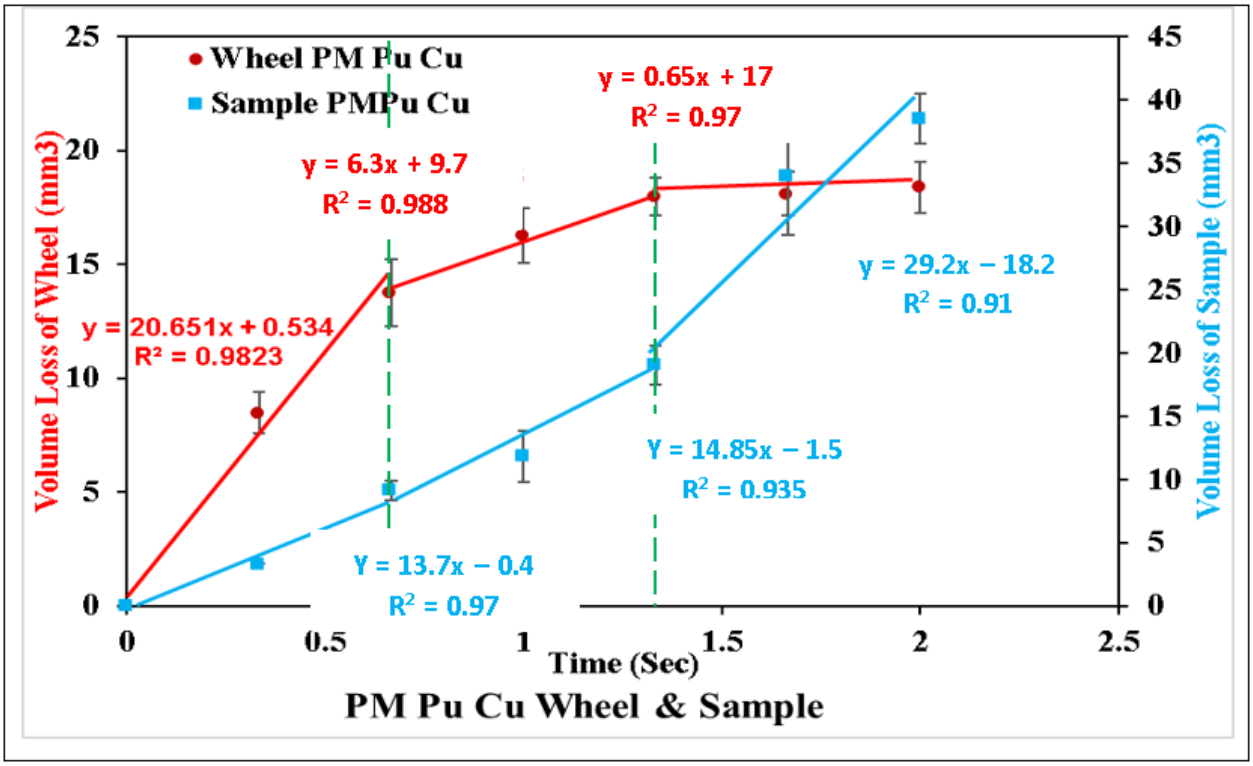

Figure (7-11): Volume loss against cutting time of PM-pure Cu samples and wheels cut them.

7.4.1 Mathematical Models Applied to Wear Estimation

Generally, where there is a complex behaviour such as wear, it is desirable to find a mathematical description to aid analysis. This is the case for the abrasion tester device developed in this study. The calculation included each reading to be as precise as possible allowing the standard deviation (SD) of the samples to be calculated by having at least three readings for the cutting sample and wheel at each specific time.

Most experimental studies express their data distribution by using either the standard deviation (SD) or the standard error of the mean (SE). There can be confusion between the SD and SE in research. Nevertheless, they are statistically different and each of them has its own calculation process and meaning. SD refers to how close the mean is to the actual sample data (it is a dispersion of data in a normal distribution), while SE statistically extracts this sampling distribution (it is the SD of the theoretical distribution of the sample means), therefore, the SE is a result of SD per square root of the number of data points [224]. The standard deviation is calculated by applying equation (7-5) [224]. In this work,

Microsoft Excel software was used to find the standard deviation and to plot results to represent wear curves of cut-off wheel and samples against cutting time.

$\boldsymbol{SDev.} = \sqrt{\frac{\sum(\boldsymbol{x}-\boldsymbol{x}`)}{\boldsymbol{n}-\mathbf{1}}}$ ………………………………………………………………*Equation 7-5*

At this point the scatter plot can be used to estimate wear properties of the testing samples, using the plotted curves with error bars (see Figure (7-9) for example), to find wear properties of samples.

In many experiments regression analysis is a useful tool to understand the behaviour of data and the trend (here this is the volumetric wear (W)). Where there is a linear relationship between two parameters plotted against each other, the regression equation can be used to estimate the relationship between the dependent variable and the independent one [225] (W/t in the current study).

Here, we have assumed that the curve is divided into three stages, each of near-linear form, by which the Linear Least Squares Method equation (7-6) can be applied for data fitting.

$Y = b\,X + a$ ……………………………………………………………………… *Equation 7-6*

where: Y represents dependent variable (volumetric lose in mm^3)

X represents independent variable (time in Sec)

b is slope of line , $b = \frac{\sum \boldsymbol{XY} - \frac{\mathbf{1}}{\boldsymbol{n}}\sum \boldsymbol{X} \sum \boldsymbol{Y}}{\sum[\boldsymbol{X}^{\mathbf{2}}] - \frac{\mathbf{1}}{\boldsymbol{n}}(\sum \boldsymbol{X})^{\mathbf{2}}}$……………………………………………………*Equation 7-7*

a is y intercept (that fixed value of Y when X=0), $a = \frac{\sum \boldsymbol{Y} - \boldsymbol{b}\sum \boldsymbol{X}}{\boldsymbol{n}}$**…***Equation 7-8*

n is a number of data points

An important assumption in linear regression is that the relationship is indeed linear, that the slope does not change. The assumption of linearity is used when it can at least offer a measure of the trend [225]. Another important factor therefore when using the linearity assumption is to estimate how close it is to reality; this factor is called a Coefficient of determination $r^2_{(XY)}$ or (R^2) [226]**,** a value between 0-1 (close to 1 means the regression linearity is high, and vice versa if it is close to zero). This factor can be found by equation (7-9).

R2 = $1 - \frac{SS_{err}}{SS_{tot}}$ …………………*Equation 7-9*

where: $SS_{tot} = \sum(Y_i - \bar{Y})^2$

$SS_{err}=\sum(Y_i - Y^*)^2$

The linear regression model is used for prediction of Y with given X (if they are independent). When using it, it is good practice to state the R^2 of the equation [226], [227].

Many computer programs can be used to do these calculations, particularly for a large amount of data. One of the most widely available is Microsoft Excel which is used here. An example result, for the first stage of wheel wear in the cutting of Ni, Figure (7-9), is shown below.

The first step is filling first two columns in Table (7-1) from raw data (data readings from test), then calculating the next two columns and finding the summation of all values. The next step is substituting these values in to equations (7-7 and 7-8) to find the slope and intercept of the least square fitting line (b and a) as follows:

$$b=\frac{260.3975-\frac{1}{5}\times 5\times 180.165}{7.5-\frac{1}{5}\times 25}=32.092$$

$$a=\frac{180.165-32.092\times 5}{5}=3.9394$$

Now the linear regression equation is ready substituting a and b in Equation 7-6

to be Y= 32.092 X + 3.9394 *…….....Equation 7-10*

at this point we can find R^2 when using Sum. values of SS_{err} and SS_{tot} from Table (7-1) as that shown with green highlighted in this table.

Table (7-1): Values used in least square regression method analysis and correlation.

X	Y	X*Y	X^2	Y^2	Y*(bX+a)	SS_{tot}	SS_{err}
0	0	0	0	0	3.94	1298.38	15.52
0.5	23.53	11.77	0.25	553.66	19.99	156.33	12.56
1	35.06	35.06	1.00	1229.20	36.03	0.95	0.94
1.5	59.16	88.73	2.25	3499.31	52.08	534.62	50.09
2	62.42	124.84	4.00	3896.26	68.12	696.27	32.53
Sum	180.17	260.40	7.50	9178.44		2686.55	111.65
Mean	36.03					SS_{err}/ S_{tot}	0.0416
						R^2	1-0.0416
							=0.9584

Chapter 8 Abrasion Wear Assessment of AMDCs (Cutting Test)

This chapter will focus on the primary abrasive wear test, which assesses the resistance of a material to a process sometimes named cutting wear [134]. A test is developed and described which can be used to assess the performance of the MMDCs produced here under conditions of abrasive cutting.

To verify the test and be sure the observed wear in the cutting blade was caused by composite effects only we have also cut one of the empty mild steel moulds (without filling by composite) showing no noticeable wear on the cutting blade.

Displaying the tested wear properties of all samples (Al, Sn and epoxy matrices) processed by molten metal infiltration in histogram plots together, allows comparison of the wear behaviour, Figure (8-1) a and b for samples and wheels, respectively and Figure (8-2) for relative wear of composites.

Through this study the effect on abrasive wear of a number of material parameters is assessed, including the effects of diamond particle size and its surface condition. These are explored for the fixed condition of aluminium as the matrix and processing by the gas infiltration process. After it is found which particle size is the best, the result will be compared with aluminium reinforced by the same size reinforcement processed by other manufacturing methods; conventional powder metallurgy (PM) and spark plasma sintering (SPS). Then ceramic particles (alumina and silicon carbide) are substituted for the reinforcement using the same way of manufacturing (GI).

In the next chapter, other matrices are used with different production methods applied to study their impact on wear behaviour in MMDCs. This chapter continues with composites manufactured by melting matrices.

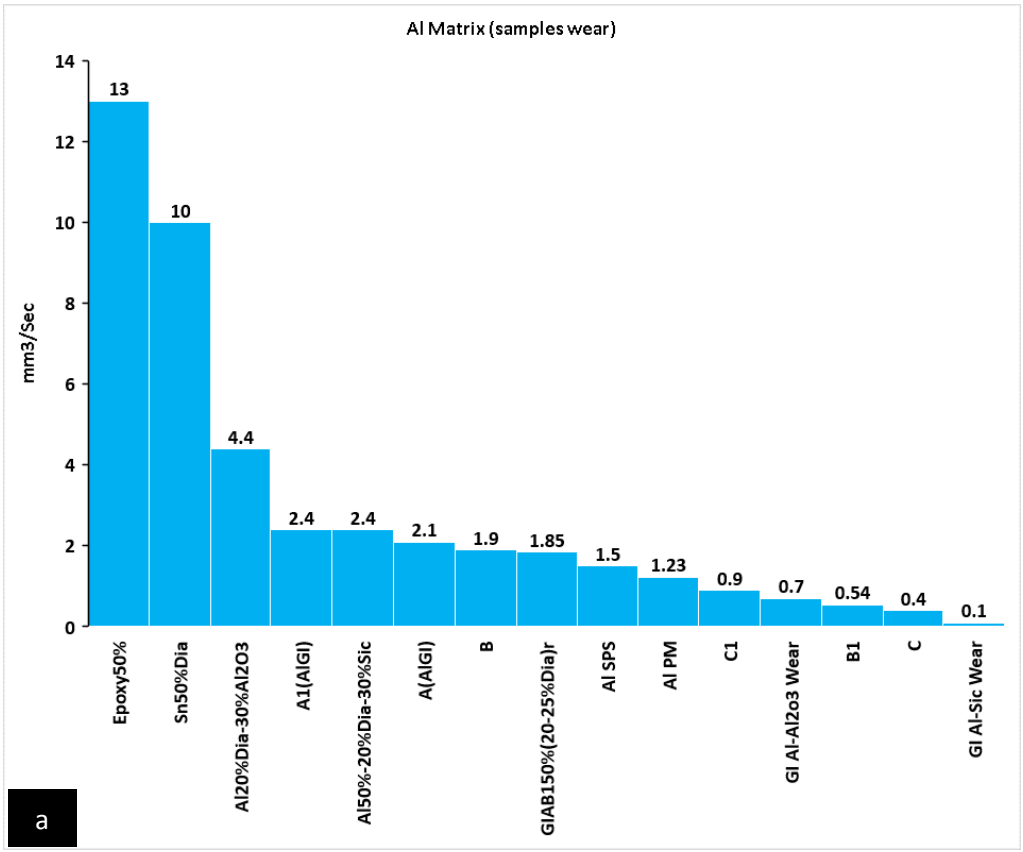

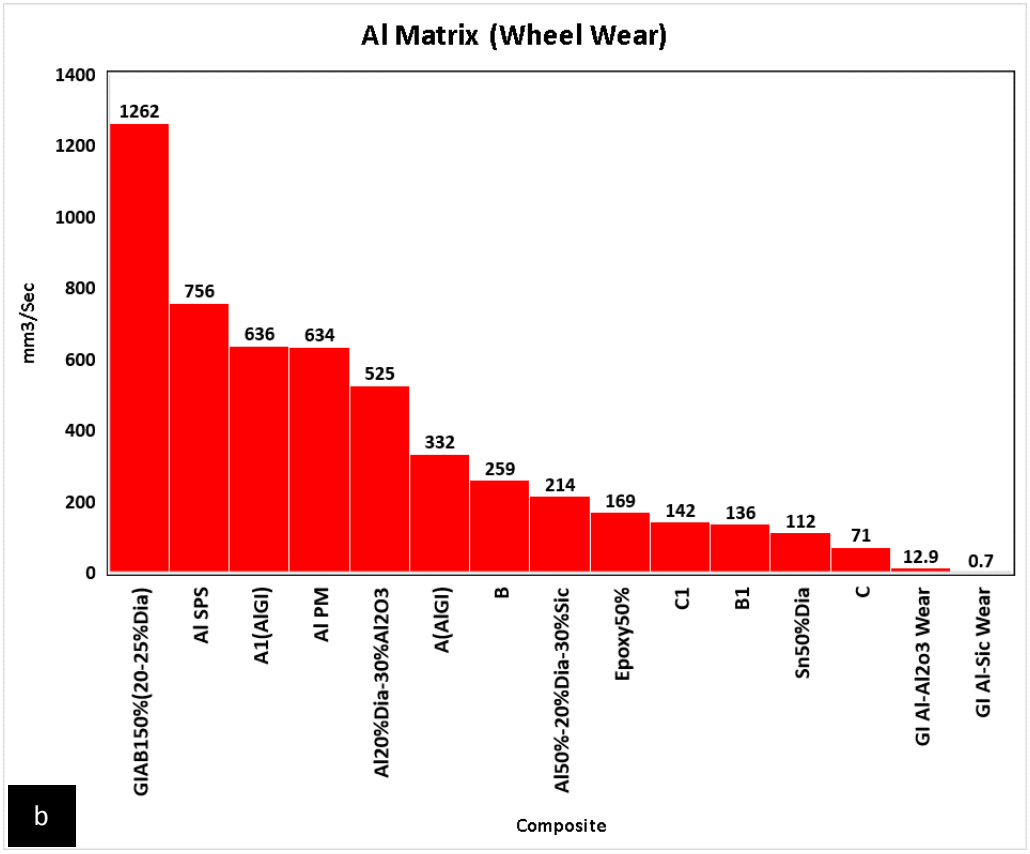

Figure (8-1): Summary of abrasive wear of composites a-samples and b-wheels used to cut composites.

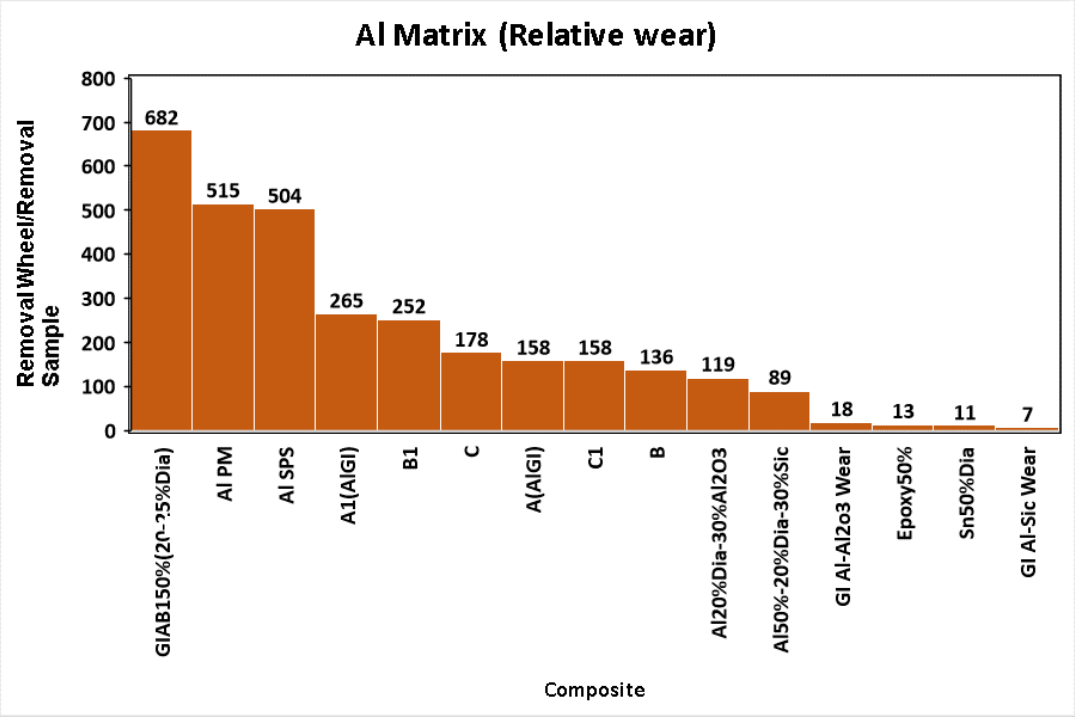

Figure (8-2): Summary of relative wear of composites.

8.1 Effects of Different Diamond Particle Sizes and Surface Conditions

At the beginning of this study, the Gas Infiltration technique (GI – described in chapter six in more detail) was utilized to manufacture Aluminum Matrix Diamond Composites (AMDCs) by using three different particle sizes of diamond with different modified surface conditions (coated with Ti and uncoated) combined with aluminum-1wt. % Mg as a matrix. Many studies have reported that the addition of Mg to aluminium enhances wettability of aluminium to reinforcements by decreasing its surface tension [15], [97], [99] with the Mg addition at a limited percentage (<3%) [15], [99] to eliminate carbide formation and remain in the solid solution region at the process temperature, as shown in Figure (3-2) [98] (pp. 39). These materials and technique were applied to achieve sufficient bonding between phases in the molten state of the matrix, in order to judge which particle size and surface condition can achieve highest abrasive wear resistance behaviour. The wear data of this Al-diamond composite could then be used as a fundamental reference to identify the best particle size and surface condition that showed the highest wear resistance behaviour (relative wear) for further later development with other matrices and techniques. Figure (8-3 a and b) show the trend of samples and wheel

wear during abrasive cutting of AMCs reinforced by the larger particle size used which is 420-500 µm for both surface conditions (Ti-coated and uncoated). The composites reinforced with this particle size are identified as A and A_1 when the subscript number 1 indicates that the AMCs are reinforced with coated Ti diamond particles while the letter A without subscript number means the AMCs are reinforced by uncoated diamond. The volume lost (calculated from the depth of cut and reduction in wheel diameter) in both abrasive elements engaged in the test (sample and wheel) is plotted versus cutting time to reveal how the reinforcement conditions effect the abrasive wear properties of the sample itself, and how much each sample causes degradation of the cutting wheel by abrasive effects. Hence, the high reduction in the wheel volume compared with the wear of the MMDCs is an indication of rapid abrasive wheel wear during the cutting process. Some MMDCs results showed that the first and third wear stages were not clear and were dominated by the second stage, which will be discussed in more detail through this chapter.

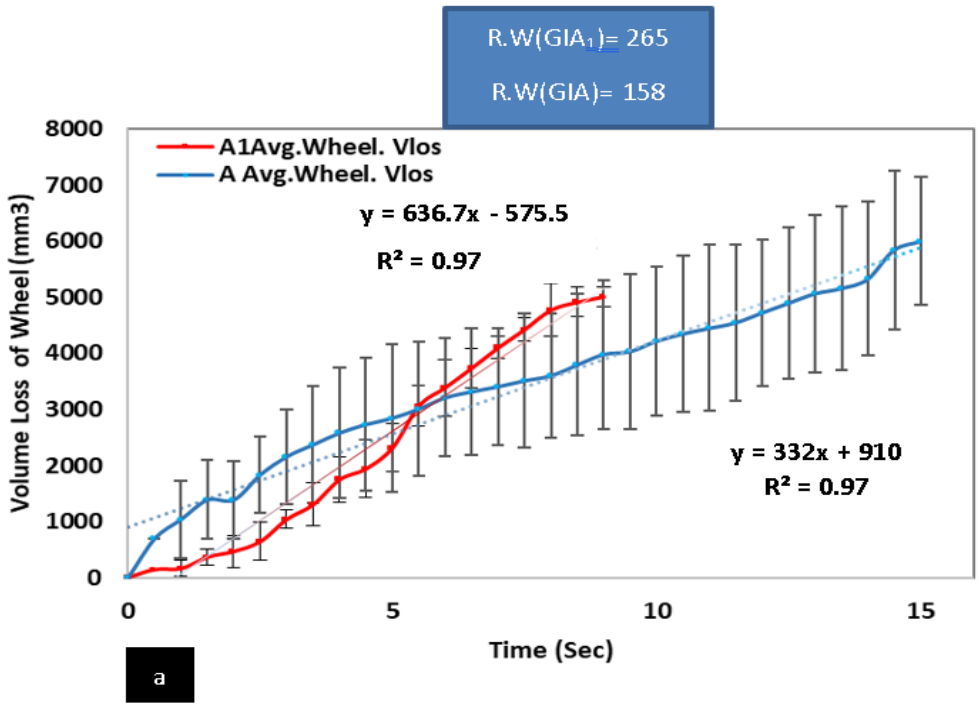

a

Cut-off wheel of A&A1 MMDCs

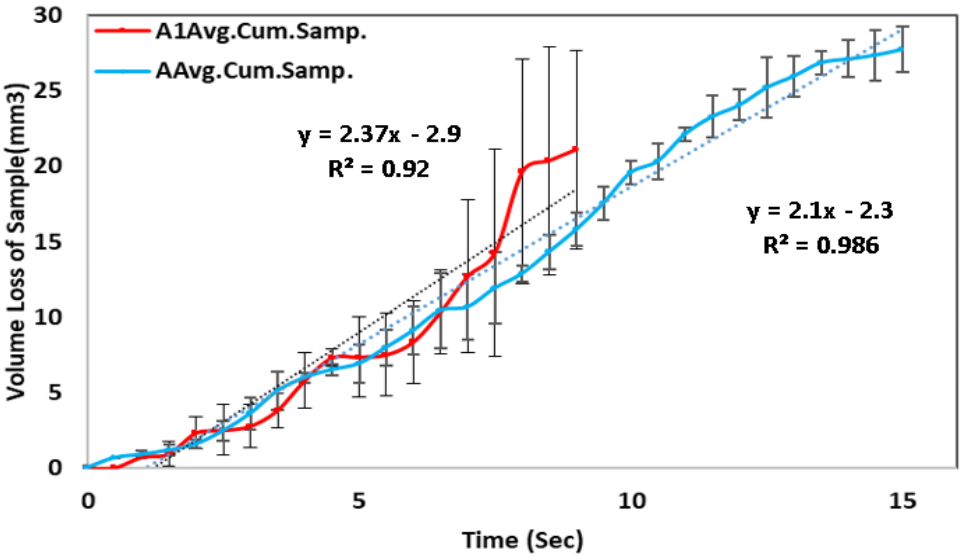

b

A & A1 MMDCs

Figure (8-3): a) Volume loss of wheel cut through A_1 sample (AMDCs reinforced with Ti- coated 35/40 grit (420-500 µm) diamond particles-red curve) and A sample(AMDCs reinforced with uncoated 35/40 grit (420-500 µm) diamond particles-blue curve) versus cutting time (the 1st wear stage is too small and neglected for the purposes of comparison) and b) Volume loss of A and A_1 samples versus cutting time.

As shown in Figure (8-3 a) for both wheels, which were used to cut the samples and the two AMDCs samples (A&A_1) Figure (8-3 b) there is approximately a linear wear trend with some fluctuation. The variations from linear behaviour may come from some pulled out reinforcement particles or cavities in either of the wear elements, or could be related to the nature of the test where the resolution depends on the distances being extracted from the video images. Differences in wear behavior are noticeable between A and A_1 although the penetration of the cutting wheel in the sample is somewhat similar in both, especially at the beginning of the wear test until about 7 s as shown in Figure (8-3b). The acceleration of wear in the cutting wheel on the other hand was initially more in the wheel which cuts A sample, though at later times the wear in the wheel that cuts A_1 sample is at a higher rate, Figure (8-3a). This correlates with the time at which the depth of cut becomes more in A_1 sample. The differences in wear behaviour will be more obvious when the relative wear is found (by dividing the slope of wheel wear curve by the slope of sample wear curve, assuming there is a linear trend of wear with time). The resulting relative wear can be considered a performance metric for the samples, as it relates to both the relative wear of the samples themselves, but also how they degrade the cutting blade (an important aspect for security applications).

Nevertheless, the linearity of the curves may decrease to about 91%, for example in the wear curve of A_1 sample Figure (8-3b). Examination of the error however allows for a linear trend to still be consistent with the data. The results of this study indicated that the relative wear values were 158 and 265 (wheel vol. lost/s ($mm^3 s^{-1}$) / sample vol. lost/s ($mm^3 s^{-1}$)) for A and A_1, respectively.

That means the increase of relative wear was about 68% in A_1 sample compared with A. This increase may be interpreted as arising from the existence of the Ti coating, which leads to good bonding at interfaces and prevents or eliminates carbide formation at interfaces [184].

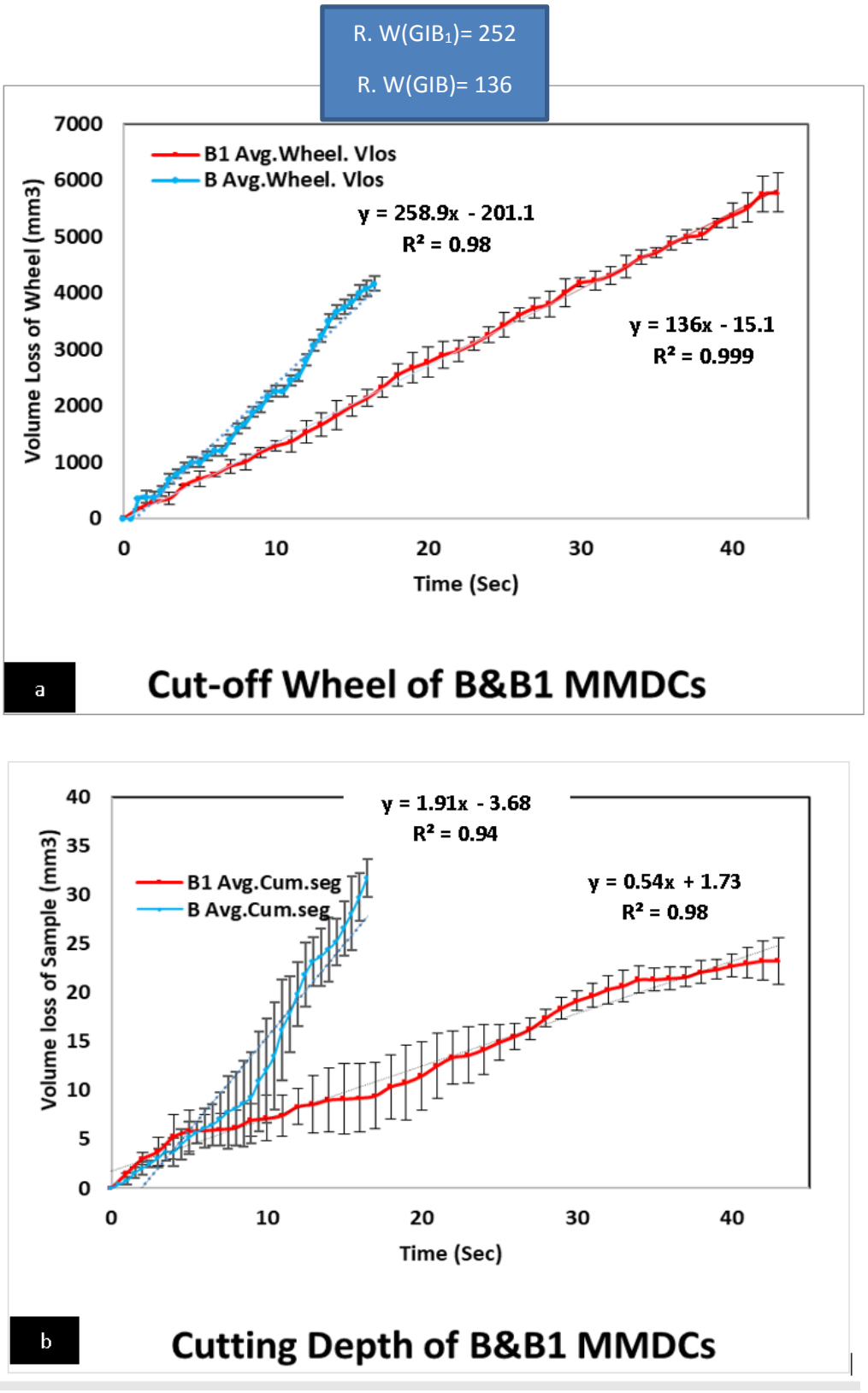

Figure (8-4): a) Volume loss of wheel cut through B_1 sample (AMDCs reinforced with Ti- coated 60/70 grit(212-250 µm) diamond particles-red curve) and B sample(AMDCs reinforced with uncoated 60/70 grit(212-250 µm) diamond particles-blue curve) versus cutting time and b) Volume loss of B and B_1 samples versus cutting time (the 1st wear stage is too small and neglected for the purposes of comparison).

Figure (8-4a) shows the wear gradient of the wheels used to cut B and B_1 samples. The slopes of the curve here are scientifically different from the wheels used to cut A and A_1 samples, but the slope is still greater with the uncoated reinforcement (B Sample). As mentioned previously, this slope represents wear of the wheel, thus the absolute wear of the wheel that cuts the B sample was higher than wheel that cuts the B_1 sample neglecting any differences in how they penetrate the sample. Considering how the samples are cut in each case shows that the cutting rate was also higher with uncoated reinforcement, and when both effects are taken together the relative wear is greater for the uncoated sample. The enhancement of relative wear in composite reinforced with coated particles (B_1) sample was about 85% compared with a composite reinforced with the same particle size uncoated diamond (B) sample.

Because of the increased number of cutting edges, which result from the breaking of some of the coated particles and the rough surface of the coated particles themselves which probably contributes to enhancing mechanical bonding between the composite constituents, the resistance to cutting is greater in a coated sample. There is increased difficulty to remove particles from matrix due to two bonding effects; chemical bonding, from the formation of intermetallic compounds at the interface, and mechanical bonding, which results from the interlocking of matrix and particles at micro cracks in the coating layer. Such cracks could result from the differences in thermal extension of diamond and Ti and its compound formed at a coated layer [60] as that was discussed in Chapter 6. Those cracks in the surface layers may promote the separation of particles to many small particles, which may be more mobile between the contacting cutting surfaces to attack the cutting blade, thus increasing the number of cutting edges, with some of small pieces of particles acting as a third body of wear. These pieces of particle probably lead to additional wear of the wheel resulting in the high rate of wear of the wheel with limited wear of sample in B_1 compared with B.

R. W(GIC_1)=158

R. W(GIC)=178

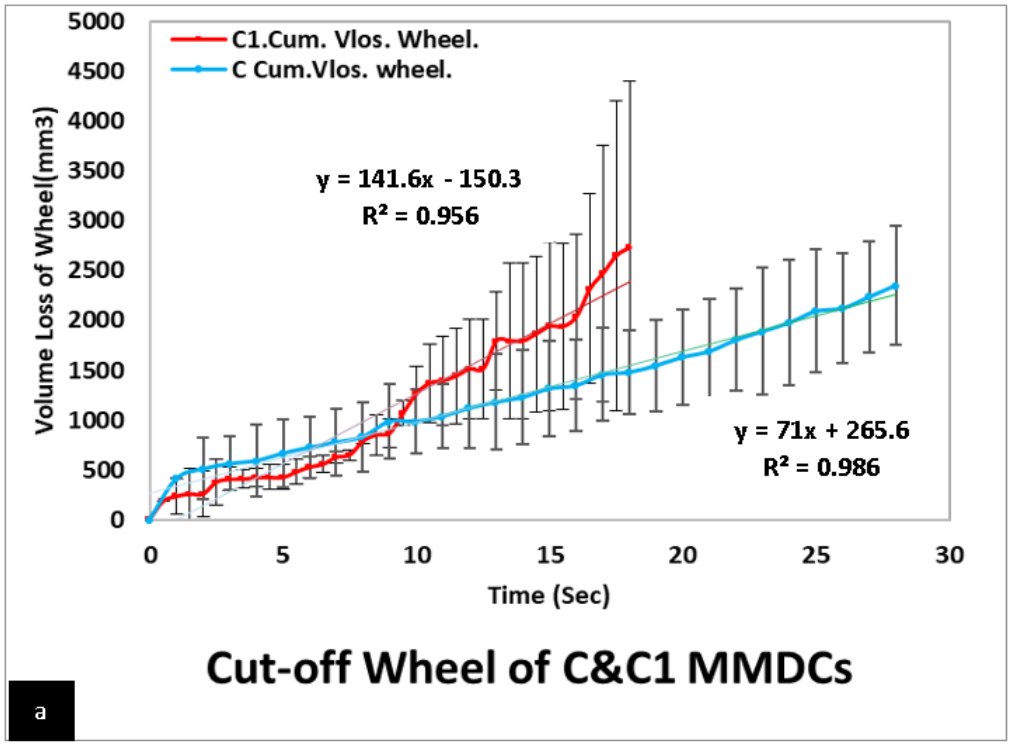

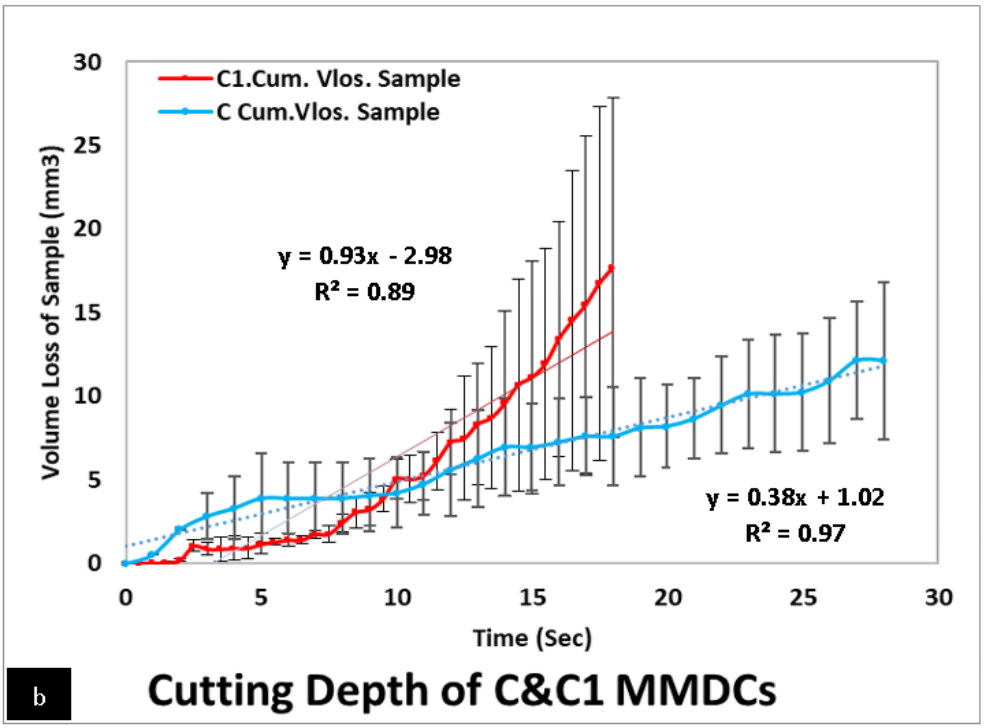

Figure (8-5):a) Volume loss of wheel cut through C_1 sample (AMDCs reinforced with Ti-coated 200/230 grit(75-63 µm) diamond particles-red curve) and C sample(AMDCs reinforced with uncoated 200/230 grit(75-63 µm) diamond particles-blue curve) versus cutting time and b) Volume loss of C and C_1 samples versus cutting time (the 1st wear stage is too small and neglected for the purposes of comparison).

Figure (8-5) shows wear behavior of samples (C and C_1) and the cut-off wheels used to cut them. These samples were reinforced with the smallest particle size diamond and were utilised in this study (63-75 µm diameter). the wear behavior in this composite was slightly different from the last two groups of composites (A, A_1 and B, B_1, with larger particle sizes), where the relative wear for coated reinforced composites (C_1) here was less than uncoated reinforced composites (C). The relative wear of C_1 was 158, about 12.65% less in comparison to the relative wear of C (178). In spite of that, the trends for wear of sample and wheel behaved similarly to A and A_1 samples and wheels with a comparable slope of lost volume with time for the separate wear elements (wheels and samples) as shown in Figure (8-5a) and b). This change of wear behavior may relate to the small particle size and the resulting increased surface area of reinforcement. This means that high portion of the total particle volume is influenced by surface processes during infiltration casting or during the coating process; in small particles such processes will affect material further toward the center of the particles. That can be experimentally shown through series of investigations which start with SEM images, Figure (6-23), Figure (6-24), and Figure (8-6), and end with optical microscope images of these composites, Figure (6-25). These tests showed that the uncoated particles were strongly affected by the process to produce a thick layer of graphite and some intermetallic compounds, which may act in the manner of solid lubrication at the contact surface, especially when the surface of diamond has graphitized. That would result in the long time observed for cutting of the sample and wearing of the blade faster than the sample. Therefore, there is a limit to penetration of the cut-off blade into samples as shown by the slope of the blue line in Figure (8-5b). On the other hand, the coated Ti diamond particles were easily removed from matrix due to cracks propagating through the particles resulting in the fine particles as seen under SEM images Figure (8-6). These cracks may have initiated in the coating layer due to thermal mismatch between diamond and Ti coating [60].

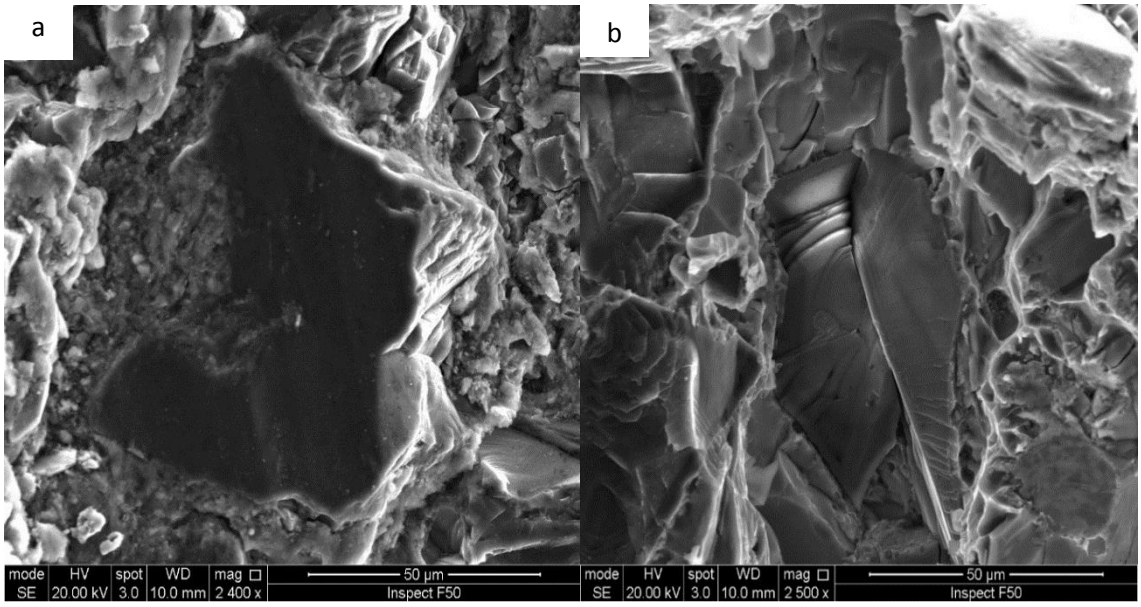

Figure (8-6): SEM images a)C_1 sample(AMDCs reinforced with Ti- coated 200/230 grit(75-63 µm) diamond particles) and b) C sample(AMDCs reinforced with uncoated 200/230 grit(75-63 µm) diamond particles. Show that the microcutting wear mechanism in C_1 while the fracture wear (sliding wear) in C sample.

Finally, as a part of studying the particle size effects on abrasive behavior of AMDCs Ti-coated diamond particles 20/25 grit (710-840 µm) were utilised to reinforce aluminium in order to confirm that the abrasive behavior of AMDCs increases with particle size of diamond particles. When tested this composite shows a relative wear of about 686 (mm^3 wheel V_{loss} /mm^3 sample V_{loss}) as shown in Figure (8-7). This more than double the relative wear of AMDCs reinforced by 35/40 grit.

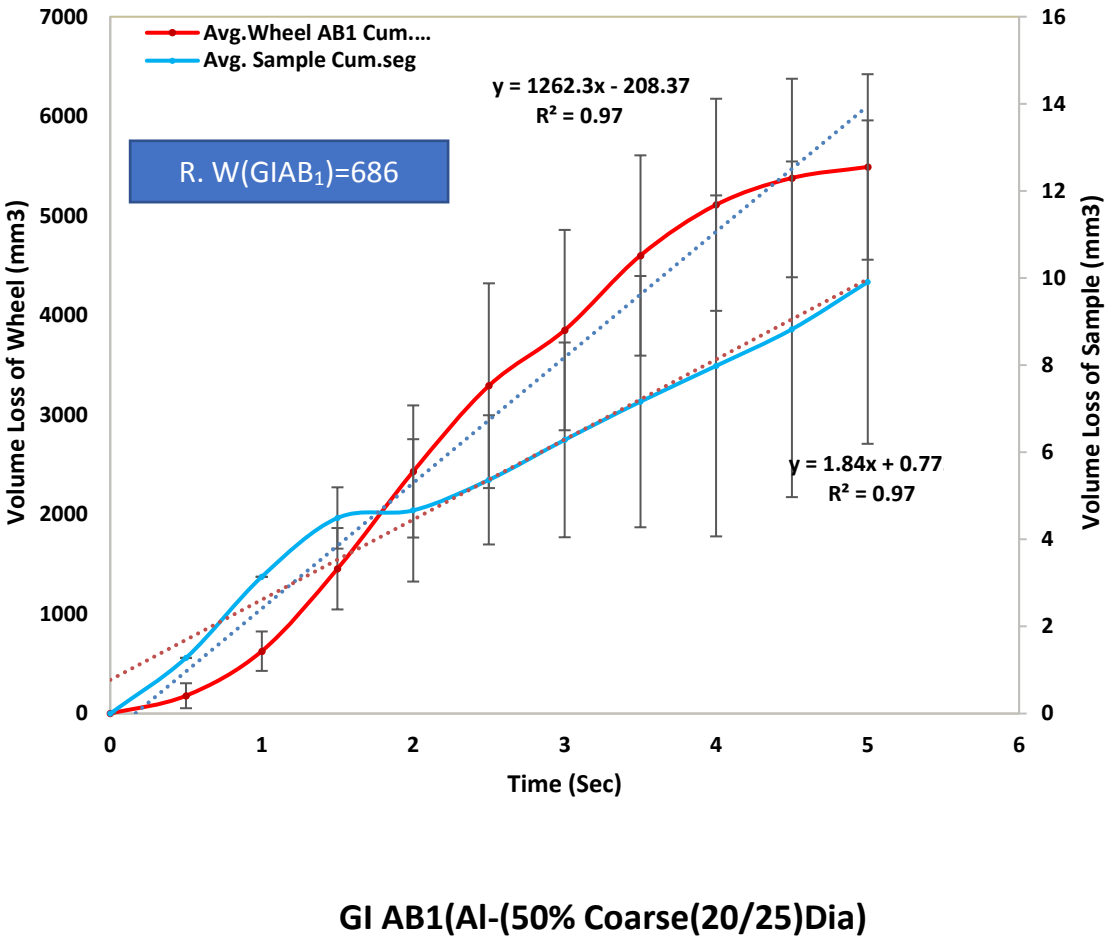

Figure (8-7): Volume loss of wheel and AB_1 sample (AMDCs reinforced with Ti-coated 20/25 grit(710-840 µm) diamond particles) versus cutting time.

To sum up, the coarsest particle size tends to offer the highest increase in wear behavior. this is in agreement with other research [163] because during cutting every hard particle works as a cutting edge that leads to wear of the blade quickly. In spite of the fact that the cutting edges should be higher in number in the samples that are reinforced with the smallest particles, these particles are less well embedded in the matrix and are more easily removed [228] (their contact area for bonding is less per particle than with the large particles). In addition, the relative size difference between the abrasive particles of the wheel and the sample (the sample having the coarser reinforcement) will have a role. In this case it would be expected that the composite would have a superior relative wear as reported by [138], [166]. Therefore, they will not be as effective as the coarsest particles. This study has found that the wear rate of the wheel is increased by increasing the reinforcing particles size, corresponding to the abrasive wear concept that the wear rate and friction coefficient should increase with increasing particle size reinforcement of the

counter face (the harder surface or that which contains harder particles, in our case AMDCs). This agrees with the behaviour for example of grinding or polishing papers used to prepare samples, as reported in literature [229], [230]. While in regard to surface condition effects, the situation was different. There is no clear trend when comparing cut-off wheel wear isolated from sample wear, which was discussed previously where there are some fluctuations in behaviour. For example, in the composite with large particle size reinforcement (A, A_1 and B, B_1) the wear with coated particles was better than uncoated, while with small particles (C and C_1) the opposite trend was seen. Efforts have been spent in the current work to understand this fluctuation by using instruments such as SEM, EDX, XRD and optical microscope and even Raman spectroscopy. The results seem to reveal that these fluctuations are related to the differences in interfacial bonding, particle sizes and nature of surface morphology of reinforcement previously discussed in detail (in comparing microstructure chapter 6 and wear behaviour in the current chapter above).

Generally, by finding the different wear behaviours of samples according to the variation in a particle size and coated/ uncoated nature for the same particle size, it can be seen from Figure (8-3), Figure (8-4), and Figure (8-5) that the relative wears of the samples increase faster in the cutting of composites that are reinforced with coated diamond particles than with uncoated diamond of the same particle size. The result of dividing the slope of blade wear by sample wear of A_1 and B_1 cutting samples is higher than the result of dividing the slope of blade wear by sample wear of A and B cutting samples. Even so, there are some occasional fluctuations in the wear of the blade in cutting of composite with the uncoated or coated diamond reinforcement, which may relate to some inhomogeneity in cutting samples and the existence of some graphite transported by the cutting action from interfaces to form a thin layer of solid lubricant, especially through the cutting of the coarsest particle size reinforcement, A and A_1.

Furthermore, there is slightly different abrasive behaviour noted for samples with the finest particles, C and C_1, where the relative wear of uncoated particles was higher than coated, as clearly shown in *Figure* (8-5*).* This behaviour may be related to the coating process of particles or even to infiltration processes, where some of each of the smaller particles was already converted to carbides or graphite during the process cycles due to its small size, which offers a wide surface area as that shown in Figure (6-23**),** Figure (6-24**),** and Figure (6-25).

8.2 Comparison of Manufacturing Routes for Aluminium Matrix

The study of particle size and surface condition effects on abrasive wear behaviour of composites produced by the GI technique has allowed the best particle size and surface condition of diamond particle reinforcement to be found. From this, 420-500 µm Ti coated-diamond particle size has been chosen to reinforce aluminium by other production techniques to explore effects of manufacturing route. These methods are conventional Powder Metallurgy (PM) and Spark Plasma Sintering (SPS) in order to compare their effects on abrasive wear properties of AMDCs.

Figure (8-8) shows a comparison of wear behavior of AMDCs produced by three different production methods (PM, SPS, GI), where the Figure (8-8 a) represents wear behavior of cut-off discs used to cut these composites and Figure (8-8 b) refers to sample wear behavior. These figures reveal a high difference in wear behavior between GI methods and powder sintering methods (PM and SPS) where is the enhancement in relative wear was about 90% in the case of SPS over GI, and about 94% for conventional Powder metallurgy. This means that the powder sintering methods (PM and SPS) give much more favourable properties. It could be that the solid state nature of these techniques eliminates or reduces the intermetalic compound formation at interfaces due to the lower temperature used (550 ˚C in both cases, compared to 780˚C in GI). This high temperature may give enough energy to form intermetallic compounds at interfaces, and at the same time it may result in oxidation or graphitisation of the diamond structure in the interfacial area. The short time of the SPS method may also have a similar effect to that of PM.

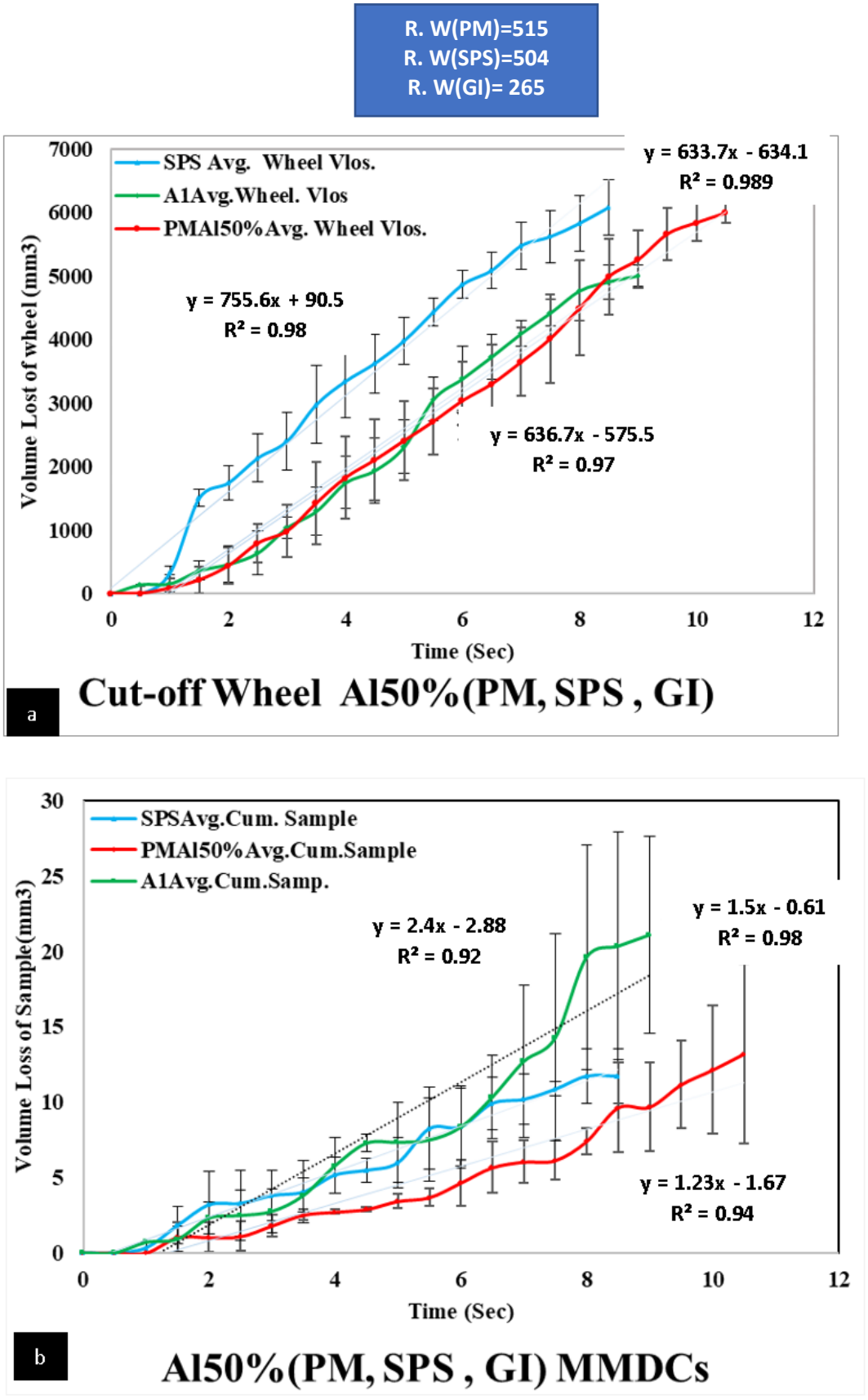

Figure (8-8): Volume loss of wheels versus cutting time (left) and Volume loss of AMDCs reinforced with Ti-coated 35/40 grit(420-500 µm) diamond particles versus cutting time of three manufacturing processes of AMDCs (GI, PM and SPS).

8.3 Abrasion Resistance with Other Reinforcements

To investigate more about abrasive wear resistance of AMCs, samples with other types of abrasive reinforcement particles were produced. Other abrasive particles which can be used to manufacture commercial cut-off discs were chosen to reinforce AMCs. These composites were manufactured by using GI under the same conditions of production AMDCs as previously. Figure (8-9a) and b) below shown the abrasive wear behavior of Al-SiC and Al-Al_2O_3. Generally, in both cases the wear trend was completely different from that in AMDCs, where the wear curve can be divided into three main stages of wear, related to the relatively low rate of removal which leads to a relatively long-time test. Under these circumstances the three stages of wear appear clearly. This behavior can be compared to a conventional wear curve, which consists of three stages of wear, but here the wear curve is shorter in time because the conditions are different. The abrasive element is exposed to quite an extreme wear environment, where both sides of the contact contain abrasive materials, in contrast to the normal machining process where the conventional wear curve is derived from. This type of test takes minutes, while in the tests used here the duration is a number of seconds. The first stage of the curves is a little short which can be represented as the initial accelerated wear when the wear elements (wheel and sample) begin to engage in the cutting process. It can be seen at this stage that the wear starts to be a little higher than in the second stage. At the wheel (red curve) this may be related to the nature of the wheel, where the outer circumference of the new wheel contains more resin and less abrasive than other parts of wheel. This is shown in Figure (8-15) where SEM imaging of different areas along wheel radius reveals that the fiber reinforcement layer at the edge of wheel gets thinner towards the center, down to about 85 μm while towards the outer edge it exceeds 185 μm. The second stage is the main wear stage. At this stage both wheel and sample seem to be affected by sliding, which may come from some solid lubricants extruded from the composite when the temperature starts to rise during cutting (glazing wear). These components form a very smooth sliding interface for the wheel at this contact area as shown in Figure (8-11) and Figure (8-13) for SiC and alumina composites, respectively, a thin layer, which is building up, extruded on the sides of wheel (cutting surface). This layer may be damaged during a continuous cutting process [138], [231] by an adhesive wear mechanism and thermal effects. The wear at this stage was about 0.67 mm^3/s and 0.09 mm^3/s for the cut-off wheel and SiC reinforced composite sample respectively, Figure (8-9a). For alumina reinforced composite the wear at this

stage was higher (12.93 and 0.69 mm^3/sec in the cut-off wheel and Al_2O_3 reinforced composite sample respectively). Figure (8-9b) shows these values were very low in comparison with the next stage. There is a very short stage in the curves directly after the second stage, which is possibly related to the gradual disappearance of a solid lubricant layer [138]. Similar features may appear in pure metal wear and are called glaze oxide layers, especially in wear at elevated temperature [231]. The third stage begins after that, which may correspond to the failure stage of wear (the last wear stage) in a conventional wear curve. This is when the cut-off disc has failed because of exceeding the temperature limit of the resin bond; this would occur at temperatures higher than 150℃ [232]. The actual temperature, checked by infrared gun directly outside the contact cutting area, is about 140 ℃ as that shown in Figure (8-9 a), and it is likely that the localised temperature at the wear surface would be higher than this. At this stage the wear of the cut-off wheel was very high in both composites (the wear rate for wheel and sample was 153 and 1.32 mm^3/s with the SiC sample and 72.8 and 1.61 mm^3/s in the case of alumina composites.

To compare the abrasive relative wears between Al-SiC and Al-Al_2O_3 composites the wear rate of the cutting wheel should be divided by the wear rate of the sample as before. As the wear rate is not steady throughout the test, the wear curve was divided into three stages, as described above, to produce stage-dependent values. The wear ratio values were different at each stage of wear; 93.4 for SiC and 32.5 for Al_2O_3 composite samples in the first stage, 7.5 and 18.7 in the second stage and 116.4 and 45.2 in the third stage. This comparison reveals that the Al- Al_2O_3 composites have a higher relative wear during the steady wear stage (second stage). This is the longest wear stage, taking up around 40% and 37% of the time of the test in SiC and Al_2O_3 composite samples, respectively while other stages are quite short, and may be affected by other factors, such as thermal and manufacturing issues. Therefore, while it may be difficult to judge which composite is the best under these two-short stages, a high relative wear ratio can be clearly identified at the secondary stage in Al-Al_2O_3, probably governed by sliding wear. The stage persists until the particles fracture, creating a layer from matrix material behind cutting edges in the wheel, as clearly shown in Figure (8-14). But overall the Al-SiC composites can be last longer under cutting process, that is possibly because a balance of the sliding and fracture wear mechanism control the abrasive wear where there are some fragments of SiC still stick together or in matrix even it was cracked as a result of its good strength [233] as that shown in Figure (8-11).

Furthermore, the edge of the cutting discs have been designed to be more abrasive (denser population of abrasive particles than other regions [234] and are compacted better than other parts of disc to a depth of about 3 mm from the outside circumference toward the center Figure (8-15). Factors such as this may affect the wear trends observed.

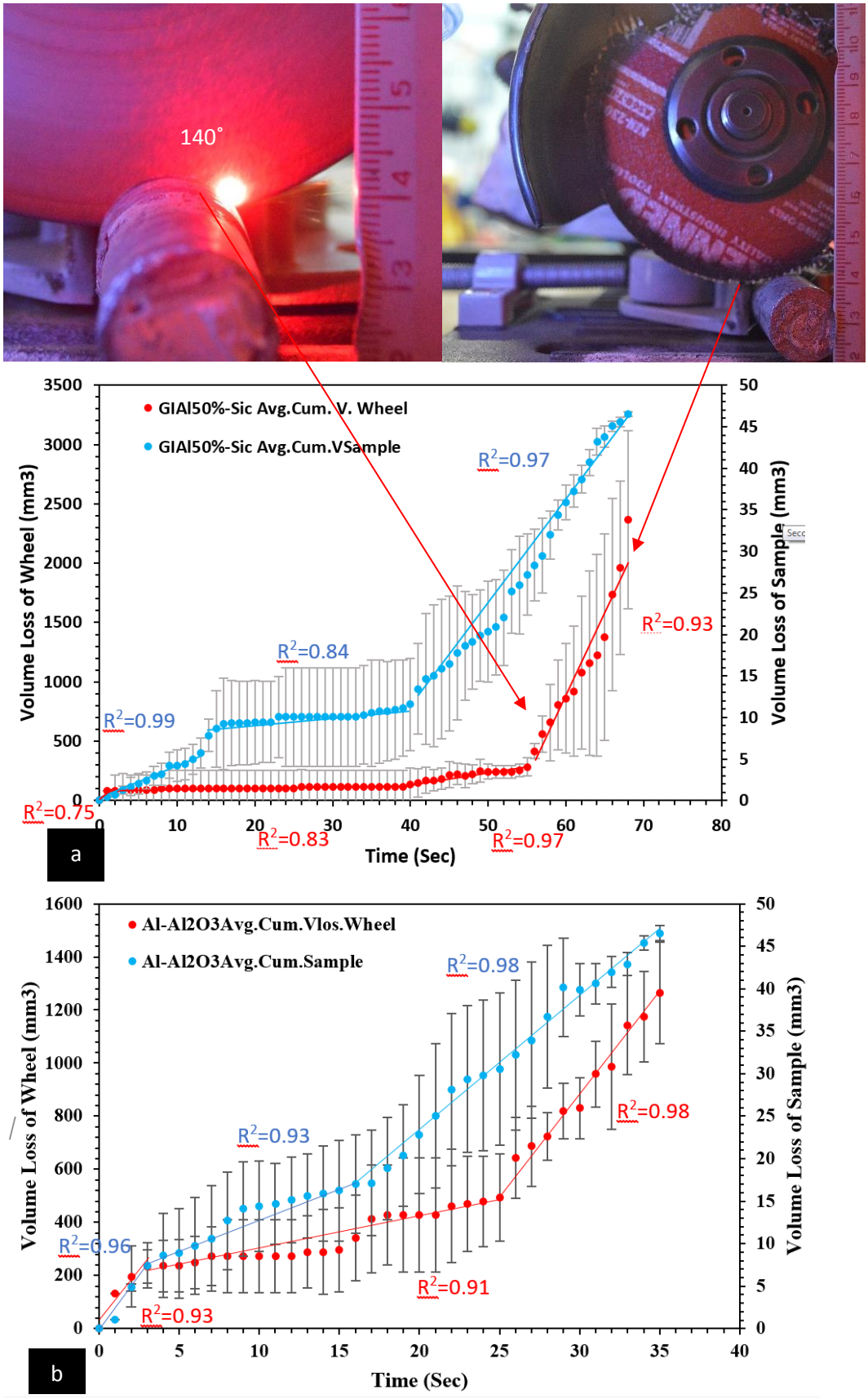

Figure (8-9): Volume loss of wheels and Sample versus cutting time a) GI Al-SiC composites b) GI Al- Al_2O_3 composites.

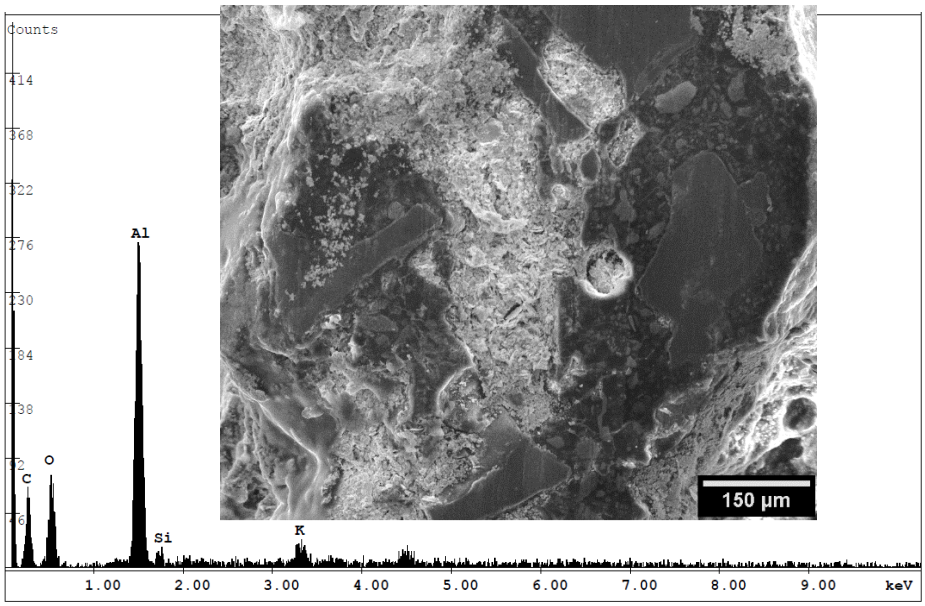

Figure (8-10): SEM and EDX of the wheel surface, which cuts Al-SiC, due to adhesive wear of wheel in steady stage wear, because the cutting edge of wheel look likes it has become glazed.

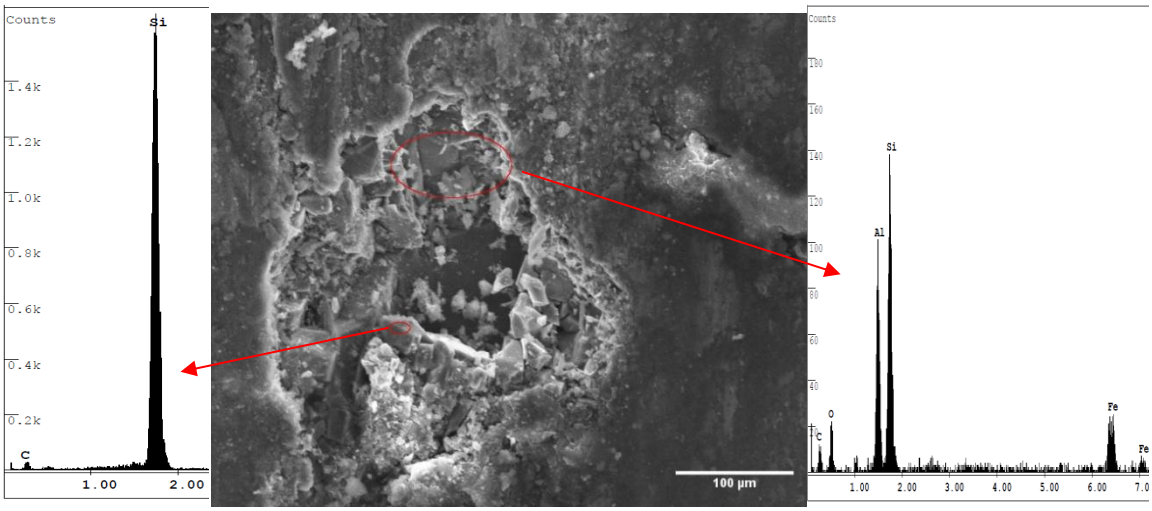

Figure (8-11): SEM and EDX of GIAl-SiC cutting surface showing that the cut go through the particles where the fracture and sliding wear occurred in reinforcement and matrix, respectively.

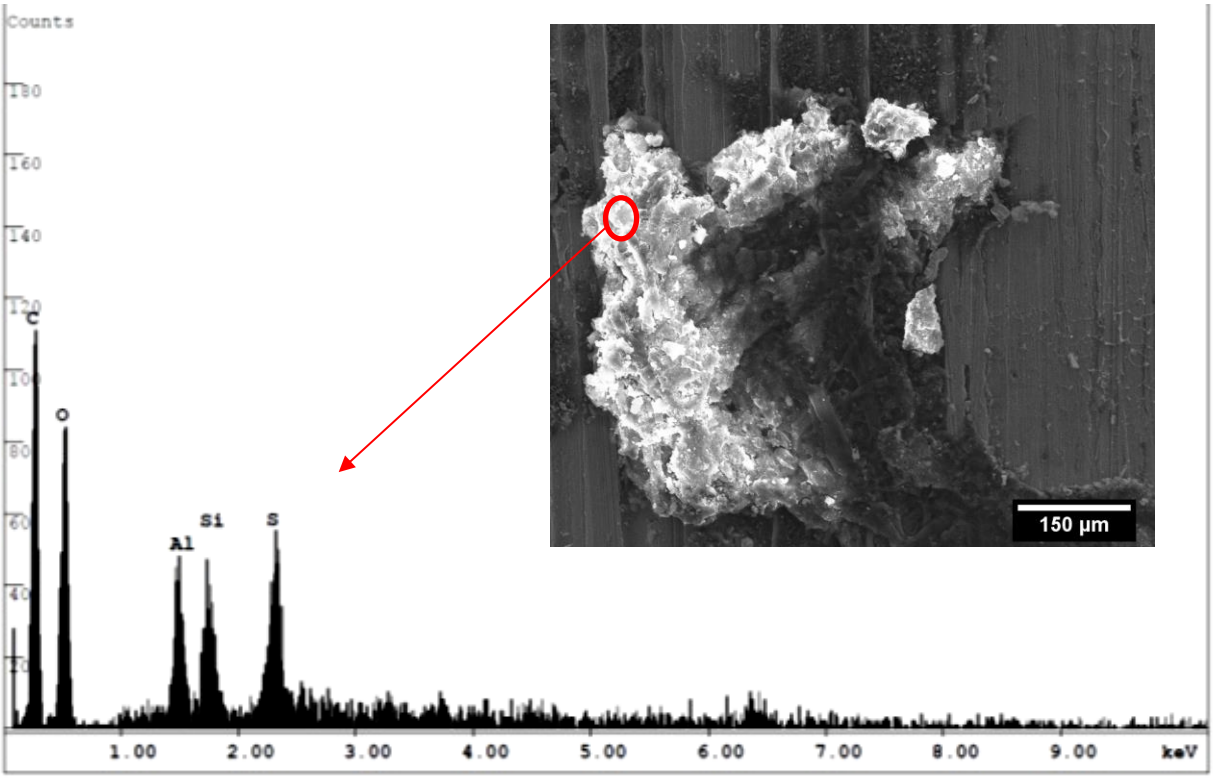

Figure (8-12): SEM image and EdX of cutting surface of GIAl-SiC shows extrude some materials from interface, which is thought to be contributed in formation sliding layer.

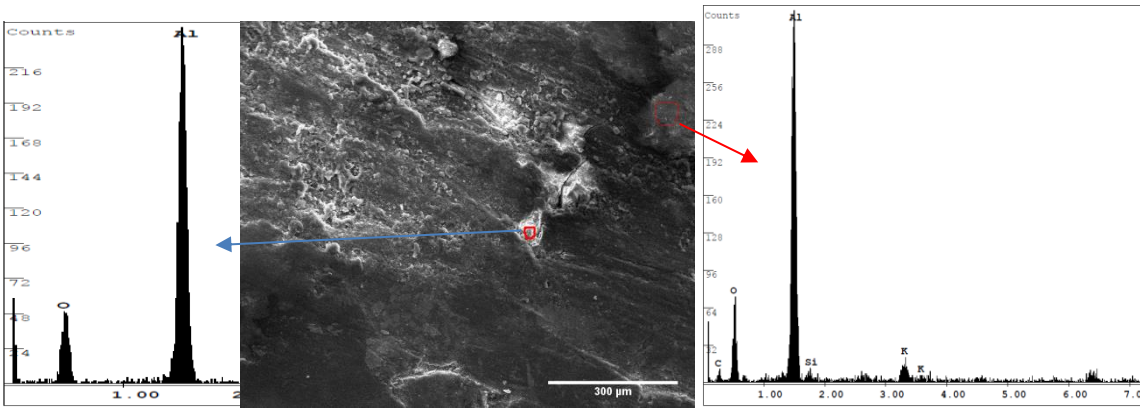

Figure (8-13): SEM image of cutting surface of GIAl- Al_2O_3 shows that the dominant wear mechanism was a sliding wear rather than fracture wear mechanism in Al_2O_3 particles.

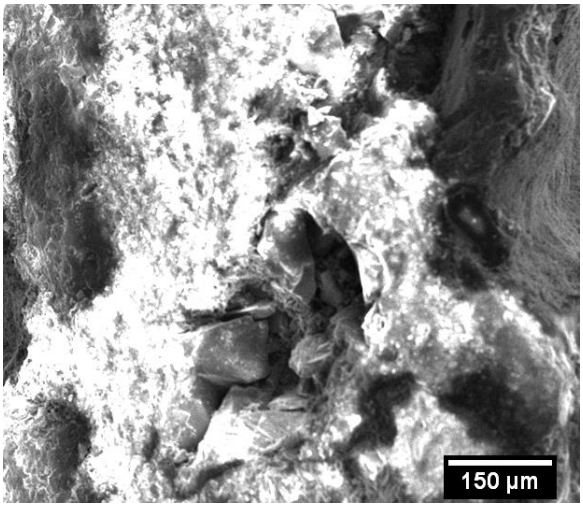

Figure (8-14): SEM of cut-off Wheel surface which cut GIAl- Al_2O_3 show fracture wear occurred in reinforcement particle in addition to sliding wear.

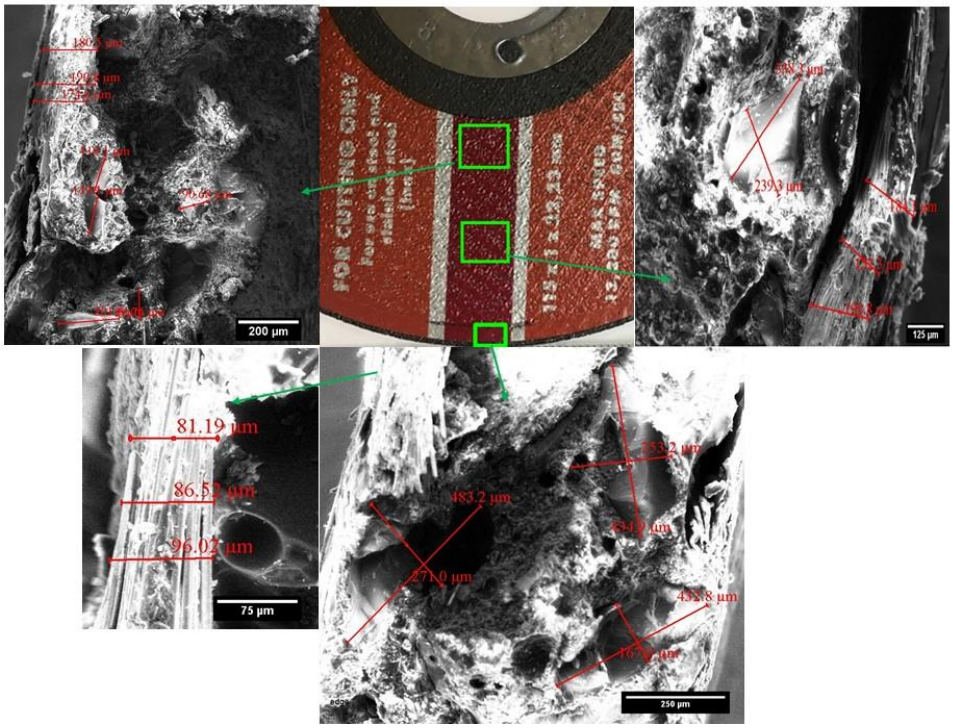

Figure (8-15): Wheel photo and SEM images of different area of wheel from edge toword center along a diameter.

8.3.1 Aluminum-Ceramic Composites (GIAMCCs) Loaded with 20% vol. Diamond

To increase the relative wears of AMCCs a proportion of diamond particles have been added to form hybrid AMCCs. These contain 20% volume fraction of diamond, being mixed with ceramic reinforcement at 30% volume fraction to give a 50/50 ratio of matrix to reinforcement, counting all the reinforcement together (20% diamond-30% ceramics with 50% aluminum matrix). In these composites the wear behavior has changed in comparison with plain AMCCs by minimizing or eliminating the third short wear stage or merging the second and third stages together. These appeared in plain AMCCs and made the second steady state stage of wear dominant as clearly shown in Figure (8-16). Al- 30% vol. Al_2O_3 composites loaded with 20% vol. diamond have a higher relative wear, which was about 120.4, than Al-30% vol. SiC loaded with the same volume fraction of diamond, which obtained about 89.1 relative wear, even though the hardness of alumina (15.7 GPa) is lower than the hardness of SiC (22GPa) [235], [236]. This difference in relative abrasive behaviour is probably because the nature of SiC, which can offer kind of solid lubricant layer, and in these composites the chemical compatibility between aluminium matrix and alumina is probably higher than the compatibility between SiC and aluminium. While alumina is considered inert in molten aluminium, SiC has been reported to react with molten aluminium, particularly between 657-827 ˚C (which includes processing temperature (780 ˚C)) by releasing some carbon atoms to the aluminium to create Al_4C_3 [237], consequently the bonding strength between alumina and aluminium may be higher without this interfacial reaction by mechanical support from the matrix. This can be interpreted from the differences in the dominant mechanism of wear that occurred in each composite, where the SEM images revealed that the dominant mechanism of wear occurring in Al-Al_2O_3-diamond was fracture wear, whereas in Al-SiC-diamond the wear mechanism was adhesive wear and the wear debris was more clear.

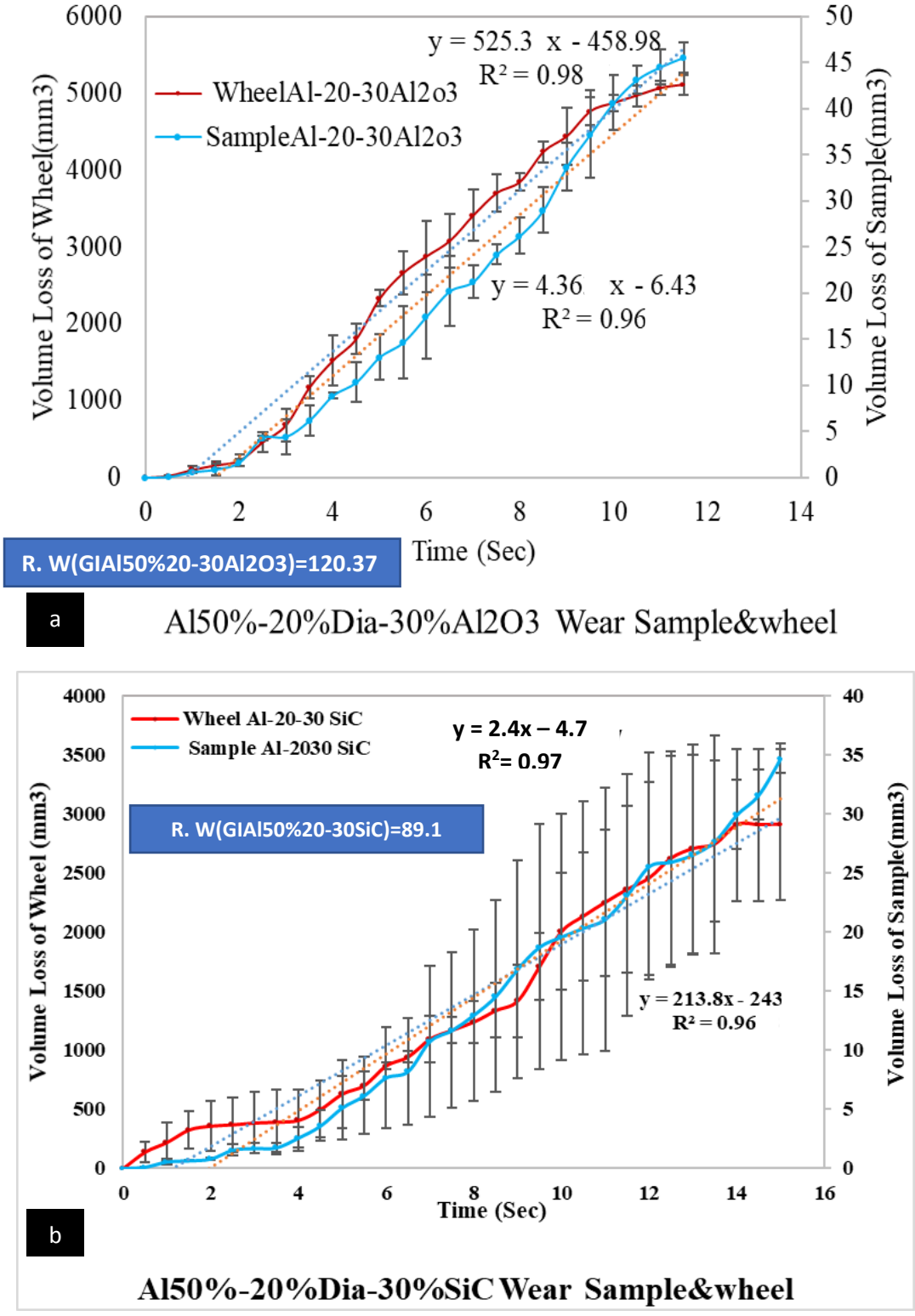

Figure (8-16): Volume loss of wheels and Sample verssus cutting time a) GI Al-30% vol. Al_2O_3-20% diamond composites b) GI Al-30% SiC-20% Dia. vol. composites.

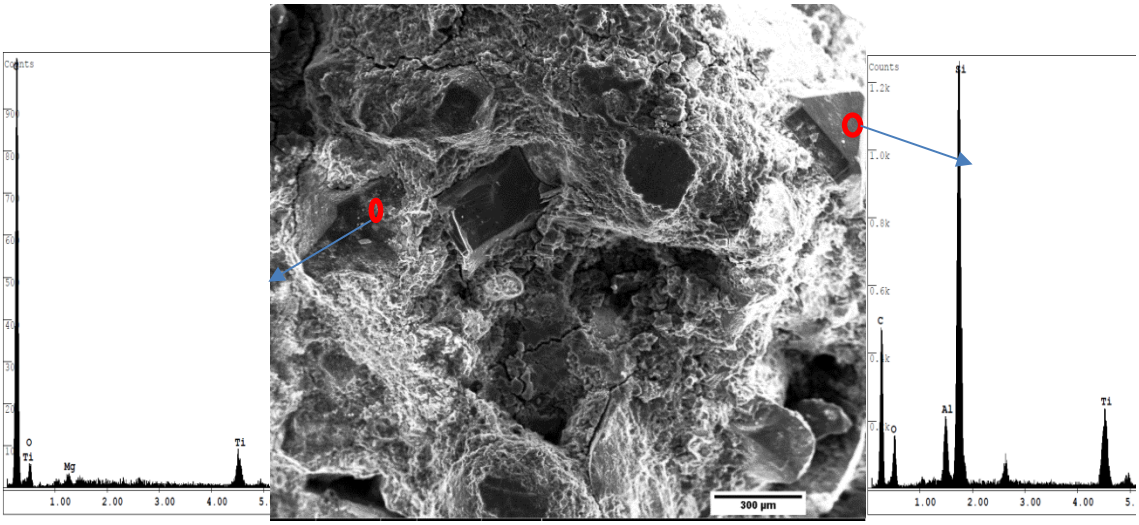

Figure (8-17): GIAl50%20-30SiC Cut show the sliding and pull out particles wear mechanism which is dominant.

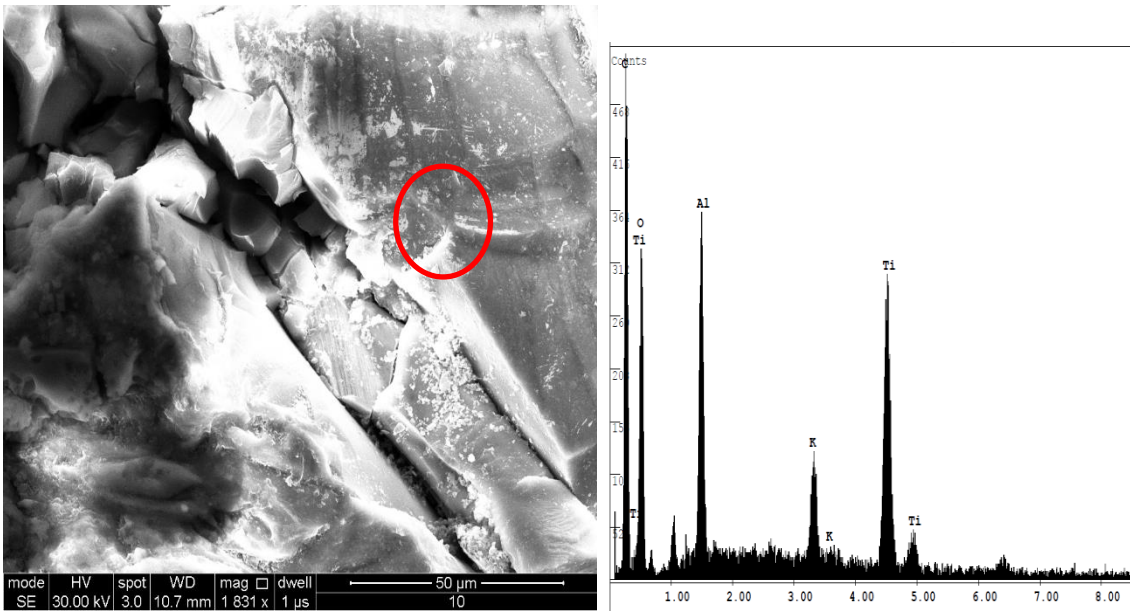

Figure (8-18): GIAl50%20-30 Al_2O_3 Cut shows the fracture and sliding wear dominant the wear mechanism.

8.4 Abrasion Wear of Tin-Diamond and Epoxy-Diamond Composites

Figure (8-19a) shows the wear trend of tin matrix-diamond composites produced by gas pressure infiltration (GI SMDCs). It appears that the wear behavior was still approximately linear but less in value than the AMDCs or AMCCs which were discussed earlier in this chapter, where the relative wear of wheel to composite (relative wear) was about 11. The linear trend was achieved as a result of the presence of extremely abrasion resistant particles, which are the diamond as in case of AMDCs, meaning the weakness in terms of relative wear is probably related to the matrix nature which is soft and inactive. These kind of matrices do not tend to generate intermetallic compounds, unlike where there is a thin Ti layer or a diamond itself as in the other materials discussed earlier, due to its low melting point and reactivity. This leads to only mechanical bonding at interfaces and, due to softening of tin which may occur in relatively low temperature due to the low melting point, which may happen during cutting process, it will be easy to pull out the diamond reinforcement particles from the matrix. The SEM imaging of Sn50%diamond composites revealed clean interfacial bonding between the Sn matrix and diamond reinforcement, Figure (8-20). This means only the mechanical holding of particles will operate, which is already weak due to the soft properties of tin at room temperature, and even less at the high temperature generated from the cutting process.

To support this concept, the relative wear of epoxy matrix with diamond composites (EMDCs) was studied; these were processed by self-gravity infiltration due to its good wettability for diamond particles, unlike in the case of a metal matrix (Al). This matrix should also be mechanically weaker and should not lead to any interfacial reaction. As is shown in Figure (8-19b), the trend of volume lost was still approximately linear while the relative wear value was slightly higher than the wear values in Sn composites (about 12.7). This is probably related to nature of epoxy as the temperature increases, where, it will soften, it will retain some adhesive character, while the Sn will melt and be pulled away from the diamond by the surface tension, as is shown in the SEM images in Figure (8-21). As a result the epoxy may hold the diamond particles slightly more effectively than the tin. In addition to previous reason there is a difference in matrix hardness which may contribute to the high relative wear of EMDCs, where the hardness was about 16.25 kg/mm^2 while the Sn composite hardness was about 11.2 kg/mm^2. Furthermore, some epoxy at the interface may act as a lubricant, Figure (8-21 b)

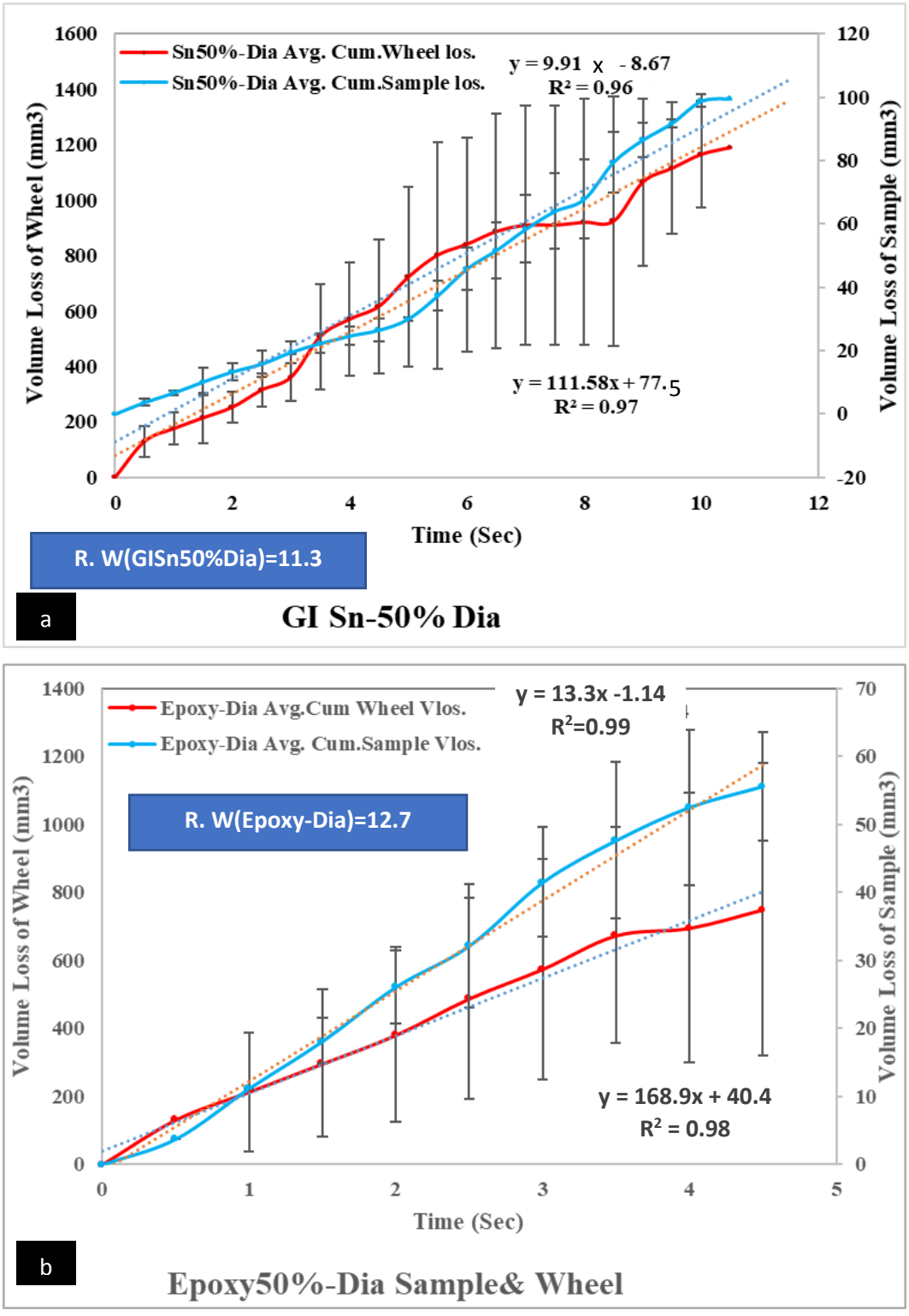

Figure (8-19): a) Volume loss of Sn-diamond sample and wheel versus Cutting Time and b) Volume loss of Epoxy-diamond sample and wheel versus cutting time.

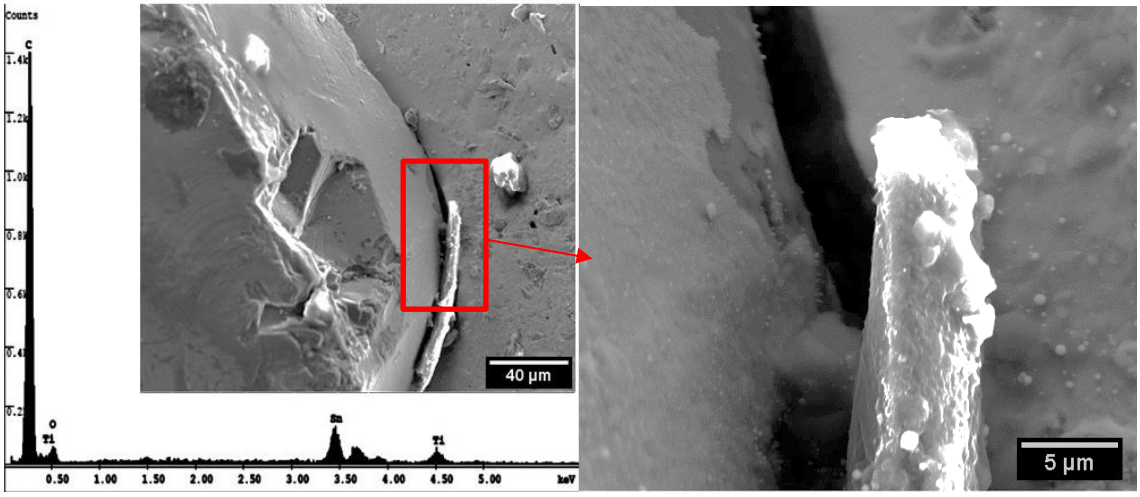

Figure (8-20): SEM images of (GISD) Sn50%Dia. show clean interfacial bonding from compounds.

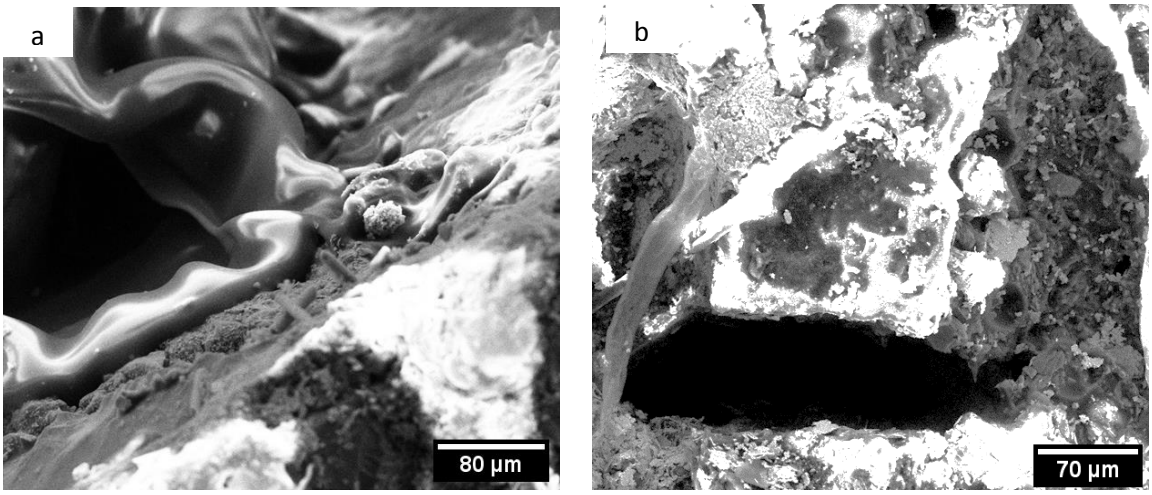

Figure (8-21): a) SEM image of Epoxy-diamond show sticky matrix on the diamond at interface and b) SEM image of Wheel cuts Epoxy-diamond show some epoxy stick on the cutting surface.

8.5 Summary

To sum up, of this chapter, it can be concluded that the main points, which were studied, revealed the following:

- An idea of the general wear behaviour of the composites can be gained, and is summarised in Figure (8-2) pp.160, according to the relative wear parameter (the result of dividing the slope of wear curves of the wheel cutting the composites,

Figure (8-1 b), by the slope of wear curves of cutting the samples Figure (8-1 a) pp. 159), further AMDCs with different reinforcements (SiC and Al_2O_3) have been compared with other low melting matrices (Sn and epoxy).

- Some results show the whole wear curve of the composite exhibiting near-linear wear curve, while others show the second stage of the wear curve exhibiting three wear stages. The relative wear was taken as a suitable criterion for comparison.
- Generally, by finding the different wear behaviours of samples according to the variation in a particle size and coated/ uncoated nature for the same particle size, it can be seen from Figure (8-3) and Figure (8-4) pp. 162 and 164 respectively, that the relative wears of the samples increase faster in the cutting of composites that are reinforced with coated diamond particles than with uncoated diamond of the same particle size. The result of dividing the slope of blade wear by sample wear of A_1 and B_1 cutting samples is higher than the result of dividing the slope of blade wear by sample wear of A and B cutting samples.
- One of the important observations was that the relative wear increases with reinforcement particle size and the Ti-coated diamond particle reinforcement enhanced wear properties, most likely by improving wettability between molten aluminium and the diamond surface.
- The high processing temperature encourages formation of intermetallic compounds at interfaces. Raman spectroscopy Figure (6-27) and SEM Figure (6-21), Figure (6-22), and Figure (6-24) in Chapter 6 reveal some of these, which may affect the diamond structure and result in the decrease of relative wear of GI AMDCs in comparison with sintered AMDCs (PM and SPS).
- AMCCs showed that 50vol% of either SiC or AL_2O_3 is insufficient to stop a single abrasive cutting wheel from cutting the sample, while when these loaded with 20vol% diamond the same type of cutting wheel is prevented from passing through a sample of the chosen diameter (8 mm).
- The other two matrices examined (Sn and epoxy) exhibited similar relative abrasive wear, even though there was a slight deference in the value of relative wear. This may be related to the differences in hardness of the matrices. All wear values of composites reinforced with 50% vol. reinforcement are shown in the tables and figures above.

Chapter 9 Abrasive Wear Assessment of Transition Metal in MMDCs

Most of transition elements, such as (Ni, Fe, Cu, Ti …) may be used as catalysts during diamond formation from carbon. These elements could have a reverse effect toward graphitization of diamond when they are present as a coating or matrix, especially at high temperature, where the graphitization at the surface that is in contact with these elements may possibly occur [209].

In general, the reactivity of transition metals toward carbon is determined by the d-orbitals contribution of electron-vacancies. Where these metals tend to form carbides or solid solution with carbon, depending on the number of electrons in their d-orbitals, such elements with a high number of electron (copper, zinc) become inactive toward carbon. Other metals with high vacancy number (titanium, chromium) have the ability to react with carbon to make carbides [238], [239]. In between these extremes there will be a moderate tendency to form carbides, and elements can be divided in to three groups, depending on their carbide forming potential [240], (Table (9-1) in addition to Si and Al are probably considered as having high tendency to form carbides. Therefore, in this research three transition elements were chosen, one from each group (Ti, Ni and Cu) to study their abrasive performance as matrices in MMDCs by investigation of possible reactions which may happen between them and diamond reinforcement, and how this may impact the abrasive behaviour of MMDCs. The wear behaviour of all samples is shown as histogram plots to give a general idea of behaviour, Figure (9-1 a and b) for samples and wheels, respectively and Figure (9-2) for relative wear of transition metal matrix composites.

Table (9-1): Classification of transition metals depending on their tendency to form carbides with carbon [240].

Period No. in periodic table	High tendency to form Carbides	Moderate tendency to form carbides	No tendency to form carbides
4th Period	Mn, Ti, Cr, V	Ni, Co, Fe	Cu, Zn
5th Period	Nb, Y, Zr, Mo	Pd	Ag
6th Period	Ta, Hf, W		Au, Hg

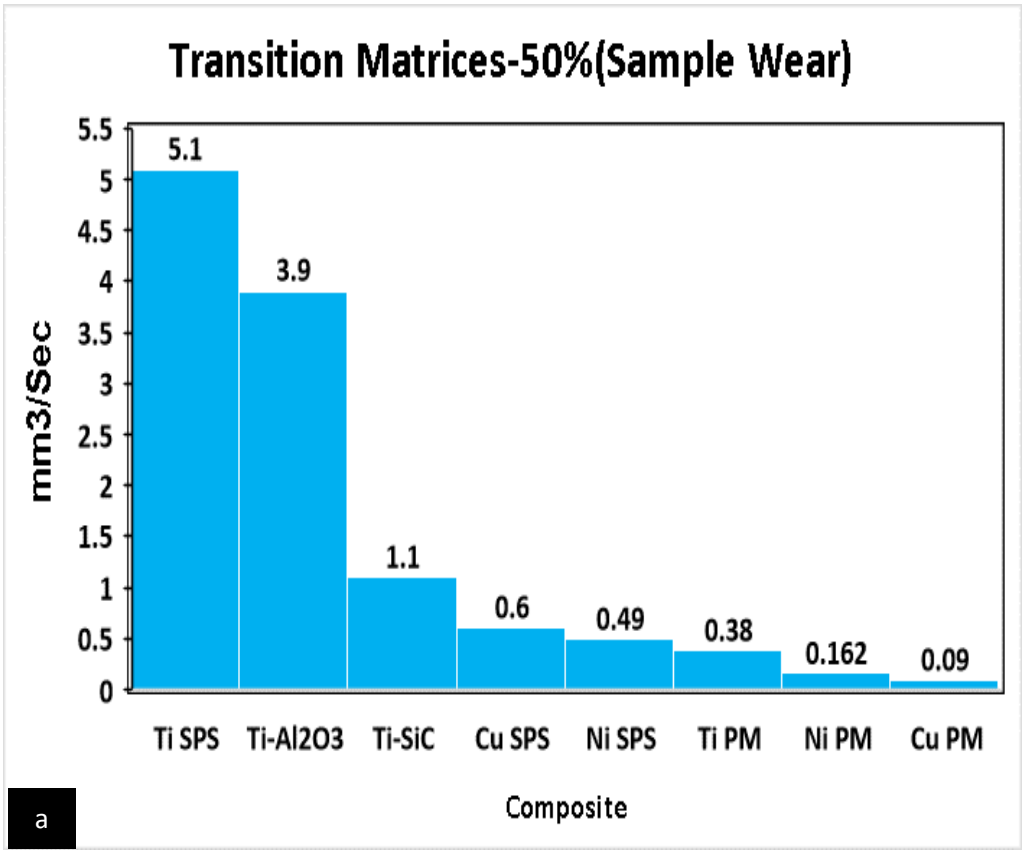

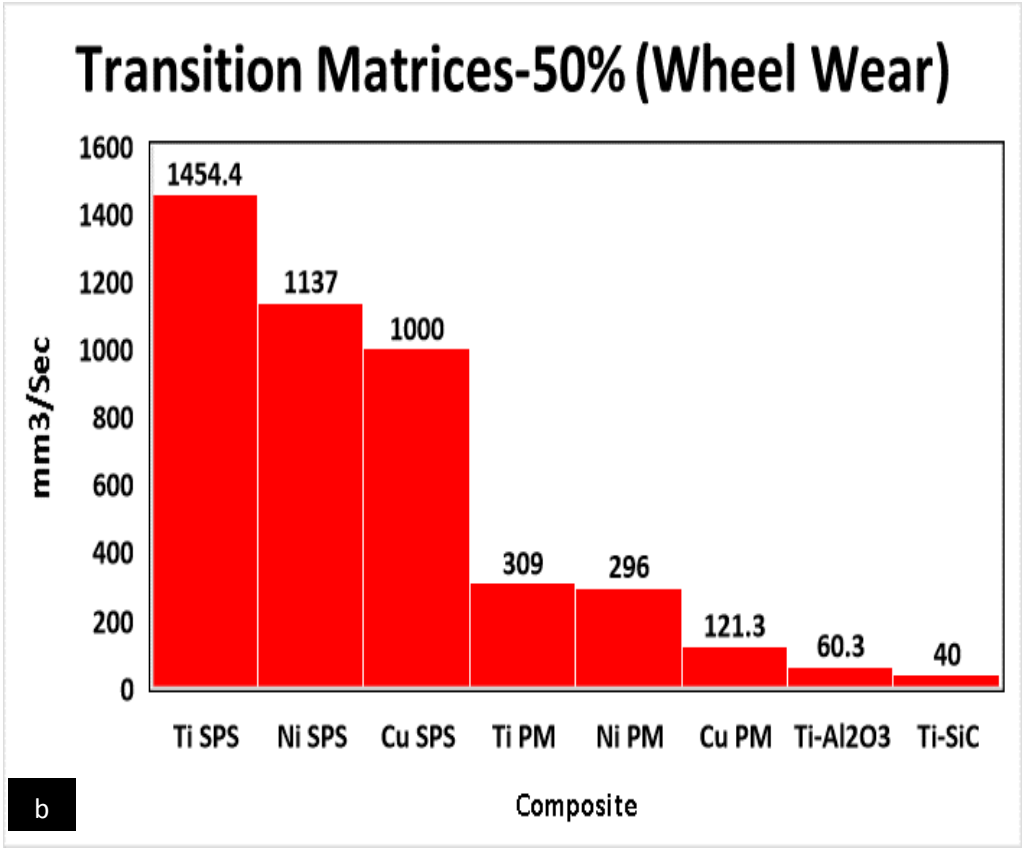

Figure (9-1): Summary of abrasive wear of composites, a-samples and b-wheels used to cut composites.

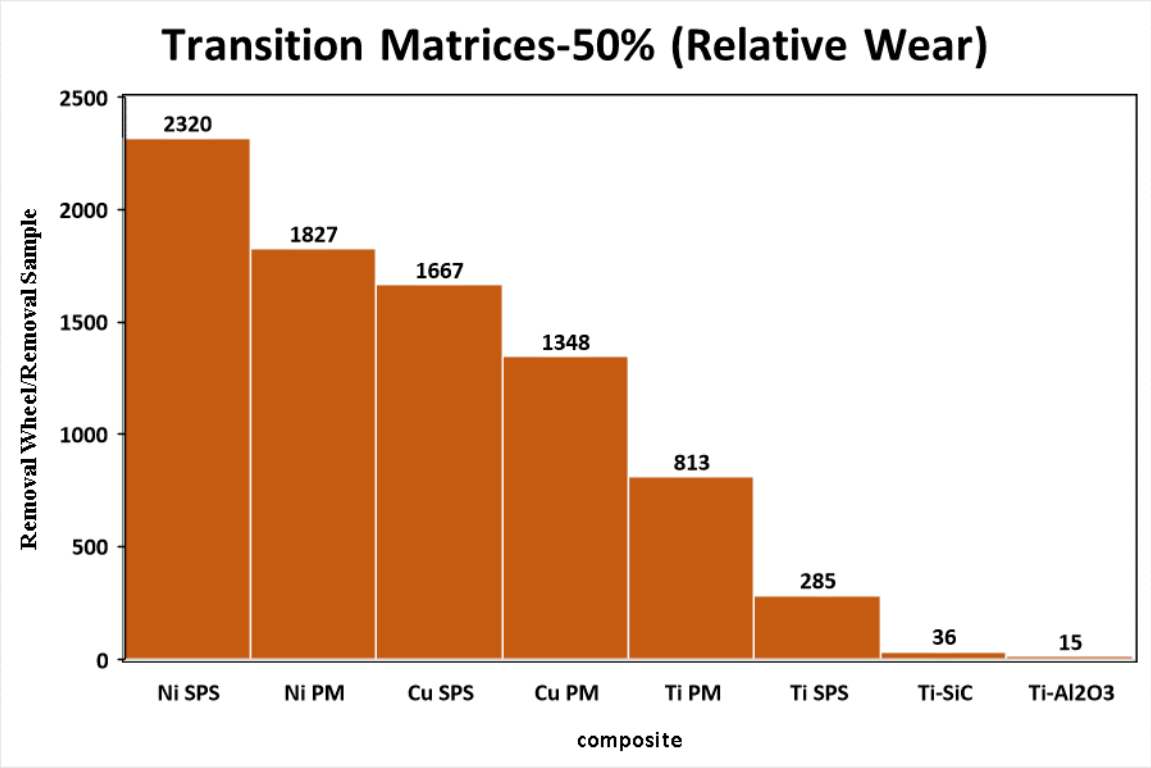

Figure (9-2): Summary of relative wear of composites.

9.1 Ti-Diamond Composites

In this class of composites two different sintering methods have been utilised in order to study the effects of interfacial interaction and compounds those may generate at interfaces. The Ti matrix was chosen because the chemical activity of Ti suggests carbides will be formed, in addition to its high melting point and light weight, which would be desirable characteristics as well as wear resistance. These features make it a good candidate to manufacture a composite with diamond with a different volume fraction and two sintering techniques (PM and SPS) to compare which will offer the best abrasive resistance. The wear of pure matrix material, fabricated by the same production conditions as the composite has also been tested under the same abrasive conditions, in order to see how much the relative wear is enhanced by diamond additives. The value of relative wear of pure titanium processed by PM was about 1.3 which result of dividing wear rates of abrasive element at cutting (wheel/sample), where the wear rates were 5.3 mm^3/s and 4.08 mm^3/s for cut-off wheel and pure titanium PM sample respectively. That means the relative wear of pure Ti matrix (relative wear) is about 1.3 (mm^3 wheel/ mm^3 sample). The wear

behavior of composites with different volume fraction of diamond reinforcement will be shown in Figure (9-3) to Figure (9-6), but before this discussion it is important to know what occurs between the Ti and diamond at this relatively elevated sintering temperature and the possible kind of bonding mechanism at interfaces, whether this is a purely mechanical holding for a particle by matrix or by aid of some intermetallic phases that may be generated.

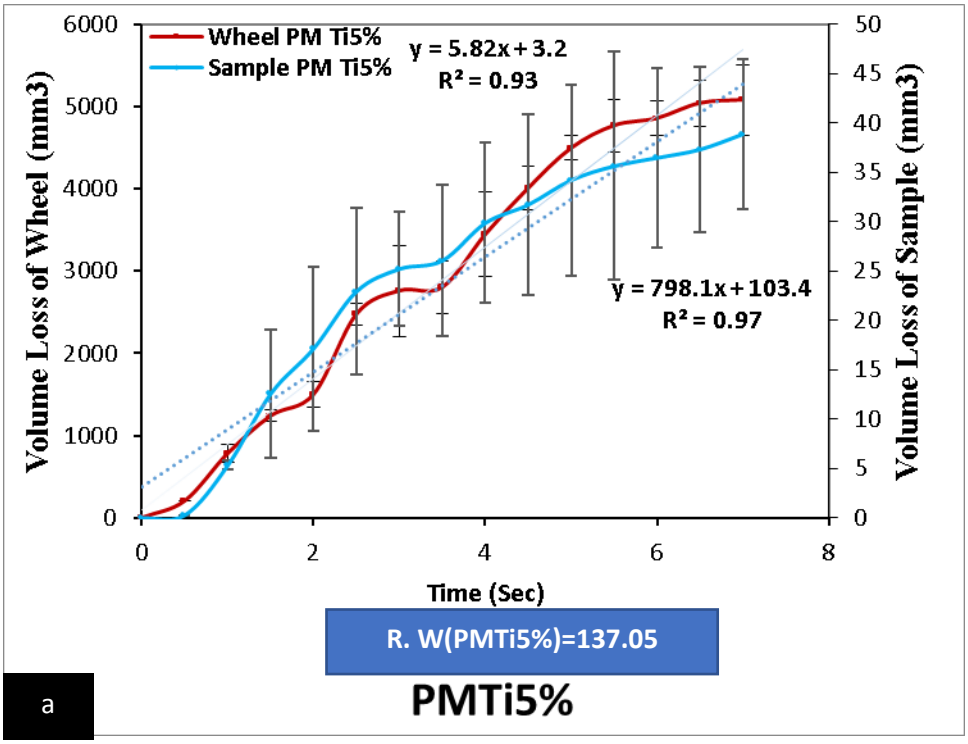

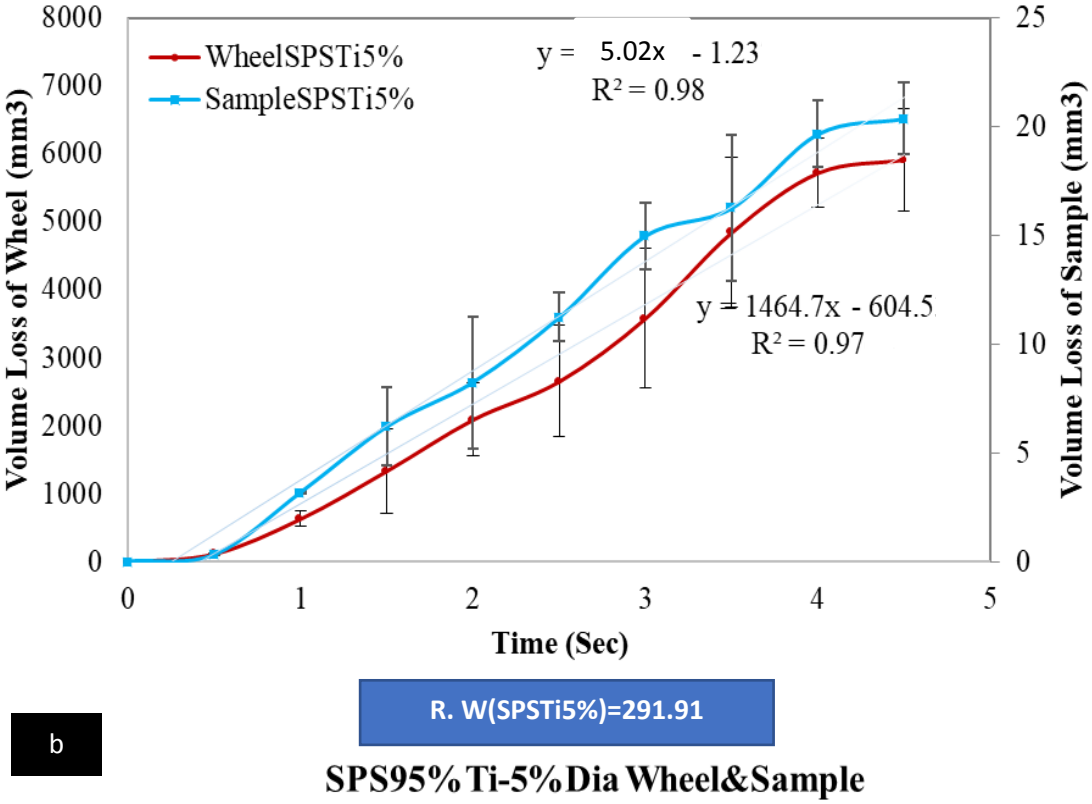

Figure (9-3): a) Volume loss of wheels cut through PM Ti-5%Dia. samples and samples themselves versus cutting time and b) Volume loss of wheels cut through SPS Ti-5%Dia. samples and samples themselves versus cutting time.

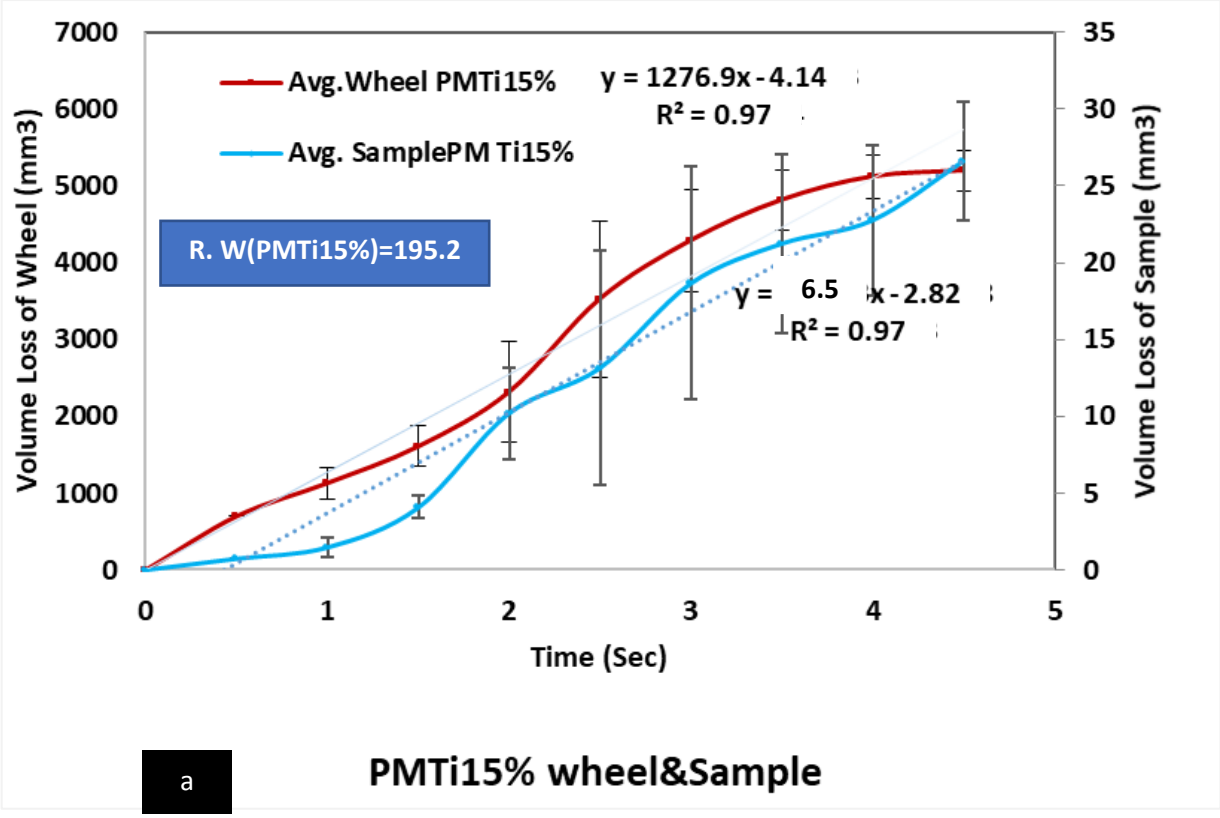

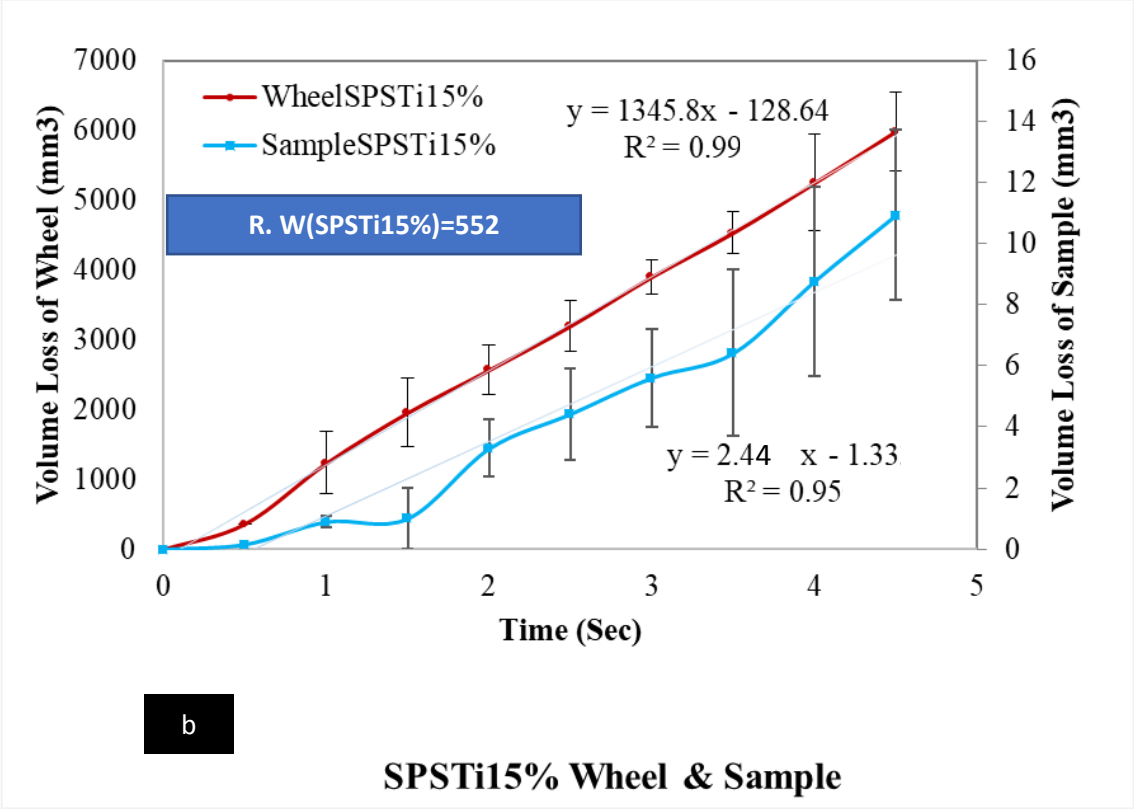

Figure (9-4): a) Volume loss of wheels cut through PM Ti-15%Dia. samples and samples themselves versus cutting time and b) Volume loss of wheels cut through SPS Ti-15%Dia. samples and samples themselves versus cutting time.

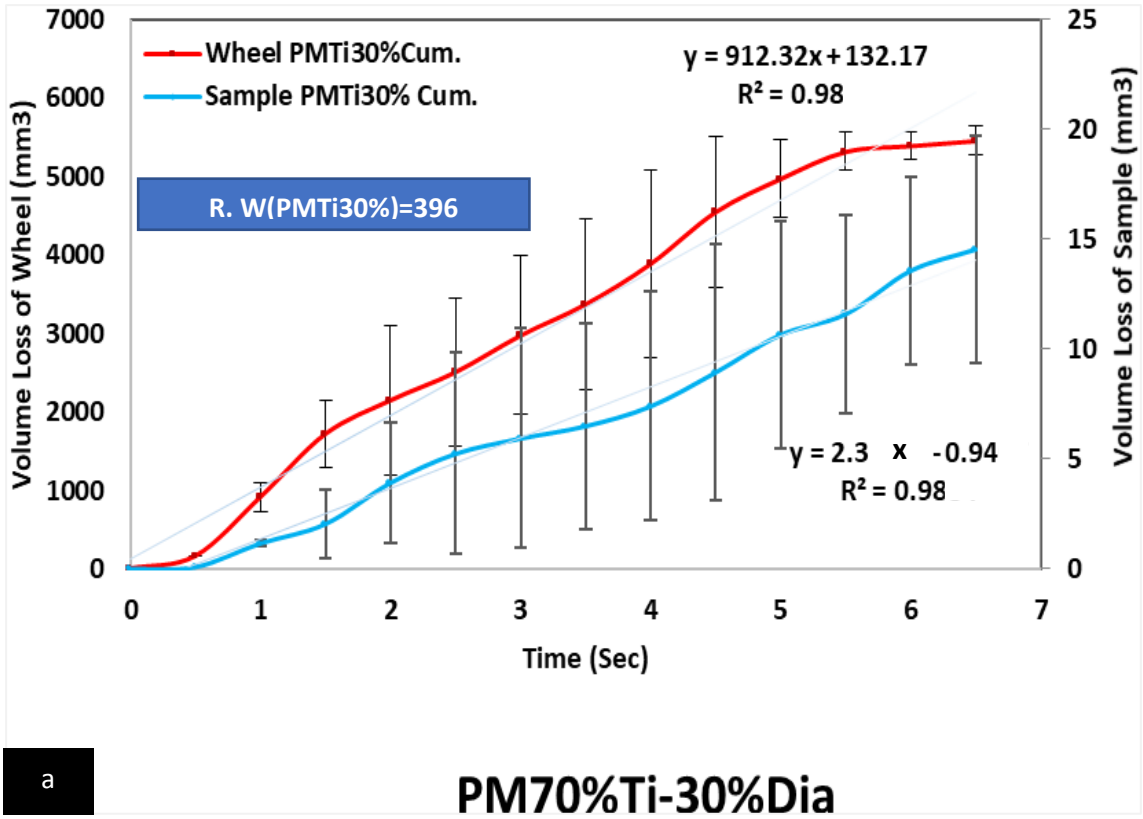

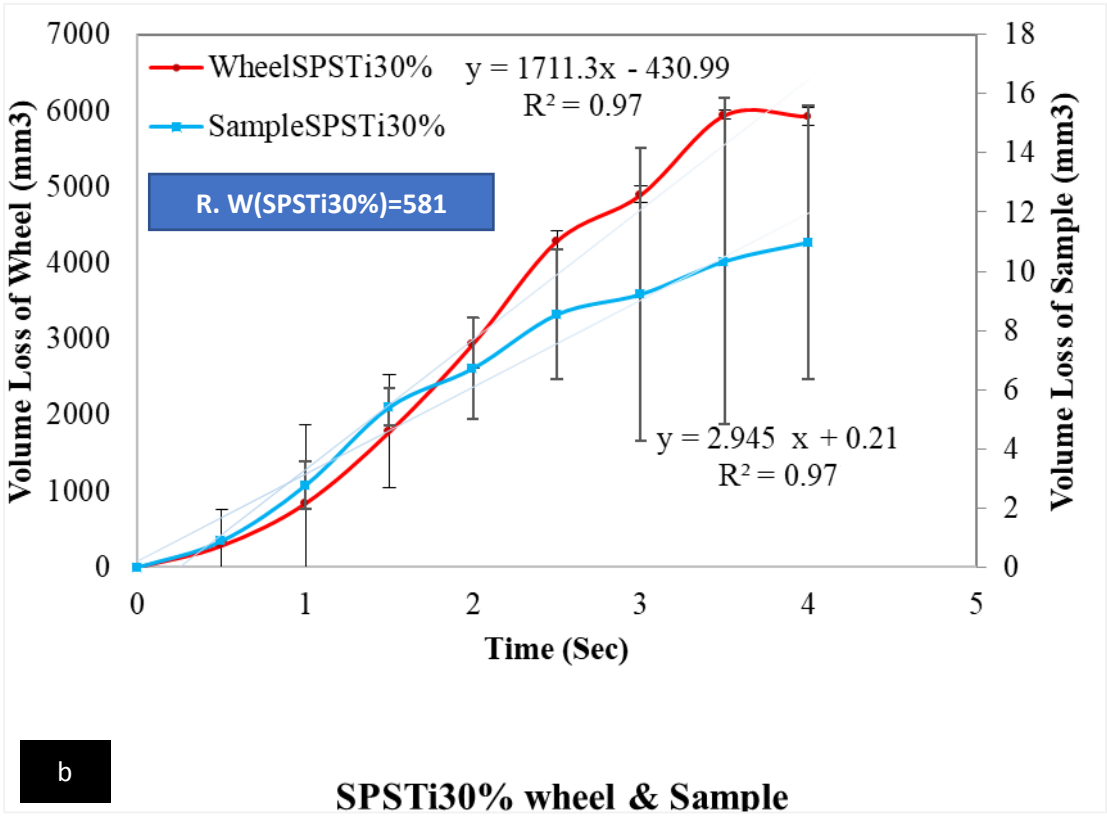

Figure (9-5): a) Volume loss of wheels cut through PM Ti-30%Dia. samples and samples themselves versus cutting time and b) Volume loss of wheels cut through SPS Ti-30%Dia. samples and samples themselves versus cutting time.

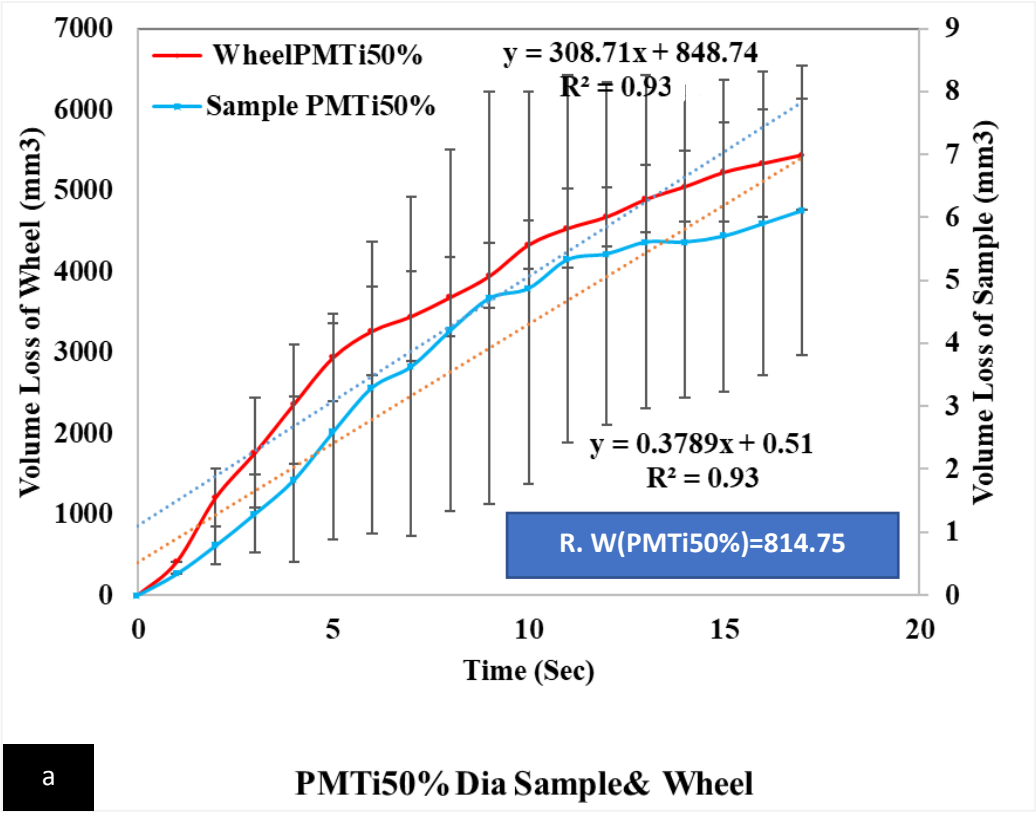

a

PMTi50% Dia Sample& Wheel

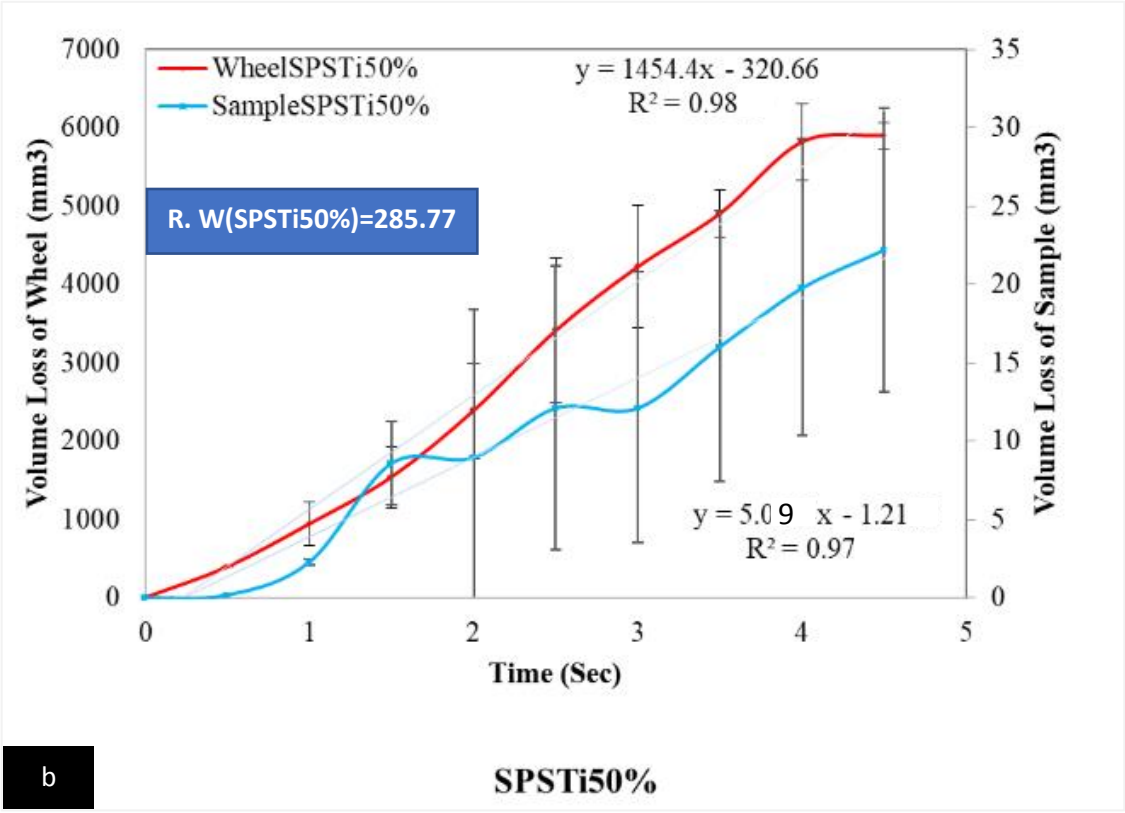

b

SPSTi50%

Figure (9-6): a) Volume loss of wheels cut through PM Ti-50%Dia. samples and samples themselves versus cutting time and b) Volume loss of wheels cut through SPS Ti-50%Dia. samples and samples themselves versus cutting time.

Figures (Figure (9-3) to Figure (9-6)) show the wear behavior of Ti-diamond composites. Each one contains two scatterplots of wear against time for the two wear elements. These plots form two groups; the (a) group shows the wear trend of PM samples of Ti-diamond composites reinforced with 5%, 15%, 30% and 50% vol. fraction of diamond reinforcement and the wheels cutting them, which achieved relative wear of 137.1, 195.2, 396.3 and 814.8 (mm^3 wheel Vol./ mm^3 sample Vol.) respectively, while (b) group presents the wear trend of SPS samples for equivalent volume fraction of reinforcement and the wheels cutting them, which achieved relative wears of about 291.9, 551.8, 581.1 and 285.8 (mm^3 wheel Vol./ mm^3 sample Vol.), respectively. It can be noticed that from these values the relative wear of all groups (relative wear) of Ti-diamond composites increased with volume fraction, in agreement with other researchers, who studied the effects of different volume fractions on the dry sliding wear of AMCs reinforced by SiC [241] and Ramamurthy, who studied the effects of weight fraction and particle size of alumina reinforcement in an aluminum matrix [242]. The increments of relative wears were in different proportions to and were not consistent with the amount of volume reinforcement in both manufacturing processes, indicating and influence of the process as summarised in Figure (9-8). The relative wear of composites processed by PM was approximately consistent with increasing volume fraction reinforcement, while in SPS processing this increment in relative wear was not consistent with reinforcement increment, even though the SPS composites have higher relative wear values than the equivalent PM composites at low volume fraction of reinforcement (5, 15 and 30 vol %). The increase in relative wear is lost with increasing volume fraction of reinforcement.

Generally, the composites produced by the SPS technique achieved higher wear than PM products at the same volume fraction of reinforcement, except for the highest volume fraction of reinforcement (50% vol.) where the relative wear of the SPS product was less than half that of the equivalent reinforced of PM product. This possibly comes from a low amount of intermetallic compound at interfaces, which may contribute to bonding of the reinforcement in the PM case. At high levels of reinforcement, the particles may not be fully surrounded by matrix, meaning that mechanical holding only would not be effective. The relatively large particle size of the particles forming the matrix (Ti), up to 45 µm, may also have a role. Differences in interfacial bonding between the two production methods appeared under SEM imaging, Figure (6-38) and Figure (6-39).

Furthermore, the existence of some intermetallic compounds at interfaces was confirmed by Raman spectroscopy, Figure (6-36) and by XRD, Figure (6-37). The weak bonding by an interfacial compound can be important when these intermediate phases are combined with matrix around the reinforcement particles. Then these compounds can reduce the span of matrix which is required to hold neighbouring reinforcement grains mechanically by acting as intermediate compounds in PM composite, as shown schematically in Figure (9-7). It could be concluded from the relative wear values of 50% vol. reinforcement in both composites (PM and SPS), that there is sufficient reinforcement being held by growth of the intermetallic compound.

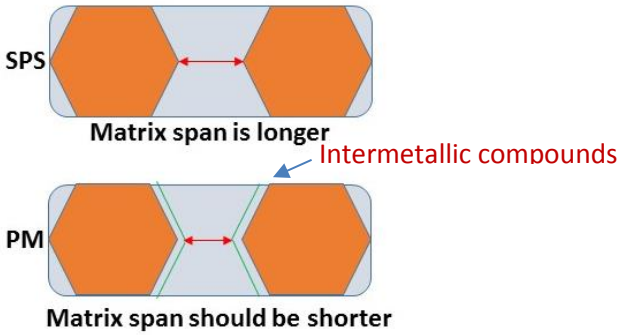

Figure (9-7): The differences between spans filled by matrix in cases of SPS and PM route.

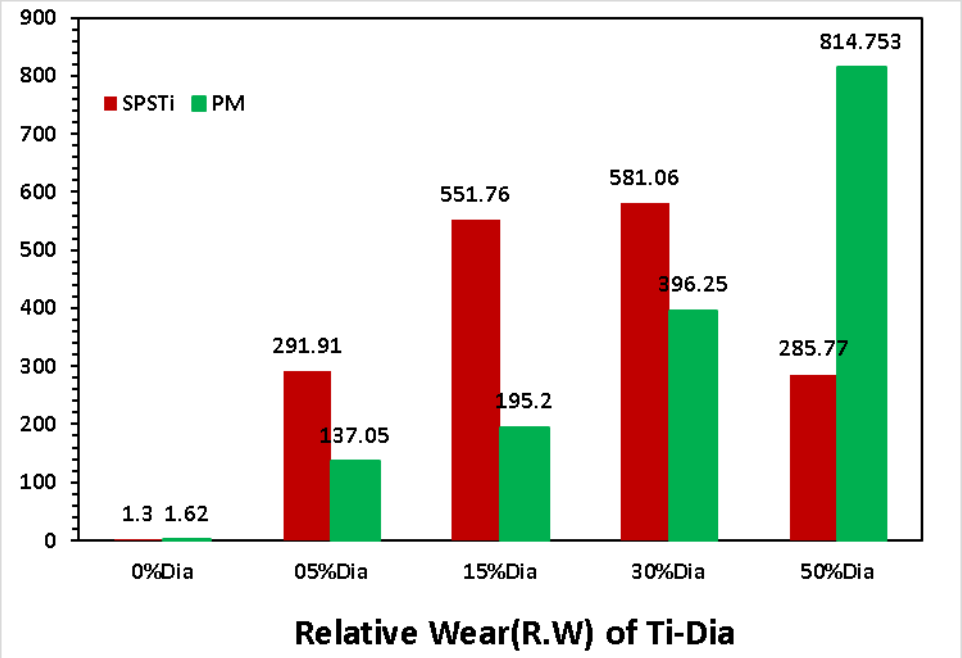

Figure (9-8): Change in the relative wear trend with volume fraction and manufacturing methods.

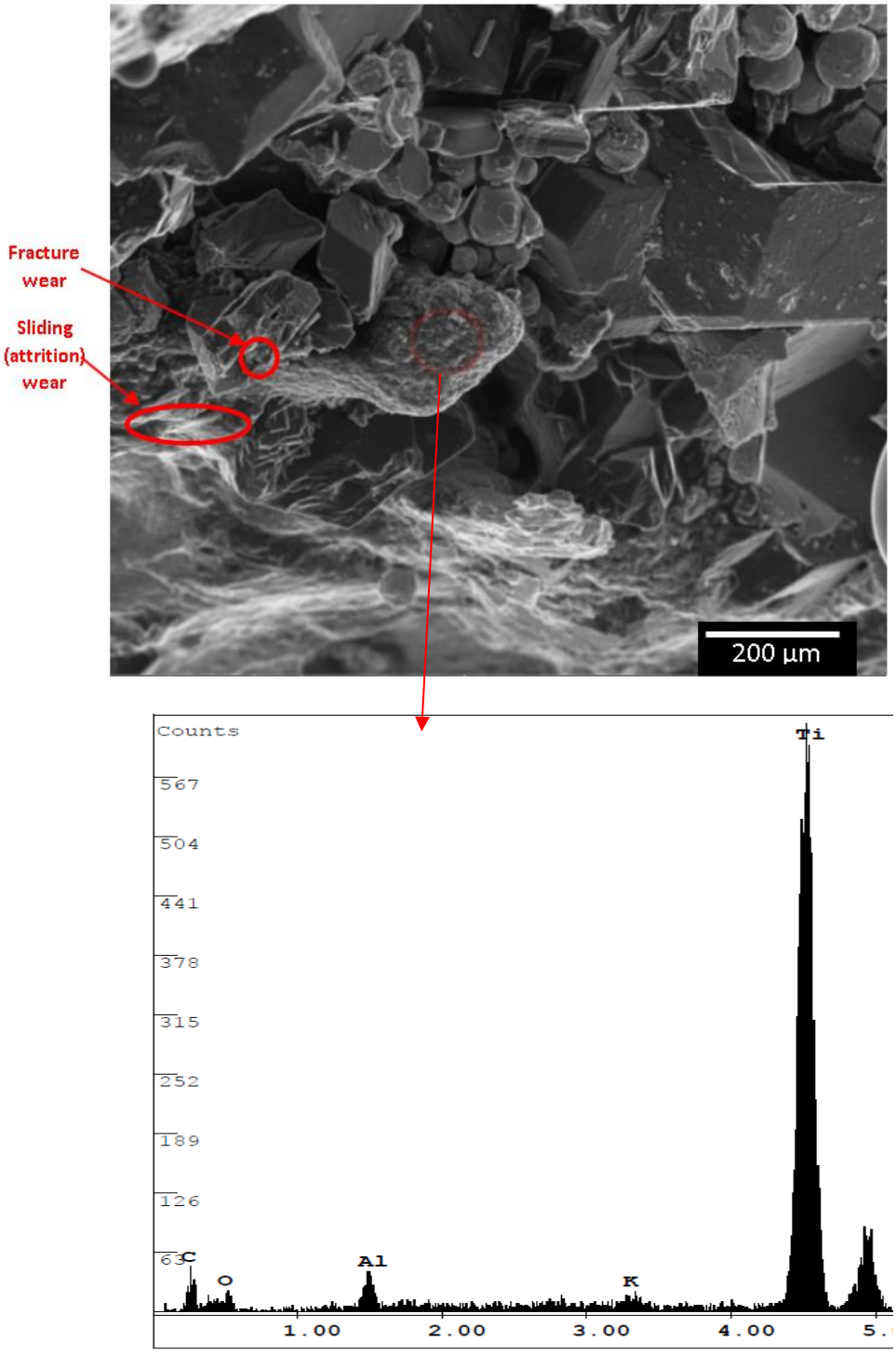

Figure (9-9) : SEM and EDX result of the cutting surface of SPSTi50% showing there are two main mechanisms of abrasive wear and agglomeration of some matrix behind diamond particles as a result of continuous sliding.

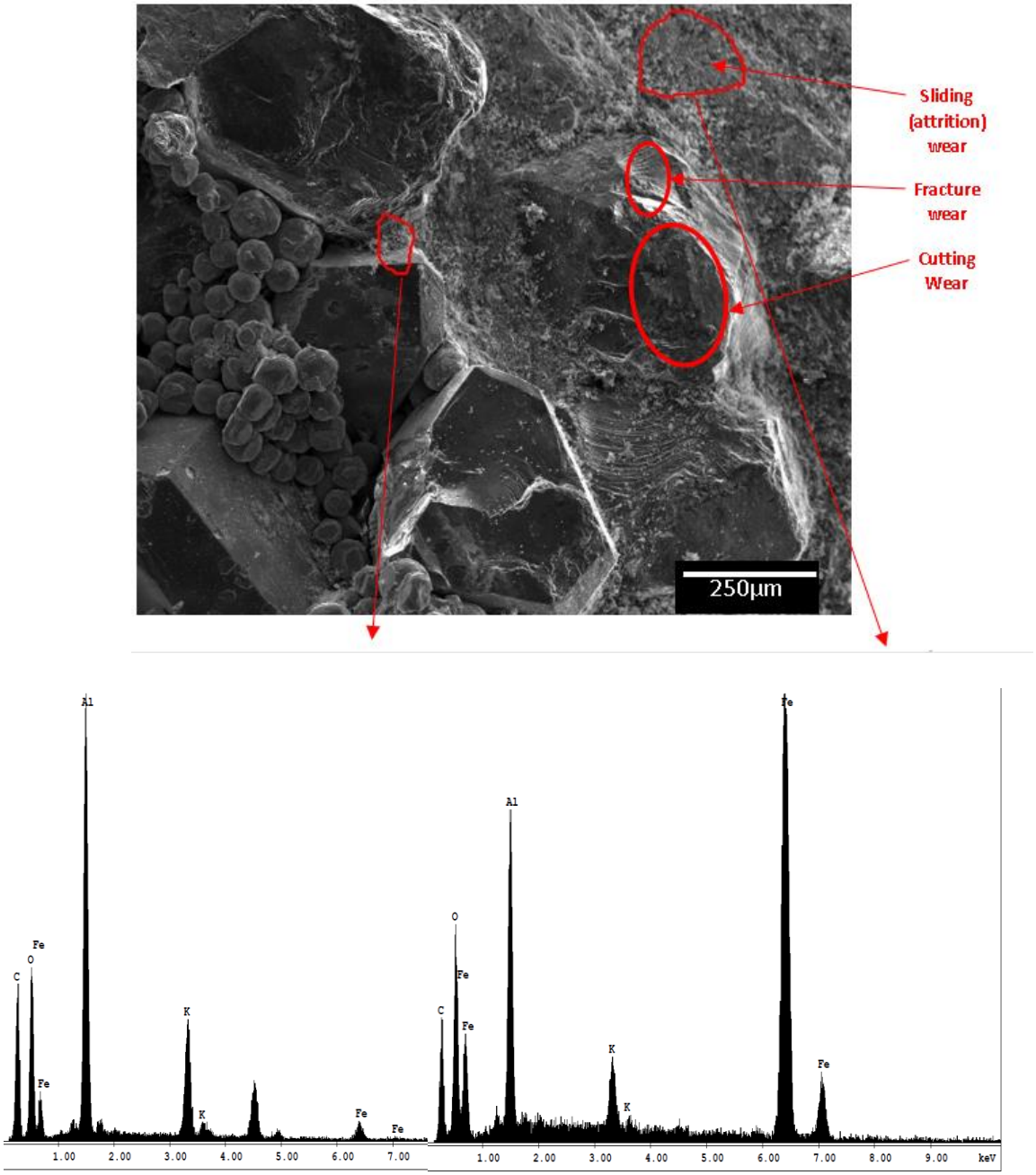

Figure (9-10): SEM and EDX result of the cutting surface of PM Ti-diamond showing that sliding wear is dominant and results in cutting through the diamond particles.

Figure (9-9) and Figure (9-10) reveal there are clear differences in which dominant wear mechanisms appear through the cutting process of SPS and PM composite. While the cutting surface of SPS composites shows the most dominant mechanisms are fracture [149] and attrition wear in addition to some pulling out of particles, in PM product the cutting surface under SEM shows that sliding wear (attrition) and cutting wear (abrasive) mechanisms were dominant, in addition to some fracture, probably due to the exposure of

diamond to relatively high temperature [209], leading to weakness or graphitization, especially where Ti is in contact with diamond [209]. Ti is known as an element which encourages carbide formation, and carbide formation at the diamond surface in PM would allow the wheel to penetrate the diamond structure more easily by sliding or attrition wear rather than fracture of the diamond particles.

In addition to this, titanium has been reinforced by 50% Vol. of 20/25 grit (710-840 µm) diamond and sintered under argon flow (PM) to see what happened with this relatively large particle size reinforcement compared to the previous group of particle size reinforcement, which was 35/40 grit (400-520 µm). The abrasive wear test, Figure (9-11), shows a drop in the relative wear value of this composite (466.6 mm^3 wheel/mm^3 sample) in comparison with Ti-diamond reinforced with 35/40 grit. The reason for this is thought to be due to the spaces between reinforcement particles being increased by the intermetallic bonding mechanism (the dominant mechanism in PM), with additional contributions from any oxidation happening at the surface of the Ti particles themselves before bonding of these together that will be lead to easy pull out of reinforcement particles. Reinforcement in the Ti composites may bond by the formation of intermetallic compounds as some peaks corresponding to such compounds appear under Raman and XRD of PM samples, Figure (6-36) and by XRD, Figure (6-37). There may be a relatively long span between reinforcement particles as a result of the nature of the low compaction factor of large particles [243] and the low load profile in these relatively long spans, especially in the PM case, which is only the route used to manufacture composites with this size of reinforcement [244].

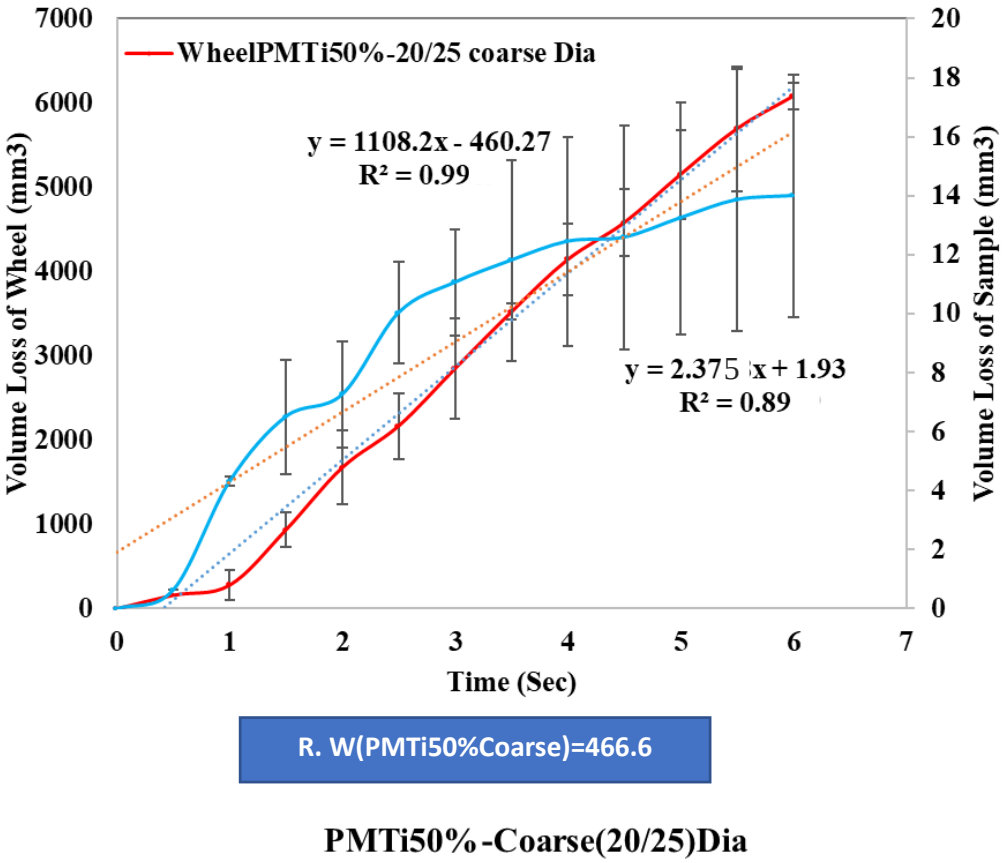

Figure (9-11): Volume loss of sample and wheels of TMDCs reinforced by 20/25 grit (710-840 µm) diamond particles.

9.1.1 Titanium-Ceramic Composites (PMTCCs) Ti-SiC & Ti- Al_2O_3

The wear behavior of (PMTCCs), shown in Figure (9-12), shows not great difference from AMCCs, especially in the wear behavior of wheels that cut Ti-SiC composites, which have three main stages of wear. The time of the cutting test was relatively longer than the test time of the equivalent composite reinforced with diamond reinforcement. This means the wheel and sample are not aggressively attacking each other, which may relate to the nature of the rubbing abrasive particles, which both show relatively similar wear properties or even in the case of the SiC particles, which have higher hardness than the alumina particles which reinforce the wheel. The longer test gives enough time for cutting tool (wheel) to be distinguished among the three conventional wear curve stages, which, as has previously been discussed in this chapter (4), occur in machining tools utilized in moderately abrasive conditions of cutting process. Another reason may behind this relatively slow volume

removed from wear elements may be that a thin layer of solid lubricant is formed [138], [231], [244], which may arise from smashed particles with some matrix particles and burned resin bond of the wheel to minimize friction coefficient at contacted abrasive interface. This layer has been extruded gradually on both sides of the embedded cutting wheel to coat the cutting surfaces of the sample, which was parallel to cutting process direction due to high temperature generated at contact cutting surface[138], [231], [244] (which reached 140°C at some points of the cutting process, as captured by a laser gun thermometer) as this extruded film appeared (red square) in SEM imaging of cutting surface of sample Figure (9-13) for SiC and Figure (9-15) for Al_2O_3. Therefore, it can been noticed in Figure (9-12a) that the wear rate of the wheel is changeable, starting with a relatively low value, about 9.6 mm^3/s, then at the end of this stage reaching about 40 mm^3/s. This stage of wear may correspond to the early formation of the solid lubricant layer which then starts to be removed with continuous friction and rise in temperature at the end of this stage, moving to another higher wear rate stage (at about 237 mm^3/s). This is the final stage (the failure stage) where at the end of this stage the wheel smashed due to its weak bonding of binder and the rising temperature. Its stated tolerance for temperature has a limit at 150-200°C. In Figure (9-12b) for Ti-alumina the situation is slightly different where the relative wear is about 15.6 (mm^3 wheel/mm^3 sample) and the stages of the conventional wear curve were not visible. As a result of that, the abrasive particle reinforced Ti composites have the same hardness of wheel reinforcement, which is alumina. This may lead to the cutting wheel being exposed to higher abrasive wear particles than in case of Ti-SiC, thus there is not enough time to distinguish these wear stages.

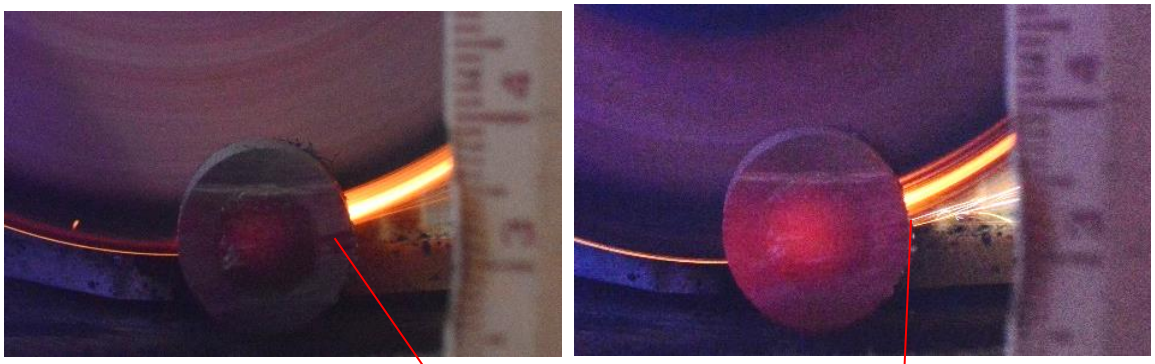

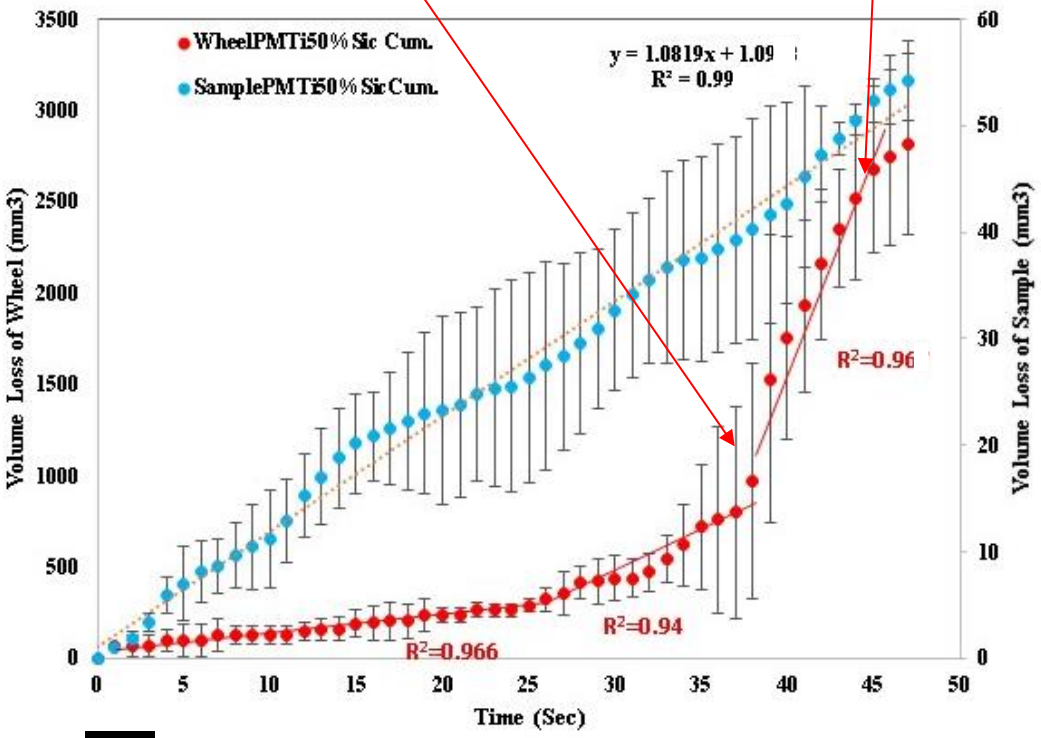
WheelPMTi50% Sic Cum.
SamplePMTi50% Sic Cum.
y = 1.0819x + 1.09
R² = 0.99
R²=0.96
R²=0.94
R²=0.966
Volume Loss of Wheel (mm3)
Volume Loss of Sample (mm3)
Time (Sec)
0
500
1000
1500
2000
2500
3000
3500
0
10
20
30
40
50
60
0
5
10
15
20
25
30
35
40
45
50

a

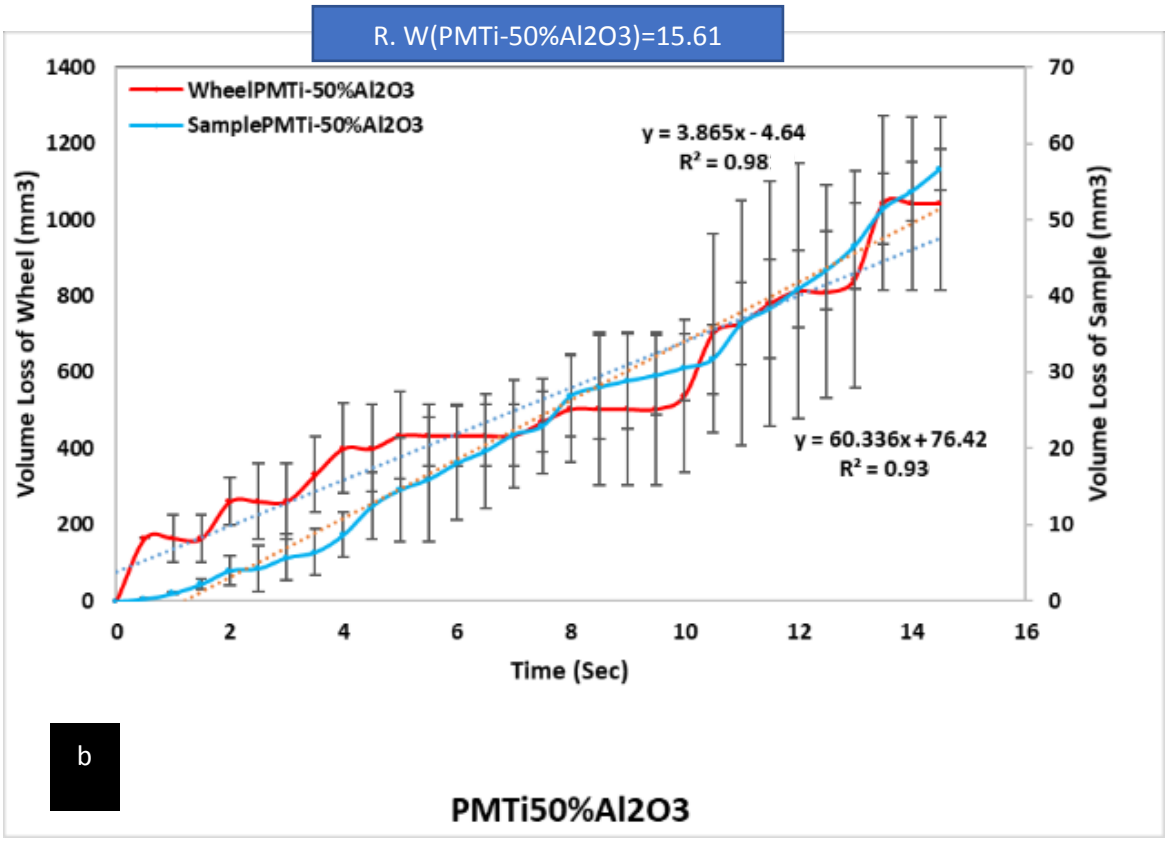

Figure (9-12): Volume loss of wheels and samples of TMCCs a) reinforced by SiC and b) reinforced by alumina (Al_2O_3).

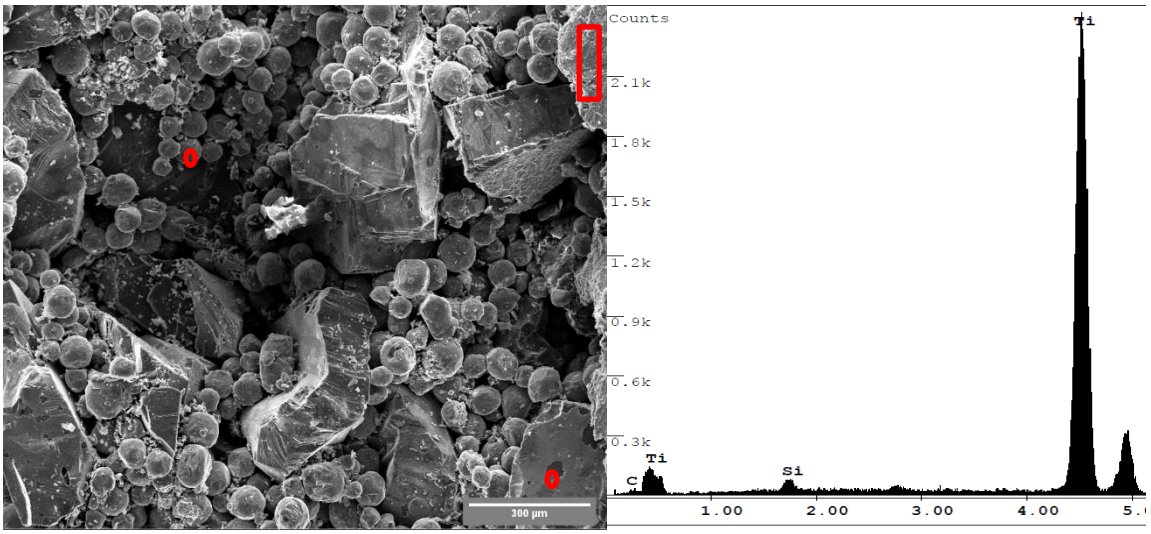

Figure (9-13): SEM broken and cutting surface of PMTi-50%SiC show that the bonding was limited by contact interfacial areas and the cutting surface form a melting sliding layer (top right red square).

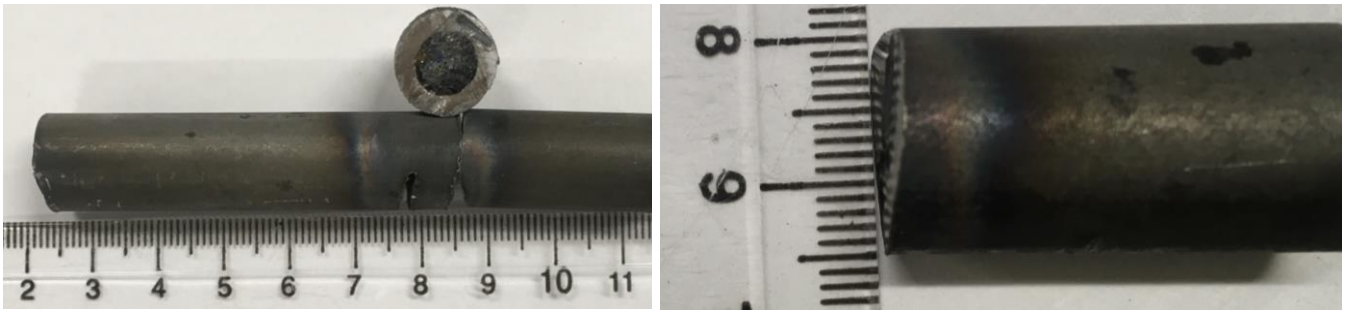

Figure (9-14): Images of Ti-Sic cutting sample shows the effect of heat generated during cutting.

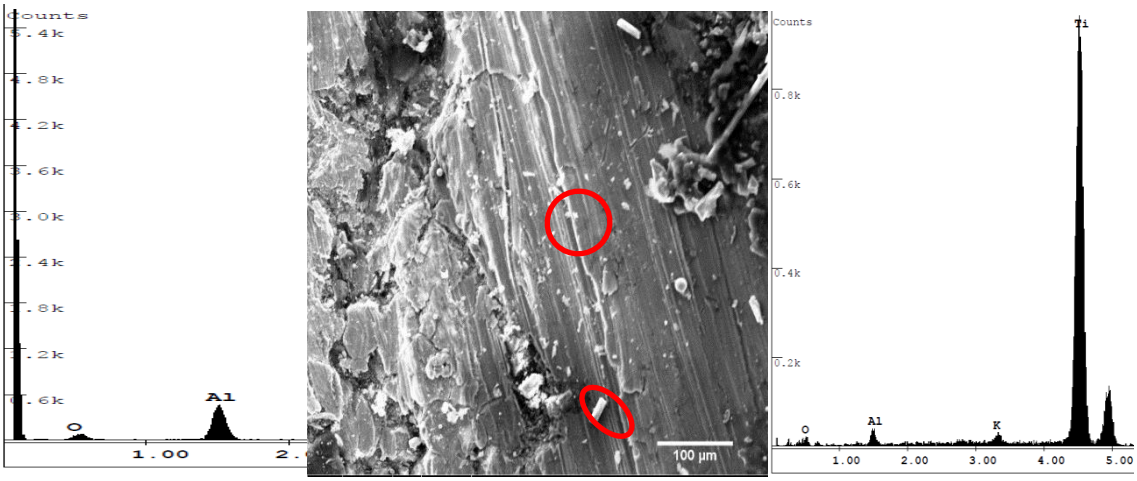

Figure (9-15): SEM image and EdX spectra of cutting surface of PMTi-50% Al_2O_3 show the sliding layer which form during cutting.

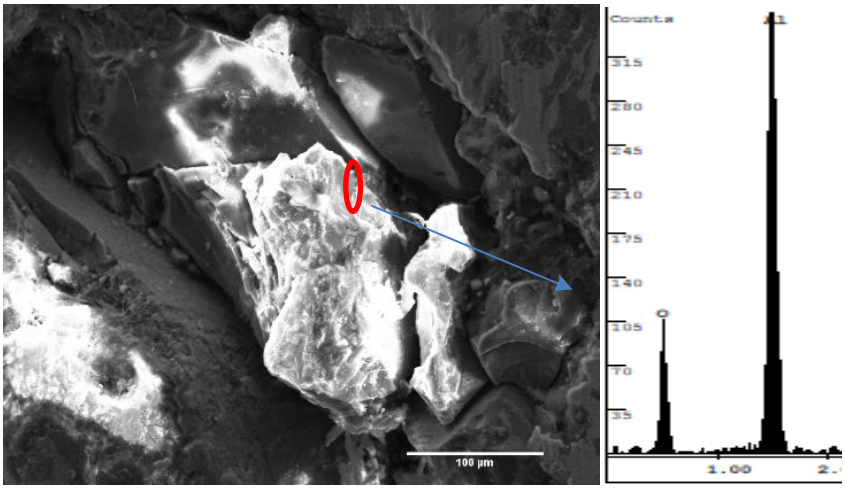

Figure (9-16): Broken surface by SEM of PMTi-50% Al_2O_3 shows that there is poor interfacial bonding.

9.2 Ni-Diamond Composites.

As well as studying carbide forming elements, which have ability to form carbides by reaction with carbon (such as Al and Ti) the current work explores other matrices such as nickel and copper, where carbides will not form or will not be stable. These elements have been utilised as a matrix reinforced with diamond in this study in order to eliminate the carbide effects on interfacial bonding. Hence, two main production methods (PM and SPS) were used in this investigation to see which of them is suitable to produce a Ni-diamond composite, and which has a higher relative wear. The comparable wear tests of these composites are shown in Figure (9-17a and b). These tests have shown that the Ni-diamond composite manufactured by SPS exhibited higher abrasive wear resistance (relative wear), about 2322.3 (mm^3 wheel/ mm^3 sample) while composite manufactured by PM gave about 1829.73 (mm^3 wheel/ mm^3 sample) relative wear. Even though, the relative wear of the Ni matrix made by PM without reinforcement was about 2.5 (mm^3 wheel/ mm^3 sample).

The SPS product seems to exhibit a higher relative wear than the PM product. This behavior possibly relates to the difference in mechanism of bonding between phases in the composite according to which production method was applied. This may indicate the formation of some interfacial compounds in PM products (Raman peaks Figure (6-45), which may cause weak bonding at interfaces and that makes the pulling out of the reinforcement particles easier. These compounds probably come from absorbed oxygen reactions and lead to oxidize the surface of constituent particles (Ni and diamond) or even formation some unstable carbides at interfaces with relatively long sintering time (1 hour) that was given for the PM product in comparing to SPS sintering time (about 10 minutes).

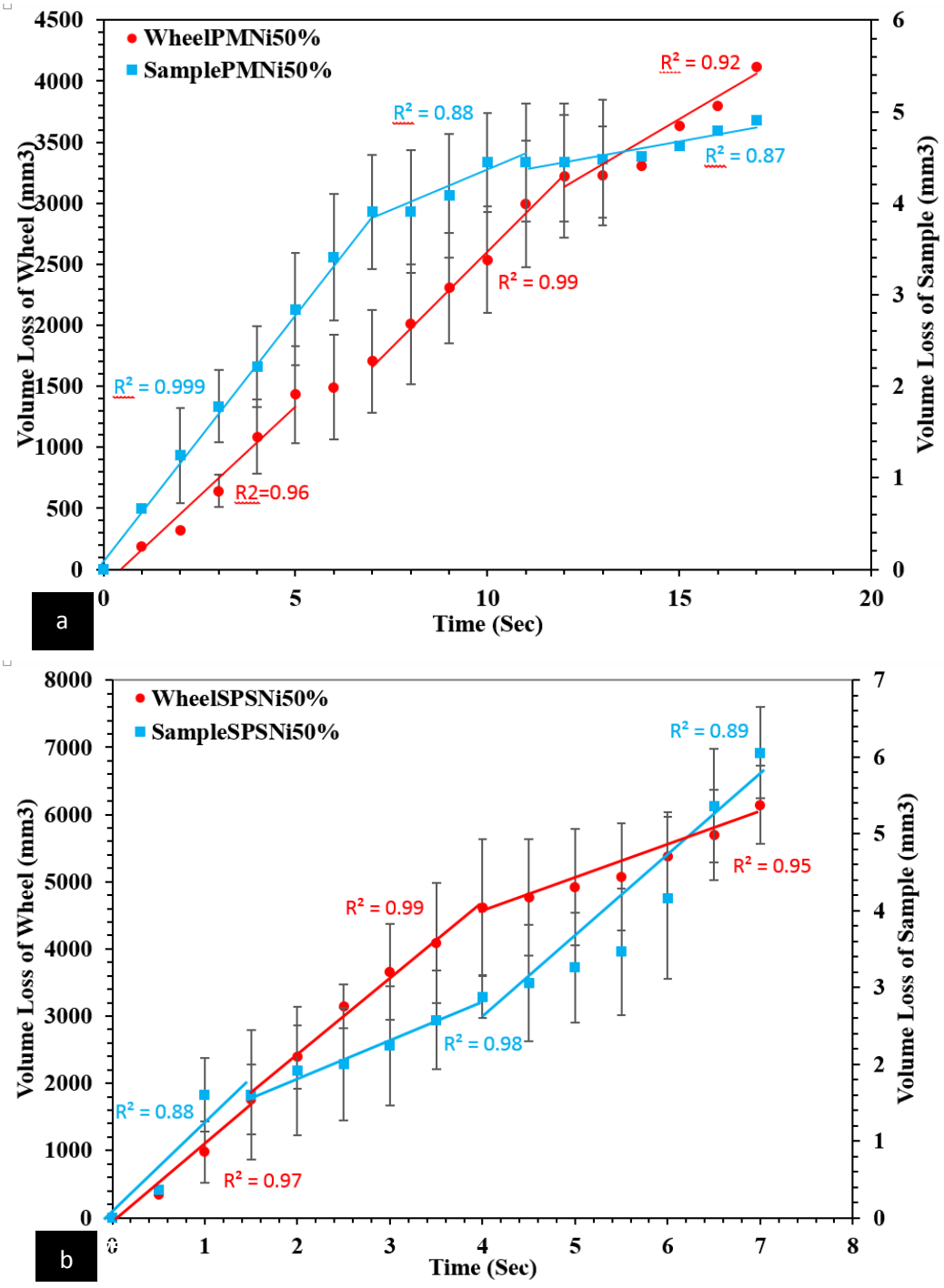

Figure (9-17): Volume loss of wheels and samples versus cutting time of Ni-Dia. composites a) PM and b) SPS.

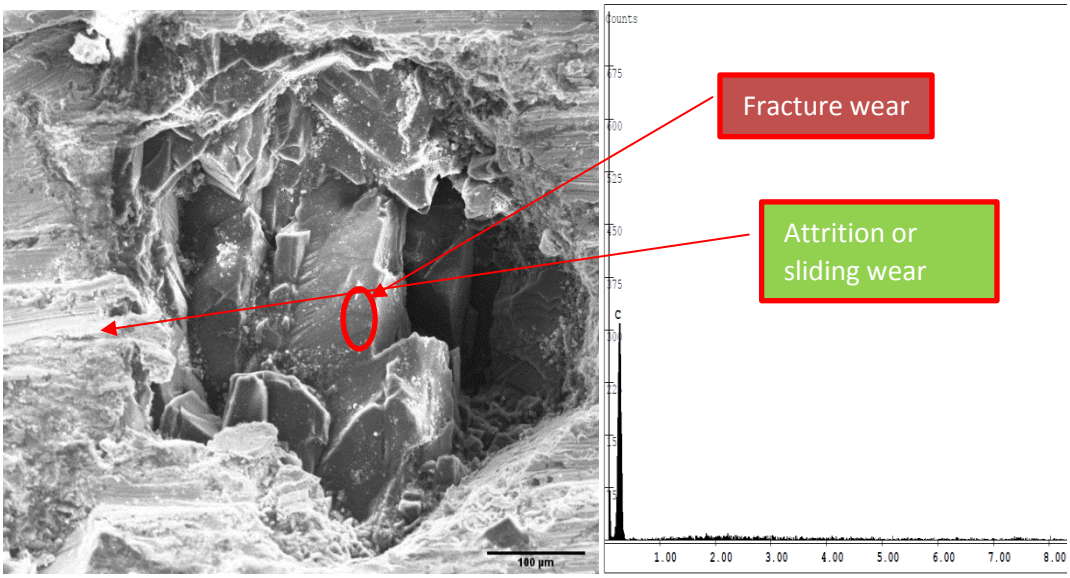

Figure (9-18): SEM image of the cutting surface of SPSNi50% samples reveals that fracture wear occurred in diamond particles during the cutting process.

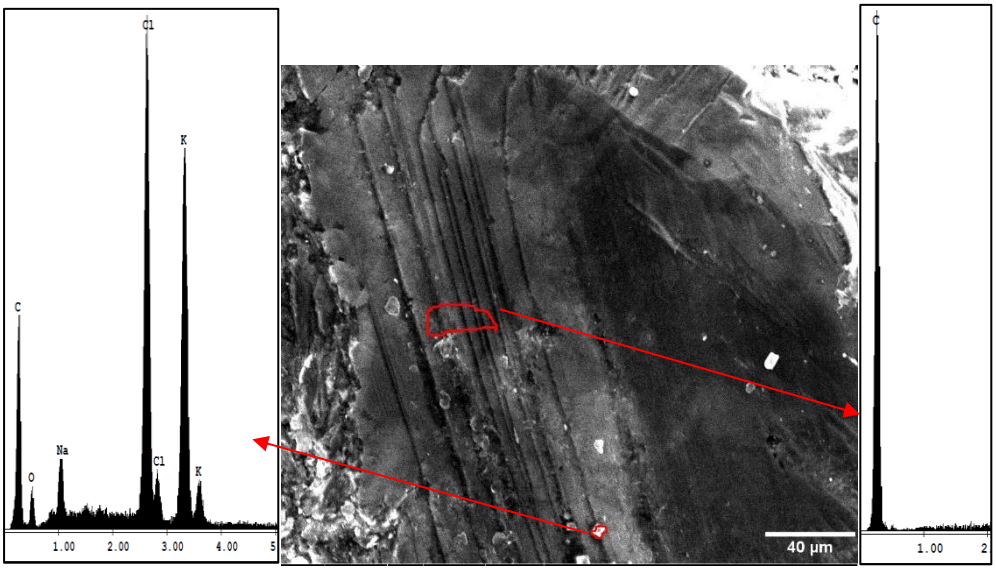

Figure (9-19): SEM image of PM Ni-diamond cutting surface reveals that the dominant mechanism of wear is sliding wear or (micro cutting wear mechanism) as a result of weakness in diamond structure due to the sintering temperature and relatively long holding time.

Figure (9-18) and Figure (9-19) show the SEM images of the cutting surface of Ni-diamond composites of SPS and PM, respectively. The wear debris impression can be clearly seen, and there are differences in wear mechanism which may dominate in each composite. In SPS the abrasive wear is combined of two main mechanisms, fracture wear in particles and attrition wear or sliding in the matrix. The dominant wear mechanism in PM material was a micro cutting with sliding wear in reinforcement particles with some wear debris which comes from abrasive wheel breakage between sliding surfaces [245].

9.3 Cu-Diamond Composites

The diamond base copper matrix composites are commonly applied in high thermal transport applications [72], [106]. Therefore, it is important to study their tribological properties in the current study to see if there are any interesting aspects for these composites in tribology, which relate to their high thermal conductivity, and may make them attraction candidate in tribological applications as well. These results will be compared with another composite with diamond reinforcement at the same volume fraction of reinforcement. There are also two main manufacturing methods (PM and SPS) utilised to process Cu-diamond composites, as for the other matrices (Ti and Ni) in order to compare the impact of the production technique on the structure and interfacial bonding, then on the wear behavior properties of composites. Figure (9-20 a and b) shows the volume loss of wheels and samples against the abrasive test time. Figure (9-20 a) displays the volume loss of Cu-diamond composite manufactured by PM technique and Figure (9-9 b) displays the same composite manufactured by SPS technique. But before the comparison of different processing methods, some important effects should be discussed.

There is an important phenomenon, noticed here, Figure (9-20). The curves of volume losses with time display three obvious main stages of wear, which could be corresponding to the conventional wear curve of machining tools. The wear rates of Cu-diamond composite fabricated by PM were about 0.51 and 270 mm^3/s for sample and wheel respectively, at the initial wear stage, 0.0915 and 121.3 mm^3/s for sample and wheel respectively, at the second steady stage while at the third rapid wear stage there is no wear occurred to the sample but the wear rate of the wheel continued to increase, at this stage preparing to fail, probably due to thermal effects. That means the relative wear of PM composites, which can be represented by the second wear stage, is about 1325.7 (mm^3 wheel/mm^3 sample). Whereas, the wear rates of the SPS Cu-diamond composite were about 1.75 and 643.13 mm^3/s for the sample and wheel respectively, at the first initial stage

of wear, 0.6 and 1000 mm^3/s for the sample and wheel respectively, at the second steady stage of wear and 0.7 and 197.6 mm^3/s for the sample and wheel respectively, at the third stage of wear. That means the Cu-diamond composites manufactured by SPS exhibited slightly higher relative wear, which was about 1666.7 (mm^3 wheel/mm^3 sample) at the second, relatively long stage of wear curves. However, the relative abrasive wear for Cu matrix without reinforcement, which was produced by PM, was very low in comparison to Cu-diamond composites, which achieved about 0.4.

This wear behavior is slightly different from the wear behavior of previous matrices. This is because the thermal effects here should be different to other matrices, due to the high thermal conductivity of Cu-diamond composites, which helps to reduce these thermal effects on wear by dispatching the generated heat from the abrasive cutting interface relatively quicker than other composites. Therefore, the wear behavior appears to show the effect of cutting speed more purely than before. In most previous samples the volume loss is affected by two conflicting factors, the heat generation at the contact surface, which increases wear rate, and the speed reduction as a result of the reduction in wheel diameter due to abrasive wear, which reduces wear rate.

Another reason for this behavior may be the very poor tendency of copper to react with carbon to create carbides. Consequently, there is a clean interface opposite to the matrices which have ability to create carbides at interface, where these compounds work as a barrier for heat dissipation if their thickness exceeds the desirable range [81], [246]. Growth of these compounds during cutting or even their existence at the interfaces after production may reduce the heat dissipation from the system (wheel-sample cutting surface) and lead to an increase in wear. In matrices which are able to form carbides, the three wear stages were not clear enough to be separated, or the steady state wear might dominate. Therefore, comparable wear behavior between the composites made by different processing methods (PM and SPS) depended on the steady state wear behavior (second stage of wear curves) because this stage is the longest and may be more representative for the relative wear of composite [117].

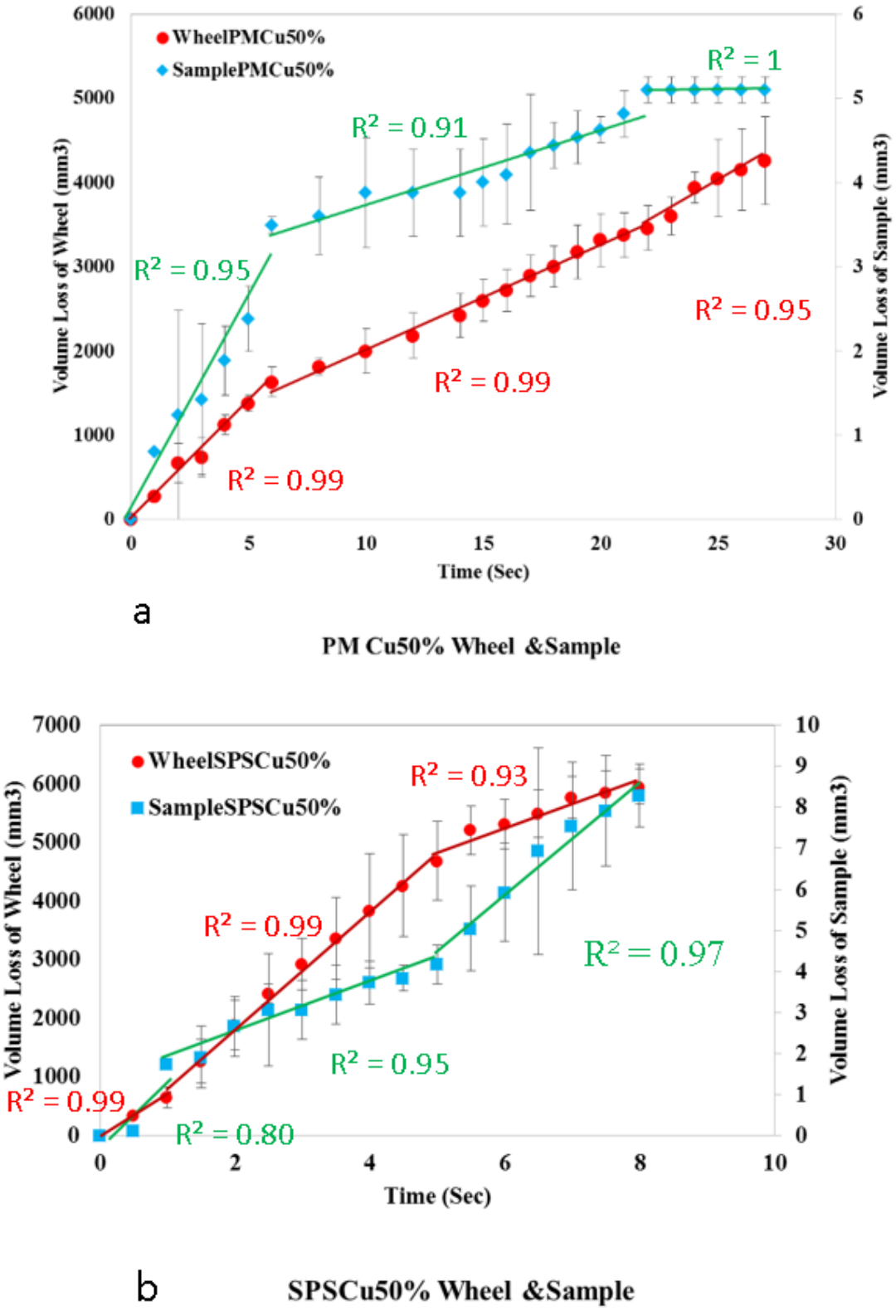

Figure (9-20): Volume loss of wheels and samples of Cu-diamond composites processed by a) PM and b) SPS.

While the cutting surface of both composites, Figure (9-21) and Figure (9-22), show there are differences in wear mechanisms occurring during the cutting process. In PM composites the sliding wear was dominant which probably relates to weakness or graphitization in the diamond structure due to the relatively long sintering time and high temperature [209]. In addition to some reaction such as oxidation or carbide formation that may happen in PM, this makes the abrasive wheel penetrate the diamond structure more easily by sliding or attrition wear rather than fracture of the diamond particles. In SPS composites the abrasive wear mechanisms were a combination of fracture and attrition, consequently, the latter production method achieved higher relative wear.

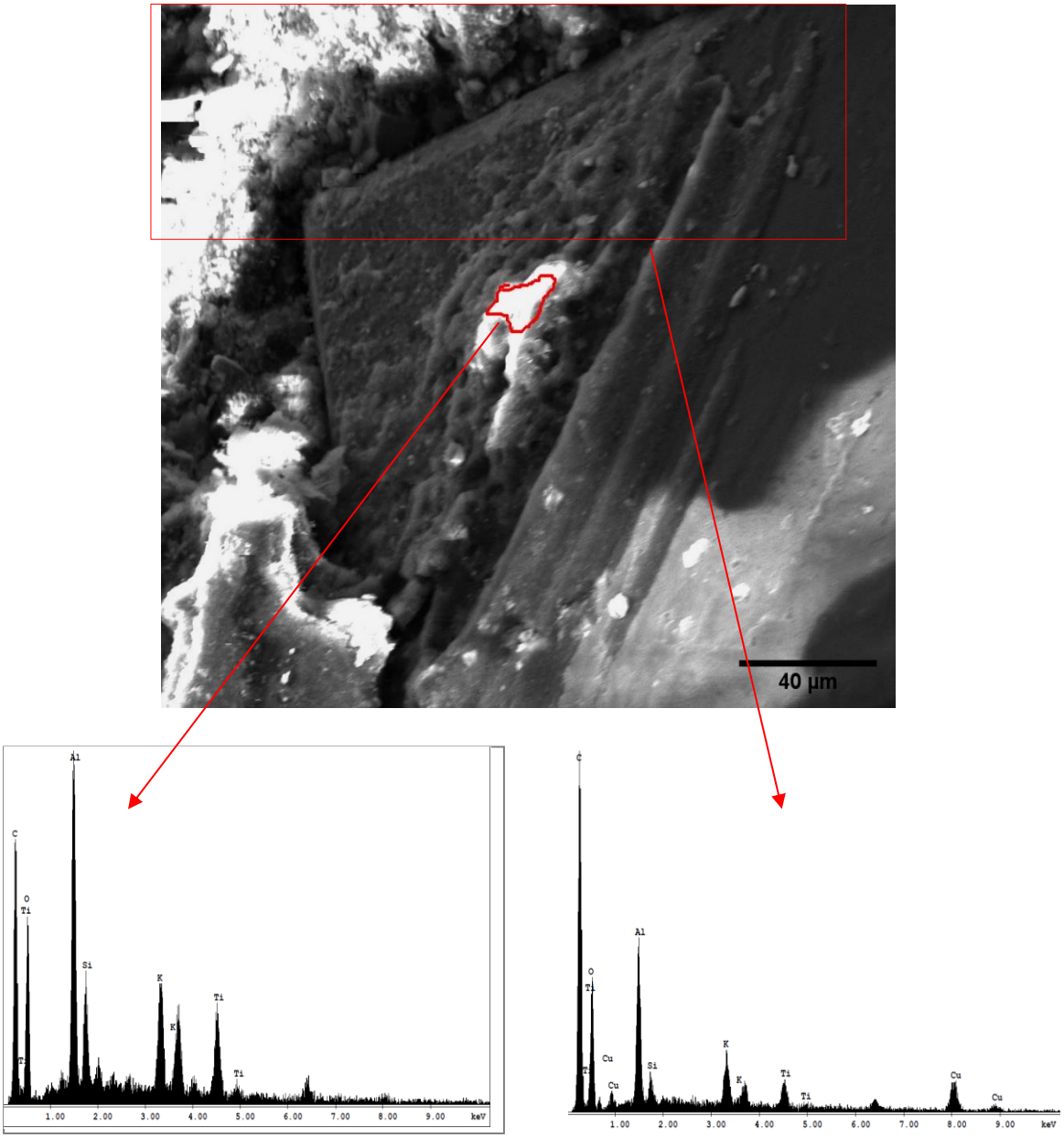

Figure (9-21): PM Cu-diamond cutting surface shows swarf sticking to the diamond surface due to sliding wear.

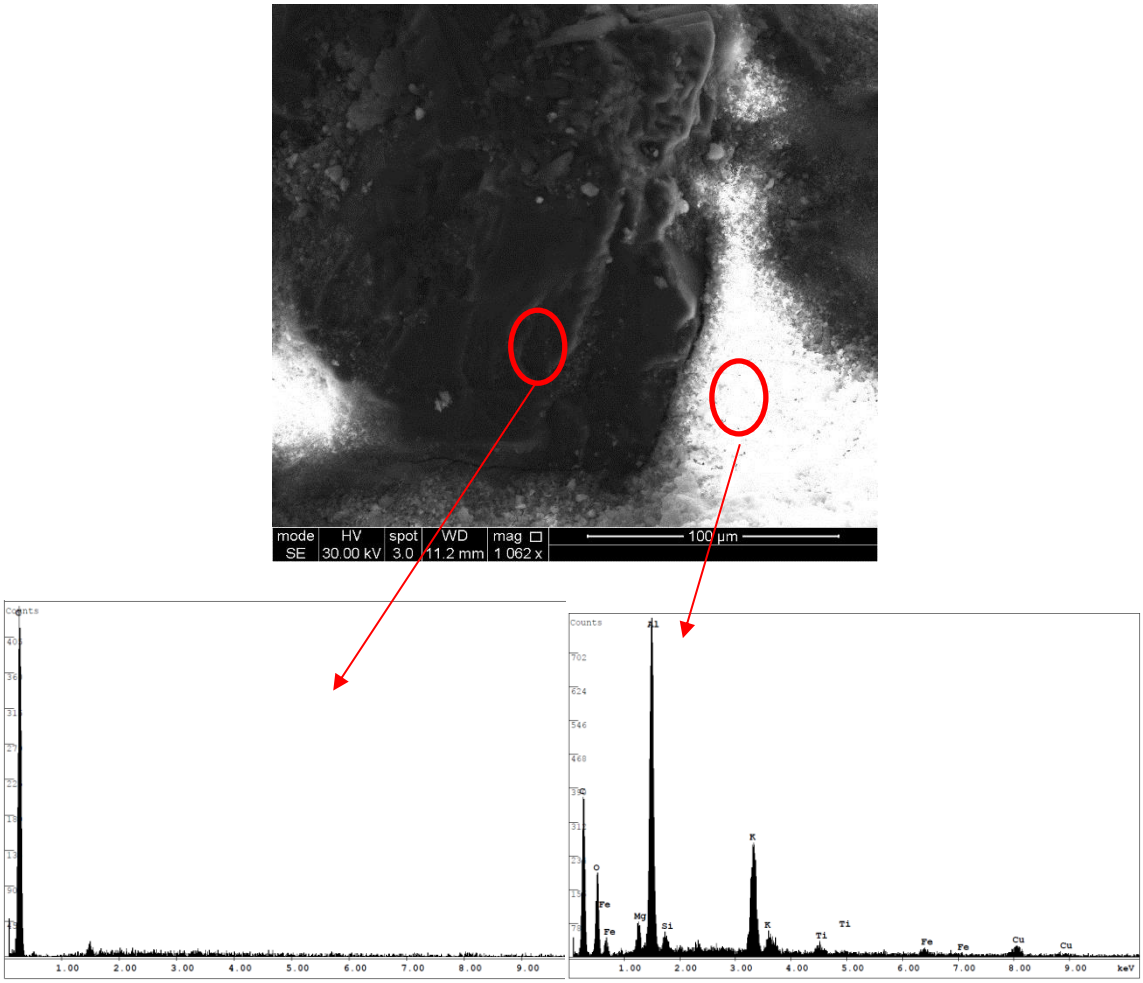

Figure (9-22): SEM image and EDX analysis of cutting surface of SPSCu50%-diamond, showing that the cut passes throughout the diamond particle and some cutting swarf left in matrix.

9.4 Summary

To sum up,

- This chapter compares and discusses some transition metals reinforced with diamond or ceramic reinforcement (SiC and alumina). These results may be summarised in the histogram plots shown in Figure (9-1 a and b), giving the wear of samples and wheels respectively, while Figure (9-2) displays the relative wear of composites.
- From the relative wear, our criterion of comparison, the wear behaviour of the composites is affected by the processing temperature and the nature of the matrix in terms of whether it encourages carbide formation, more than the hardness of the

matrix. This is seen in the Ti composite having lower relative wear than Ni and Cu composites, even though the Ti matrix has higher hardness.

- Another important observation is that composites produced by SPS generally achieved higher relative wear than those produced by the PM route, except for the Ti composite. The highest relative wear was Ni reinforced with diamond followed by Cu and then Ti composites.
- Ti matrix reinforced by ceramic reinforcement (SiC and Al_2O_3) showed higher relative wear than pure Ti (1.3 relative wear), but are still insufficient to prevent cutting of the 8 mm diameter sample by a single abrasive wheel. Different wear mechanisms have been seen in cutting composites such as fracture wear, attrition wear and cutting wear mechanisms.
- In regard to the other two wear parameters (wheel and sample wear), the wear behaviour was not consistent in a way that could allow comparison. The effects of these two parameters on wear behaviour can be separately studied, so this study may be valid for estimating the suitability of these materials for other applications such as brake discs and gears. In the current study the composite is required to achieve a balance between preventing a cut-off wheel from penetration through the sample, and destroying the wheel by abrasive attack. For example, the wear behaviour of Ti-diamond composite and Ni-diamond composite is compared for wheel wear, sample wear, and relative wear parameters. The Ti composites caused higher wear rate for the wheel than Ni composite, Figure (9-1 b), but the wheel has penetrated more in the Ti composite than in the Ni composite, Figure (9-1 a). Consequently, the relative wear of the Ni composite was higher than the Ti composite. In other words the Ni composite has higher abrasive wear resistance against abrasive cutting than the Ti composite, under the measure applied here. These parameters are discussed in more detail in the next chapter.

Chapter 10 Discussions of Abrasive Wear Results

This discussion chapter comprises further critical analysis of the results and discussion concerning the wear properties of both elements in the process (the cut off wheels and the samples) separately, rather than the relative wear value which describes their relative values in a single number, and was used as the comparison criterion in the last three chapters (7, 8 and 9).

Before independent wear property analysis of each element can begin, some concepts need to be defined. Firstly, the same type of abrasive cut-off wheel was used in all experiments and the main target was to develop new high wear resistance abrasive composites. Therefore, when high wear rate occurs in the wheel, a high degree of abrasive attack is generated by the composites towards the wheel. Secondly, when a high wear rate occurs in a composite sample, then this composite has low wear resistance, and the wheel has penetrated more due to abrasive wear attack of the composite. For the main aim of this work in developing effective materials to resist abrasive cutting, especially for security applications, finding a particularly high or low wear rate in one of the contacting wear elements (the wheel and the composite sample), meaning that this element has a high or low wear resistance, is not enough without looking to how much this has affected the opposite surface, in terms of how it will perform. This is the reason for the adoption of the relative wear as the criterion of proportional wear effects, combining the behavior of both wear elements in the system.

As the behavior of the elements separately is also relevant, this chapter discusses wear data of both contacted surfaces as well as their combined behaviour. The analysis and discussion are developed according to the two key aspects of the investigation:

1. Relationships between the different AMDCs and the cut-off wheel according to variable particle size, surface conditions and types of reinforcement (either diamond or ceramics) with different processing methods.

2. The effect of the different transition metal matrices reinforced by diamond/ceramics and cut-off wheel with different processing methods.

10.1 Wear Behavior of AMDCS

The grinding process is a complex phenomenon of combined wear mechanisms due to undefined cutting edges [146]. Therefore, the grinding process trend with time normally fluctuates, and this fluctuation would be expected to be increased in grinding composite materials. This can be interpreted from the high error bars that were calculated for the wear trend of composites (see section 8.1). Consequently, the creation of a predictive model by applying linear regression of wear for each wear element (the wheel and the composite) was required in order to estimate wear properties depending on the relative wear, as was discussed in chapter 7. There are differences in wear behavior when we look at each side of the contacted surface in the wear system separately. Here there appears to be no clear trend of wear rate either with size or with surface condition of the reinforcement, as shown in Chapter 8 (histogram figures (8-1) and (8-2)) in addition to Table (10-1). This table displays the trend of wear rate in ascending and descending order toward poorer performance of the composite materials, according to three different values:

i- Wheel wear values (descending order), showing the trend towards lower abrasive wear from the composite samples.

ii- Sample wear values (ascending order), showing the trend towards greater cutting of the composite samples

iii- Relative wear values (descending order), showing the trend towards more cutting of the sample for a given amount of wheel wear.

Whatever criterion is used to rank abrasive wear, it should achieve the purpose of material selection for design. For example, for security barrier applications as envisaged here, it is required to prevent the abrasive wheel cutting through the composite and aggressively (via abrasion) attack the cut-off wheel used at the same time. This behaviour can be easily assessed by the relative wear values as these combine both effects and offer a balance between them. Table (10-1) also shows sample and wheel behavior which give rise to these values. Before discussing these, it is important to define an important parameter that is normally used with grinding processes, the G ratio. This parameter applied in most grinding process to assess abrasive wear in the blade and sample, via the standard Archard equation, widely used for wear and discussed earlier in chapter 4. This equation requires an accurate value for the

contact distance for the blade with the workpiece during cutting. This distance frequently cannot be obtained as it changes throughout the cutting process in a way that is difficult to measure and account for. To deal with this, some previous researchers have taken the approach of defining a parameter representing a wheel wear resistance, which is the G ratio. This is the material removal volume divided by volume of wheel worn away, so a high G ratio indicates a minimum amount of wheel lost, and vice versa [147], [149], [151]–[153]. In the current work the wheel wear is very high, meaning very low values of the G ratio for tests on MMDCs would be expected. We apply calculations depending on volume lost to represent the wear in both parts of the wear system, with the results plotted with cutting time. The high reduction seen in the wheel radius in comparison with much lower depth of cut of the sample can be considered as an indicator of the amount of abrasive wear (proportional wear) of the cut-off blade; at the same time, it refers to the degree to which the specimen is strong enough to resist the cutting process. This type of model was applied by tribologists in the Commonwealth Scientific and Industrial Research Organisation (CSIRO) in Australia, to study wear behavior of a composite of 80% diamond with 20% Si, designed for use in cutting elements, with mass loss used to measure wear behaviour. The wear rate (relative wear) of the different composites was found to be between 300 to 818,900 (material cut (wt%)/ tool loss (wt%)) [100]. Most of the relative wear values of manufactured composites in the current study are in this range, even when volume loss was applied for measuring wear.

However, the grinding ratio is not truly an expression of grinding wheel wear in all cases [149] because abrasive wear can occur in a grinding wheel by pulling out whole abrasive grains, where the diameter of these grains is greater than the depth of total wear, usually the measured parameter used to calculate the volume removed from the wheel [154]. In this situation, any variations in grinding conditions may cause unexplained changes in the grinding ratio [149].

Table (10-1): Different criteria (wheel, sample and relative wear) to show wear behaviour of composites in either ascending or descending order of AMDCs.

A

Composite	Wheel Wear (mm^3/Sec)
GIAB$_1$50%(20-25 Dia grit)	1262
Al SPS	756
A$_1$(AlGI)	636
Al PM	634
Al20%Dia-30% Al_2O_3	525
A(AlGI)	332
B	259
A$_1$50%-20%Dia-30%SiC	214
Epoxy50%	169
C$_1$	142
B$_1$	136
Sn50%Dia	112
C	71
GI Al- Al_2O_3	12.9
GI Al-Sic Wear	0.7

Descending order

÷

B

Composite	Sample Wear (mm^3/Sec)
GI Al-Sic Wear	0.1
C	0.4
B$_1$	0.54
GI Al- Al_2O_3 Wear	0.7
C$_1$	0.9
Al PM	1.23
Al SPS	1.5
GIAB$_1$50%(20-25%Dia grit)	1.85
B	1.9
A(AlGI)	2.1
A$_1$(AlGI)	2.4
Al50%-20%Dia-30%SiC	2.4
Al20%Dia-30% Al_2O_3	4.4
Sn50%Dia	10
Epoxy50%	13

Ascending order

C

Composite	Relative Wear
GIAB$_1$50%(20-25 Dia grit)	682
Al PM	515
Al SPS	504
A$_1$(AlGI)	265
B$_1$	252
C	178
A(AlGI)	158
C$_1$	158
B	136
Al20%Dia-30% Al_2O_3	119
Al20%Dia-30%SiC	89
GI Al- Al_2O_3	18
Epoxy50%	13
Sn50%Dia	11
GI Al-SiC Wear	7

Descending order

In Table (10-1), the order of values is arranged toward reduction in the composite wear performance. If a high wear rate of wheels is considered an indication of the ability of the cutting composite to resist abrasive wear and cause high abrasive wear in the wheels, then the wheel wear rate is seen to be increased with the coarsest particle size of reinforcement of the composite, which tends to offer the highest increase in abrasive wear attack of wheel. This trend agrees with other research [163], and probably occurs because during cutting every hard particle operates as a cutting edge of the blade. In spite of the fact that the cutting edges are higher in number in the samples that are reinforced with the smallest particles, these particles are less well embedded in the matrix and are more easily removed [228] (their contact area for bonding is less per particle than with the large particles). These small particles then may work as a third body between the contacting surfaces, reducing the wear occurring by acting probably in the manner of a lubricant (at least for short time once they smashed). As there is lower abrasive attack for the wheel in this case, there is lower relative wear. The same behavior probably occurred in the ceramic reinforced composite where there is limited penetration into the samples due to the nature of the gradual fragmentations that happened to the reinforcement, introducing a kind of solid lubricant at the contact surface, and leading to reduced wear rate of samples as shown in the upper part of Table (10-1B). This conclusion corresponds with other research, such as [138]. Another important factor, which may contribute to wear enhancement of Al-ceramic composites, is the high tensile properties and modulus of elasticity of Al-ceramic composites according to [125], [128] which may be enhanced with Al_2O_3 reinforcement [247] or even diamond [90]. Rao [163] reported that the wear rate of Al7075 AMCs decreases with increasing volume fraction or particle size of SiC reinforcement [163]. Pradhan [164] attributed the enhancement in wear resistance of AMCs with volume fraction of SiC reinforcement to a reduction in the coefficient of friction due to increase in the volume fraction of SiC, in addition to the formation of an oxide layer. On the other hand, cut-off wheels that cut the ceramic reinforced composite did not wear at a high rate, as shown at the bottom of Table (10-1 A). Consequently, these composites have low relative wear values in comparison with the equivalent diamond reinforced composites, Table (10-1C). Hence, the relative wear criterion can be used to judge which composite is more suitable to resist abrasive cutting resistance for security applications, while the other two criteria may be suitable to assess wear for other potential applications, such as brake discs

when long life of contact surfaces is required. According to the low wear results of AMCs, when these composites were loaded with 20 vol. % of diamond, this addition improved the composites wear attack and caused high wear rate in the wheel used to cut these composites, Table (10-1 A), consequently increasing the relative wear values of the composites, Table (10-1 C). The composites that were loaded with 20 vol. % diamond were sufficient to wear the whole abrasive cutting wheel before the cutting was completed for the designed barrier, which is about 8 mm diameter.

The composite samples made here and the cut-off wheels are very different materials. In regard to the differences of abrasive particle sizes in both contacted surfaces, the relative size of the abrasive particles of the wheel and the sample has an important role. As the sample has the coarser reinforcement, it would be expected that the composite would have a superior wear resistance, as reported by [138] and [166]. Following the same logic, the composite reinforced with fine particles will not be as effective as that with the coarsest particles in the relative wear concept. This study has found that the wear rate of the wheel is increased by increasing the reinforcement particle size, corresponding to the abrasive wear concept that the wear rate and friction coefficient should increase with increasing particle size reinforcement of the counter face (the harder surface or that which contains harder particles, in our case the AMDCs). This agrees with the behaviour for example of grinding or polishing papers used to prepare samples, as reported in literature [229], [230].

While in regard to reinforcement surface condition effects, the situation was different. There is no clear trend when comparing cut-off wheel wear isolated from sample wear; as was discussed previously there are some fluctuations in behaviour. For example, in the composite with large and small particle size reinforcements (A, $A_1$and C, C_1) the wheel suffers from greater abrasive wear with coated rather than uncoated particle reinforcement, while with median particles (B and B_1) the opposite trend was seen as shown in Table (10-1A). Table (10-1B) in comparison the trend of samples to resist wheel penetration for cutting composite was generally better with uncoated particle reinforcement, except for the median particles (B and B_1). This was probably because some graphite (considered to act as a solid lubricant) and Al_4C_3 formation took place on the surface of diamond particles, while in coated particles these effects are prevented. It has been reported that the coating of diamond reinforcement with

SiC prevents Al_4C_3 formation during the casting process (for a pressureless infiltration method) [248].

Efforts have been spent in the current work to understand this fluctuation in wear behaviour among composites that are reinforced with different particle size reinforcements and surface conditions, by investigation of specific samples with SEM, EDX, XRD, optical microscopy and Raman spectroscopy. The results generally reveal that these fluctuations are related to the differences in interfacial bonding, particle sizes and nature of surface morphology of the reinforcement (comparison of microstructure chapter 6 and wear behaviour in chapter 8 above).

Generally, by finding the different wear behaviours of samples according to the variation in a particle size and coated/uncoated nature for the same particle size, it can be seen from Figure (8-3), Figure (8-4), and Figure (8-5) (pp. 162, 164 and 166) that the relative wear values of the samples increase more rapidly in the cutting of composites that are reinforced with coated diamond particles than with uncoated diamond of the same particle size. The result of dividing the gradient of blade wear with time by sample wear of A_1 and B_1 samples is higher Nevertheless, there are some occasional fluctuations in the wear of the blade in cutting composite with both the uncoated and coated diamond reinforcement, which may relate to some inhomogeneity in the samples themselves, or the existence of some graphite transported by the cutting action from interfaces to form a thin layer of solid lubricant, especially through the cutting of the coarsest particle size reinforcement, A and A_1.

Furthermore, there is slightly different abrasive behaviour noted for samples with the finest particles, C and C_1, where the relative wear of uncoated particles was seen to be higher than coated, as clearly shown in Table (10-1C) and Figure (8-5). This behaviour may be related to the coating process of particles, or even to the infiltration processes, where an appreciable proportion of the smaller particles may convert to carbides or graphite during the process due to its small size, which offers a large surface area, as shown in Figure (6-23), Figure (6-24), and Figure (6-25) (pp. 112 and 113). Another possible factor that may reduce the wear resistance of fine particle reinforcement is the high compaction factor of fine particles (the small spacing formed between particles). A high packing fraction may mean these particles touch each other, and not being fully surrounded by matrix, they will be easily removed during

abrasive cutting. This conclusion could be in agreement with Weber & Tavangar, who studied the effect of a high volume fraction of diamond particles (60-75 vol. %) on opposing the contraction of diamond particles during thermal expansion of composite [86].

The production methods and ranges of temperatures that can be used to produce composites have a crucial impact on the structural and tribological properties of AMCs. The range of temperature for processing diamond or diamond coated reinforcement has been reported to need be under 800°C to overcome the oxidation and graphitization problems of diamond [249]. In the current research the range of processing temperature that was utilised with the GI technique was very close to 800°C (780°C). It is thought this may be one reason for the decreased wear properties of the GI composite in general comparing with AMCs processed by sintering techniques (PM and SPS) as that revealed in Table (10-1 A, Table (10-1 B, and C) with no differences in the three criteria; wheel wear rates of PM and GI composites are close to each other as shown in Table (10-1 A). This was probably because of some graphite layer formation on the diamond surface which may introduce a solid lubricant during cutting in both products, but to different amounts, as that shown in Raman spectra, Figure (6-30), pp. 119. The conflicting effects of combining the two different criteria (Table (10-1A and B)) can be clearly shown in Table (10-1 C). This table reveals a large difference in wear behavior between the GI methods and powder sintering methods (PM and SPS) where the enhancement in relative wear was about 87% in the case of SPS over GI, and about 90% for conventional powder metallurgy. This means that the powder sintering methods (PM and SPS) give much more favourable properties. It could be that the solid state nature of these techniques eliminates or reduces the intermetalic compound formation at interfaces due to the lower temperature used (550 ˚C in both cases,which was even less than that has been reported by Natishan & Morrish [249] (600 ˚C), compared to 780˚C in GI). The higher temperature may give enough energy to form intermetallic compounds at interfaces, and at the same time it may result in oxidation or graphitisation of the diamond structure in the interfacial area. The short time of the SPS process in comparison with the powder sintering methods may also have a similar effect. The promotion of wear properties in the powder sintering composites may also be related to enhanced tensile properties for the products that were manufactured with such techniques; Natishan & Morrish achived an elastic modulus of 97.7 GPa for AMCs reinforced with only 20 vol.% of diamond, processed under 600 ˚C for half an hour [249].

10.2 Wear Behavior of Transition Metals as Matrices in MMDCs

Generally, the study of transition metals as matrices was motivated by the idea that the transition metals having different tendencies for the formation of carbides would induce different behavior with the diamond. Three elements were considered according to their reactivity toward carbon from high to low (Ti, Ni, and Cu) as was discussed in more detail in the last chapter (chapter 9). As well as the evident differences in mechanical behavior of the matrices, this variation in reactivity toward carbon has an impact on interfacial bonding between diamond and matrix, and consequently this leads to a variety of effects in the wear behavior of these matrices. Again, like AMDCs, the wear test results of transition metal-diamond composites, in addition to histogram figures (9-1) and (9-2)) in Chapter 9, are summarised in three separate tables (Table (10-2 A, B and C). These tables are constructed for the three wear criteria, wheel wear, sample wear, and relative wear. The wear values have been arranged depending on these criteria in to three categories to show the trend of wear toward low wear properties of the composite materials in the three different criteria.

Table (10-2): Different criteria (wheel, sample and relative wear) to show wear behavior of composites in either ascending or descending order of transition metal matrices with diamond reinforcement.

A

Descending order

Composite	Wheel Wear (mm^3/Sec)
Ti SPS	1454.4
Ni SPS	1137
Cu SPS	1000
Ti PM	309
Ni PM	296
Cu PM	121.3
Ti- Al_2O_3	60.3
Ti-SiC	40

÷

B

Ascending order

Composite	Sample Wear (mm^3/Sec)
Cu PM	0.09
Ni PM	0.162
Ti PM	0.38
Ni SPS	0.49
Cu SPS	0.6
Ti-SiC	1.1
Ti- Al_2O_3	3.9
Ti SPS	5.1

=

C

Descending order

Composite	Relative Wear (wheel/sample)
Ni SPS	2320
Ni PM	1827
Cu SPS	1667
Cu PM	1348
Ti PM	813
Ti SPS	285
Ti-SiC	36
Ti-Al_2O_3	15

Table (10-2 A and B) display the results of wear rate for wheel and composite, respectively. A high rate of wheel wear is considered to be an indication of how effectively the cutting composites attack the wheel abrasively. According to this criterion Table (10-2 A) (wheel wear rate) the SPS Ti composite causes the highest wear rate of the wheel, which means it was the most effective composite against abrasive cutting by abrasively attacking the wheel. On the other hand, in Table (10-2 B) with the sample wear criterion shows a totally different situation, where the wear rate of this sample was highest, based on wear values (at the bottom of the table), which means the penetration of the wheel into the samples was very high and the resistance of the sample to abrasive wear was lower than other composites. At this point, where the two criteria conflict, the logical interpretation is that the high penetration of wheel into the sample was the main cause of the high wear rate for the wheel due to rapid renewal of cutting edges, quickly generated during progress of the wheel through the composite. This concept partially agrees with Levashov et al. [250] who compared Co-WC with diamond composite tools, and concluded that the number of active cutting edges of diamond would be determined by the proportion of the wear rate of diamond particles and matrix, leading to an increased number of cutting edges when the matrix is worn faster [250]. Consequently, those two criteria become invalid for interpretation of the grinding behavior, at least in this type of grinding configuration, although they may be useful in other kinds of applications like gears or brake discs to find surface couples with greater lifetimes which cannot be abrasively attacked by each other. Therefore, the relative wear criterion is more accurate in this situation (especially in the grinding process) because it combines the wear of both surfaces in a proportional measurement. Additionally, this criterion has been employed by many researchers like tribologists in the Commonwealth Scientific and Industrial Research Organisation (CSIRO) in Australia, to study wear behavior of composites formed from 80% diamond with 20% Si for cutting elements, although mass loss was used for measuring wear behavior [100]. There are many reasons for the reduced abrasive wear resistance of Ti-diamond composites. Firstly, and most significantly, is the high range of processing temperature (950°C) which may affect the diamond structure [209], causing graphitization and oxidation of diamond. The wear mechanisms which occurred during abrasive cutting, were investigated by SEM imaging for the cutting surface. This SEM imaging, Figure (9-9) and Figure (9-10) pp. 197-198, reveals there are clear differences in wear mechanisms

appearing through the cutting process of SPS and PM composites. While the cutting surface of SPS composites shows the dominant mechanisms are fracture [149] and attrition wear, in addition to some pulling out of particles, in PM products the cutting surface under SEM shows that sliding wear (attrition) and cutting wear (abrasive) mechanisms were dominant, in addition to some fracture, probably due to the exposure of diamond to relatively high temperature [209], leading to weakness or graphitization, especially where Ti is in contact with diamond [209]. Ti is known as an element which encourages carbide formation, and carbide formation at the diamond surface in PM would allow the wheel to penetrate the diamond structure more easily by sliding or attrition wear rather than fracture of the diamond particles. The second reason is the weakness in interfacial bonding between diamond and the Ti matrix, due to the existence of some intermetallic compounds at interface, as shown by SEM, Figure (6-38) and Figure (6-39) pp. 129-130, and Raman spectroscopy, Figure (6-36) p. 128. These conclusions may be in agreement with other researchers, who studied Ti-diamond composites such as [251]–[253], and applied an even higher range of temperature; these thermal effects would be more limited in the present case, but may still caused some reduction in wear properties. In comparison, Ni and Cu based composites both still have higher wear resistance (low wear rate) than Ti based composites in Table (10-2 B and C) according to the wear rate of composite samples criterion (table B) and the relative wear criterion (table C). The Ni base composite exhibited the best wear resistance by achieving lowest wear rate according to the sample wear criterion and highest relative wear according to the relative wear criterion. The enhancement in hardness of Ni base composites, combined with the more moderate processing temperature range (800°C), was one important factor leading to increased wear properties of Ni base composites in both techniques (PM and SPS). Generally, the relationship between hardness of materials and their wear enhancement is considered to be directly proportional and the hardness of Ni- diamond composites has been reported to be increased with diamond content by some authors, like Ogihara et al. [254], who reported that the hardness of Ni-diamond composites can be brought to 1000 HV with 50 vol.% of diamond reinforcement [254]. Despite the inactive or limited reactivity nature of Ni toward carbides formation, Michalski and Cymerman [102] found nickel carbide (Ni_3C) was formed at the interfaces of Ni_3Al/diamond composites when they used the Plus Plasma Sintering (PPS) technique for 5 min at 1000℃ to manufacture Ni_3Al and Ni_3Al/diamond

composites. In order to compare the hardness and observe the interfacial bonding phase they applied Ni and aluminium together to obtain Ni_3Al as a matrix during the process. The hardness of Ni_3Al-30% diamond composites was more than double the Ni_3Al hardness, being about 650 HV in comparison with 305 HV of Ni_3Al [102]. While in the current work the temperature was less than 1000℃, there is still the possibility of formation of undesirable compounds, especially in the SPS route due to the short time (10 mins), while the time for the PM route was relatively longer (1 hrs) at the same sintering temperature (800 °C). This processing temperature was lower than used by other researchers such as Twomey et al. [104] who also did similar comparative study of different manufacturing processes, tube furnace and rapid discharge plasma sintering (RDS) techniques. In both paths 80% Ni-20% diamond powder was compacted into 20mm diameter pellets in varied pressures 100, 200 and 300 MPa and sintered at two different temperatures (850 and 1000℃) under inert gas atmosphere to produce composites. The results showed that using RDS to manufacture Ni-diamond composites was better than using a furnace because the RDS samples, which had less graphitization of the diamond than furnace samples (even though an atmosphere of 3 to 1 H_2/N_2 was used in both techniques), lead to higher hardness and abrasive wear resistances, especially for 850 ℃ [104]. Mechnik [105] utilised same sintering temperature as the PM route of this study (800℃ for 1 hr), with a complex alloy as a matrix to produce cutting element metal-diamond composites; 51 vol.% of iron (Fe)–32 vol.% of copper (Cu)–9 vol.% nickel (Ni)–8 vol.% tin (Sn) combined with 35 vol.% of 302-455 μm diamond particles. The solid solution was found to contain iron, copper, $NiSn_3$ and Cu_9NiSn_3. This author also found that the graphitised surface of diamond reacted with α-Fe to form a 5-40 nm layer of Fe_3C, and they attributed wear resistance enhancement to the formation of this layer, hypothesising that it helps to prevent pull out of the diamond particles from the matrix during abrasion [105].

The low processing temperature (700°C) of Cu base composites contributed to improvement of wear properties, as this temperature is below the range of temperatures that cause graphitic transformation or oxidation of diamond [249]. The trend in for Cu base composites reinforced with diamond was higher than Ti-diamond composites in two wear criteria Table (10-2 B) and C except Table A, the wheel wear criterion, where more wheel wear was caused by cutting Ti composites than Cu composites. This low wear rate of wheels that cut Cu-diamond composites was probably as a result of the high thermal conductivity of Cu-diamond composites, which

helps to reduce the thermal effects on wear by dispersing the generated heat from the abrasive cutting interface quicker than other composites. Therefore, the wear behavior appears to show the effect of cutting speed and abrasive wear more clearly than before. In most previous samples the volume loss is affected by other factors, such as the heat generation at the contact surface, which increases wear rate, especially for the wheel, which will be most affected by this factor due to degradation of the resin bonding at elevated temperature Another reason for this behavior may be the very poor tendency of copper to react with carbon to create carbides. Consequently, there is a clean interface opposite to the matrices which have the ability to create carbides at the interface, where these compounds work as a barrier for heat dissipation if their thickness exceeds the desirable range (some microns) [81], [246]. Growth of these compounds during cutting, or even their existence at the interfaces after production, may reduce the heat dissipation from the system (wheel-sample cutting surface) and lead to an increase in wear. In matrices which are able to form carbides (Ti and Al), the three wear stages were either not distinct enough to be separated, or the steady state wear might dominate. Therefore, comparable wear behavior between the composites made by different processing methods (PM and SPS) depended on the steady state wear behavior (second stage of wear curves) because this stage is the longest and may be more representative for the relative wear of composite [117]. Additionally, apart from the wheel wear criterion shown in Table (10-2 A) the Cu-diamond composites, manufactured by both techniques (SPS) and (PM), were more resistant to abrasive cutting than Ti-diamond composites as shown in Table (10-2 B and C). Part of this enhancement in wear properties can be attributed to an expected improvement in tensile properties [90] and hardness [4], [106] of Cu reinforced by diamond as has been found by some authors, who studied these features of Cu-diamond composites such as [4], [90], [106]. In regard to Ti-ceramic composites the wear rate was higher in the wheels cutting Ti-Al_2O_3 composites than the wear rate in wheels that cut Ti-SiC, as shown in Table (10-2 A) (wheel wear rate criterion). By contrast, the wear rate in Ti-Al_2O_3 composites themselves was higher than Ti-SiC composites, as shown in Table (10-2 B). The latter behaviour is considered an indication of low wear resistance of Ti-Al_2O_3 composites in comparison with Ti-SiC composites, the rapid penetration of the wheel into alumina composites leads to continuous generation of new alumina cutting edges, and consequently leads to a high wheel wear rate, Table (10-2 A). The last criterion, which is relative wear criterion, is commonly used in

grinding processes. This criterion, which was more consistent with the second criterion in Table (10-2 B), also reveals that the Ti-SiC composites had higher wear resistance than Ti-Al_2O_3 composites (Ti-SiC composites having higher relative wear). These high wear resistance properties of Ti-SiC composites can be attributed to the nature of SiC reinforcement to form kind of glazing wear layer, which works as a solid lubricant layer for some time before elimination with continued cutting process in the Ti-SiC composites. This conclusion would be partially in agreement with other authors [138], [231]. However, both composites were insufficiently effective at resisting the abrasive wear caused by a single wheel cutting through the designed example barrier structure.

Chapter 11 Conclusions and Recommendations for Future Work

11.1 Conclusions

The main goal of this research was developing a new composite material reinforced with diamond for security barrier applications against abrasive cutting. Through developing this material many problems were encountered; apart from the processing difficulties, one of the crucial issues was the capability of testing these extremely hard materials with standard conventional ways of testing engineering materials. That led to the creation of a novel device, which can be used to make a measurable wear impression in the MMDCs, from which can be found the relative wear of the composites (wheel/composite), which is considered to be our criterion of comparison. However, the fabrication composites and assessing their wear performance came through many steps, from which can be drawn conclusions of this study in different aspects. The following conclusions can be detailed from the performed study:

- The metal-diamond composites are more challenging than most other composite materials for selection of a manufacturing method, due to the unique reactivity of the diamond structure under typical manufacturing conditions such as high temperature and reactive atmosphere. Therefore, a gas pressure infiltration process was chosen to produce aluminium-diamond composites with a volume fraction about 50-55 vol. % of different diamond particle sizes and surface conditions (coated/uncoated), seeking to achieve the best abrasion resistance of the composites.
- The results have shown that the bonding between matrix and diamond reinforcement was better in composites that are reinforced with coated Ti diamond particles than those with uncoated diamond.
- The abrasion resistance of composites tended to increase with increasing particle size of diamond reinforcement for both groups (coated/uncoated). In addition to this, the composites that are reinforced with coated Ti of diamond particles showed better abrasion resistance than those that were reinforced with uncoated. Therefore,

the choice of reinforcement was the largest particle size of coated diamond for manufacturing the remaining of composites with other matrices (Sn, Ti, Ni, Cu and epoxy).

- Choosing other types of ceramic reinforcement such as SiC and Al_2O_3 from an economic perspective may reduce the cost of MMDCs while achieving the purpose that the composites were produced for.
- Metal matrices, either Ti or Al, reinforced by ceramic reinforcement (SiC and Al_2O_3) showed higher relative wear than pure metal matrices, but are still insufficient to prevent cutting of the 8 mm diameter sample by a single abrasive wheel.
- The AMCCs loaded with 20 vol. % of diamond were sufficient to prevent a single cut-off wheel cutting through the chosen thickness (8 mm).
- Choosing matrices with low melting point, such as epoxy and tin for MMDCs were insufficient to resist the abrasive cutting of the chosen sample thickness.
- The conventional PM by sintering under argon atmosphere and SPS was chosen to produce other composites with different high melting point matrices (Ti, Ni, Cu), seeking to achieve the best abrasion resistance of the metal- diamond composites.
- The high processing temperature encourages formation of intermetallic compound at interfaces and may affect on the diamond structure and properties. Some of these compounds and diamond structure effects were indicated with using XRD, SEM, EDX, and Raman spectra microscope. This was especially the case, at diamond-matrix interfaces.
- The wear behaviour of composites is affected by the processing temperature and the nature of the matrix whether it encourages carbide formation or not, more than its effects on the hardness of the matrix, which may be considered the main crucial property determining the wear properties of metals and alloy. This can be seen from the Ti composite having lower relative wear than Ni and Cu composites even though the Ti matrix has higher hardness and the SPS products of the transition metal matrix- diamond composites achieve higher relative wear than those produced by PM route, due to elimination of the interfacial compounds in SPS route compared to PM.
- In regard to the wear properties of transition metal- diamond composites, the highest relative wear was obtained by Ni reinforced with diamond followed by Cu

and then Ti composites. Different wear mechanisms have been seen in cutting these composites such as fracture wear, attrition wear and cutting wear mechanisms. The fracture wear mechanism was the most dominant in cutting Ni-diamond composites rather than other mechanisms.

- Finally, from the cost point of view, it can be said that the MMCs loaded with 20 vol. % diamond would be suitable for security barriers, with a likely acceptable increment in cost for some applications; compared to the commercial product the cost rise would be between 3.3-5.2% for both case study examples. Even if greater protection were needed, for the same aluminum matrix reinforced with 50 vol. % diamond the cost would only increase to about 7.9-12.1% over the commercial products in both case study examples.

Another novel approach of this research was the application of a mathematical-volumetric model to study and assess the wear behaviour of MMDCs and it may can be applied for assessing other extremely hard materials. This model was simplified according to the cumulative volume loss concept, which is considered more reliable than weight loss in tribological studies, and it is applied here in comparative study of different composites in order to achieve as accurate as possible wear data and eliminate the error effects on the wear results. A simple linear predictive approach was applied for estimation of wear behaviour of comparable MMCs under the same test conditions. Therefore, this model is still in the early stage of development to broadly apply to other materials rather than composites and it needs more analysis testing and validation. Some suggestions will be made in the next section (future work) to improve MMDCs for other applications.

11.2 Recommendations for future work

Developing MMDCs and studying the abrasive wear behaviour of these materials in order to optimize their performance against abrasive cutting would not be the only potential use of these extraordinary materials. There are wide potential applications, such as semiconductor and thermal management applications, due to their high thermal conductivity. Therefore, it is worth to study the thermal properties of these composites and optimize their properties by control of the structure and volume fraction reinforcement. At this point, when there will be sufficient thermal and tribological data is available about these composites, another aspect, which could be studied, is linking between thermal properties and tribological properties and explore any effect of use at high temperature on wear behaviour.

Moreover, tungsten carbide (WC), which can be a good candidate for abrasion resistant applications, could be studied as a reinforcement in future work, and compared with the ceramic reinforcement applied in this study. This could be combined with some volume fraction of diamond and different matrices to enhance wear properties of the composite as well.

Extra work may offer further supporting information on the mechanisms of abrasive wear in MMDCs to further understand the effects of other processing and structural factors on the effectiveness of the composites. In a security application the nature of the method by which a lock may be cut cannot be predicted. Even though, the angle grinder cutter is the currently most commonly used for these purposes, other relevant mechanical properties of the composites may be assessed. Additionally, the possible interfacial reactions between diamond and molten metal can be investigated in more details to see if there are any preferable diamond crystal planes for interfacial reactions with molten metal. That means additional micro-mechanical tests and structure investigations may be required to improve strategies and find other possible applications of these composites, apart from security applications.

References

[1] C. Zweben, “Advanced Composites And Other Advanced Materials For Electronic Packaging Thermal Management,” Int. Symp. Adv. Packag. Mater., vol. 324, pp. 222–287, 2001.

[2] M. Caccia, A. Rodríguez, and J. Narciso, “Diamond surface modification to enhance interfacial thermal conductivity in Al/diamond composites,” Jom, vol. 66, no. 6, pp. 920–925, 2014.

[3] “Super Abrasives - EPoS.” [Online]. Available: http://www.eposintering.com/materials/super-abrasives-2/. [Accessed: 02-Jan-2019].

[4] J. B. Correia, V. Livramento, N. Shohoji, E. Tresso, and K. Yamamoto, “Bulk Copper-nanodiamond Nanocomposites ; Processing and Properties,” vol. 588, pp. 443–447, 2008.

[5] “Angle grinder gang thefts: Damage put at £109k caused - BBC News,” BBC News, 2014. [Online]. Available: https://www.bbc.co.uk/news/uk-england-london-27778727. [Accessed: 18-Jul-2018].

[6] C. Moore, “CCTV video captures Sicilian thieves cutting open ATM | Daily Mail Online,” Daily Mail, 2016. [Online]. Available: http://www.dailymail.co.uk/news/article-3577940/Shocking-moment-Sicilian-thieves-attempt-cut-open-petrol-station-ATM-angle-grinder-sending-sparks-flying-nearby-fuel-pump.html. [Accessed: 18-Jul-2018].

[7] D. Owen, “Thieves use angle grinder to try and steal cash from Castle Donington ATM - Leicestershire Live,” leicestershire live, 2018. [Online]. Available: https://www.leicestermercury.co.uk/news/leicester-news/thieves-use-angle-grinder-try-1599072#comments-section. [Accessed: 18-Jul-2018].

[8] B. Vonow, “Moped thieves release shocking videos showing them using angle grinders to steal bikes as they terrorise London streets,” thesun, 2017. [Online]. Available: https://www.thesun.co.uk/news/4204893/london-moped-thieves-video-angle-grinder/. [Accessed: 18-Jul-2018].

[9] A. K. Kaw, Mechanics of Composite Materials, S econd Ed. US: Taylor & Francis Group, LLC, 2006.

[10] S. V Hoa, Principles of the Manufacturing of Composite Materials. Lancaster, Pennsylvania 17602 U.S.A.: DEStech Publications, Inc., 2009.

[11] O. Ridge, Materials Science and Technology Teachers Handbook. Pacific Northwest National Laboratory, U S A, 2008.

[12] N. Prasad, "Development and Charactrization of Melal Matrix Composite Using Red Mud an Industrial Waste for Wear Resistant Applications," PhD Thesis, National Institute of Technology Rourkela - India, 2006.

[13] P. Mishra, "Development and Characterization of Low Cost Composite from Sugarcane Bagasse Waste," PhD Thesis, National Institute of Technology Rourkela - India, 2011.

[14] B. S. Mitchell, Materials Engineering and Science an Introduction To Materials Engineering and Science for Chemical and Materials Engineers. 2003.

[15] J. Hashim, "The Production of Metal Matrix Composites Using The Stir Casting Technique," PhD thesis, School of Mechanical and Manufacturing Engineering, Dublin City University- Ireland, 1999.

[16] A. N. Guz' and G. V. Guz', "Mechanics of composite materials with large-scale curving of filler," Mechanics of Composite Materials, vol. 18. pp. 434–439, 1983.

[17] M. Balasubramanian, "Introduction to Composites," in Composite Materials and Processing, 2014, pp. 1–16.

[18] F. C. Campbell, "Introduction to Composite Materials Science," ASM Int., vol. 68, pp. 331–332, 2010.

[19] B. Harris, "Engineering composite materials," Inst. Mater. London, vol. 18, p. 261, 1999.

[20] C. Cayron and Lausanne, "TEM study of interfacial reactions and precipitation mechanisms in Al_2O_3 short fiber or high volume fraction SiC particle reinforced Al-4Cu-1Mg-0.5Ag squeeze-cast composites," PhD Thesis, Materials technology, Ingénieur Civil diplômé de l'Ecole des Mines de Nancy originaire de Dijon

(France), 2000.

[21] H. Mil, Composite materials handbook- Metal matrix composites., vol. 4, no. 33, Arizona, USA, 2002.

[22] D. B. Miracle, “Metal matrix composites - From science to technological significance,” Compos. Sci. Technol., vol. 65, no. 15–16 SPEC. ISS., pp. 2526–2540, 2005.

[23] A. Macke, B. F. Schultz, and P. Rohatgi, “Metal matrix: Composites offer the automotive industry an opportunity to reduce vehicle weight, improve performance,” Adv. Mater. Process., vol. 170, pp. 19–23, 2012.

[24] K. U. Kainer, Basics of Metal Matrix Composites., Elsevier, 2006.

[25] S. Durante, G. Rutelli, and F. Rabezzana, “Aluminum-based MMC machining with diamond-coated cutting tools,” Surf. Coatings Technol., vol. 94–95, pp. 632–640, 1997.

[26] M. E. Shamekh, “Processing and Characterization of Mg Matrix Composites Reinforced with TiC and TiB_2 Phases using an In-situ Reactive Infiltration Technique,” PhD Thesis, Mechanical and Industrial Engineering Presented,Concordia University Montreal, Quebec, Canada, 2011.

[27] Y. Wu, “Fabrication of metal matrix composite by semi- solid powder processing,” PhD Thesis, Mechanical Engineering, Lowa State University, 2011.

[28] Z. Y. Xiu, X. Wang, M. Hussain, C. Feng, and L. T. Jiang, “Effect of heat treatment on microstructure and thermophysical properties of diamond/2024 Al composites,” Trans. Nonferrous Met. Soc. China (English Ed., vol. 23, no. 12, pp. 3584–3591, 2013.

[29] D. Muscat and R. A. L. Drew, “Infiltration Kinetics of Aluminium in Titanium Carbide Preforms,” in Conf. High Temperature Capillarity, Venice, July 1997.

[30] K. K. Chawla and N. Chawla, “Metal-Matrix Composites,” (University of Alabama at Birmingham and Arizona State University, 2004.

[31] B. Pulkit, “Mechanical Behaviour of Aluminium Based Metal Matrix Composites Reinforced with SiC and Alumina,” 2011.

[32] M. Lee, M. Fu, J. Wu, C. Chung, and S. Lin, “Diamond & Related Materials Thermal properties of diamond / Ag composites fabricated by eletroless silver plating ☆,” Diam. Relat. Mater., vol. 20, no. 2, pp. 130–133, 2010.

[33] F. A. Khalid, O. Beffort, U. E. Klotz, B. A. Keller, and P. Gasser, “Microstructure and interfacial characteristics of aluminium-diamond composite materials,” Diam. Relat. Mater., vol. 13, pp. 393–400, 2004.

[34] B. Huchler, “Pressure Infiltration Behaviour and Properties of Aluminium Alloy - Oxide Ceramic Preform Composites by Bernd Arthur Huchler,” PhD Thesis, School of Metallurgy and Materials , University of Birmingham, 2009.

[35] K. C. Russell, S. Oh, and A. Figueredo, “Theoretical and Expérimental Studies of Ceramic : Metal Wetting,” pp. 46–52, 2000.

[36] A. Mortensen and I. Jin, “Solidification processing of metal matrix composites,” Int. Mater. -Reviews, vol. 37, no. 3, 1992.

[37] G. S. Rohrer, “Introduction to Grains, Phases, and Interfaces—an Interpretation of Microstructure,” Trans. AIME, 1948, vol. 175, pp. 15–51, by C.S. Smith, vol. 41, no. May. 2010.

[38] A. K. T. Hartaj Singh, Sarabjit, Nrip Jit, “An Overview of Metal Matrix Composite : Processing and Sic Based Mechanical,” J. Eng. Res. Stud., vol. II, no. 4, pp. 72–78, 2011.

[39] M. K. Surappa, “Aluminium matrix composites: Challenges and opportunities,” Sadhana - Acad. Proc. Eng. Sci., vol. 28, no. 1–2, pp. 319–334, 2003.

[40] D. J. Lloyd, “Particle reinforced aluminium and magnesium matrix composites,” Int. Mater. Rev., vol. 39, no. 1, pp. 1–23, 1994.

[41] T. North and A. Defense, “Technology Base Enhancement Program Metal Matrix Composites,” Organization, 1993.

[42] B. C. Giessen, “Constitution of Non-Equilibrium Alloys after Rapid Quenching from the Melt,” in Developments in the Structural Chemistry of Alloy Phases, Boston, MA: Springer US, 1969, pp. 227–281.

[43] K. Chu, Z. Liu, C. Jia, H. Chen, X. Liang, W. Gao, W. Tian, and H. Guo, “Thermal

conductivity of SPS consolidated Cu/diamond composites with Cr-coated diamond particles," J. Alloys Compd., vol. 490, pp. 453–458, 2010.

[44] U. Department of Defense, "Ceramic Matrix Composites - Vol 5," Compos. Mater. Handb. -, vol. 5, no. June, p. 260, 2002.

[45] S. N. Trinh and S. Sastry, "Processing and Properties of Metal Matrix Composites," 2016.

[46] K. H. Habig, "Chemical vapor deposition and physical vapor deposition coatings: Properties, tribological behavior, and applications," J. Vac. Sci. Technol. A Vacuum, Surfaces, Film., vol. 4, no. 6, pp. 2832–2843, Nov. 1986.

[47] K. Sudipt, "Metal Matrix Composite Production and Characterisation of Aluminium-Fly Ash Composite Using Stir Casting Method Production and Characterisation of Aluminium-Fly Ash Composite Using Stir Casting Method," Bachelor of Technology In Metallurgical & Materials Engineering,National Institute of Technology, India, 2008.

[48] J. Llorca and C. González, "Microstructural factors controlling the strength and ductility of particle-reinforced metal-matrix composites," J. Mech. Phys. Solids, vol. 46, no. I, pp. 1–28, 1998.

[49] J. D. Eshelby, "The Determination of the Elastic Field of an Ellipsoidal Inclusion, and Related Problems," Proc. R. Soc. A Math. Phys. Eng. Sci., vol. 241, no. 1226, pp. 376–396, 1957.

[50] J. D. Eshelby, "The elastic field outside an ellipsoidal inclusion," Peoceedings R. Soc. London. Ser. A, Math. Phys. Sci., vol. 252, no. 1271, pp. 561–569, 1959.

[51] J. C. Halpin and J. . Kardos, "The Halpin-Tsai equations: A review," Polym. Eng. Sci., vol. 16, no. 5, pp. 344–352, 1976.

[52] I. A. Ibrahim, F. A. Mohamed, E. J. Lavernia, M. K. Surappa, J. Llorca, and C. González, "Particulate reinforced metal matrix composites - a review," J. Mater. Sci., vol. 26, no. 5, pp. 1137–1156, 1991.

[53] Q. Meng and Z. Wang, "Prediction of interfacial strength and failure mechanisms in particle-reinforced metal-matrix composites based on a micromechanical model," Eng. Fract. Mech., vol. 142, pp. 170–183, 2015.

[54] N. Kanetake, M. Nomura, and T. Choh, “Continuous observation of microstructural degradation during tensile loading of particle reinforced aluminium matrix composites,” Mater. Sci. Technol., vol. 11, no. 12, pp. 1246–1252, Dec. 1995.

[55] L. Babout, E. Maire, J. Y. Buffière, and R. Fougères, “Characterization by X-ray computed tomography of decohesion, porosity growth and coalescence in model metal matrix composites,” Acta Mater., vol. 49, no. 11, pp. 2055–2063, 2001.

[56] Y. Su, Q. Ouyang, W. Zhang, Z. Li, Q. Guo, G. Fan, and D. Zhang, “Materials Science & Engineering A Composite structure modeling and mechanical behavior of particle reinforced metal matrix composites,” Mater. Sci. Eng. A, vol. 597, pp. 359–369, 2014.

[57] D. S. Dugdale, “Yielding of steel sheets containing slits,” J. Mech. Phys. Solids, vol. 8, no. 2, pp. 100–104, 1960.

[58] Y. N. Li and A. P. Hong, “Prediction of failure in notched infinite strips by the cohesive crack model,” Int. J. Solids Struct., vol. 29, no. 23, pp. 2815–2828, 1992.

[59] L. Babout, Y. Brechet, E. Maire, and R. Fougères, “On the competition between particle fracture and particle decohesion in metal matrix composites,” Acta Mater., vol. 52, no. 15, pp. 4517–4525, 2004.

[60] D. Margaritis, “Interfacial Bonding in Metal-Matrix Composites Reinforced Diamonds with Metal-Coated,” PhD Thesis, University of Nottingham, 2002.

[61] M. A. Prelas, A. Benedictus, L.-T. S. Lin, G. Popovici, and P. Gielisse, Diamond Based Composites and Related Materials. Dordrecht / Boston / London: Kluwer Academic Publishers-Published in cooperation with NATO Scientific Affairs Division, 1997.

[62] Bain and Company, “The Global Diamond Industry,” World Diam. Cent. Priv. Found., p. 82, 2011.

[63] C. M. Breeding and J. E. Shigley, “The ‘type’ classificantion system of diamonds and its importance in geology,” Gems Gemol., vol. 45, no. 2, pp. 96–111, 2009.

[64] S. Ferber, “Synthetic diamonds and identification,” Gemol. Cent. INC (I. G. C), 1954.

[65] T. Hainschwang and F. Notari, “The Challenge of Identifying Recent Generations of Melee-Sized Synthetic Diamonds,” Gemol. Work. Univ. Geneva, 2014.

[66] H. Chen, C. Jia, and S. Li, “Interfacial characterization and thermal conductivity of diamond/Cu composites prepared by two HPHT techniques,” J. Mater. Sci., vol. 47, pp. 3367–3375, 2012.

[67] J. Flaquer, A. Ríos, A. Martín-Meizoso, S. Nogales, and H. Böhm, “Effect of diamond shapes and associated thermal boundary resistance on thermal conductivity of diamond-based composites,” Comput. Mater. Sci., vol. 41, no. 2, pp. 156–163, 2007.

[68] A. M. Abyzov, S. V. Kidalov, and F. M. Shakhov, “High thermal conductivity composites consisting of diamond filler with tungsten coating and copper (silver) matrix,” J. Mater. Sci., vol. 46, pp. 1424–1438, 2011.

[69] K. Chu, C. Jia, X. Liang, H. Chen, W. Gao, and H. Guo, “Modeling the thermal conductivity of diamond reinforced aluminium matrix composites with inhomogeneous interfacial conductance,” Mater. Des., vol. 30, no. 10, pp. 4311–4316, 2009.

[70] M. Seal, “Thermal and Optical Applications of Thin Film Diamond,” Philos. Trans. R. Soc. A Math. Phys. Eng. Sci., vol. 342, no. 1664, pp. 313–322, 1993.

[71] S. V. Kidalov and F. M. Shakhov, “Thermal conductivity of diamond composites,” Materials (Basel)., vol. 2, pp. 2467–2495, 2009.

[72] Y. Zhang, H. L. Zhang, J. H. Wu, and X. T. Wang, “Enhanced thermal conductivity in copper matrix composites reinforced with titanium-coated diamond particles,” Scr. Mater., vol. 65, no. 12, pp. 1097–1100, 2011.

[73] P. Man’kowski, A. Dominiak, R. Domansk, M. J. Kruszewski, and Lu. Ciupinski, “Thermal conductivity enhancement of copper-diamond composites by sintering with chromium additive,” J. Therm. Anal. Calorim., pp. 1–5, 2014.

[74] Z. A. Hamid, “Fabrication and characterization copper/diamond composites for heat sink application using powder metallurgy,” Nat. Sci., vol. 03, no. 11, pp. 936–947, 2011.

[75] J. W. Zimmer and G. Chandler, “Challenges in Matching Die to Package CTE’s for

High Thermal Flux Devices," 2008.

[76] R. B. Robert and N. S. Sussmann, "Diamond composite heat sink for use with semiconductor devices," United States Pat., vol. 255259, pp. 423–446, 1991.

[77] M. Schöbel, H. P. Degischer, S. Vaucher, M. Hofmann, and P. Cloetens, "Reinforcement architectures and thermal fatigue in diamond particle-reinforced aluminum," Acta Mater., vol. 58, pp. 6421–6430, 2010.

[78] Peroni. L, "Investigation of the Mechanical Behaviour of Metal Diamond Composites," in Composites, 2013, vol., no. ECCM15–15th European Conference on Composite Materials, Venice, Italy, 24–28 June 2012, p. .

[79] K. W. A. B. Spierings, C. Leinenbach, C. Kenel, "Processing of metal-diamond-composites using selective laser melting," Review Paper, 2014.

[80] C. Y. Chung, M. T. Lee, M. Y. Tsai, C. H. Chu, and S. J. Lin, "High thermal conductive diamond/Cu-Ti composites fabricated by pressureless sintering technique," Appl. Therm. Eng., vol. 69, no. 1–2, pp. 208–213, 2014.

[81] S. Ren, X. Shen, C. Guo, N. Liu, J. Zang, X. He, and X. Qu, "Effect of coating on the microstructure and thermal conductivities of diamond-Cu composites prepared by powder metallurgy," Compos. Sci. Technol., vol. 71, no. 13, pp. 1550–1555, 2011.

[82] Y. Xia, Y. Q. Song, C. G. Lin, S. Cui, and Z. Z. Fang, "Effect of carbide formers on microstructure and thermal conductivity of diamond-Cu composites for heat sink materials," Trans. Nonferrous Met. Soc. China (English Ed., vol. 19, no. 82129, pp. 1161–1166, 2009.

[83] M. T. Lee, C. Y. Chung, S. C. Yen, C. L. Lu, and S. J. Lin, "High thermal conductive diamond/Ag-Ti composites fabricated by low-cost cold pressing and vacuum liquid sintering techniques," Diam. Relat. Mater., vol. 44, pp. 95–99, 2014.

[84] Z. Yupeng, Y. Jianglong, L. Ziyi, X. Lei, C. Hexing, and D. Mingjiang, "Structural View Study on Diamond and Copper Bonding with AlNi Micro/nano Multilayers," Rare Met. Mater. Eng., vol. 43, no. 11, pp. 2597–2601, 2014.

[85] W. A. Ferrando, A. Va., J. B. Clark, and E. City, "Dimond/silver composites," United States Am. as Represent. by Secr. Navy, Washington, DC., no. 105,324,

1994.

[86] L. Weber and R. Tavangar, “Diamond-Based Metal Matrix Composites for Thermal Management Made by Liquid Metal Infiltration — Potential and Limits,” Adv. Mater. Res., vol. 59, no. January, pp. 111–115, 2009.

[87] R. R. Scott, D. Jesso, and W. Jordan, “Heat Sink for Dental Curing Light Composing a Plurality of Different Materials,” United States Pat. Trademark, vol. 2, no. 12, 2006.

[88] R. Tavangar, J. M. Molina, and L. Weber, “Assessing predictive schemes for thermal conductivity against diamond-reinforced silver matrix composites at intermediate phase contrast,” Scr. Mater., vol. 56, pp. 357–360, 2007.

[89] K. Mizuuchi, K. Inoue, Y. Agari, M. Sugioka, M. Tanaka, T. Takeuchi, M. Kawahara, Y. Makino, and M. Ito, “Composites : Part B Processing of diamond-particle-dispersed silver-matrix composites in solid – liquid co-existent state by SPS and their thermal conductivity,” Compos. Part B, vol. 43, no. 3, pp. 1445–1452, 2012.

[90] K. A. Weidenmann, R. Tavangar, and L. Weber, “Mechanical behaviour of diamond reinforced metals,” Mater. Sci. Eng. A, vol. 523, no. 1–2, pp. 226–234, 2009.

[91] S. R. Holloway and N. S. Paul, “Aluminum Composite for Gun Barrels,” United States Pat., vol. 1, no. 12, 2002.

[92] E. C. Supan, J. F. Dolowy, Jr., and B. A. Webb, “High thermal conductivity metal matrix composite,” United States Pat. Trademark, no. 19, pp. 2–5, 1992.

[93] P. W. Ruch, O. Beffort, S. Kleiner, L. Weber, and P. J. Uggowitzer, “Selective interfacial bonding in Al(Si)-diamond composites and its effect on thermal conductivity,” Compos. Sci. Technol., vol. 66, pp. 2677–2685, 2006.

[94] I. E. Monje, E. Louis, and J. M. Molina, “Aluminum/diamond composites: A preparative method to characterize reactivity and selectivity at the interface,” Scr. Mater., vol. 66, no. 10, pp. 789–792, 2012.

[95] I. E. Monje, E. Louis, and J. M. Molina, “Optimizing thermal conductivity in gas-pressure infiltrated aluminum/diamond composites by precise processing control,”

Compos. Part A Appl. Sci. Manuf., vol. 48, pp. 9–14, 2013.

[96] Z. Tan, Z. Li, D. B. Xiong, G. Fan, G. Ji, and D. Zhang, "A predictive model for interfacial thermal conductance in surface metallized diamond aluminum matrix composites," Mater. Des., vol. 55, pp. 257–262, 2014.

[97] C. Millière and M. Suéry, "Fabrication and properties of metal matrix composites based on SiC fibre reinforced aluminium alloys," Mater. Sci. Technol., vol. 4, no. 1, pp. 41–51, 1988.

[98] ASM International Handbook prepared under the direction of Committee' H. baker, H. Okamoto, S. D. Henry, G. M. Davidson, M. A. Fleming, L. Kacprzak, H. F. Lampman, William W. Scott Jr. and Robert C. Uhl,' Volume editors, Schlesinger, Mark E., Okamoto and Hiroaki '' alloys phase diagrams'', vol. 3, Materials Park, Ohio, ASM International, 1992.

[99] Y. Kimura, "Composite materials review," J. Mater. Sci., vol. 19, p. 3107, 1984.

[100] J. N. Boland and X. S. Li, "Microstructural characterisation and wear behaviour of diamond composite materials," Materials (Basel)., vol. 3, no. 2, pp. 1390–1419, 2010.

[101] P. Larsson, N. Axén, T. Ekström, S. Gordeev, and S. Hogmark, "Wear of a new type of diamond composite," Int. J. Refract. Met. Hard Mater., vol. 17, no. 6, pp. 453–460, 1999.

[102] A. Michalski and K. Cymerman, "Ni_3Al/diamond composites produced by pulse plasma sintering (PPS) with the participation of the SHS reaction," J. Alloys Compd., vol. 636, pp. 196–201, 2015.

[103] L. Wang, Y. Gao, Q. Xue, H. Liu, and T. Xu, "Effects of nano-diamond particles on the structure and tribological property of Ni-matrix nanocomposite coatings," Mater. Sci. Eng. A, vol. 390, pp. 313–318, 2005.

[104] B. Twomey, A. Breen, G. Byrne, A. Hynes, and D. P. Dowling, "Rapid discharge sintering of nickel-diamond metal matrix composites," J. Mater. Process. Technol., vol. 211, no. 7, pp. 1210–1216, 2011.

[105] V. A. Mechnik, "Production of Diamond -(Fe - Cu - Ni - Sn)," Mterals Process., vol. 52, no. 9, pp. 577–587, 2014.

[106] D. Nunes, V. Livramento, J. B. Correia, K. Hanada, P. A. Carvalho, R. Mateus, N. Shohoji, H. Fernandes, C. Silva, E. Alves, and E. Osawa, "Consolidation of Cu-nDiamond Nanocomposites: Hot Extrusion vs Spark Plasma Sintering," Mater. Sci. Forum, vol. 636–637, pp. 682–687, 2010.

[107] I. V Rigou, G. Mărginean, D. Frunzăverde, and C. V Câmpian, "The effect of diamond particle size on the wear resistance of silver / diamond electroplated dispersion coatings," pp. 219–222.

[108] B. Wielage and A. Dorner, "Bonding and sliding wear behavior of diamond-like carbon coatings on fiber reinforced aluminum," Surf. Coatings Technol., vol. 108–109, pp. 473–478, 1998.

[109] J. Sugishita, N. Kawabata, and K. Kumamoto, "Grinding performance of an aluminium- bonded diamond wheel on ceramics and glass," pp. 184–188, 1991.

[110] K. Holmberg and A. Mathews, "Coatings tribology: a concept, critical aspects and future directions," Thin Solid Films, vol. 253, no. 1–2, pp. 173–178, 1994.

[111] ASM International Handbook prepared under the direction of Committee; 'Peter J. Blau, Oak Ridge, William P. Koster and Edward L. Langer', Volume editors, Totten, George E., Sally Fahrenholz-Mann, Bonnie Sanders, Scott Henry, Grace Davidson, Randall Boring, Robert Braddock, Kathleen Dragolich, and Audra Scott '' Friction, Lubrication, and Wear Technology", vol. 18, Materials Park, Ohio, ASM International, 1992.

[112] J. F. Archard, "Contact and rubbing of flat surfaces," J. Appl. Phys., vol. 24, no. 8, pp. 981–988, 1953.

[113] J. M. Thompson and M. K. Thompson, "A Proposal for the Calculation of Wear Mechanisms of Wear," Int. ANSYS Conf., pp. 1–14, 2002.

[114] W. Wood, "Processing, wear and mechanical properties of polyethylene composites prepared with pristine and orgaosilane-treated carbon nanofibers," PhD Thesis, School of Mechanical and Materials Engineering, Washington State University, 2012.

[115] C. S. Abreu, "Tribological Properties of CVD Diamond Coated Ceramic Surfaces," PhD Thesis-University of Minho, 2008.

[116] A. Zmitrowicz, “Wear Patterns and Laws of Wear – a Review,” J. Theor. Appl. Mech., vol. 44, no. 1803, pp. 219–253, 2006.

[117] S. M. Nahvi, “Abrasive Wear Behaviour of Steels and Advanced HVOF-Sprayed WC-M Coatings,” The University of Nottingham, 2011.

[118] A. Abdullah, “Machining Of Aluminium Based Metal Matrix Composite (MMC),” PhD Thesis, University of Warwick, 1996.

[119] A. Ersoy and U. Atici, “Wear characteristics of circular diamond saws in the cutting of different hard abrasive rocks,” Diam. Relat. Mater., vol. 13, no. 1, pp. 22–37, 2004.

[120] M. Farrow, “Selecting Wear Resistant Surface Treatments: with Particular Reference to Ion-Plated TiN,” in 13th International Conference on Metallurgical Coatings, 1986.

[121] T. S. Eyre, “The mechanisms of wear,” Tribol. Int., vol. 11, no. 2, pp. 91–96, 1978.

[122] M. Farrow and C. Gleave, “Wear resistant coatings,” Trans. IMF, vol. 62, no. 1, pp. 74–80, Jan. 1984.

[123] K. Kato and K. Adachi, “Wear Mechanisms,” in Modern Tribology Handbook. Vol 1, CRC Press LLC, 2001, p. 28.

[124] M. Varenberg, “Towards a unified classification of wear,” Friction, vol. 1, no. 4, pp. 333–340, 2013.

[125] A. Vencl, A. Rac, and B. Ivković, “Investigation of abrasive wear resistance of ferrous-based coatings with scratch tester,” Tribol. Ind., vol. 29, no. 3–4, pp. 13–16, 2007.

[126] M. M. Khruschov and M. A. Babichev, “Resistance to abrasive wear of structurally heterogeneous materials,” Frict. Wear Mach., vol. 12, pp. 5–24, 1958.

[127] B. S. Mitchell, Materials Engineering and Science an Introduction To Materials Engineering and Science for Chemical and Materials Engineers. New Jersey, United State of America: A John Wiley & Sons, Inc., Publication, 2004.

[128] M. M. Khruschov, “Principles of abrasive wear,” Wear, vol. 28, no. 1, pp. 69–88, 1974.

[129] T. L. Oberle, “Properties Influencing Wear of Metals,” J. Met., no. 438, 1951.

[130] A. Leyland and A. Matthews, “On the significance of the H/E ratio in wear control: A nanocomposite coating approach to optimised tribological behaviour,” Wear, vol. 246, no. 1–2, pp. 1–11, 2000.

[131] M. F. Ashby, Materials Selection Mechanical Design Second Edition. Elsevier, 1999.

[132] K. Nogi, A. Tomsia, N. Eustathopoulos, A. Mortensen, R. Riman, O. Milosevic, S. Ohara, and M. Naito, “Wettability of solid by liquid at high temperature,” Report, no. 2001, 2004.

[133] L. Wu, X. Guo, and J. Zhang, “Abrasive Resistant Coatings—A Review,” Lubricants, vol. 2, no. 2, pp. 66–89, 2014.

[134] Y. Choudhury and P. Gupta, “Recent Trends in Nanomaterials,” Adv. Struct. Mater., vol. 83, 2017.

[135] I. K. Ř. Íková, B. Szewczyková, P. Blaškovitš, E. Hodúlová, and E. L. Č, “Study and Characteristic of Abrasive Wear Mechanisms,” pp. 1–9, 2012.

[136] J. R. Davis, “Metals Handbook,” Met. Handb., p. 2571, 1997.

[137] S. Z. Kure-Chu et al., “Sliding friction, wear and tribofilm formation of silver films electro-plated on copper alloy sheets,” Electr. Contacts, Proc. Annu. Holm Conf. Electr. Contacts, vol. 2016–Decem, pp. 135–140, 2016.

[138] S. Das, D. P. Mondal, S. Sawla, and S. Dixit, “High stress abrasive wear mechanism of LM13-SiC composite under varying experimental conditions,” Metall. Mater. Trans. A Phys. Metall. Mater. Sci., vol. 33, no. 9, pp. 3031–3044, 2002.

[139] K. Kendall, T. P. Weihs, and I. M. Hutchings, “Ductile-brittle transitions and wear maps for the erosion and abrasion of brittle materials,” J. Phys. D Appl. Phys, vol. 25, pp. 212–221, 1992.

[140] A. R. Warmuth, P. H. Shipway, and W. Sun, “Fretting wear mapping: the influence of contact geometry and frequency on debris formation and ejection for a steel-on-steel pair,” Proc. R. Soc. A Math. Phys. Eng. Sci., vol. 471, no. 2178, pp. 20140291–20140291, 2015.

[141] E. Kulesza, J. R. Dabrowski, J. Sidun, A. Neyman, and J. Mizera, “Fretting wear of materials - Methodological aspects of research,” Acta Mech. Autom., vol. 6, no. 3, pp. 58–61, 2012.

[142] D. A. Devaraju, “A Critical Review on Different Types of Wear of Materials,” Int. J. Mech. Eng. Technol., vol. 6, no. 11, pp. 77–83, 2015.

[143] Y. Berthier and L. Vincent, “Fretting fatigue and fretting wear,” vol. 235, no. ii, 1989.

[144] E. Gutierrez-Miravete, “Wear,” in Friction, Wear and Lubrication of Materials, 2013, pp. 1–13.

[145] I. Celal, “Theories on Rock Cutting, Grinding and Polishing Mechanisms,” Tribol. Eng., 2013.

[146] R. I. Singleton, “Utilisation of Chip Thickness Models in Grinding,” PhD Thesis, University of Sheffield, 2014.

[147] T. W. Liao, K. Li, L. J. O’Rourke, and S. B. McSpadden, “Wear of diamond wheels in creep-feed grinding of ceramic materials II. Effects on process responses and strength,” Wear, vol. 211, no. 1, pp. 104–112, 1997.

[148] S. Malik and N. H. Cook, “The Wear of Grinding Wheels Part 1—Attritious Wear,” J. Eng. Ind., vol. 70–prod–A, no. ASME Paper, pp. 1120–1128, 1971.

[149] S. Malkin and N. H. Cook, “The Wear of Grinding Wheels: Part 2—Fracture Wear,” J. Eng. Ind., vol. 93, no. 4, ASME Paper, p. 1129, 1971.

[150] J. Tilon, “Chapter 3- Mechanics of Grinding,” , Elsevier, 2010.

[151] M. J. Jackson, “Fracture dominated wear of sharp abrasive grains and grinding wheels,” Proc. Inst. Mech. Eng. Part J J. Eng. Tribol., vol. 218, no. 3, pp. 225–235, 2004.

[152] X. U. N. Chen, W. B. Rowe, B. Mills, and D. R. Allanson, “Analysis and simulation of the grinding process. Part IV: Effects of wheel wear,” Int. J. Mach. Tools Manuf., vol. 38, no. 1–2, pp. 41–49, 1998.

[153] M. H. Miller, X. Fan, and A. Showa, “Wheel Wear During Intermittent Grinding,” 2006.

[154] Y. Novoselov, S. Bratan, and V. Bogutsky, “Analysis of Relation between Grinding Wheel Wear and Abrasive Grains Wear,” Procedia Eng., vol. 150, pp. 809–814, 2016.

[155] G. Y. Lee, C. K. H. Dharan, and R. O. Ritchie, “A physically-based abrasive wear model for composite materials,” Wear, vol. 252, no. 3–4, pp. 322–331, 2002.

[156] T. Jian-min, S. Ye-ying, Z. Hua-yi, Z. Ching-an, and K. Xian-wu, “Investigation of abrasive wear resistance and wear mechanism of composite alloys,” Tribol. Int., vol. 18, no. 2, pp. 101–105, 1985.

[157] W. M. Garrison Jr., “Khruschov’s rule and the abrasive wear resistance of multiphase solids,” Wear, vol. 82, no. 2, pp. 213–220, 1982.

[158] S. Wang, Y. Wang, and C. Li, “The Dry Sliding Wear Behavior of Interpenetrating Titanium Trialuminide / Aluminium Composites,” pp. 129–144, 2007.

[159] K. H. Zum-Gahr, “Abrasive wear of two-phase metallic materials with a coarse microstructure,” in International Conference on Wear of Materials, 1985, no. 793 p.

[160] S. Ilo, C. Just, E. Badisch, J. Wosik, and H. Danninger, “Effects of interface formation kinetics on the microstructural properties of wear-resistant metal – matrix composites,” Mater. Sci. Eng. A, vol. 527, no. 23, pp. 6378–6385, 2010.

[161] T. Rong, D. Gu, Q. Shi, S. Cao, and M. Xia, “Effects of tailored gradient interface on wear properties of WC/Inconel 718 composites using selective laser melting,” Surf. Coatings Technol., vol. 307, pp. 418–427, 2016.

[162] J. I. Harti, T. B. Prasad, M. Nagaral, P. Jadhav, A. B. V, and G. N. Sahadev, “Evaluation of Wear Properties of TiC Particulates Reinforced Al2219 Alloy Composites,” vol. 020058, 2017.

[163] T. B. Rao, “An Experimental Investigation on Mechanical and Wear Properties of Al7075/SiCp Composites: Effect of SiC Content and Particle Size,” J. Tribol., vol. 140, no. 3, p. 031601, 2017.

[164] S. Pradhan, T. K. Barman, P. Sahoo, and G. Sutradhar, “Effect of SiC weight percentage on tribological properties of Al-SiC metal matrix composites under acid environment,” vol. 13, no. April, pp. 21–35, 2017.

[165] F. Ahmad, S. H. J. Lo, M. Aslam, and A. Haziq, “Tribology behaviour of alumina particles reinforced aluminium matrix composites and brake disc materials,” Procedia Eng., vol. 68, no. 0, pp. 674–680, 2013.

[166] I. M. Hutchings, “Advanced Materials and Processes, University of Cambridge,” in Advanced Materials and Process, University of Cambridge, 1991, p. 56.

[167] Inland Craft, “Home | Inland Craft.” [Online]. Available: https://inlandcraft.com/. [Accessed: 15-Apr-2018].

[168] I. Lists, “Inland Equivalent US convention.” p. 170. Available: https:// Inland Equivalent US convention.com/. [Accessed: 13-Apr-2018].

[169] “Particle Size Conversion Chart- ANSI - Washington Mills.” [Online]. Available: https://www.washingtonmills.com/guides/grit-sizes-ansi/particle-size-conversion-chart-ansi/. [Accessed: 26-Oct-2018].

[170] E. Elizondo, “Investigation of Porous Metals as Improved Efficiency Regenerators,” PhD Thesis-University of Sheffield, 2016.

[171] T. Thompson, “The fundamentals of Raman spectroscopy,” Electro Opt., vol. 2, no. 114, p. 2, 2012.

[172] A. C. Ferrari, “A Model to Interpret the Raman Spectra of Disordered, Amorphous and Nanostructured Carbons,” MRS Proc., vol. 675, p. W11.5.1, 2001.

[173] F. Rosenburg and E. Ionescu, “High-Temperature Raman Spectroscopy of Nano-Crystalline Carbon in Silicon Oxycarbide,” Materials (Basel)., vol. 11, no. 1, p. 93, 2018.

[174] M. A. Pimenta, G. Dresselhaus, M. S. Dresselhaus, L. G. Cançado, A. Jorio, and R. Saito, “Studying disorder in graphite-based systems by Raman spectroscopy,” Phys. Chem. Chem. Phys., vol. 9, no. 11, pp. 1276–1291, 2007.

[175] R. J. Nemanich and S. A. Solin, “First- and second-order Raman scattering from finite-size crystals of graphite,” Phys. Rev. B, vol. 20, no. 2, pp. 392–401, 1979.

[176] F. Adar, “Depth Resolution of the Raman Microscope : Optical Limitations and Sample Characteristics Depth Resolution of the Raman Microscope ,” 2016. [Online]. Available: http://www.spectroscopyonline.com/depth-resolution-raman-

microscope-optical-limitations-and-sample-characteristics. [Accessed: 16-Jan-2019].

[177] N. Reeves, “Standard Operating Procedures - Renishaw inVia Raman Microscope Step 1 : Switch On,” 2017.

[178] Cromwell Tools, “Kennedy 115x1x22.23mm AS60 INOX BF CUT-OFF DISC - Pack of 10 1111240 | Cromwell Tools,” 2018. [Online]. Available: https://www.cromwell.co.uk/shop/abrasives/cutting/product/p/KEN2304430K. [Accessed: 28-Aug-2018].

[179] O. Beffort, S. Vaucher, and F. A. Khalid, “On the thermal and chemical stability of diamond during processing of Al/diamond composites by liquid metal infiltration (squeeze casting),” Diam. Relat. Mater., vol. 13, no. 10, pp. 1834–1843, 2004.

[180] R. A. Munson, “Surface energies of liquid metal interfaces with carbon,” Carbon N. Y., vol. 5, no. 1, pp. 471–474, 1967.

[181] N. Sobczak, J. Sobczak, R. Asthana, and R. Purgert, “The mystery of molten metal,” China Foundry, vol. 7, no. 4, pp. 425–437, 2010.

[182] E. Illeková, P. Švec, and D. Janičkovič, “Influence of the processing on the ordering process in the Al-Ti binary system with composition close to Al3Ti,” J. Phys. Conf. Ser., vol. 144, no. January, pp. 3–9, 2009.

[183] C. A. Leon, V. H. Lopez, E. Bedolla, and R. A. L. Drew, “Wettability of TiC by commercial aluminum alloys,” J. Mater. Sci., vol. 37, no. 16, pp. 3509–3514, 2002.

[184] R. Sara, V. and G.G. Liversidge, K.C. Cundy, J.F. Bishop, “Chemically bonded aluminum coating for carbon via monocarbides,” United States Pat., vol. 96, no. 19 North Olmsted, Ohio, pp. 62–66, 1983.

[185] P. E. P. Porta and A. E. Chu, “Chemically Bonded Aluminum Coated Carbon via Monocarbides,”J. Mat. Tech., vol. 21, 1993.

[186] G. Requena, D. C. Yubero, J. Corrochano, J. Repper, and G. Garcés, “Stress relaxation during thermal cycling of particle reinforced aluminium matrix composites,” Compos. Part A Appl. Sci. Manuf., vol. 43, no. 11, pp. 1981–1988, 2012.

[187] P. Schulson, Erland M.;Duval, “Cambridge Books Online © Cambridge University Press,” Paleodemography Age Distrib. from Skelet. Samples, no. June 1999, pp. 80–83, 2009.

[188] A. Technologies, Agilent Laser and Optics User ’ s Manual, Fifth edit., vol. I. 5301 Stevens Creek Boulevard Santa Clara, California 95052-8059: Agilent Technologies USA, 2007.

[189] A. Technologies, Agilent Laser and Optics User ’ s Manual , Volume I, vol. 1. 2007.

[190] K. E. Spear and J. P. Dismukes, Synthetic Diamond-Emerging CVD Science and Technology. NY: Wiley, 1994.

[191] D. N. Talwar, W. Grochala, and W. Grochala, “Related content Thermal Expansion Coefficient of Synthetic Diamond Single Crystal at Low Temperatures,” 1992.

[192] K. Miyoshi, “Structures and mechanical properties of natural and synthetic diamonds,” no. June 1998, p. 26, 1998.

[193] ASM, “ASM Material Data Sheet.” [Online]. Available: http://asm.matweb.com/search/SpecificMaterial.asp?bassnum=mtu010. [Accessed: 18-Apr-2018].

[194] J. Emi and S. Iizuka, “Diamond Particles Deposited among Nickel / Copper Particles in Energy Controlled CH_4 / H_2 RF Discharge Plasmas,” vol. 2012, no. July, pp. 158–162, 2012.

[195] A. Gupta, G. Chen, P. Joshi, S. Tadigadapa, and P. C. Eklund, “Raman scattering from high-frequency phonons in supported n-graphene layer films,” Nano Lett., vol. 6, no. 12, pp. 2667–2673, 2006.

[196] F. Inzoli, D. Dellasega, V. Russo, R. Caniello, C. Conti, F. Ghezzi, and M. Passoni, “Nanocrystalline diamond produced by direct current micro-plasma: Investigation of growth dynamics,” Diam. Relat. Mater., vol. 74, pp. 212–221, 2017.

[197] C. Spudat, C. Meyer, and C. M. Schneider, “Oxidation induced shifts of Raman modes of carbon nanotubes,” Phys. Status Solidi Basic Res., vol. 245, no. 10, pp. 2205–2208, 2008.

[198] L. A. Dobrzański, T. Błażej, and M. Macek, “Fabrication, Composition, Properties

and Application the $AlMg_1SiCu$ Aluminium Alloy Matrix Composite Materials Reinforced with Halloysite or Carbon Ma," in World ' s largest Science , Technology & Medicine Open Access book publisher, Intech Open, 2017, pp. 139–160.

[199] D. J. Woo, J. P. Hooper, S. Osswald, B. A. Bottolfson, and L. N. Brewer, "Low temperature synthesis of carbon nanotube-reinforced aluminum metal composite powders using cryogenic milling," J. Mater. Res., vol. 29, no. 22, pp. 2644–2656, 2014.

[200] S. Boullosa-Eiras, E. Vanhaecke, T. Zhao, D. Chen, and A. Holmen, "Raman spectroscopy and X-ray diffraction study of the phase transformation of ZrO_2-$Al_2O_3$and CeO_2-Al_2O_3nanocomposites," Catal. Today, vol. 166, no. 1, pp. 10–17, 2011.

[201] R. Ren, Z. Wen, S. Cui, Y. Hou, X. Guo, and J. Chen, "Controllable Synthesis and Tunable Photocatalytic Properties of Ti3+-doped TiO_2," Sci. Rep., vol. 5, no. 1, p. 10714, 2015.

[202] M. Lubas, J. J. Jasinski, M. Sitarz, L. Kurpaska, P. Podsiad, and J. J. Jasinski, "Raman spectroscopy of TiO_2 thin films formed by hybrid treatment for biomedical applications," Spectrochim. Acta - Part A Mol. Biomol. Spectrosc., vol. 133, pp. 867–871, 2014.

[203] A. C. Ferrari, "Raman spectrum of graphene and graphene layers," Phys. Rev. Lett., vol. 97, no. 18, pp. 1–4, 2006.

[204] T. Peng, Z. Kou, H. Wu, and S. Mu, "Graphene from amorphous titanium carbide by chlorination under 200°C and atmospheric pressures," Sci. Rep., vol. 4, pp. 4–9, 2014.

[205] Q. Liu, D. Ding, and C. Ning, "Anodic fabrication of Ti-Ni-O nanotube arrays on shape memory alloy," Materials (Basel)., vol. 7, no. 4, pp. 3262–3273, 2014.

[206] X. Yuan, L. Cheng, L. Kong, X. Yin, and L. Zhang, "Preparation of titanium carbide nanowires for application in electromagnetic wave absorption," J. Alloys Compd., vol. 596, no. 3, pp. 132–139, 2014.

[207] C. Adelhelm, M. Balden, M. Rinke, and M. Stueber, "Influence of doping (Ti, V,

Zr, W) and annealing on the sp^2 carbon structure of amorphous carbon films," J. Appl. Phys., vol. 105, no. 3, p. 033522, 2009.

[208] X. H. Gao, Z. M. Guo, Q. F. Geng, P. J. Ma, A. Q. Wang, and G. Liu, "Structure, optical properties and thermal stability of SS/TiC–ZrC/Al_2O_3 spectrally selective solar absorber," RSC Adv., vol. 6, no. 68, pp. 63867–63873, 2016.

[209] Y. I. Naidich, V. P. Umanskii, and I. A. Lavrinenko, Strength of the Metal-Diamond Interface and Brazing of Diamonds. Cambridge, UK: Cambridge International Science Publishing Ltd, 2007.

[210] M. Setton, J. V. derspiegel, and B. Rothman, "Formation of a ternary silicide for Ni/Ti/Si(100) and Ni/TiSi structures," J. Mater. Res., vol. 4, no. 5, p. 1218, 1989.

[211] C. Mattevi, H. Kim, and M. Chhowalla, "A review of chemical vapour deposition of graphene on copper," J. Mater. Chem., vol. 21, no. 10, pp. 3324–3334, 2011.

[212] B. Predel, O. Madelung, and W. Martienssen, Phase equilibria, crystallographic and thermodynamic data of binary alloys, vol. 5, no. 12. Berlin,: Springer-Verlag., 1992.

[213] D. J. Mcadam and G. W. Geil, "Rate of oxidation of typical nonferrous metals as determined by interference colors of oxide films," J. Res. Natl. Bur. Stand. (1934)., vol. 28, no. 5, p. 593, 1942.

[214] N. Catalyst, "Ammonia Generation via a Graphene-Coated Nickel Catalyst," Coatings, vol. 7, no. 6, p. 72, 2017.

[215] S. Chen, L. Brown, M. Levendorf, W. Cai, S. Y. Ju, J. Edgeworth, X. Li, C. W. Magnuson, A. Velamakanni, R. D. Piner, J. Kang, J. Park, and R. S. Ruoff, "Oxidation resistance of graphene-coated Cu and Cu/Ni alloy," ACS Nano, vol. 5, no. 2, pp. 1321–1327, 2011.

[216] D. Zappa, A. Bertuna, E. Comini, N. Kaur, N. Poli, V. Sberveglieri, and G. Sberveglieri, "Metal oxide nanostructures: Preparation, characterization and functional applications as chemical sensors," Beilstein J. Nanotechnol., vol. 8, no. 1, pp. 1205–1217, 2017.

[217] B. B. Bokhonov, A. V. Ukhina, D. V. Dudina, A. G. Anisimov, V. I. Mali, and I. S. Batraev, "Carbon uptake during Spark Plasma Sintering: Investigation through the analysis of the carbide 'footprint' in a Ni-W alloy," RSC Adv., vol. 5, no. 98, pp.

80228–80237, 2015.

[218] H. E. Taylor, J. H. Gibson, and R. K. Skogerboe, “Determination of trace impurities in argon by microwave induced excitation,” Anal. Chem., vol. 42, no. 8, pp. 876–881, 1970.

[219] S. Ib, “Copper as electrical conductive material with above-standard performance properties,” pp. 1–38, 2015.

[220] S. S. Dalgic and M. Celtek, “Glass forming ability and crystallization of CuTi intermetallic alloy by molecular dynamics simulation,” J. Optoelectron. Adv. Mater., vol. 13, no. 11–12, pp. 1563–1569, 2011.

[221] J. M. J. Santillán, F. A. Videla, M. B. Fernández Van Raap, D. C. Schinca, and L. B. Scaffardi, “Analysis of the structure, configuration, and sizing of Cu and Cu oxide nanoparticles generated by fs laser ablation of solid target in liquids,” J. Appl. Phys., vol. 113, no. 13, 2013.

[222] D. Neves, A. E. Diniz, and M. S. F. Lima, “Microstructural analyses and wear behavior of the cemented carbide tools after laser surface treatment and PVD coating,” Appl. Surf. Sci., vol. 282, pp. 680–688, 2013.

[223] Y. Koren, “Flank Wear Model of Cutting Tools Using Control Theory,” J. Eng. Ind., vol. 100, no. 1, p. 103, 1978.

[224] D. K. Lee, J. In, and S. Lee, “Standard deviation and standard error of the mean,” Korean J. Anesthesiol., vol. 68, no. 3, pp. 220–223, 2015.

[225] R. L. Ott and M. Longnecker, An Introduction to Statistical Methods and Data Analysis, Sixth Edit. Canada: Brooks/Cole, Cengage Learning, 2010.

[226] J. Lawal, “Physical Vapour Deposition of Aluminium-Rich Nanostructured/Amorphous Metallic Coatings for Wear and Corrosion Protection,” , PhD thesis, University of Sheffield, 2017.

[227] A. Kaplan, “Linear Least Squares Fitting with Microsoft Excel.” 2010.

[228] K. Weinert and W. König, “A Consideration of Tool Wear Mechanism when Machining Metal Matrix Composites (MMC),” CIRP Ann. - Manuf. Technol., vol. 42, no. 1, pp. 95–98, 1993.

[229] C. Trevisiol, A. Jourani, and S. Bouvier, “Effect of abrasive particle size on friction and wear behaviour of various microstructures of 25CD4 steel,” J. Phys. Conf. Ser., vol. 843, no. 1, 2017.

[230] H. Sin, N. Saka, and N. P. Suh, “Abrasive wear mechanisms and the grit size effect,” Wear, vol. 55, no. 1, pp. 163–190, 1979.

[231] J. Jiang, F. H. Stott, and M. M. Stack, “A mathematical model for sliding wear of metals at elevated temperatures,” Wear, vol. 181–183, no. PART 1, pp. 20–31, 1995.

[232] M. A. Brochure, Grinding Wheels Solutions for Industry, ISO 9001, vol. EN 12413, on www.master-abrasives.co.uk. pp. 45-74, 2007.

[233] L. Jaworska, “Diamond Composites with TiC , SiC and Ti_3 SiC_2 Bonding Phase,” vol. 7959, pp. 3–6, 2010.

[234] Health Safety Executive, “Safety in the use of abrasive wheels,” pp. 1–53, 2000.

[235] Kyocera, “Physical - Rigidity | Characteristics of Fine Ceramics | FINE CERAMICS WORLD - All About Advanced Ceramics -,” Fine Ceramics World, 2015. [Online]. Available: https://global.kyocera.com/fcworld/charact/strong/hardness.html. [Accessed: 25-Sep-2018].

[236] R. Ziaur Rehman, “Ceramics.” [Online]. Available: https://www.slideshare.net/ZiaRehman18/ceramics-58777015?from_action=save. [Accessed: 25-Sep-2018].

[237] M. Yan and Z. Fan, “Review: Durability of materials in molten aluminum alloys,” J. Mater. Sci., vol. 36, pp. 285–295, 2001.

[238] W. Tillmann, C. Kronholz, M. Ferreira, A. Knote, W. Theisen, P. Schütte, and J. Schmidt, “Comparison of Different Metal Matrix Systems for Diamond Tools Fabricated by New Current Induced Short-Time Sintering Processes,” Proceeding Powder Metall. 2010 World Congr., 2010.

[239] C. M. Sung and M. F. Tai, “Reactivities of Transition Metals with Carbon: Implications to the Mechanism of Diamond Synthesis Under High Pressure,” Int. J. Refract. Met. Hard Mater., vol. 15, no. 4, pp. 237–256, 1997.

[240] C. Artini, M. L. Muolo, and A. Passerone, “Diamond-metal interfaces in cutting tools: A review,” J. Mater. Sci., vol. 47, no. 7, pp. 3252–3264, 2012.

[241] F. Gul and M. Acilar, Effect of the reinforcement volume fraction on the dry sliding wear behaviour of Al-10Si/SiCp composites produced by vacuum infiltration technique, vol. 64, no. 13–14. 2004.

[242] V. S. Ramamurthy, “Effect of Particle Size and Weight Fraction of Alumina Reinforcement on Wear Behavior of Aluminum Metal Matrix Composites,” vol. 3, no. 4, pp. 11191–11198, 2014.

[243] M. Santl, I. ILIc, F. Vrecer, and S. Baumgartner, “A compressibility and compactibility study of real tableting mixtures: The effect of granule particle size,” Acta Pharm., vol. 62, no. 3, pp. 325–340, 2012.

[244] A. Maleque and R. Karim, “Tribological behavior of dual and triple particle size SiC reinforced Al- MMCs: a comparative study,” Ind. Lubr. Tribol., vol. 60, no. 4, pp. 189–194, 2008.

[245] A. Zmitrowicz, “Wear Debris: a Review of Properties and Constitutive Models,” J. Theor. Appl. Mech., vol. 43, no. 1, pp. 3–35, 2005.

[246] Q. L. Che, J. J. Zhang, X. K. Chen, Y. Q. Ji, Y. W. Li, L. X., Wang, S. Z. Cao, L. Guo, Z. Wang, S. W. Wang, Z. K. Zhang, and Y. G. Jiang, “Spark plasma sintering of titanium-coated diamond and copper-titanium powder to enhance thermal conductivity of diamond/copper composites,” Mater. Sci. Semicond. Process., vol. 33, pp. 67–75, 2015.

[247] S. C. Tjong, “Novel nanoparticle-reinforced metal matrix composites with enhanced mechanical properties,” Adv. Eng. Mater., vol. 9, no. 8, pp. 639–652, 2007.

[248] W. B. Johnson and B. Sonuparlak, “Diamond/Al metal matrix composites formed by the pressureless metal infiltration process,” J. Mater. Res., vol. 8, no. 5, pp. 1169–1173, 1993.

[249] P. M. Natishan and A. M. Morrish, “Diamond-Reinforced Matrix Composites,” US Pat. Appl., no. 698, pp. 0–16, 1993.

[250] E. Levashov, V. Kurbatkina, and Z. Alexandr, “Improved Mechanical and

Tribological Properties of Metal-Matrix Composites Dispersion-Strengthened by Nanoparticles," Materials (Basel)., vol. 3, pp. 97–109, 2009.

[251] Y. Mu, J. Guo, B. Liang, and Q. Wang, "Rapid fabrication of the Ti_3SiC_2 bonded diamond composite by spark plasma sintering," Int. J. Refract. Met. Hard Mater., vol. 29, no. 3, pp. 397–400, 2011.

[252] S. Roy, M. Das, A. K. Mallik, and V. K. Balla, "Laser melting of titanium-diamond composites: Microstructure and mechanical behavior study," Mater. Lett., vol. 178, pp. 284–287, 2016.

[253] O. A. Voronov and B. H. Kear, "Diamond-Hardfaced TiC / Ti Composite for Submersible Pump Bearings in Geothermal Systems," Clean Technol., vol. ISBN 978-1, no. 1787–2, pp. 9–12, 2009.

[254] H. Ogihara, A. Hara, K. Miyamoto, N. K. Shrestha, T. Kaneda, S. Ito, and T. Saji, "Synthesis of super hard Ni-B/diamond composite coatings by wet processes," Chem. Commun., vol. 46, no. 3, pp. 442–444, 2010.

[255] LexisNexis, "LexisNexis® - Sign In to LexisNexis® via Athens or Your Institution," 2018. [Online]. Available: https://www.lexisnexis.com/start/shib/wayf. [Accessed: 08-Sep-2018].

[256] A. Evans, C. San Marchi, and A. Mortensen, Metal Matrix Composites in Industry. Boston, MA: Springer US, 2003.

[257] D. stefan Szyniszewski, K. Fivaesh, D. R. Vogel, and D. T. Hipke, "Metallic-Ceramic Multi-Material Composite for Protection from Forcible Entry MSE Congress: Postersession," 2016.

[258] I. Society, "ASM International the Materials Information Society - ASM International," 2018. [Online]. Available: https://www.asminternational.org/. [Accessed: 22-Sep-2018].

[259] InvestmentMine, "Aluminum Prices and Aluminum Price Charts - InvestmentMine," 2018. [Online]. Available: http://www.infomine.com/investment/metal-prices/aluminum/. [Accessed: 10-Sep-2018].

[260] Epoxy, "price of epoxy resin | davidneat," 2015. [Online]. Available:

https://davidneat.wordpress.com/tag/price-of-epoxy-resin/. [Accessed: 10-Sep-2018].

[261] Epoxy Composite, “EL2 Epoxy Laminating Resin for use with Carbon Fibre, Kevlar or Glass Reinforcement. - Easy Composites,” 2018, 2018. [Online]. Available: http://www.easycomposites.co.uk/#!/resin-gel-silicone-adhesive/epoxy-resin/EL2-epoxy-laminating-resin.html. [Accessed: 10-Sep-2018].

[262] The Global Source for Metals Pricing, “Mineralprices.com - The Global Source for Metals Pricing,” 2018. [Online]. Available: http://mineralprices.com/. [Accessed: 10-Sep-2018].

[263] T. Prices, “MetalMiner Prices: Titanium Prices,” 2018. [Online]. Available: https://agmetalminer.com/metal-prices/titanium/. [Accessed: 10-Sep-2018].

[264] E. Edge, “Densities of Metals and Elements Table | Engineers Edge | www.engineersedge.com,” 2018. [Online]. Available: https://www.engineersedge.com/materials/densities_of_metals_and_elements_table_13976.htm. [Accessed: 10-Sep-2018].

[265] J. King, “Engineering Materials,” Mater. Process. J, vol. 12, pp. 1–13, 2015.

[266] N. A. Wholesale, “Buy An ATM Machine | ATM Machine Sales | National ATM Wholesale,” 2018. [Online]. Available: https://atmmachines.com/available-atms/. [Accessed: 31-Aug-2018].

[267] WRG, “WRG | WRG ATM | WRG Apollo ATM Machine.” [Online]. Available: https://www.atmexperts.com/wrg_apollo_atm.html. [Accessed: 12-Sep-2018].

[268] E. Cycles, “Abus Granit Extreme 59 Lock | LOCKS & SECURITY | Evans Cycles,” 2018. [Online]. Available: https://www.evanscycles.com/abus-granit-extreme-59-lock-00104612?lsft=esvt:54464-OUKE2191442,esvq:,esvadt:999999-0-1213402-1,esvcrea:183847436579,esvplace:,esvd:c,esvtg:pla-300126404561,esvo:00104612-NA-NA,esvaid:50080&esvt=54464-GOUKE2191442&esvq=&esvad. [Accessed: 19-Sep-2018].

Appendix1: Assessment of Applicability in a Commercial Setting

The focus of this thesis has been the study of some fundamental behaviours underlying the end goal of producing extremely abrasion resistant materials. With this in mind, the object of the current chapter is to undertake an initial commercial assessment study of some of the aspects of applying the product in the market, applying the technical knowledge that has been obtained. It should be noted that this discussion does not focus on financial or marketing aspects.

The emphasis is more on the potential application of the MMDCs, essential production costs compared to commercially available products intended to solve angle grinder-thief attacks, comparison of the cost and practical effectiveness.

A.1 Market Assessments

Comprehensive details of the global market require huge amounts of commercial information about general metal matrix composites (MMCs) and MMDCs more specifically. The current study is not going to discuss in depth details about MMCs marketing, but it will offer an overview of some recent studies dealing with MMCs marketing and will compare MMDCs capability and affordability with specific case study examples.

In recent years the MMCs global market has grown rapidly, according to Technavio (a market research reports institute), in the 2016 report about the MMC market. The report, which includes a study of the MMCs market in Europe, Middle East, Latin America and Africa, estimated the use of MMCs to be more than 30 kilotons by 2020. For example, in some industrial countries like the UK, Germany, and France the demands of MMCs have been raised by the use in automotive and electronics applications. According to these marketing requirements Technavio expects that there will be a higher requirement of MMCs in the markets of central and Eastern Europe countries, as well as the Western European countries in the near future [255]. There are two other recent reports which have been conducted evaluating the market for MMCs, which considered independent evaluations of the MMC market. The most recent report published by a specialised organization for MMCs [256], introduces the industrial view about MMCs. However, they did not include any security or critical military information, while there are many military applications which include MMCs [257]. Miracle [22] adressed most market constituents, such as customers, suppliers, second tier agencies, materials, properties and applications.

These reports can be considered as a guide for MMCs business and marketing, where information is available in [22], [256]. Additional recent data and information, which should be updated regularly about MMCs in general, can be found on the ASM international website [17], [22], [258].

A.2 Assessment of MMCs with Diamond Reinforcement

The materials with diamond reinforcement were found effective at resisting abrasive cutting. There are many possible applications for this, such as protection from angle grinder thieves for example; as was mentioned in the motivation for study in **chapter 1** such crimes have been reported in relatively recent news**.** We will take two main examples of this application of MMDCs as security applicantions which are an ATM machine and a U shape bike lock. The Table (A-1) shows the prices and densities of materials used, and it is considered a guidance of the cost calculation in the next two examples.

Table (A-1): Prices and densities of materials that were used to make composites.

Material	Price (£/Kg) [259], [260], [261], [262], [263]	Density (g/cm3) [264], [265]
Al	1.4-1.61	2.7
Sn	14.5	7.26
Epoxy	20.1	1.25
Ni	9.6	8.9
Cu	4.6	8.95
Ti	43.3	4.5
Diamond	423	3.55
SiC	10.2-14.6	3.19
Al2O3	12.8-19.2	3.92

A.2.1 ATM Machine Reinforced Against Abrasive Cutting Attacks

The economic reinforcement of ATM machine is probably in the form of a sandwich panel filled with a net arrangement of MMDC rods with 8 mm diameter. The distance between them should be equal to or less than the radius of the common grinding wheel which can be used in portable angle grinders (which is assumed here to be 57.5 mm) as shown in

Figure (A-1) (the dimensions of this ATM machine were taken from [266]). This would ensure wherever a cut was attempted it would be very likely to meet with diamond reinforcement. The cost calculation of materials, which can be used to manufacture this net, was according on the cost of raw composite constituents that contribute in composite formation (metal matrix and diamond reinforcement). It is noted that this neglects processing costs, but these are expected to be low in comparison. The cost was calculated in grams as that reflects per mass units in Table (A-1) after applying the density of materials in equation A-1 **below** to convert constituent's volume to mass.

$$\boldsymbol{\rho}=\frac{\boldsymbol{M}}{\boldsymbol{V}} \quad \text{…….. } \textit{Equation 11-1}$$

where: $\boldsymbol{\rho}$ is the density of material (g/cm^3)

M: mass (g)

V: volume (cm^3)

Nowadays, consumption of the space is important, and there will be a trend towards more compact designs for ATMs, which can offer a full capability of ATM machines with a convenient size. This type of ATM is sold by WRG Apollo ATM group with selectable properties and setting up features to optimize space demand [267]. Product dimensions were considered as an example, shown in Figure (A-1) for the use of an MMDCs mesh as reinforcement of one face of ATM against angle grinder thieves. The net shaped obstacle is required to cover a rectangular area of 508 × 266.7 mm (these dimensions of a mini ATM machine were taken from [266], [267] as an example).

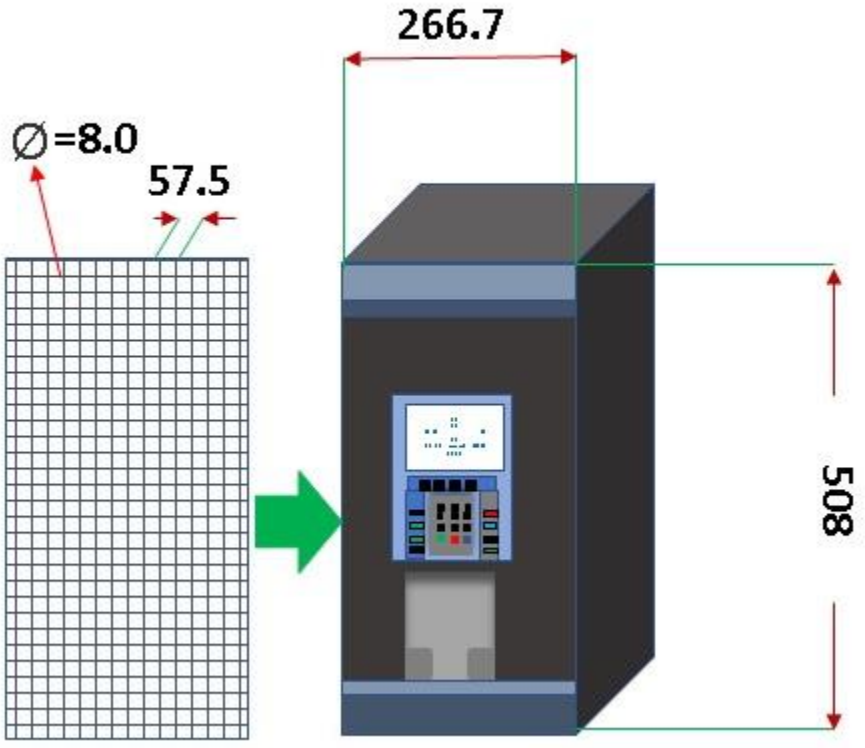

Figure (A-1): ATM Machines and MMDC mesh design with dimensions.

Such a mesh requires 9 horizontal bars and 5 vertical bars to form a structure as that is shown on the left in Figure (A-1). These dimesions were found according to the assumption that the required distance between bars should be no more than 57.5 mm, which is the radius of the cut-off wheel. If the dimeter of each rod making up the mesh is assumed to be 8 mm (to give consistent behaviour with the tests performed here), the volume of materials required can be calculated according to equation A-2

$$V = (\pi \times r^2 \times L) \times n + (\pi \times r^2 \times L) \times n \qquad \text{....Equation A-2}$$

120 cm^3	127.7 cm^3	= 247.7 cm^3
horizontal bars	vertical bars	

where : V is the volume of net (cm^3)= 247.7 cm^3

r: bar radius (cm)= 0.4 cm

L: one dimension of the net (Width or Hieght) (cm)

n: the number of required bars

After we know the volume of the required net, we can calculate the required volume of each constituent of composite by multiplying the net volume by the vol% of each constituent, and then can find the weight of each component (in grams) by applying the density formula (equation A-1). At this point we can estimate the cost of the product according to Table (A-1) above. For the example of the MMC mesh required to reinforce the selected ATM machine this is shown in Table (A-1).

Hence, to apply the MMDCs mesh to reinforce the front of an ATM machine would increase the commercial price of the machine should be increased by the cost of the MMDC mesh. The prices of such ATM machines (National ATM Wholesale) are about $2000 to $2500 (≈ £1538.5- £1923) according to the model and brand [266]. The increnents in price of ATM machines reinforced with MMDC meshes with various diamond contents and matrices are displayed in the last column in Table (A-1) showing the highest increment in price is less than 14%, and can be as low as 3.4% of the original (the cost increase for any MMDCs component is within the overall price range of the machines.

Table (A-1): Cost of possible MMDC meshes and increment in price in comparison with the commercial product.

MMDCs GI	**Net volume (cm^3)**	**Matrix mass (g)**	**Dia. mass (g)**	**Matrix cost (£)**	**Dia. cost (£)**	**MMDCs cost (£)**	**Increment (1538.5 to 1923 £)**
Al-50% Dia.	**247.7**	**333.45**	**439.66**	**0.55**	**185.97**	**186.52**	**9.7-12.1%**
Sn-50% Dia.	**247.7**	**899.15**	**439.66**	**13.04** [259]	**185.97**	**199.01**	**10.3-12.9%**
Epoxy-50% Dia.	**247.7**	**154.80**	**439.66**	**3.11**	**185.97**	**189.08**	**9.8-12.3%**
Either SPS or PM							

Ni-50% Dia.	**247.7**	**1102.26**	**439.66**	**10.58** [259]	**185.97**	**196.55**	**10.2-12.8%**
Cu-50% Dia.	**247.7**	**1109.70**	**439.66**	**5.07** [259]	**185.97**	**191.04**	**9.9-12.4%**
Ti-5% Dia.	**247.7**	**1058.9**	**43.97**	**45.85**	**18.60**	**64.45**	**3.4-4.2%**
Ti-15% Dia.	**247.7**	**947.45**	**131.9**	**41.02**	**55.80**	**96.82**	**5-6.3%**
Ti-30% Dia.	**247.7**	**780.25**	**263.8**	**33.79**	**111.6**	**145.4**	**7.6-9.5%**
Ti-50% Dia.	**247.70**	**557.33**	**439.66**	**24.13**	**185.97**	**210.10**	**10.9-13.7%**

The above costs of MMDC meshes could be further reduced by the use of less expensive reinforcement and ceramic particle reinforcements (alumina and silicon carbide) were tested with two specific matrices, Al and Ti, as shown in Table (A-2). However, these MMCs were found to have insufficient abrasive wear resistance to prevent cutting by a single abrasive cut-off wheel as shown in Figure (8-9) in Chapter 8 and Figure (9-12) in Chapter 9. To choose the optimum material, the cost and the performance must be considered, and data for the abrasive cutting test and wear resistance were used to calculate the diamond content of 8mm rods needed to prevent one standard cutting wheel passing through the barrier, Table (A-1). This is based on the idea that the practical difficulties in interrupting a cut to change a wheel would deter a theif. The volume fraction of diamond required to resist one cut-off wheel was found to be 20 vol. %, This amount of reinforcement can be distributed across 8 mm bar diameter by substituting part of the volume by ceramic reinforcement (30 vol. %) to retain an overall reinforcement percentages of 50 vol. % for processing reasons. Aluminium matrix was considered for this purpose for two reasons, one economic (Al is the cheapest metal matrix among those applied) and the second as Al is suitable to fabricate by melting techniques (GI here) without effects on reinforcement properties, which allows it to be formed in a complex shape product relatively cheaply. The cost of this product (Al-20%Dia-30% ceramic) is

reduced by more than half compared to Al-50% Diamond. The minimum cost increase for an effective product is therefore assessed as just over 4% (about £78).

Table (A-2): Cost of prospecting MMCCs net and increment in comparing with commercial product.

Ceramic Ren. Or Dia loaded	**Net volume (cm^3)**	**Matrix mass (g)**	**Rein. mass (g)**	**Matrix cost (£)**	**Rein. cost (£)**	**MMDCs cost (£)**	**Increment (1538.5 to 1923 £)**
Al GI-50% SiC	**247.7**	**333.45**	**395.08**	**0.55**	**5.77**	**6.32**	**0.33-0.41%**
Al GI-50% Al2O3	**247.7**	**333.45**	**485.50**	**0.55**	**9.32**	**9.87**	**0.51-0.64%**
Ti PM-50% SiC.	**247.70**	**557.33**	**395.08**	**24.13** [263]	**5.77**	**29.90**	**1.6-1.9%**
Ti PM-50% Al2O3	**247.70**	**557.33**	**485.50**	**24.13** [263]	**9.32**	**33.45**	**1.7-2.2%**
Al GI 30% Sic-20% Dia.	**247.7**	**333.45**	**237.05-175.87**	**0.55**	**3.46+ 74.4**	**78.40**	**4.1-5.1%**
Al GI 30% Al2O3-20% Dia.	**247.7**	**333.45**	**291.30-175.87**	**0.55**	**5.6+ 74.4**	**80.55**	**4.2-5.2%**

A.2.2 ''U'' Bike Lock Reinforced Against Abrasive Cutting Attacks

Many critical security applications can be reinforced by MMDCs (doors, walls of buildings as a shield or sandwich panel style, bike locks and padlocks). The reinforcement can be applied as a core in the centre of the material that form the external frame of the application to reduce cost and to potentially introduce additional physical support. As an example, this section estimates the cost of a U shape bike lock as commercial information

about these products is available. The same procedures were followed as in the previous section to calculate the cost of making the lock, where the same equation A-1 above was used to convert volume to the density, while equation A-2 was modified to be suitable to calculate the volume of the U shape bike lock assuming that is formed from two bars of 260 mm length (the lock height from base until the arc of ‘’U’’ shape).

The comparison was made to a top of the range U bike lock [268], the Abus Granit Extreme 59 Lock, retailing at £249.99. the dimensions of this lock are shown in

Figure (A-2). This is described as being made from armoured hardened steel, and is intended for high risk applications, especially motorcycles [268]. The possible cost increases due to reinforcement of the lock with a core of MMDCs is shown in Table (A-3) and Table (A-4), the percentage increment in comparison with commercial prices is displayed in the last column of the same tables.

The same steps can be taken with ATM reinforcement to reduce the manufacturing cost by the use of reinforced metal matrices with some ceramic particles such as alumina and silicon carbides replacing a portion of the diamond. The estimated costs for the MMCCs and those loaded with diamond reinforcement are shown in Table (A-5). These materials were made in the same way that was discussed above in section A.2.1 ATM Machine Reinforced Against Abrasive Cutting Attacks.

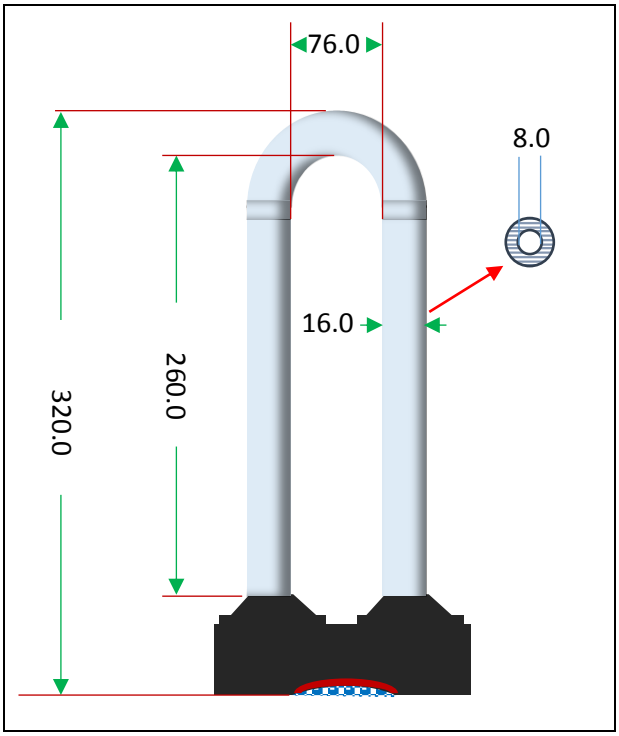

Figure (A-2): Shape and dimension of prospecting bike lock case study.

Table (A-3): Cost of a possible MMDCs reinforced bike lock and increment in comparison with a commercial product.

MMDCs GI	Lock core volume (cm^3)	Matrix mass (g)	Dia. mass (g)	Matrix cost (£)	Dia. cost (£)	MMDCs cost (£)	Increment (249.99 £)
Al-50% Dia.	**26.14**	**35.3**	**46.4**	**0.06**	**19.63**	**19.69**	**7.9%**
Sn-50% Dia.	**26.14**	**94.88**	**46.4**	**1.38** [259], [262]	**19.63**	**21.01**	**8.4%**
Epoxy-50% Dia.	**26.14**	**16.34**	**46.4**	**0.33**	**19.63**	**19.96**	**8%**

Table (A-4): Cost of prospecting MMDCs reinforced bike locks (SPS and PM) and increment in comparing with commercial product.

Either SPS or PM	Lock core volume (cm^3)	Matrix mass (g)	Dia. mass (g)	Matrix cost (£)	Dia. cost (£)	MMDCs cost (£)	Increment (249.99 £)
Ni-50% Dia.	**26.14**	**116.32**	**46.4**	**1.12** [259]	**19.63**	**20.75**	**8.3%**
Cu-50% Dia.	**26.14**	**117.1**	**46.4**	**0.54** [259]	**19.63**	**20.17**	**8.1%**
Ti-5% Dia.	**26.14**	**111.75**	**4.64**	**4.84**	**1.96**	**6.8**	**2.72%**
Ti-15% Dia.	**26.14**	**100**	**13.92**	**4.33**	**5.89**	**10.22**	**4.1%**
Ti-30% Dia.	**26.14**	**82.34**	**27.84**	**3.57**	**11.78**	**15.35**	**6.1%**
Ti-50% Dia.	**26.14**	**58.82**	**46.4**	**2.55** [263]	**19.63**	**22.18**	**8.9%**

Table (A-5): Cost of prospecting MMCCs reinforced bike lock and increment in comparing with commercial product.

Ceramic Ren.	Lock core volume (cm^3)	Matrix mass (g)	Rein. mass (g)	Matrix cost (£)	Rein. cost (£)	MMDCs cost (£)	Increment (249.99 £)
Al GI-50% SiC	**26.14**	**35.3**	**41.7**	**0.06**	**0.6**	**0.66**	**0.26%**
Al GI-50% Al2O3	**26.14**	**35.3**	**51.23**	**0.06**	**0.98**	**1.04**	**0.41%**

Ti PM-50% SiC.	**26.14**	**58.82**	**41.7**	**2.55** [263]	**0.6**	**3.15**	**1.3%**
Ti PM-50% Al2O3	**26.14**	**58.82**	**51.23**	**2.55** [263]	**0.98**	**3.53**	**1.4%**
Al GI 30% Sic-20% Dia.	**26.14**	**35.3**	**25.02-18.56**	**0.06**	**0.37+7.85**	**8.28**	**3.3%**
Al GI 30% Al2O3-20% Dia.	**26.14**	**35.3**	**30.74-18.56**	**0.06**	**0.6+7.85**	**8.51**	**3.4%**

It can be seen that the minimum increase in cost can be reduced to 3.3% (around £8), making these reinforcements potentially viable from a commercial point of view.

A.3 Assessment of MMDCs against Other Types of Cutting

The MMDCs developed in this work have not been extensively tested by other means of cutting, which could possibly be used by thieves such as oxyacetylene gas flame to cut the MMDCs barrier. Even though this was not one of the main targets of this study, a cover of a steel plate could offer some resistance against this type of attack, in addition to the distributed diamond or ceramic particles in general have high thermal resistance, which may act to disperse the energy of the flame. The high thermal conductivity of the reinforcement particle (either diamond or ceramic) could allow the thermal energy to disperse, consequently leading to at least some delay in the cutting process.

To sum up from cost information above, it can be conducted that the MMCs loaded with 20 vol. % diamond would be suitable for security barriers in two reasons. One of them is that these composites are able to wear a whole cut-off wheel with a design as a rod structure of 8 mm diameter. Secondly, the increment in cost for some applications is probably acceptable; compared to the commercial product the cost rise would be between 3.3-5.2% for both case study examples. Even if greater protection were needed, the same aluminum matrix reinforced with 50 vol. % diamond the increment would only increase to about 7.9-12.1% over the commercial products in both case study examples.